Technische Universität München
Department Chemie
Lehrstuhl II für Organische Chemie

Synthesis and Conformational Study of N-Methylated Cyclic Peptides

Jayanta Chatterjee

Vollständiger Abdruck der von der Fakultät für Chemie der Technischen Universität München zur Erlangung des akademischen Grades eines

Doktors der Naturwissenschaften (Dr. rer. nat)

genehmigten Dissertation.

Vorsitzender: Univ.-Prof. Dr. Steffen Glaser

Prüfer der Dissertation:

1. Univ.-Prof. Dr. Horst Kessler
2. Priv.-Doz. Dr. Rainer Jordan

Die Dissertation wurde am 08.05.2008 bei der Technischen Universität München eingereicht und durch die Fakultät für Chemie am 29.05.2008 angenommen.

Dedicated to my parents

Chemists are a strange class of mortals, impelled by an almost maniacal impulse to seek their pleasures amongst smoke and vapor, soot and flames, poisons and poverty, yet amongst all these evils I seem to live so sweetly that I would rather die than change places with the King of Persia."

- Johann Joachim Becher, *Physica subterranea* (1667)

Acknowledgements

Research described in this thesis was carried out in the laboratory of Prof. Dr. Horst Kessler of Technische Universität München and supervised by Prof. Dr. Horst Kessler during July 2004 till April 2008.

I will be ever grateful to Prof. Horst Kessler for giving me an opportunity to work in his lab in spite of being having any previous exposure to his lab. I am highly inspired by his scientific knowledge and vision, critical view and extremely cordial nature from which I learnt a lot. The experience, skill and the knowledge I gained during my stay in his lab is invaluable and will help me in my future career.

I thank Dr. Rainer Haessner for not only making the spectrometers and computers running for us but for his timely indispensable help and ever cheerful face.

My labmates Dr. Timo Weide and Burkhardt Laufer for scientific discussions which enriched my views at several instances. Some fruitful scientific discussions with Florian Manzenrieder during the writing of my thesis were very helpful. Burkhardt is to be thanked again, for not only reading meticulously my thesis but also for helping me out with several projects related to the studies of conformational impact of N-methylation on cyclic peptides.

A special acknowledgement goes to Dr. Eric Biron for involving me in several of his ongoing projects and invaluable suggestions, which helped me a lot in improving my scientific skills.

I also greatly acknowledge my labmate Florian Opperer who helped me out in acting as an interpreter and the great fun we had in the lab.

I thank Mona Wolff for timely ordering of the chemicals which are indispensable for going on in the chemical lab. And also for her timely help in some synthesis.

I thank Mrs. Martha Fill for her timely help in the official matters, which otherwise would have been real difficult.

I remember the people who have helped me, those are,

- Prof. Chaim Gilon and Prof. Amnon Hoffman at The Hebrew University of Jerusalem for collaboration on the bioavailability project.
- Luciana Marinelli for the help in MD calculation and docking studies.

- Jochen Klages for some initial help in the MD calculations.
- Dr. Georg Voll for help in the MD calculations.
- Dr. Grit Zahn, Jerini Berlin for measuring the integrin ligands.

I also thank my former supervisor Prof. Dilip Dhavale at Pune University for a nice exposure into his lab.

I also wish to thank many of my present and past colleagues for invaluable discussions and for making the lab a great place to work in. They are namely, Lucas, Dominik, Sebastian, Oliver, Andreas, Timo, Marcus, Elke and several others.

I express my sincere gratitude towards my parents, who bear silent pain to be apart but still encouraging me ever to excel in my field. I am also indebted to Rupashree for her support during my stay in Munich. I also thank Sekhar kaku and Christina aunty for their extended help during my stay outside lab.

The acknowledgement would not complete, if I forget to show my affection towards my brother, Shyamal and Abhishek, for their support, faith and encouragement to me throughout the period of my scientific life.

München, 30 April 2008 Jayanta Chatterjee

Parts of this thesis have already been published:

From Chapter 2: N-Methylated peptides-

Optimized Selective *N*-Methylation of Peptides on Solid Support. E. Biron, J. Chatterjee and H. Kessler (2006) *J. Pept. Sci.* **12**, 213-219.

From Chapter 3: N-Methylated cyclic pentaalanine peptides-

***N*-Methylated Cyclic Pentaalanine Peptides as Template Structures.** J. Chatterjee, D. Mierke and H. Kessler (2006) *J. Am. Chem. Soc.* **128**, 15164-15172.

Conformational Preference and Potential Templates of *N*-Methylated Cyclic Pentaalanine Peptides. J. Chatterjee, D. F. Mierke and H. Kessler (2008) *Chem. Eur. J.* **14**, 1508-1517.

From Chapter 4: Oral bioavailability of peptides-

Improving Oral Bioavailability of Peptides via Multiple *N*-Methylation: Somatostatin Analogs. E. Biron, J. Chatterjee, O. Ovadia, D. Langenegger, J. Brueggen, D. Hoyer, H. Schmid, R. Jalenik, C. Gilon, A. Hoffman and H. Kessler (2008) *Angew. Chem. Int. Ed.* **47**, 2595-2599.

From Chapter 5: N-Methylated cyclic hexapeptide GPIIb-IIIa ligands-

Multiple *N*-Methylation by a Designed Approach Enhances Receptor Selectivity. J. Chatterjee, O. Ovadia, G. Zahn, L. Marinelli, A. Hoffman, C. Gilon and H. Kessler (2007) *J. Med. Chem.* **50**, 5878-5881.

Contents

ABBREVIATIONS

Å	Ångstrom, 10^{-10} m
Ac	Acetyl-
ACN	Acetonitrile
ADMET	Absorption, distribution, metabolism, excretion, toxicology
Boc	*tert*-Butyloxycarbonyl-
t-Bu	*tert*-Butyl
Cbz	Benzyloxycarbonyl-
Conc.	Concentrated
COSY	Correlated spectroscopy
d	Doublet or days
δ	Chemical shift
1D, 2D, 3D	One / two / three- dimensional
DBU	1,8-diazabicyclo[5,4,0]undec-7-ene
DCM	Dichloromethane
dd	Doublet of doublets
DEAD	Diethyl azodicarboxylate
DIAD	Diisopropylazodicarboxylate
DIEA	Diisopropylethylamine
DMA	*N*,*N*-Dimethylacetamide
DMAP	4-Dimethylaminopyridine
DMF	*N,N*-Dimethylformamide
DMSO	Dimethylsulfoxide
DPPA	Diphenylphosphoric acid azide
ECM	Extracellular matix
ESI-MS	Electrospray ionization mass spectrometry
Fmoc	9-Fluorenylmethoxycarbonyl
h	hour
HATU	*O*-(7-Azabenzotriazol-1-yl)-*N*,*N*,*N'*,*N'*,-tetramethyluronium-hexafluorophosphate
HMBC	Heteronuclear multiple bond correlation
HMQC	Heteronuclear multiple quantum coherence
HOAc	Acetic acid
HOAt	1-Hydroxy-7-azabenzotriazol
HOBt	1-Hydroxybenzotriazol
HPLC	High performance liquid chromatography
HSQC	Heteronuclear single quantum coherence
Hz	Hertz
IC	Inhibitory capacity
J	Scalar coupling constants
kDa	Kilodalton

LC-MS	Liquid chromatography mass spectrometry
M	Multiplett
M	Molar
Me	Methyl
MeOH	Methanol
MHz	Megahertz
MIDAS	Metal ion dependent site
min.	Minutes
mL	Milliliter
Mmol	Millimol
MS	Mass spectroscopy
MTBD	7-methyl-1,5,7-triazabicyclo[4.4.0]dec-5-ene
MW	Molecular weight
^{N}J	Scalar coupling over n-bonds
N	Normal
NMe	N-methyl
NMP	*N*-Methylpyrrolidone
NMR	Nuclear magnetic resonance
o-NBS	*o*-nitrobenzenesulfonyl
PPh_3	Triphenylphosphine
Ph	Phenyl
ppm	parts per million
q	Quartet
RGD	Arginine-Glycine-Aspartic acid
R_f	Retention factor
ROESY	rotating frame nuclear Overhauser and exchange spectroscopy
R_t	Retention time
RT	Room temperature
s	Singlet
sat.	Saturated
SPPS	solid phase peptide synthesis
SRIF	Somatostatin release inhibitory factor
sst	Somatostatin receptor subtype
t	Triplet
TBTU	*O*-(1H-Benzotriazol-1-yl)-*N*,*N*,*N*',*N*'-tetramethyluronium-tetrafluoroborate
TCP	Tritylchlorid-Polystyrene-resin
TEA	Triethylamine
TFA	Trifluoroacetetic acid
TFE	Trifluoroethanol
THF	Tetrahydrofuran
TIPS	Triisopropylsilane

TMS	Trimethylsilyl-
TOCSY	total correlation spectroscopy

1. Conspectus

Peptides are the biomolecules whose long standing interest among the scientific community has resulted in its wide and diverse application in various fields spanning drug discovery[1] to nanomaterials.[2] The chemistry of peptides which began in the laboratories of Theodor Curtius[3] and Emil Fischer[4] with the synthesis of a protected peptide and a free dipeptide, respectively, has been revolutionized in such an extent, that today synthesizing a fully functional enzyme[5] is a matter of few days, which was long before envisioned by Emil Fischer. Further seminal contributions of Bergmann,[6] Wieland,[7] Merrifield,[8] and many others are invaluable and contributed in the everlasting nurture of peptide chemistry. However, in spite of groundbreaking inventions, the development of peptide based drugs is a downtrodden field due to the poor pharmacokinetic profile of peptides. Peptides are rapidly degraded by the enzymes in the gut and serum; to overcome this, peptide cyclization was suggested resulting in the lack of a free C- or N- terminal, which is generally required for the recognition by an enzyme.[9] In addition to this, other approaches were also envisioned like, introduction of retro-inverso peptides,[10] peptoids- where the amino acid side chain is shifted on the nitrogen of the amide bond,[11] and a plethora of peptidomimetics.[12] Another major drawback of peptides are the poor absorption through the cell membranes.[13] Peptides traverse across the intestinal membrane by either transcellular (across the apical cell membrane through the cell interior) or the paracellular pathway (aqueous extracellular route across the epithelia).[14] It is known that di- and tripeptides are transported across the membrane by active transport via the transcellular pathway;[15] on the other hand, larger peptides owing to their hydrophilicity, pass the membrane by the paracellular pathway via passive diffusion which is generally much slower and is dependant on their size and charge.[14] To circumvent this, various prodrug approaches have been envisioned,[16] but still there is a lack of a general approach to avert both the enzymatic stability and membrane permeability of peptides.

The oral bioavaiability of drug candidates are predicted by the ‘rule of 5’ originally formulated by Lipinski et al.[17] and later modified by Veber et al.[18] These rules although are used as a rule of thumb for screening drug candidates in pharmaceuticals, but they do not hold good for peptides. Cyclosporin A, an undecapeptide with seven of its eleven peptide bonds N-methylated, violates all the Lipinski’s rules but is an orally available immunosuppressant drug.[19] At this point we envisioned that the enormous stability and subsequently the oral bioavailability of Cyclosporin A are owing to its multiply N-methylated backbone. Thus, our

investigation started to reveal the versatile effects of multiple N-methylation on the backbone of cyclic peptides.

To begin with, we concentrated on the synthesis of N-methylated amino acids and peptides, as the methods available at our disposal for the synthesis of multiply N-methylated libraries of peptides were either expensive or impractical for the synthesis of large libraries. So in the beginning I will describe the synthesis of N-methylated amino acids and peptides on the solid phase which we reported for the fast and inexpensive synthesis of multiply N-methylated libraries. Then the conformational modulation of the peptidic backbone by multiple N-methylation of model alanine cyclic peptides will be described. Finally, I will wind up with the achievement of enhanced selectivity and oral bioavailability of functionalized bioactive cyclic peptides by multiple N-methylation. I would like to mention here that, when several of these projects started couple of years ago, it was like finding a needle in a stack of hay; however, today with the endless efforts of our group we seem to approach our goal, when multiple N-methylation will be used by the scientific community to modulate the pharmacokinetic properties of peptides, especially in context to drug molecules.

2. N-Methylated Peptides

2.1 Biological background

N-methyl amino acids are constituents of several biologically active natural products commonly occurring in plants, marine sources and various microorganisms, such as: Cyclosporine, Dolastatin, Didemnins etc. exhibiting highly interesting therapeutic profiles.[20-22]

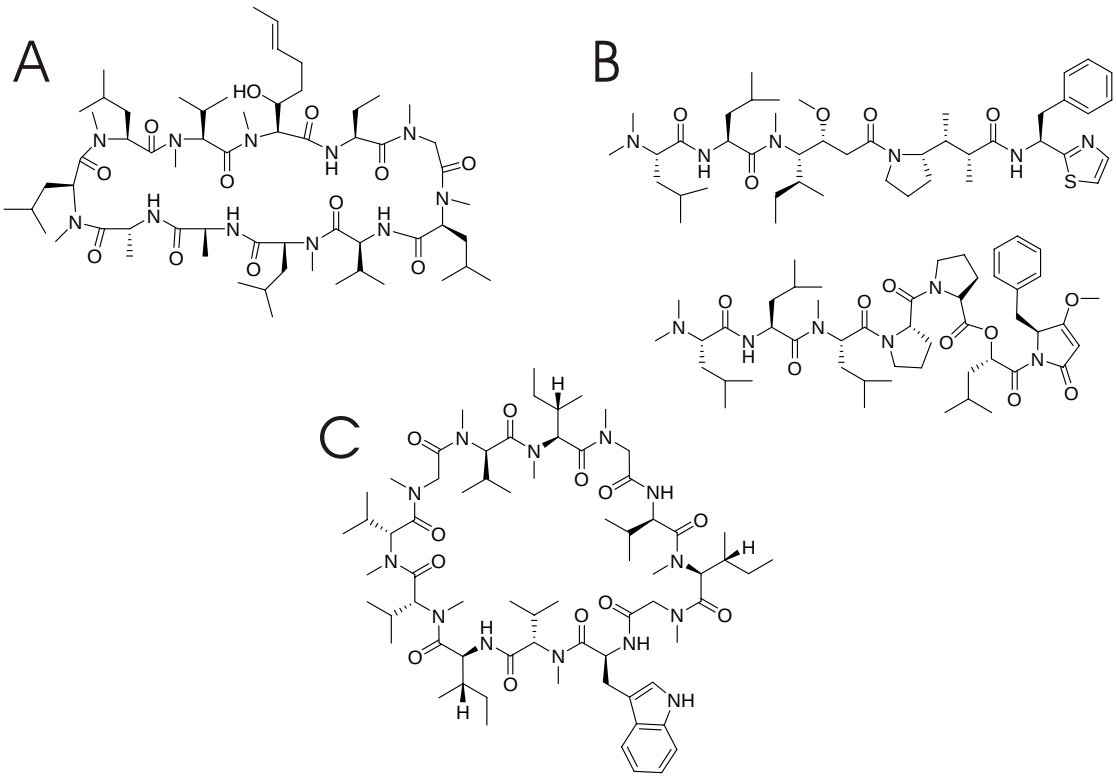

Figure 2.1. *A) Cyclosporine A. B) Dolastatin 10 (top) and Dolastatin 15 (bottom). C) Omphalotin A.*

Cyclosporine A, isolated from *Trichoderma polysporum*[23] is a lipophilic cyclic undecapeptide with seven sterically hindered N-methylated amino acids. It has various biological activities, but its immunosuppressive effects combined with low toxicity and improved pharmacokinetic activity has made it one of the most successful drugs used during organ transplantation. The first chemical synthesis of Cyclosporine was reported by Wenger.[24] The synthesis was carried out in solution using Boc chemistry, and fortunately owing to the lack of diversely functionalized amino acids in Cyclosporine, the difficult couplings on the N-methylated terminal was carried out by the formation of reactive acid chloride. Dolastatin are another group of N-methylated peptides which have received great attention. They were isolated from the sea hare *Dolabella auricularia*,[25] among them, Dolastatins 10 and 15 exhibit promising antitumor activity and show antiproliferative effects on murine and human

leukemia cell lines. Another highly N-methylated cyclic dodecapeptide, Omphalotin has been isolated from the basidiomycete *Omphalotus olearius*.[26] This peptide shows selective activity against phytopathogenic nematodes. Recently, the total synthesis of Omphalotin was reported concurrently by Sewald and Jung et al.[27,28]

N-methylated cyclic depsipeptides comprises of another class of naturally occurring cyclic peptides. E.g. IB-01212 is a cytotoxic symmetric octadepsipeptide isolated from the mycelium extract of *Clonostachys sp.*, shows growth inhibition (GI50) in the order of 10^{-8} M against Ln-CAP (prostate cancer), SK-BR3 (breast cancer), HT29 (colon cancer) and HELA (cervical cancer).[29]

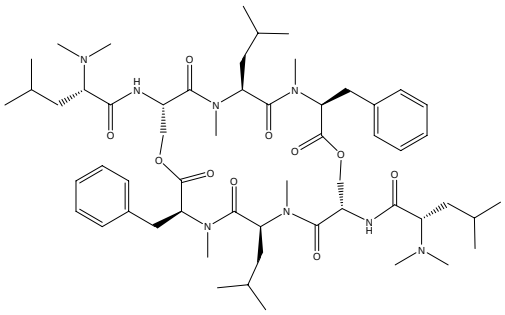

Figure 2.2. *Structure of depsipeptide IB-01212.*

Albericio and co-workers reported three solid phase strategies for the synthesis of IB-01212, of which a convergent method proved to be the most successful one. In this strategy, two symmetrical tetrapeptide fragments were prepared separately, and then finally were coupled together in solution using MSNT, NMI and DIPEA in DCM/DMF.[30]

Thus, N-methyl amino acids are abundant in natural products conferring them stability and interesting biological properties.

2.2 Structural effects

Incorporation of N-methyl amino acids into biologically active peptides, replacing the natural amino acids has resulted in analogs with improved pharmacological properties such as: enzymatic stability,[31,32] receptor selectivity,[33-35] enhanced potency[36-38] and bioavailability.[39] Thus, structural modification of the peptide backbone via N-methylation is a powerful tool to modulate pharmacokinetic profile and biological activity of peptides.

N-Methylation affects not only the conformation of the modified amino acid but also of the preceding residue.[40] In addition, it facilitates the occurrence of a *cis*-peptide bond, which in comparison to the *trans*-peptide bond is thermodynamically less unfavored compared to a secondary amide bond.[41] In case of cyclic peptides, N-methylation has further long-range impact on the entire backbone conformation. N-Methylation affects the backbone of the peptide by reducing the number of hydrogen-bond donors preventing intramolecular and

intermolecular hydrogen bonding, and potentially enhances the pharmacokinetic properties of the peptide by blocking the proteolytic cleavage sites. The presence of N-methyl backbone groups also increases the hydrophobicity of the peptide bond and, consequently, its ability to interact more selectively with the complementary hydrophobic pocket eventually resulting in enhanced membrane permeability.[42,43] Therefore, mono to multiple N-methyl scan of peptides is and will continue to be a useful approach to search for better lead structures and/or improve pharmacokinetic properties of peptides. It is worth mentioning that the concept of N-methyl scan was first introduced by Sugano et al.[44] by synthesizing a series of N-methylated analogs of the Eledoisin related peptide H-Lys-Phe-Ile-Gly-Leu-Met-NH_2, which finally resulted in a biologically active and metabolically stable analog.

2.3 Synthesis of N-methylated peptides

2.3.1 Previous approaches

Commercially available N-methyl amino acids are still very expensive in spite of various methods developed for the synthesis of optically pure N-methyl amino acids.[45] The most widely methods employ the direct N-methylation of the N^{α}–protected amino acids or amino acid esters.[46-48]

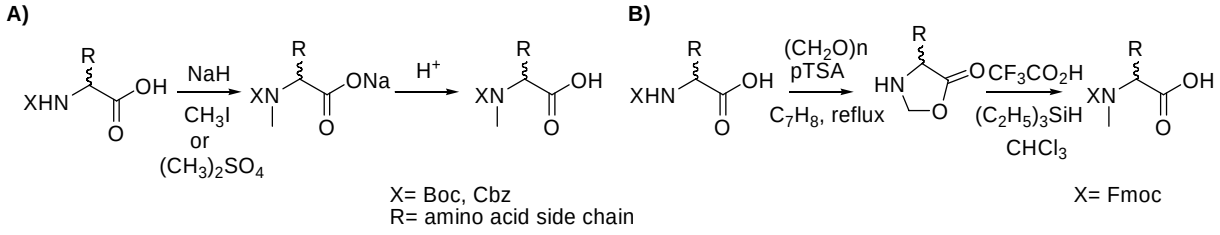

Figure 2.3. *A) Direct approach of N-methylation. B) The oxazolidinone approach.*

The direct method for preparing Cbz- and Boc-N-methylamino acids of acceptable enantiomeric purity was developed in the early 1970s, when it was shown that methylation of Cbz and Boc amino acids with methyl iodide and sodium hydride generated the products without esterifying the carboxyl groups when the reaction was carried out in tetrahydrofuran at ambient temperature (Figure 2.3A). Fmoc amino acids however, can not be produced by the direct alkylation. The most commonly accepted procedure for the synthesis of Fmoc N-methylated amino acids is the 5-oxazolidinone approach developed by Freidinger et al. at Merck.[49] This method employs the formation of oxazolidinones by reaction with formaldehyde under dehydrating conditions followed by the ring opening and methylation using trifluoroacetic acid and triethylsilane; this results in excellent yields of the Fmoc N-methyl amino acid (Figure 2.3B). Unfortunately, most of these methods are limited to

aliphatic amino acids or are characterized by harsh reaction conditions or long synthetic sequences, and some cause partial racemization of the substrate.[50,51]

It is worth mentioning that, recently the scope of the Freidinger's method was further expanded to some more protected amino acids by employing Lewis acid catalyzed reductive ring opening of the oxazolidinone instead of using the strong acidic condition by trifluoroacetic acid (Figure 2.4).[52] However, unlike the Freidinger's procedure, this method involves an additional step of purification of the final product, either by extraction or by a flash chromatography.

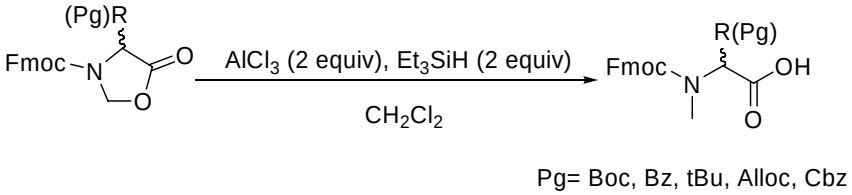

Figure 2.4. *Lewis acid catalyzed reduction of oxazolidinone.*

In addition, this reaction was also studied under microwave irradiation and was found to be extremely fast. The formation of the oxazolidinone was complete in 3 min, and the subsequent ring opening with Lewis acid was achieved in 1 min compared to the total of ~1 day required for the Freidinger's method.[53]

Thus, in literature there was a lack of a general procedure for the easy and efficient solution synthesis of N-methylated amino acid with diverse protecting groups. Hence, our group started to investigate a method which could be generalized for all the amino acids irrespective of the side chain functionality.

Till date, the most efficient procedure for selective N-methylation of peptide on solid support is a three step procedure involving amine activation by protection with *o*-nitrobenzenesulfonyl group (*o*-NBS),[54] followed by alkylation on the activated nitrogen and a final deprotection of the *o*-NBS group (Scheme 2.1).[55,56]

Scheme 2.1. *Selective N-methylation of peptide on solid support.*

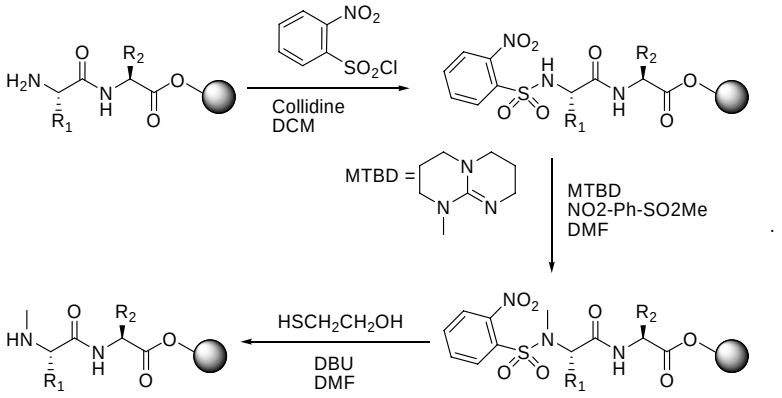

However, this method suffers from two drawbacks: i) three additional steps are needed along with the normal coupling and deprotection steps which can be time consuming and confusing while synthesizing N-methylated peptide libraries, and ii) very small quantities of N-methylated amino acids can be prepared on solid phase. Thus, a strategy was developed by Biron et al. in our group to effectively synthesize N-methylated amino acids in solution.[57] This procedure involved the activation of the amine of the amino acid by protecting with *o*-NBS group, and subsequent N-methylation by a weaker base under mild conditions in solution to use these N^{α}-methyl-N^{α}-*o*-NBS-α-amino acids directly on solid support (they preferred to deprotect the *o*-NBS group on solid phase as i) it has a longer shelf life and ii) the work-up after deprotecting the *o*-NBS group in solution could be tedious resulting in lower yields of the N-methylated amino acid) (Scheme 2.2).

Scheme 2.2. *Synthesis of N^{α}-methyl-N^{α}-o-NBS-α-amino acids in solution.*

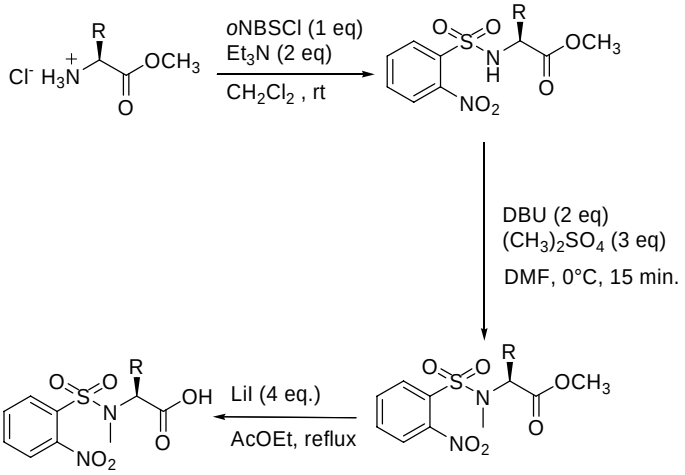

Although the synthesis of the N^{α}-methyl-N^{α}-*o*-NBS-α-amino acid ester was straightforward, Biron et al. successfully replaced the use of expensive base MTBD (7-methyl-1,5,7-triazabicyclo[4.4.0]dec-5-ene) by the inexpensive and widely used base DBU (1,8-Diazabicyclo[5.4.0]undec-7-ene) and showed the efficiency of the method towards every amino acid. The most intricate step in the synthesis was the saponification of the N^{α}-*o*-NBS-N^{α}-methylamino acid ester avoiding any racemization (N^{α}-protected-N^{α}-methylamino acids are infamous for undergoing racemization during saponification than the corresponding amino acid ester due to the absence of the amide proton).[50,51,58] To overcome this problem, the methyl ester cleavage by S_N2 dealkylation using LiI in pyridine was tested.[59,60] Initial investigations with lithium iodide in refluxing pyridine for 30 min resulted in a mixture of products (owing to non selective nucleophilic attack of iodine). However, this was overcome by replacing pyridine with refluxing ethyl acetate (having a lower boiling point and neutral); which finally resulted in the completion of the reaction in 16 h yielding the corresponding N^{α}-

methyl-N$^{\alpha}$-*o*-NBS-α-amino acids ranging from 83-99%, which could be directly used on solid support without further purification.

2.3.2 Optimized synthesis of N-methylated peptides

The most efficient solid phase procedure described by Miller and Scanlan,[55] involves a total of 3 h for the N-methylation and is expensive owing to the cost of the MTBD. Thus, we were interested in optimizing the procedure in order to reduce the cost and time while demonstrating the compatibility of the procedure to different side chain functionalized amino acid. The development of the synthetic methodology by Biron et al.[57] was the starting point for our investigation to achieve an efficient and fast synthesis of N-methylated peptides on solid support.

2.3.2.1 *o*-NBS protection

The first step uses the method developed by Fukuyama for the preparation of secondary amines.[54] In the procedure described by Miller and Scanlan,[55] protection of the resin-bound free amine peptide with *o*-nitrobenzenesulfonyl chloride (*o*-NBS-Cl) is completed in DCM at room temperature in 2 hours (Scheme 2.1) while protection is completed in 30 minutes in DMF in the procedure described by Reichwein and Liskamp.[56] Time needed for complete protection was investigated with the trityl resin-bound amine free dipeptide **1a** by treatment with *o*-NBS-Cl, and collidine in dichloromethane, tetrahydrofuran or N-methylpyrrolidone (NMP). The investigation revealed that the protection in THF needs more than 2 hours while complete conversion is observed in 1 hour in DCM and in only 15 minutes in NMP. NMP has also the advantage that no solvent changes have to be done after Fmoc deprotection.

Trityl resin (TCP resin) bound N$^{\alpha}$-*o*-NBS-protected dipeptides **2b-k** were prepared following the optimized procedure (Scheme 2.3), i.e. by treatment of the corresponding resin-bound amine free dipeptides **1b-k** with *o*-nitrobenzenesulfonyl chloride (4 equivalents) in the presence of collidine (10 equivalents) in NMP for 15 minutes. Monitoring of the reaction by HPLC revealed that protection was completed in 15 min for every tested dipeptide (purity >99%). Analysis of the *N*$^{\alpha}$-o-NBS-Xaa-Leu-OH dipeptides **2a-k** was accomplished by HPLC and ESI-MS (Table 2.1). Protection of dipeptides **1a-k** with *o*-NBS-Cl did not involve racemization as shown by HPLC of the crude product and by comparing with the corresponding *N*$^{\alpha}$-o-NBS-D-Xaa-Leu-OH dipeptides.

Scheme 2.3. *Synthesis of o-NBS protected resin-bound dipeptides* ***2a-k****.*

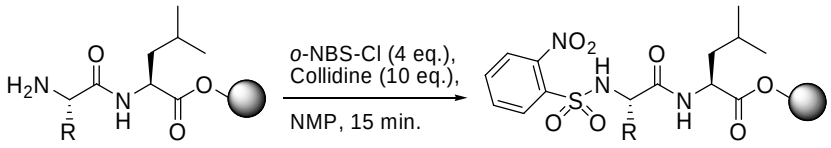

1a-k **2a-k**

Table 2.1. *Retention times and observed mass of* N^{α}*-o-NBS-Xaa-Leu-OH* ***2a-k****.*

Peptide	Xaa	HPLC[a] [rt] (min)	ESI-MS $[M+H]^+$
2a	Phe	20.9	464.2
2b	Lys(Boc)	21.4	545.3
2c	Arg(Pbf)	23.3	725.4
2d	Ser(tBu)	21.7	460.3
2e	Trp	20.7	503.2
2f	Tyr(tBu)	23.1	536.2
2g	Glu(tBu)	21.7	502.3
2h	Gln(Trt)	25.6	687.2
2i	Met	19.6	448.2
2j	Cys(Trt)	26.9	662.2
2k	His(Trt)	22.2	695.1

[a] RP-HPLC on C18 column, ACN 10-100% in 30 min.

2.3.2.2 N-methylation using DBU

In the procedure described by Miller and Scanlan, N-methylation of the resulting resin-bound sulfonamides is achieved by using 4 equivalents of methyl *p*-nitrobenzenesulfonate in combination with 3 equivalents of the hindered, nonionic guanidium base MTBD (7-methyl-1,5,7-triazabicyclo[4.4.0]dec-5-ene) in DMF and is completed in 30 min (Scheme 2.1).[55,61] The high price of MTBD led us to consider the possibility of using other less expensive structurally related hindered bases like TBD (1,5,7-triazabicyclo[4.4.0]dec-5-ene) or DBU (1,8-diazabicyclo[5,4,0]undec-7-ene). We have recently reported the successful N-methylation of *o*-NBS amino acid methyl esters in DMF using DBU as base.[57] A first investigation of the reaction on the resin-bound N^{α}-*o*-NBS-dipeptide **2a** with DBU and dimethylsulfate in DMF revealed a very important side reaction coming from the reaction of DBU with dimethylsulfate and full conversion into N^{α}-*o*-NBS-N^{α}-methyl dipeptide **3a** could not be achieved. The same problem has been observed when TBD is used as base. To overcome this problem, DBU was first reacted with the resin-bound N^{α}-*o*-NBS-protected dipeptide **2a** to ensure complete deprotonation of the sulfonamide and was characterized by the yellow coloration of the resin. After 5 minutes of reaction, dimethylsulfate was added to the resin for N-methylation and the yellow color completely disappeared. Monitoring of the reaction showed that 91% of the N^{α}-*o*-NBS dipeptide **2a** is N-methylated after 3 minutes of reaction with DBU and 2 minutes with dimethylsulfate. Full conversion (>99%) into N^{α}-

methyl-N$^{\alpha}$-*o*-NBS dipeptide **3a** is achieved when the procedure is repeated one more time (Scheme 2.4).

The newly optimized N-methylation procedure with the less expensive DBU was tested on the other resin-bound N$^{\alpha}$-*o*-NBS dipeptides **2b-k**. N-Methylation was then performed in NMP using 3 equivalents of DBU for 3 minutes followed by 10 equivalents of dimethylsulfate for 2 minutes. The sequence was repeated one more time and gave, in most cases, the corresponding N$^{\alpha}$-*o*-NBS-N$^{\alpha}$-methyl dipeptides **3b-j** in >99% purity (HPLC). Unfortunately a considerable amount of impurity was observed during N-methylation of His(Trt)-containing dipeptide **2k.** HPLC-MS analysis revealed that N-methylation also occurs on the side chain of histidine with loss of the trityl protecting group. Side-chain N-methylation of histidine was also observed in solution.[57] Analysis of the N$^{\alpha}$-o-NBS-MeXaa-Leu-OH dipeptides **3a-k** was accomplished by HPLC and ESI-MS (Table 2.2). N-Methylation of the dipeptides **2a-j** with DBU and dimethylsulfate did not involve racemization as shown by HPLC of the crude product and by comparing with the corresponding N$^{\alpha}$-o-NBS-D-MeXaa-Leu-OH dipeptides.

Scheme 2.4. *Solid phase synthesis of N$^{\alpha}$-methyl-N$^{\alpha}$-o-NBS-dipeptides* ***3a-k*** *using DBU and dimethylsulfate.*

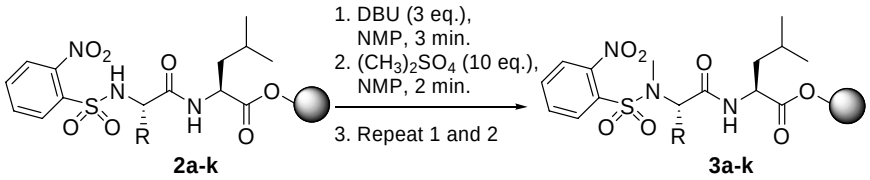

2.3.2.3 N-methylation using Mitsunobu reaction

To overcome the problem of side chain methylation, N-methylation via Mitsunobu reaction was investigated on the N$^{\alpha}$-*o*-NBS-dipeptide **2k** (Scheme 2.5). In the procedure described by Yang and Chiu,[62] N-methylation of resin-bound N$^{\alpha}$-*o*-NBS-amino acids under Mitsunobu conditions is performed with 5 equivalents of triphenylphosphine (Ph_3P), 10 equivalents of methanol and 5 equivalents of diethyl azodicarboxylate (DEAD) in THF for 1 hour. The same conditions were applied for N-methylation of the resin-bound N$^{\alpha}$-*o*-NBS-dipeptide **2k** and full conversion without side chain methylation was observed. Monitoring of the reaction versus time revealed that N-methylation of the resin-bound N$^{\alpha}$-*o*-NBS-dipeptide **2k** under Mitsunobu conditions is completed after only 5 minutes. N-Methylation under Mitsunobu conditions would be therefore the method of choice for N-methylation of His(Trt) on solid support.

N-Methylation under Mitsunobu conditions was performed on the other resin-bound N^{α}-*o*-NBS-dipeptides **2a-j** and complete conversion to corresponding N^{α}-methyl-N^{α}-*o*-NBS-dipeptides **3a-j** was observed in 10 minutes in every case. N-Methylation of resin-bound dipeptides **2a-k** by Mitsunobu reaction did not involve racemization as shown by HPLC of the crude products and by comparing with the corresponding N^{α}-o-NBS-D-MeXaa-Leu-OH dipeptides. Analysis of the N^{α}-*o*-NBS-MeXaa-Leu-OH dipeptides **3a-k** from the Mitsunobu procedure was accomplished by HPLC and ESI-MS (Table 2.2) and showed exactly the same profile as the dipeptides from the DBU procedure.

Scheme 2.5. *Solid phase synthesis of N^{α}-methyl-N^{α}-o-NBS-dipeptides* ***3a-k*** *under Mitsunobu conditions.*

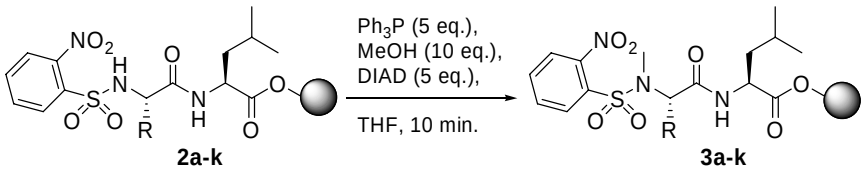

Both N-methylation procedures are very efficient and are completed in only ten minutes. One positive point about the N-methylation procedure with DBU is that no solvent changes have to be made since the reaction is done in NMP. On the other side, N-methylation under Mitsunobu conditions needs dry THF and solvent changes have to be made.

Table 2.2. *Synthesis of N^{α}-o-NBS-MeXaa-Leu-OH* ***3a-k***.

Peptide	MeXaa	HPLC [t_R] (min)	ESI-MS [M+H]$^+$
3a	MePhe	22.3	464.2
3b	MeLys(Boc)	22.5	545.3
3c	MeArg(Pbf)	23.9	725.4
3d	MeSer(tBu)	23.0	460.3
3e	MeTrp	22.3	503.2
3f	MeTyr(tBu)	24.4	536.2
3g	MeGlu(tBu)	23.1	502.3
3h	MeGln(Trt)	26.3	687.2
3i	MeMet	21.1	448.2
3j	MeCys(Trt)	28.0	662.2
3k	MeHis(Trt)	22.9	695.1

2.3.2.4 *o*-NBS deprotection

In the procedure described by Miller and Scanlan, removal of the *o*-NBS protecting group is achieved in 30 minutes with 10 equivalents of mercaptoethanol and 5 equivalents of DBU in DMF. Time needed for complete *o*-NBS deprotection was investigated on resin-bound N^{α}-methyl-N^{α}-*o*-NBS-dipeptide **3a** in NMP and revealed that the reaction is completed in only 5 minutes (Scheme 2.6). The shortened deprotection procedure was performed on the other resin-bound N^{α}-methyl-N^{α}-*o*-NBS-dipeptides **3b-k** and repeated one more time for 5 minutes to ensure complete deprotection in every case. Removal of the *o*-NBS protection was

monitored by HPLC and complete deprotection was observed after two times five minutes for every studied dipeptide. A major advantage of the *o*-NBS protecting group is that deprotection with mercaptoethanol is selective for N-methylated derivatives and does not proceed when the protected amine is not alkylated.

Scheme 2.6. *Solid phase synthesis of resin-bound N^{α}-methylamine free dipeptide* ***4a-K***.

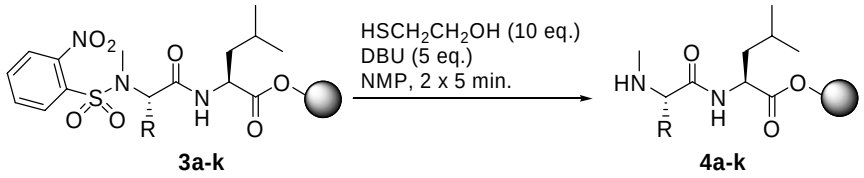

2.3.2.5 Coupling to N-methylated amino acid

Couplings on N^{α}-methylamino acids are known to be more challenging than normal couplings.[63] Coupling of Fmoc-Phe-OH to the resin-bound N^{α}-methylamino dipeptide **4a** could not be achieved when *N*-[(1H-benzotriazol-1-yl)-dimethylamino-methylene]-*N*-methylmethanaminium tetrafluoroborate *N*-oxide (TBTU) and 1-hydroxybenzotriazole (HOBt) were used as coupling mixture. The use of triphosgene has been recently described for couplings on resin-bound *N*-alkylated peptide,[64,65] but the use *N*-[(dimethylamino)-1H-1,2,3-triazolo[4,5-b]pyridine-1-yl-methylene]-*N*-methylmethanaminium hexafluorophosphate (HATU) as coupling reagent was preferred because no solvent changes are needed and the handling is easier and safer. As with triphosgene, one has to maintain an absolute dry condition and there are high chances of racemization with higher equivalents of the used base. A combination of HATU with 1-hydroxy-7-azabenzotriazole (HOAt) and diisopropylethylamine (DIEA) in NMP was used to couple Fmoc-Phe-OH to resin-bound N^{α}-methylamine free dipeptides **4a-k** (Scheme 2.7). Every coupling was completed after 3 hours (>98% purity) except coupling on the resin-bound dipeptide **5j** containing MeCys(Trt) where only 53% yield was observed. Therefore, coupling on N-methyl cysteine containing dipeptide **4j** had to be performed for 12 hours until complete conversion was observed. The tripeptide Fmoc-MePhe-MePhe-Leu-OH **6a** was efficiently prepared (>99% purity) by coupling Fmoc-MePhe-OH to the resin-bound dipeptide **4a** using HATU and HOAt for 3 hours. Analysis of the tripeptides **5a-k** and **6a** was accomplished by HPLC and ESI-MS (Table 2.3). Couplings using HATU/HOAt did not involve racemization as shown by HPLC of the crude products. The optimized three-step procedure and coupling with HATU/HOAt on the N^{α}-methyl peptides did not cause any detectable racemization of the peptide stereocenters.

Scheme 2.7. *Solid phase synthesis of N^{α}-methylamino acid containing tripeptides* ***5a-k***.

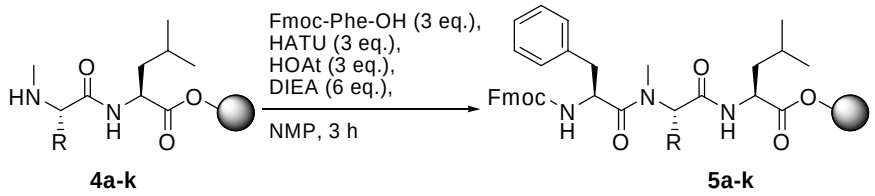

Table 2.3. *Synthesis of Fmoc-Phe-MeXaa-Leu-OH* ***5a-k***.

Peptide	-MeXaa-	HPLC [t_R] (min)	ESI-MS [M+H]$^+$
5a	MePhe	24.3	662.2
5b	MeLys(Boc)	24.5	743.3
5c	MeArg(Pbf)	25.3	923.6
5d	MeSer(tBu)	25.1	658.3
5e	MeTrp	23.9	702.3
5f	MeTyr(tBu)	26.5	734.2
5g	MeGlu(tBu)	25.0	700.2
5h	MeGln(Trt)	28.2	885.4
5i	MeMet	23.4	646.2
5j	MeCys(Trt)	30.4	860.3
5k	MeHis(Trt)	23.7	894.4

2.4 Conclusion

A simple and convenient optimized three-step procedure is developed for the preparation of N^{α}-methylpeptides on solid support. Every step of the procedure for solid-phase site-selective N-methylation of peptide described by Miller and Scanlan[55] was optimized in respect of time and economy. Protection and activation of the amino function of the resin-bound amino free peptide with *o*-NBS-Cl is performed in NMP and is completed in 15 minutes. Afterwards, the N-methylation step can be performed by direct N-alkylation using DBU and dimethylsulfate in NMP or under Mitsunobu conditions in THF. Both N-methylation reactions are completed in 10 minutes. Finally the *o*-NBS protecting group is selectively removed by using mercaptoethanol and DBU in NMP twice for 5 minutes. The optimized procedure is completed in 35 minutes instead of 3 hours for the three steps and no solvent changes are necessary. Compatibility of the procedure with every commonly used amino acid was demonstrated by using the optimized sequence to prepare tripeptides containing different N^{α}-methylamino acids. The *o*-NBS procedure on solid support is also an easy and inexpensive way to prepare peptides containing N^{α}-methyl-D- and unnatural amino acids. Coupling to N^{α}-methylamino acids on solid support can be efficiently performed with HATU and HOAt. The entire procedure and coupling with HATU/HOAt on the N^{α}-methyl peptides did not cause any detectable racemization of the peptide stereocenters. The optimized procedure is compatible with Fmoc-SPPS conditions and allows a rapid and efficient synthesis of N-methyl peptide analogues on solid support.

3. N-methylated cyclic pentaalanine peptides

3.1 Introduction

The great diversity of biological roles played by peptides and proteins is correlated with the immense number of possibilities that exist for their primary sequences and three-dimensional structure. Hence, knowledge of the 'active conformation' of a given polypeptide is a major step towards understanding its biological function. Although a large number of biophysical techniques exist to study polypeptide conformation, a major obstacle in their study is their inherent intrinsic flexibility. In majority of the polypeptides, this 'active sequence' comprises of a sequence of few amino acids and structural modification in this region leads to drastic changes in the biological activity of the polypeptide.[66] Thus, if enough efforts are carried out in rigidifying the conformation of the active sequence, it would result in the desired activity and selectivity of the target in concern. This is achieved by reducing the conformational flexibility in peptides and proteins by introducing constraints. Nature uses several such constraints to reduce the flexibility of polypeptide chains, including the incorporation of prolines and formation of macrocycles through disulfide bonds. In these ways, particular conformations of peptides and proteins are stabilized by reducing the entropy cost upon folding into such conformations.

The most general way to introduce global constraint into a peptide chain and to affect drastically its overall conformation is the formation of a covalent bond between distant parts of the active sequence is cyclization.[9] In addition to increased rigidity, cyclization can also induce preferred conformation. Cyclizations are performed by forming a link between the two backbone termini, between two side chains, or between one of the side chains and a terminus. In addition to cyclization, N-methylation introduces additional constraint into the cyclic peptide backbone. N-methylation has been used over the years in pharmaceuticals and by various academic groups to introduce additional constraint into the peptide backbone and modulate the peptide activity.[45] However, a detailed understanding of the conformational modulation by N-methylation (mono- to multiple-) in cyclic peptides was lacking, thus we set out to investigate the conformational impact by multiple N-methylation on cyclic peptide backbone.

3.2 Template structures for spatial screening

For rational design and spatial screening of distinct bioactive conformations, it is desirable to explore cyclic peptides which (i) are small enough to exhibit conformational rigidity or at

least adopt a preferred conformation, and (ii) simultaneously allow the introduction of sufficient functionality (pharmacophores) to achieve the desired biological activity.

Conformational restriction seems to be an important prerequisite for oral availability. Cyclic pentapeptides (which are the smallest peptides having strain-free all-*trans*-peptide bonds) or cyclic hexapeptides are well suited for this purpose.[67] Cyclic peptide conformation of smaller ring size is mainly dictated by the array of chirality (D- or L-) of the amino acids in the peptide sequence. Hence, peptides which consist of only alanine with a fixed pattern of chirality can be used as template structures for designing bioactive peptides when replaced with appropriate side chains containing amino acids (pharmacophores); barring glycine and proline. N-methylation introduces another dimension to this 'spatial screening'[68,69] (Figure 3.1) owing to its remarkable property of conformational modulation. N-methylation facilitates the occurrence of a *cis*-peptide bond owing to thermodynamical reasons and blocks the potential hydrogen bonds which results in a long-range impact especially on the backbone conformation of the cyclic peptides.[40,41,70,71] Thus, a library of differentially 31 N-methylated cyclic pentaalanine peptides was designed to study in detail the conformational impact of N-methylation on the cyclic peptide backbone.

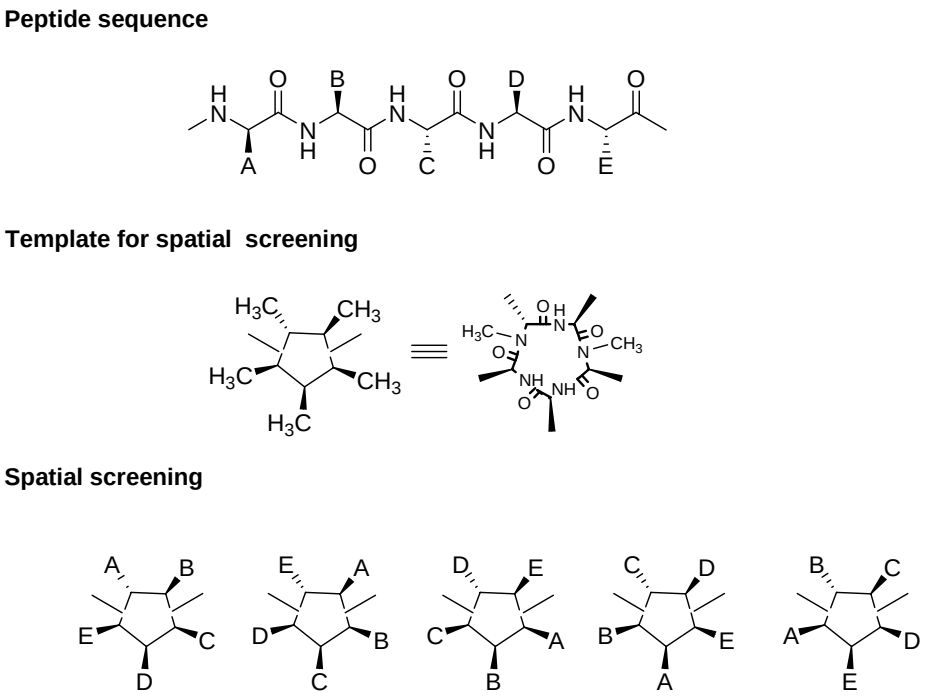

Figure 3.1. *A peptide with pharmacophoric groups A, B, C, D and E can be screened for the spatial orientation in the bioactive conformation, by synthesis of the five position shifted cyclic isomers. In the absence of N-methylation, the five isomers would have identical constitution but present pharmacophores differently. In this example, however, the five di-N-methylated analogs with shifted N-methylated peptide bonds are constitutional isomers.*

3.3 Synthesis of the N-methylated cyclic pentaalanine library

N-Methyl alanine was synthesized as described by Freidinger et al.[49] All linear peptides were synthesized using standard Fmoc solid-phase strategy using the o-chlorotrityl chloride resin.[72,73] Non-methylated or N-methylated alanine was taken as the C-terminal amino acid. However, the yields were lower in the case of a C-terminal N-methylated alanine because of the endopeptolysis by diketopiperazine formation,[63,74] which occurs when N-methylated amino acids or proline are in position one from the resin. One other unusual observation was the cleavage of the sequence Ala^2-D/L-$MeAla^1$, when a D/L-MeAla was tried to couple with it. This observation is entirely sequence specific and is not encountered with any other sequence as explained in Scheme 3.1.

Scheme 3.1. *The scheme shows the encountered problem occurred during the synthesis of the linear tripeptides.*

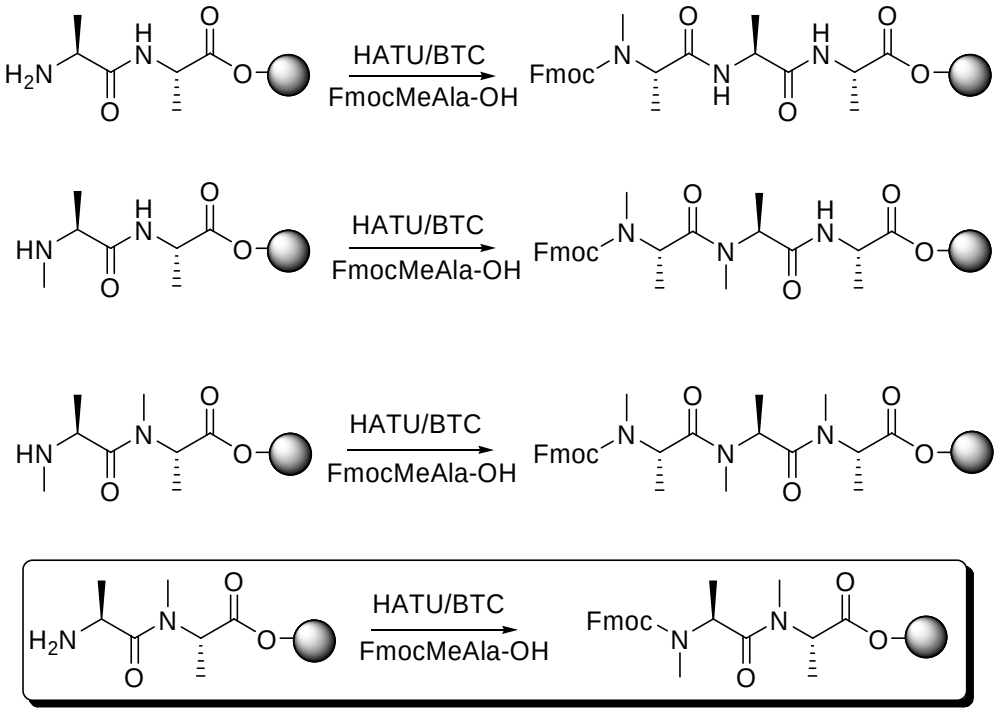

Fmoc deprotection was achieved with 20 vol % piperidine in NMP, and the other amino acids (2 equiv each) were sequentially coupled with 2 equiv of 2-(1H-benzotriazol-1-yl)-1,1,3,3-tetramethyluronium tetrafluoroborate (TBTU) and 1-hydroxybenzotriazole (HOBt) in 1-methyl-2-pyrrolidinone (NMP) as solvent.[75] N,N-Diisopropylethylamine (DIEA) was used to adjust the pH to 8. However, in the case of coupling to a N-methylated residue, 2 equiv each of N-methyl alanine or alanine, N-[(dimethylamino)-1H-1,2,3-triazolo[4,5-b]pyridine-1-yl-methylene]-N-methylmethanaminium hexafluorophosphate (HATU),[76,77] and 1-hydroxy-7-azabenzotriazole (HOAt)[78] were used along with DIEA to maintain a pH of 8 in NMP as solvent. Due to HOBt/HOAt and HBF_4 formation, the pH drops while the reaction proceeds,

leading to reduced nucleophilicity of the amino group. Therefore, in the case of insufficient couplings as monitored with the Kaiser test,[79] additional base was added, but the pH was not allowed to exceed a value of 8.5. The coupling time ranged from 20 to 45 min. The o-chlorotrityl linker allows cleaving off the linear peptide with a mild treatment of an acetic acid/2,2,2-trifluoroethanol (TFE) mixture in dichloromethane (DCM) without affecting the peptide bonds. The head-to-tail cyclization was performed with diphenylphosphorylacid azide (DPPA),[80,81] applying the solid base method using $NaHCO_3$ in N,N-dimethylformamide (DMF) under high dilution conditions (0.1-0.3 mM).[82] After the completion of cyclization, which was monitored by ESI mass spectroscopy, DMF was evaporated and the crude peptide was re-dissolved in a minimum amount of dry acetonitrile, leaving behind the cyclization reagents. The pure compound was obtained by reversed-phase high performance liquid chromatography (RP-HPLC) purification. The peptides were characterized by ESI mass spectroscopy and various NMR techniques.

A combinatorial method was adapted for the synthesis of the cyclic N-methylated analogs, a representative synthesis is shown in Scheme 3.2, where a small "a" stands for D-Ala and "A" stands for L-Ala; The underlined letters 'a' or 'A' indicate N-methylation. After each coupling, the resin was divided into two halves, one for the coupling with non-methylated and the other for the coupling with methylated alanine. We obtained all the analogs except the penta N-methylated analog, which failed to cyclize.

Scheme 3.2. *Schematic approach showing the combinatorial approach adapted to obtain the library of cyclic peptides starting with L-alanine (A) loaded to the resin. The underlined residues denote the N-methylated ones.*

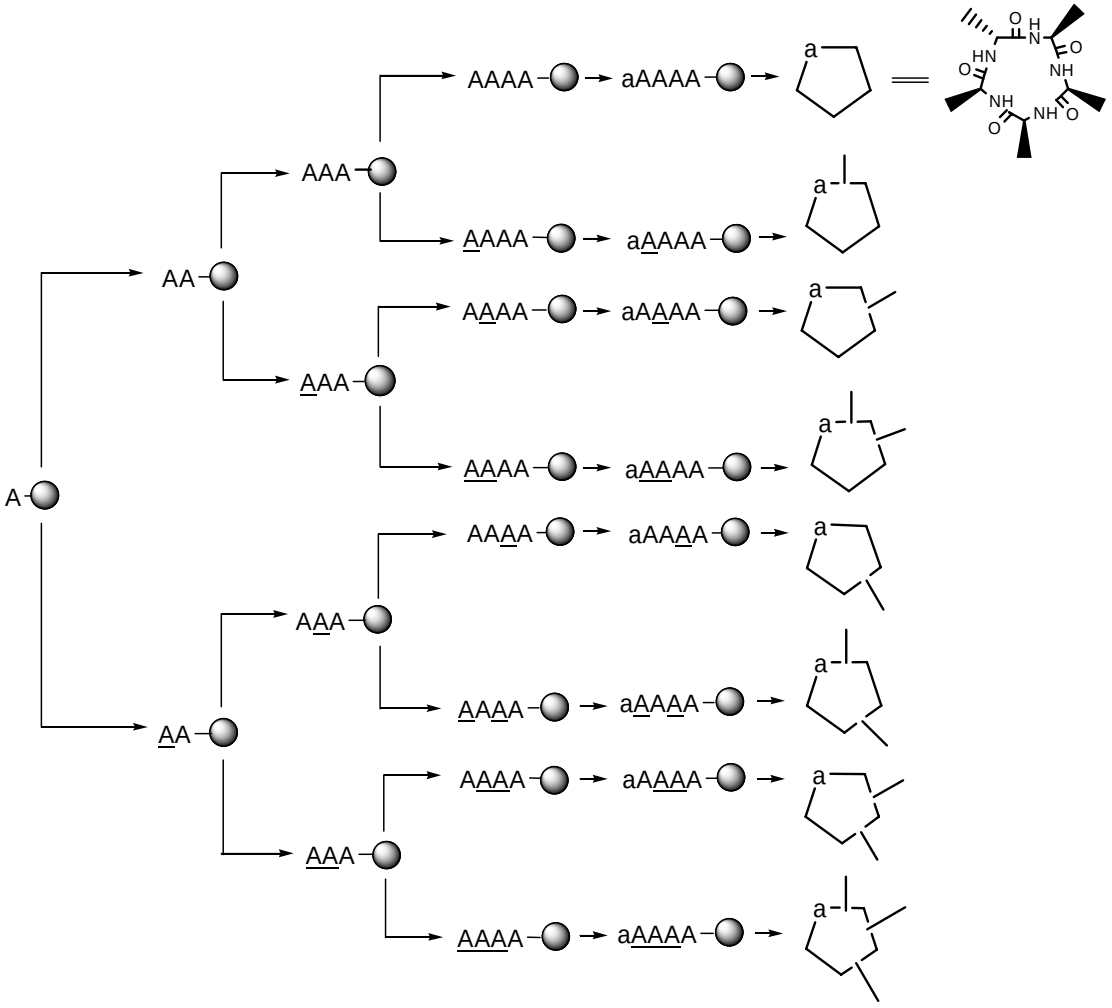

3.4 NMR assignment

Sequential assignment was accomplished by through-bond connectivities from heteronuclear multiple bond correlation (HMBC) spectrum.[83] The N-methyl group was taken as the reference for the sequential assignment, the protons of which show a correlation with the ^{13}C atom of the intra-residual α-protons by a four-bond coupling in the HMBC spectrum. The α-protons further show a correlation with the ^{13}C shift of intra-residual carbonyl by a three-bond coupling, and this carbonyl also correlates with the H^{α} shift of the same residue and the H^{N} shift of the adjacent residue (if not N-methylated) by a strong two-bond coupling. In this way the full sequence assignment was accomplished (described explicitly by the figures below). Temperature coefficients for the amide protons of each peptide were determined from one-dimensional spectra in the range from 297 to 327 K with a step size of 5 K. Many of these N-methylated analogs show more than one conformation in slow exchange on the NMR time scale of chemical shift separation at room temperature. Chemical exchange was confirmed by

exchange peaks in ROESY spectra (Figure 3.5), which show an inverted sign compared to signals caused by ROEs.[84]

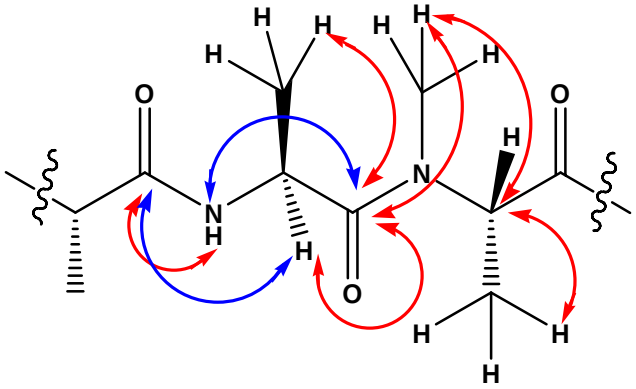

Figure 3.2. *The long range heteronuclear couplings obtained from the HMBC spectrum employed for sequential assignment are shown. The correlation shown by red arrows are obtained as strong cross peaks and the ones in blue are obtained as weak cross peaks in the HMBC spectrum.*

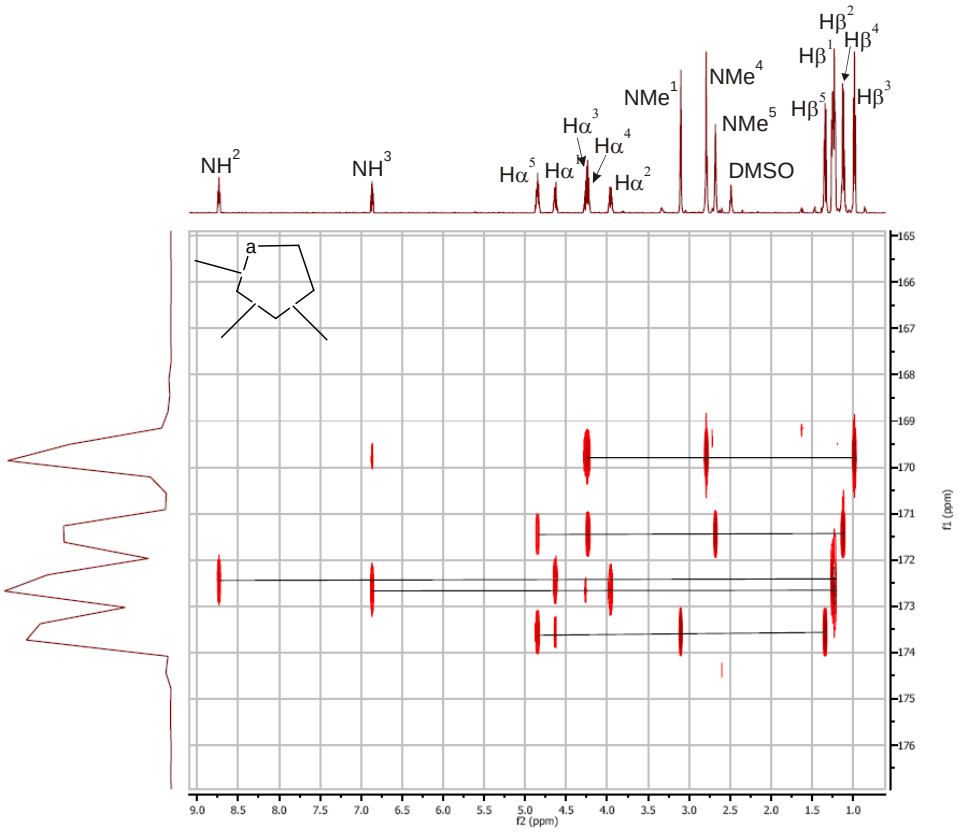

Figure 3.3. *Slice of HMBC spectrum showing the correlations between $NH^{(i)}$-$H^{\alpha(i-1)}$, $NH^{(i)}$-$H^{\beta(i-1)}$, and $H^{\alpha(i)}$-$H^{\beta(i)}$: via the $H^{\alpha(i)}$-$CO^{(i)}$, $H^{\alpha(i)}$-$CO^{(i-1)}$, and $H^{\beta(i)}$-$CO^{(i)}$ cross peaks. Inset is the schematic diagram of the compound, whose assignments are denoted.*

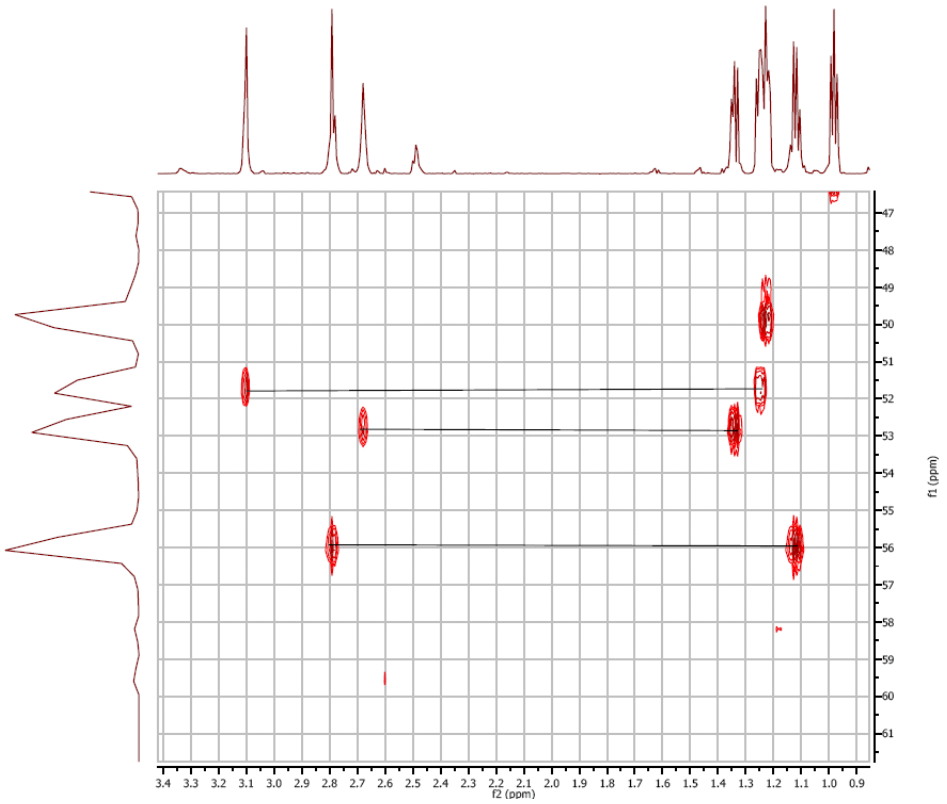

Figure 3.4. *Slice of HMBC showing the correlation between* $NMe^{(i)}$-$H^{\beta(i)}$*: via the* $NMe^{(i)}$-$C^{\alpha(i)}$*, and* $H^{\beta(i)}$-$C^{\alpha(i)}$ *cross peaks.*

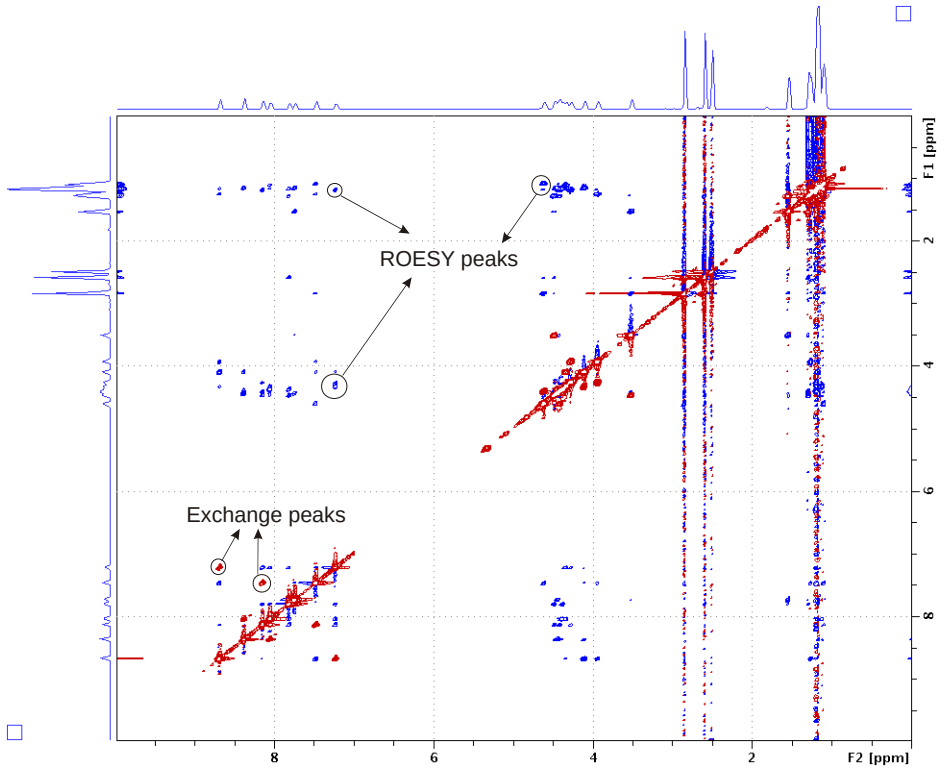

Figure 3.5. *A ROESY spectrum, showing the ROE cross peaks and the exchange peaks having opposite sign.*

3.5 Structure calculation

Proton distances were calculated according to the isolated two-spin approximation from volume integrals of rotating frame nuclear Overhauser enhancement (ROESY) spectrum.[85,86] The integrated volumes of the ROE cross-peaks were offset corrected[87] and converted to proton-proton distances employing the cross-peak intensity of Hβ-Hα of alanine as reference (2.19 Å). Restraints were obtained by adding and subtracting 10% to the calculated experimental distances, accounting for errors from the two-spin approximation and cross-peak integration. Metric matrix DG calculations were carried out with a home-written program utilizing random metrization.[88] Experimental distance constraints which were more restrictive than the geometric distance bounds (holonomic restraints) were used to create the final distance matrix. The structures were first embedded in four dimensions and then partially minimized using conjugate gradients followed by distance and angle driven dynamics (DADD),[89,90] wherein only distance constraints were used. The DADD simulation was carried out at 1000 K for 50 ps with a gradual reduction in temperature over the next 30 ps. The DADD procedure utilized holonomic and experimental distance constraints plus a chiral penalty function for the generation of the violation "energy" and forces. A distance matrix was calculated from each structure, and the EMBED algorithm was used to calculate coordinates in three dimensions. About 95-100 structures were calculated for each peptide, and >90% of the structures of every peptide did not show any significant violation. The MD calculations were carried out with the program DISCOVER using the CVFF force field.[91] The structure resulting from the DG calculation was placed in a cubic box of length 25 Å and soaked with DMSO, and a restrained MD simulation was carried out. After energy minimization using the steepest descent and conjugate gradient, the system was heated gradually, starting from 10 K and increasing to 50, 100, 150, 200, 250, and 300 K in 2 ps steps, each by direct scaling of velocities. The system was equilibrated for 50 ps with temperature bath coupling (300 K). Configurations were saved every 100 fs for another 150 ps. Finally a 150 ps free MD simulation at 300 K was carried out to prove that the stability of the calculated conformation in the solvent is similar to the structure obtained from experimental restraints.

3.6 General observation

All the N-methylated analogs were synthesized except the permethylated derivative. The NMR-based analysis of the thirty compounds displayed various populations of major and minor conformers slowly interconverting on the NMR time scale (representative ^{1}H spectrum of conformationally homogeneous and inhomogeneous ones are shown in Figure 3.6 and 3.7).

For use as templates in rational drug design we are mainly interested in those peptides which prefer a single conformation of greater than 80% abundance on the NMR time scale.

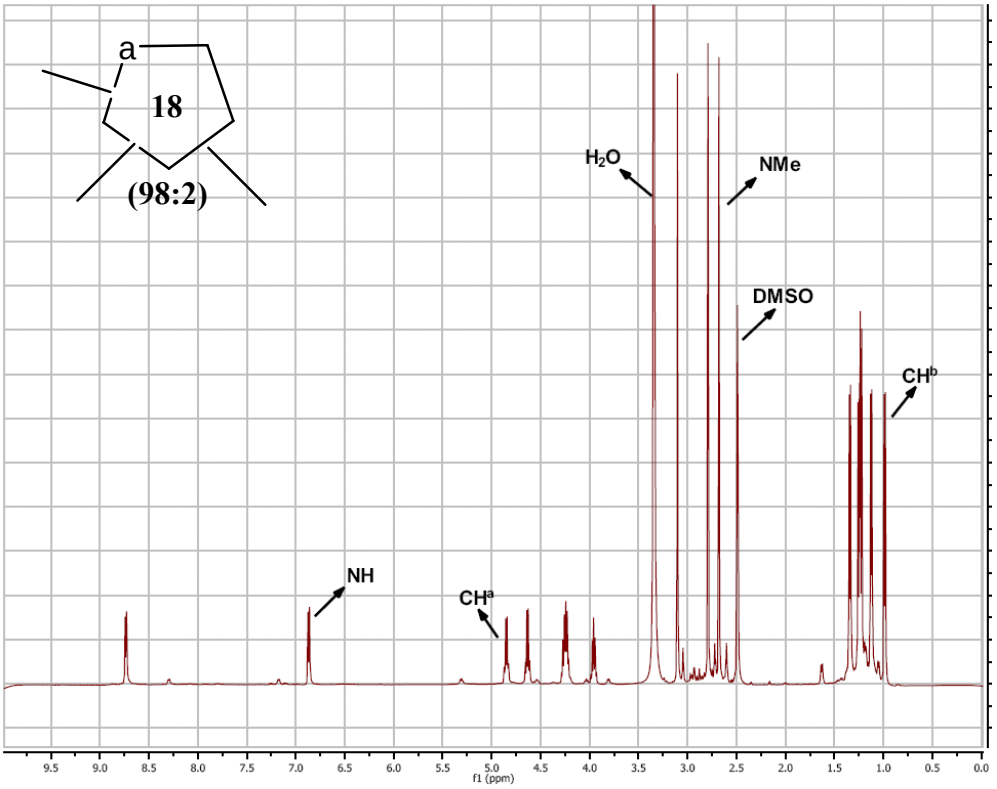

Figure 3.6. *A representative ^{1}H spectrum of a conformationally homogeneous N-methylated analog. The typical -CH_3, -NMe, -CH^{α}, and H^{N} regions in the spectrum of the N-methylated alanine cyclic peptide are marked.*

As a first pass, we examined the seven conformationally homogeneous (>98%) cyclic peptides.[92] Then we turned to the conformationally preferred ones, that have a major conformation of between 80-98% on the NMR time scale.[93] It is essential to note that in these small cyclic peptides, the conformation is strongly dependent on steric interactions rather than on internal hydrogen bonds, which was well documented over a quarter of a century ago.[94] This is in contrast to standard discussions on cyclic peptide conformations which often are claimed to be "stabilized" by intramolecular hydrogen bonds. In our N-methylated cyclic pentapeptides we rarely observe "classical" β or γ turns. It is well known that inter- or intra-molecular hydrogen bonds shift the amide proton NMR signal downfield. In DMSO, NH protons exposed to the solvent exhibit a distinct downfield shift by binding to the strongly basic sulfoxide group of the solvent. Intra-molecularly oriented NH groups even when involved in hydrogen bridges to amide carbonyls are shifted up-field and show small temperature gradients. Temperature gradients of protons which bind solvent molecules are large, indicating entropy driven hydrogen bond breaking at higher temperatures.[9]

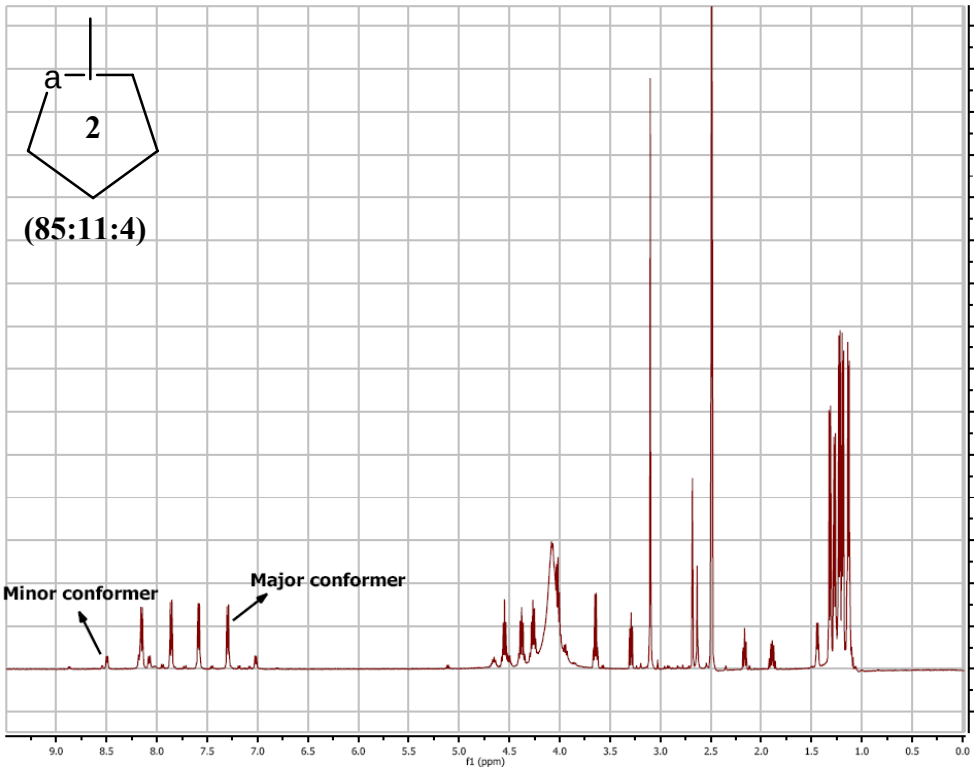

Figure 3.7. *A representative ^{1}H spectrum of a conformationally in-homogeneous analog.*

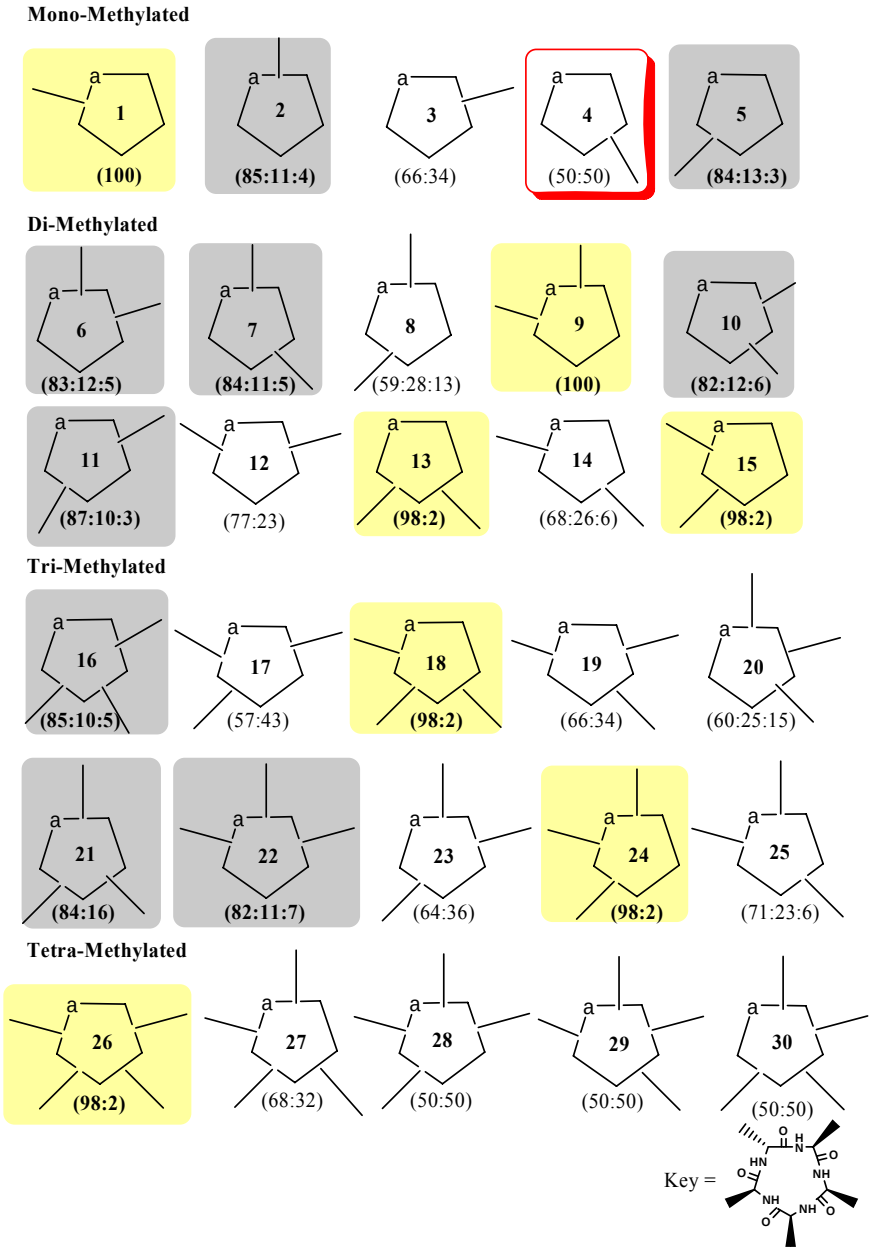

Figure 3.8. *Library of all the synthesized N-methylated peptides with their conformational abundance on the NMR time scale of chemical shift separation. The values in parentheses denote the ratio of all the conformers calculated from ^{1}H spectrum.*

Out of the mono N-methylated peptides, which do not prefer a single conformation, one analog **4** was found to exist in equilibrium between two equally populated conformers (Figure 3.9). This is due to *cis/trans*- conformational equilibrium which is slow at the NMR time scale. The conformational equilibrium of this analog is very sensitive to any change in the structure, especially towards the introduction of any branched residues, and is thus being further investigated by Laufer et al.[95]

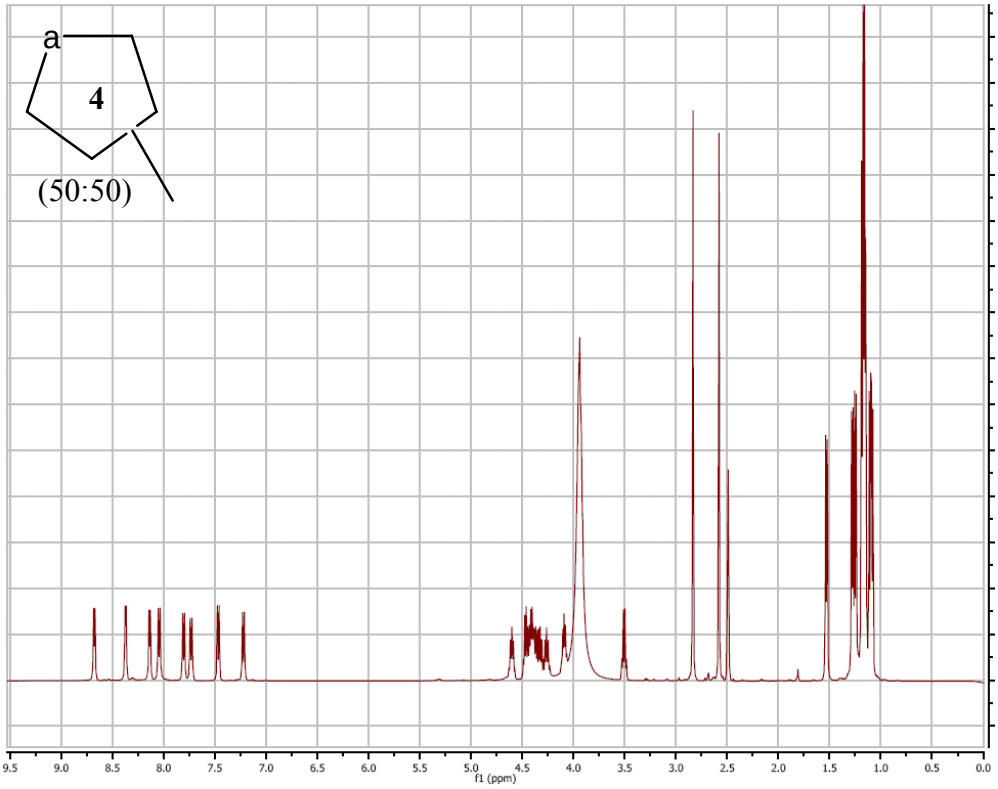

Figure 3.9. *The ^{1}H spectrum of* ***4****, showing the equally populated conformers at the NMR time scale.*

3.7 Conformational analyses

3.7.1 Conformationally homogeneous peptides

cyclo(-D-MeAla^{1}-Ala^{2}-Ala^{3}-Ala^{4}-Ala^{5}) (1). The ROESY spectrum of the compound did not show the presence of a single Hα(*i*)-Hα(*i* + 1) cross-peak,[96] so all the peptide bonds have to be in a *trans*- conformation. This peptide is the simple N-methylated analogue of the parent peptide cyclo(-aA$_4$-), which prefers a βII' on one side with D-Ala^{1} at the *i* + 1 position of the βII' turn and an equilibrium of a closed or open γ type conformation about Ala^{4}.[97,98] The spectrum reveals strong crosspeaks between the Ala^{2}H^{N}-D-Ala^{1}H^{α} and Ala^{2}H^{N}-Ala^{3}H^{N}. The conformation of **1** (Figure 3.10) in a way resembles that of the parent peptide cyclo(-aA$_4$-) without the N-methyl group. In cyclo(-aA$_4$-) a βII' turn about a^{1}A^{2} is the most characteristic feature; in this βII' turn both HN's of Ala^{3} and Ala^{2} are directed above the ring plane and have a short distance. The carbonyl group of Ala^{5} forms a bifurcated hydrogen bond to both NH protons of Ala^{2} and Ala^{3}. In **1** the peptide bond between Ala^{5} and D-Ala^{1} is turned by about -60°, resulting in the "disruption" of the hydrogen bond to Ala^{3} HN. The conformational change obviously is a consequence of the steric hindrance of the N-methyl group with the β-protons of Ala^{5} and D-Ala^{1}. It is well accepted that internal hydrogen

bonding in cyclic peptides does not lead to strong energetic stabilization, and instead stereoelectronic and steric effects are more important in determining the conformation of cyclic peptides.[94] In addition to the steric effect of methyl groups, the carbonyl group of Ala^5 is now ideally syn-oriented to the $C^{\alpha}H$ bond of D-Ala^1 (see below in the discussion).

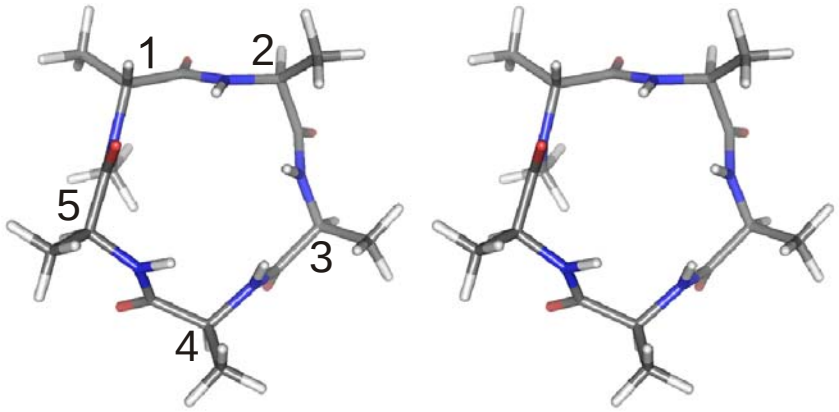

Figure 3.10. *Stereo picture of* ***1****, resulting from energy minimization of 200 steps of steepest descent of the average structure after 150 ps of restrained and free MD simulation in DMSO solvent box.*

The conformation about residues Ala^3-Ala^5 is similar to that in cyclo(-aA_4-); however, it may also form a rapid equilibrium between a γ turn and the conformation in which both the NH bonds point in the same direction as in the case of cyclo(-pA_4-).[97,98] We also observe in **1** ROEs between the NH protons; however, due to a relatively low number of data we cannot exclude the participation of a γ turn conformation in rapid equilibrium with the conformation shown in Figure 3.10. The coupling constants (Table 3.1) are in good agreement with the proposed conformation, and the Φ angles of Ala^3 and Ala^5 are close to -120° and that of Ala^2 close to -100° (Table 3.2), leading to an anti-periplanar arrangement of NH to the $C^{\alpha}H$ bond and large coupling constants. An exception is Ala^4, which may be involved partially in a γ turn structure by a twist of the peptide bond Ala^3CO-Ala^4NH, resulting in the changes of Φ and Ψ angles which are in fast equilibrium[99] and therefore exhibiting a smaller H^NH^{α} coupling constant. Only slight deviations between calculated (from the trajectory average) and observed (from the ROESY spectrum) distances are observed, with a single exception; the Ala^4H^N and Ala^4H^{α} distance is too short by about 0.4 Å, again giving evidence for a participation of the γ turn about this residue, similar to the case in the non-N-methylated cyclic pentapeptides.

Table 3.1. *The temperature gradient values of NH protons (-Δδ/ΔT) in ppb/K; the values in parenthesis are the respective $^3J(H^N\text{-}H^\alpha)$ coupling constants in Hz.*

Compound	D-Ala[1]	Ala[2]	Ala[3]	Ala[4]	Ala[5]
1	-	2.5 (9.1)	2.7 (8.1)	3.4 (6.9)	2.3 (8.3)
9	-	-	3.7 (7.4)	0.6 (7.3)	5.5 (8.2)
13	5.5 (6.2)	5.8 (6.7)	2.3 (7.6)	-	-
15	-	1.5 (9.4)	2.3 (6.2)	1.1 (7.9)	-
18	-	6.0 (6.9)	0.4 (7.5)	-	-
24	-	-	4.7 (5.7)	-1.3 (7.8)	-
26		5.1 (9.4)	-	-	-

cyclo(-D-MeAla[1]-MeAla[2]-Ala[3]-Ala[4]-Ala[5]) (9). This compound can be obtained by a further substitution of the HN of Ala[2] with an N-methyl group with respect to compound **1**. Sterically it is indeed possible; however, some steric hindrance with the β-protons of Ala[2] and HN of Ala[3] leads to further deviation from the βII' turn which is present in the non-methylated stem peptide cyclo(-aA$_4$-). The structure exhibits all carbonyl groups syn oriented to the C$^\alpha$H bond of the following residue (Figure 3.11). As this is an energetically preferred orientation, **9** exhibits only a single conformation on the NMR time scale of chemical shift separation.

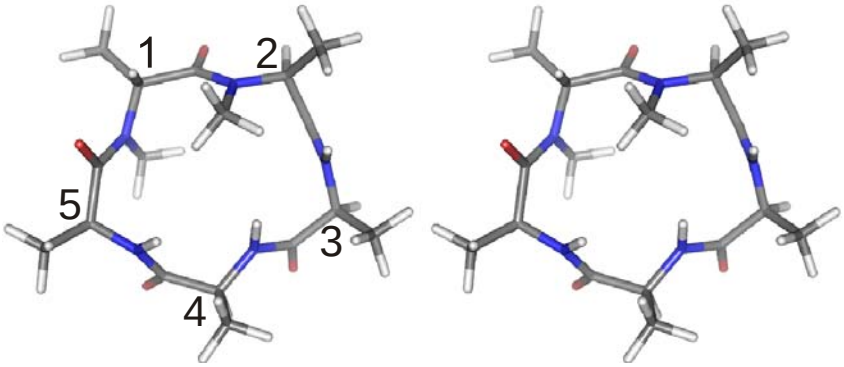

Figure 3.11. *Stereo picture of **9**.*

cyclo(-D-MeAla[1]-Ala[2]-Ala[3]-Ala[4]-MeAla[5]) (15). The structure of **15** (Figure 3.12) can be created by shifting the N-methyl groups from residue Ala[2] in **9** to Ala[5]. The steric interference of the N-methyl group with β-protons of Ala[5], results in the rotation of the peptide bond plane by about 170° in comparison to the Ala[4]-Ala[5] peptide bond plane in **9**. The rest of the molecule is almost identical to the fragment in **9**.

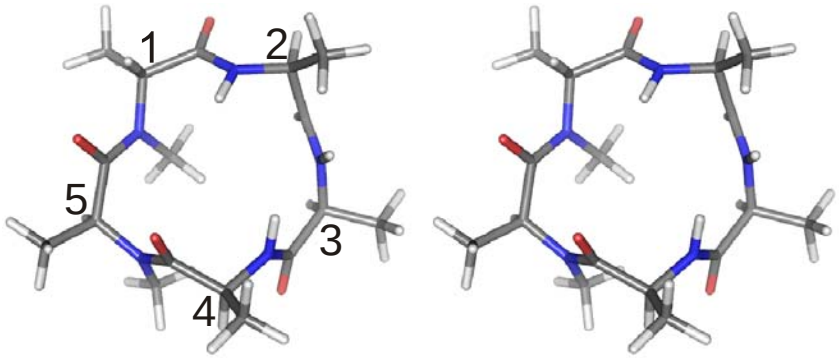

Figure 3.12. *Stereo picture of **15**.*

cyclo(-D-MeAla^1-MeAla^2-Ala^3-Ala^4-MeAla^5) (24). Compound **24** (Figure 3.13) results from the N-methylation of residue Ala^5 of **9** or the residue Ala^2 of **15**. This compound shows structural similarity with both **9** and **15**. The structure of the fragment from Ala^3 to D-Ala^1 is almost identical with the same fragment in **15**, and the one from Ala^5 to Ala^4 is identical to that of **9**.

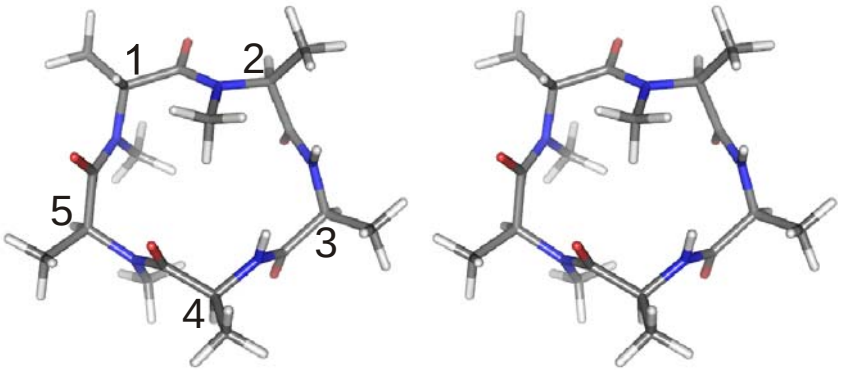

Figure 3.13. *Stereo picture of* ***24****.*

cyclo(-D-MeAla^1-Ala^2-Ala^3-MeAla^4-MeAla^5) (18). This compound results from the shifting of the N-methyl group of residue Ala^2 in **24** to residue Ala^4. The N-methylation of residue Ala^4 results in the complete rotation of the peptide bond plane between Ala^3 and Ala^4 by 170° in comparison to the previously described structures. This is because of the strong steric clash between the N-methyl of Ala^4 and β-protons of Ala^4 and Ala^3 (Figure 3.14). In addition **18** shows a *cis*-peptide bond between the residues Ala^4 and Ala^5, which might result from the steric clash between the N-methyl groups of Ala^4 and Ala^5, as the N-methyl of Ala^5 would project below the plane, if the Ala^4-Ala^5 peptide bond were *trans*-. The fragment of **18** from D-Ala^{1}H$^\alpha$ to Ala^{3}H^N resembles a βII' turn; however, the Ala^5-D-Ala^1 peptide bond has also undergone a flip of 80° in comparison to Ala^5-D-Ala^1 in **24**. This twist in the peptide bond is caused by steric interaction, which the N-methyl group would encounter with the β-protons of Ala^5, as it has been forced to project down the plane by the *cis*-peptide bond.

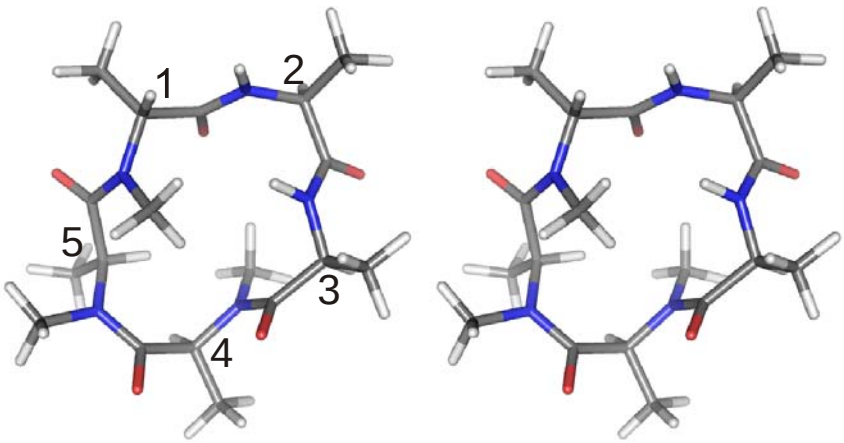

Figure 3.14. *Stereo picture of* ***18****.*

cyclo(-D-MeAla^1-Ala^2-MeAla^3-MeAla^4-MeAla^5) (26). Compound **26** can be obtained by further N-methylation of the Ala^3 residue of **18**. To our surprise this compound exhibited two *cis*-peptide bonds, one about Ala^2-Ala^3 and the other about Ala^4-Ala^5 (Figure 3.15). This is the only compound, which has an N-methylation at residue Ala^3, which results in the formation of an Ala^2-Ala^3 *cis*-peptide bond to accommodate the bulky methyl group. The compound shows a structural similarity with **18**, in the region from Ala^4 to D-Ala^1; however, it is interesting to note the orientations of the N-methyl groups of D-Ala^1 and Ala^4 with respect to their orientation in **18**. Both the Ala^3-Ala^4 and Ala^5-D-Ala^1 peptide bonds have undergone a flip of about 160° about their adjacent Φ and Ψ angles, and thus the N-methyl groups always tend to project in opposite directions of the plane to minimize their mutual steric interaction. The driving force to orient the Ala^4 N-methyl group above the plane is the Ala^2-Ala^3 *cis*-peptide bond which forces the β-protons of Ala^3 to project down the plane, which eventually reorients the N-methyl group projecting it above the plane.

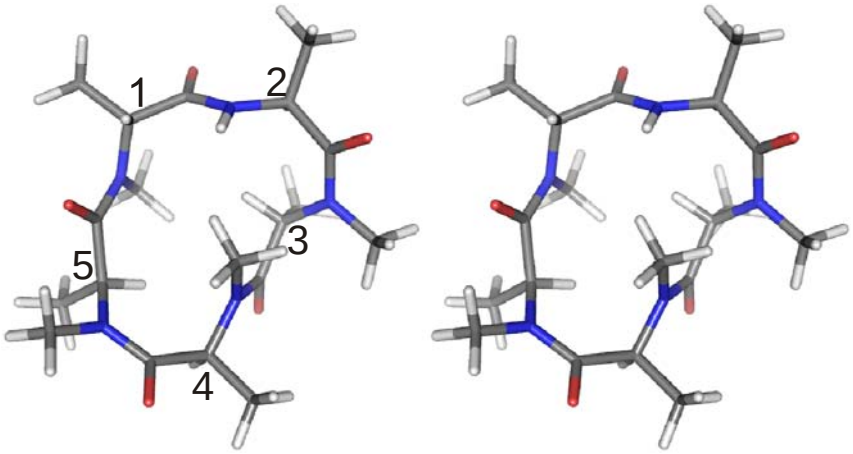

Figure 3.15. *Stereo picture of* ***26****.*

cyclo(-D-Ala^1-Ala^2-Ala^3-MeAla^4-MeAla^5) (13). This is the only compound (Figure 3.16) in the homogeneous series in which the D-Ala^1 is not N-methylated. The compound resembles **18**, in the region from Ala^2 to Ala^5 revealing the tendency of the peptides to form a *cis*-peptide bond when the N-methylation is at Ala^4 and Ala^5. The upper part of the molecule resembles a βII' turn with the D-Ala^1 at the i + 1 position of the turn, as in the case of cyclo(-aA$_4$-); however the Ψ of Ala^2 (Table 3.2), i.e., of the (i + 2) residue, deviates more than that of the (i + 1) residue from the standard angle of -120° and 0° for the (i +1) and (i + 2) residue.[66,100,101]

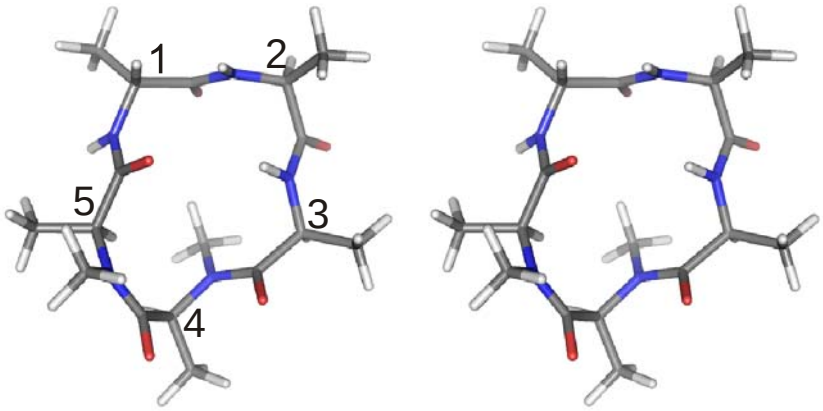

Figure 3.16. *Stereo picture of* ***13****.*

Table 3.2*. Φ and Ψ values of conformationally homogeneous peptides.*

#	Ala[1]		Ala[2]		Ala[3]		Ala[4]		Ala[5]	
	Φ	Ψ	Φ	Ψ	Φ	Ψ	Φ	Ψ	Φ	Ψ
1	117.53	-62.8	-82.89	-63.75	-131.35	-56.55	-73.57	-56.13	-133.72	83.07
9	129.15	-76.25	-97.86	-76.29	-77.53	-44.16	-120.1	-67.34	-117.55	77.32
13	84.7	-108.8	-66.6	-42.9	-144.3	78	56.3	66.9	-109.9	173.9
15	138.02	-56.34	-88.79	-87.56	-119.18	-16.03	-105.4	88.41	53.02	63.54
18	-89.12	-116.42	-65.81	-25.38	-126.34	-69.69	59.54	78.23	-124.69	62.38
24	126.26	-69.14	-105.75	-83.69	-81.68	-53.34	-108.64	102.86	57.92	70.38
26	134.82	-84.22	-142.16	78.42	-130.69	57.98	-142.45	56.28	-117.31	146.32

3.7.2 Conformationally in-homogeneous peptides

cyclo(-D-Ala[1]-MeAla[2]-Ala[3]-Ala[4]-Ala[5]-) (2). This compound is N-methylated at Ala[2] and contains a *cis*-peptide bond in the minor conformation. The analysis of the major conformation exhibits no defined classical turn structure (Figure 3.17). The strong preference of a βII' turn around the D-Ala[1]-MeAla[2] bond obviously is overcome by the N-methylation. The N-methyl group is pointing slightly inside the ring. It is remarkable that all Φ angles are adjusted to fulfill the syn orientation of the CH^{α} bond and the carbonyl bond of the preceding amino acid. Obviously this orientation is so strongly preferred energetically, that other conformations cannot compete, and the amount of the minor populated conformations is only 15%. Compound **2** exhibit a structure where three adjacent NH groups point to the same side of the molecule (upwards). Such a structure nicely exhibits that the formation of intramolecular hydrogen bonds are not essential for a preferred backbone conformation in cyclic peptides. The experimental $^{3}J(H^{N},H^{\alpha})$ coupling constant of D-Ala[1] is 6.2 Hz (Table 3.3), however, the dihedral angle calculated by averaging the dihedral angle of all the structures in the trajectory (a structure was written to the trajectory every femto-second, resulting in 1500 structures) between D-Ala[1]H^{α} and H^{N} is -14.6° which would have resulted in a coupling constant of 8.2 Hz.[102] As the peptide does not show any major violation of the ROE values (all ROEs are fulfilled within 0.1 Å) we assume that the coupling constant indicates a flip of peptide bond plane (Ala[5]-D-Ala[1]) about the adjacent Φ and Ψ. The

substitution pattern corresponds to the structure of Cilengitide [cyclo(-RGDfNMeV-)],[38] with one distinct difference: Ala^4 of **2** is substituted by a glycine in Cilengitide, which allows more flexibility for the RGD peptide. In general, both the peptides exhibit similar structures confirming our premise that the conformation of small cyclic peptides in the first approximation is determined by the sequence of the chiralities of the amino acid sequence. However, it should be kept in mind that the functional group of the amino acid side chains may affect the backbone conformation mainly with respect to the conformational homogeneity on the NMR time scale, though the backbone conformation is expected to show the same pattern of *cis*- and *trans*-peptide with similar Φ and Ψ compared with the model alanine peptides described herein.

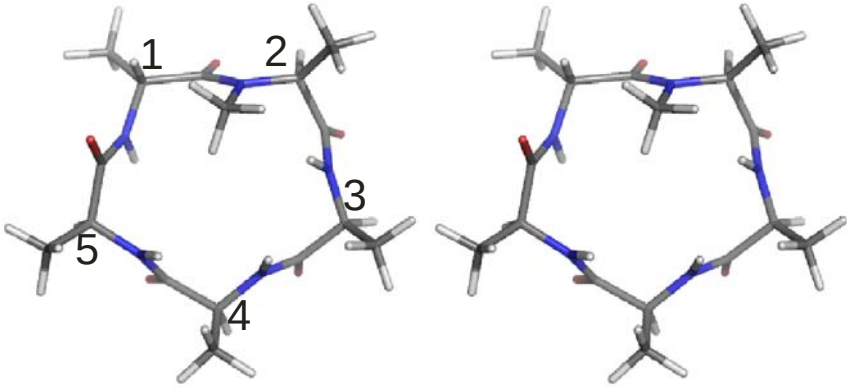

Figure 3.17. *Stereo picture of* ***2****.*

Table 3.3*. The temperature gradient values of NH protons (-Δδ/ΔT) in ppb/K; the values in parenthesis are the respective* $^3J(H^N\text{-}H^\alpha)$ *coupling constants in Hz.*

Compound	Ala^1	Ala^2	Ala^3	Ala^4	Ala^5
2	5.4(6.2)	-	2.6(7.2)	3.0(6.8)	2.0(8.4)
5	5.6(8.4)	1.3(8.2)	3.6(7.6)	1.7(7.0)	-
6	7.5(9.0)	-	-	5.1(8.2)	3.6(7.7)
7	4.3(9.0)	-	4.5(8.3)	-	4.0(8.4)
10	6.0(6.8)	0.6(8.5)	-	-	4.0(7.5)
11	3.7(8.1)	2.4(7.5)	-	4.5(8.0)	-
16	4.0(8.7)	6.0(9.8)	-	-	-
21	4.5(5.8)	-	2.0(7.4)	-	-
22	-	-	-	3.7(9.2)	1.5(9.3)

cyclo(-D-Ala^1-Ala^2-Ala^3-Ala^4-$MeAla^5$-) (5): The compound obtained by N-methylation of the parent cyclo(-aA_4-) at Ala^5 (Figure 3.18), contains only *trans*-peptide bonds. There are no major violations of the ROE values in the structure. The strong ROEs between Ala^5NMe-Ala^5H^α, Ala^5NMe-Ala^4H^α, and Ala^5NMe-D-Ala^1H^N define the spatial arrangement of the N-methyl group, which is pointing down from the plane of the peptide cycle. Most of the Φ angles are close to the preferred -120° except in position 5 (Table 3.4), where the N-methyl group avoids steric clash with the two side chain methyl groups of Ala^4 and Ala^5.

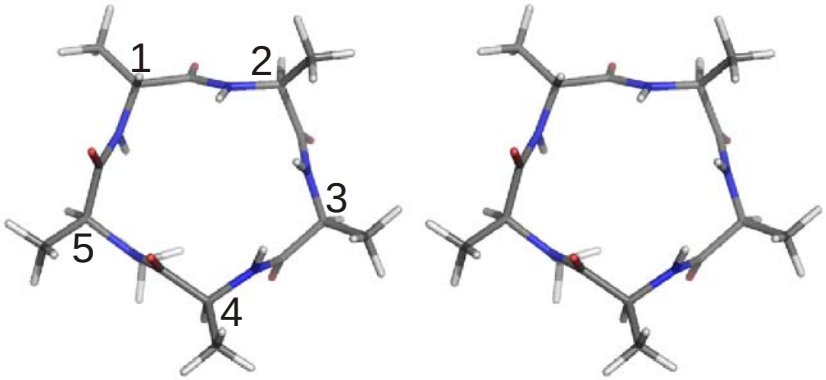

Figure 3.18. *Stereo picture of* ***5****.*

cyclo(-D-Ala^1-MeAla^2-MeAla^3-Ala^4-Ala^5-) (6): The NMR spectrum of the preferred conformation shows a strong ROE between Ala^{2}H$^\alpha$ and Ala^{3}H$^\alpha$, indicating the presence of an Ala^2-Ala^3 *cis*-peptide bond. The *cis*-peptide bond (Figure 3.19) is caused by the strong steric clash between Ala^{3}NMe and Ala^{2}NMe. Starting with the conformation of **2** and introduction of the NMe group at the Ala^3 residue (see Figure 3.17), forces the Ala^2-Ala^3 peptide bond into the *cis*- orientation. It is reassuring to observe that the structure from Ala^5 to Ala^2 is identical in **2** and **6**. The *cis*-peptide bond maximizes the distance between the methyl groups. Due to the flip of the Ala^4-Ala^5 peptide bond only three H$^\alpha$ out of five are in the preferred orientation being syn-periplanar with the CO of the adjacent residue. On the other hand, the NH of Ala^5 can now form a γ turn by bonding to CO of Ala^3. However, there are several indications that the amide bond Ala^4-Ala^5 flips around as was previously found for the amide bond Ala^3-Ala^4 in c(-pA4-); the temperature gradient (Table 3.3) of -3.6 ppb/K of Ala^{5}HN does not indicate a strong solvent shielding of Ala^{5}HN. The peptide shows strong ROE violation between Ala^{5}H^N-Ala^{4}H^N and Ala^{5}H^N-Ala^{5}H$^\beta$ (0.3 and 0.4 Å, respectively, longer than the experimental values), whereas the strong ROE between Ala^{5}H^N-Ala^{4}H$^\alpha$ is not violated. This is caused by the r^{-6} dependence of the ROE, which emphasize small distances and forces the molecule into the conformation shown in Figure 3.19, whereas the participation of the conformation with the Ala^{5}H^N pointing upwards is not exhibited. The commonly utilized restrained MD does not usually properly present such rapid conformational equilibrium and more sophisticated technologies such as ensemble-based or time-dependent restrained MD methods must be utilized.[103] For our present purposes it is sufficient to be aware of those effects when analyzing peptide conformations.

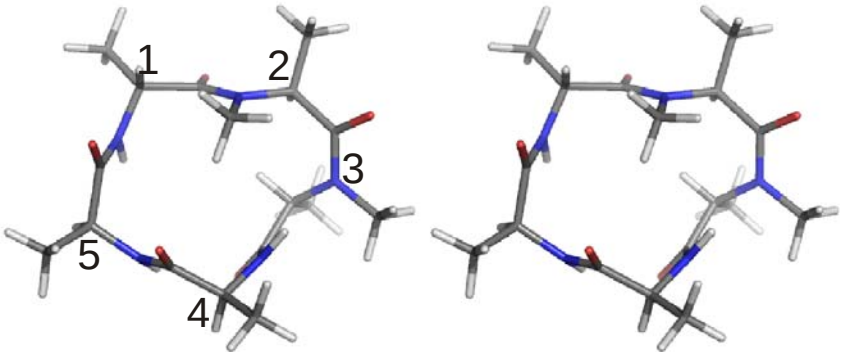

Figure 3.19. *Stereo picture of* ***6****.*

cyclo(-D-Ala^1-MeAla^2-Ala^3-MeAla^4-Ala^5-) (7): This compound differs from **6** by shifting the -NMe group from Ala^3 to Ala^4. A *cis*-peptide bond is now observed between Ala^3 and Ala^4 in the dominant conformation (Figure 3.20). On the other hand the structure in the range from Ala^4 to Ala^2 is almost identical in **6** and **7**. The latter is the only compound containing a *cis*-peptide bond at this position. In contrast to **6** there are no ROE violations. All experimental $^3J(H^N,H^\alpha)$ coupling constants are large indicating syn- or anti-periplanar arrangement of HN and Hα.

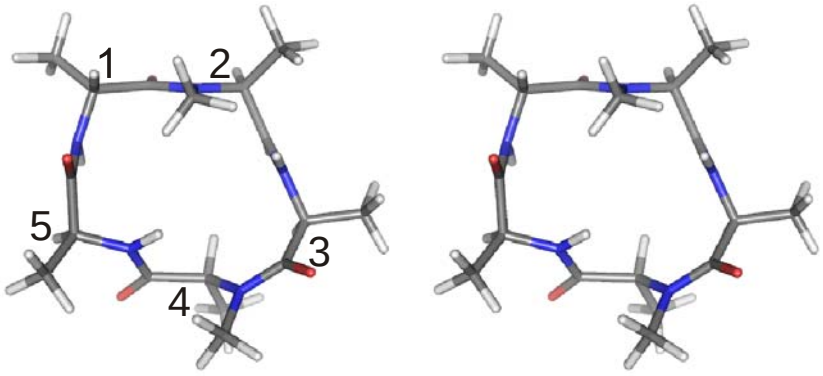

Figure 3.20. *Stereo picture of* ***7****.*

cyclo(-D-Ala^1-Ala^2-MeAla^3-MeAla^4-Ala^5-) (10): The compound is N-methylated at Ala^3 and Ala^4. The NMR spectrum of the major conformation shows the absence of any (i)H$^\alpha$-(i+1)H$^\alpha$ ROE cross peak of the major conformer, indicating that all peptide bonds are *trans*-. This is surprising because all other peptides which contain an NMeAla^3 exhibit a *cis*-peptide bond at this position. The ROEs did not clearly define the spatial orientation of the N-methyl groups. Although the calculation yields a structure with a minor violation, the result is not in agreement with the observation, because we found several missing ROE values which should be present if the calculated structure would be correct. As **10** is not conformationally homogeneous and preliminary investigations show that substitution of Ala by Val at different positions does not cause a shift to conformational homogeneity, we will not further discuss

this compound here. Usually a substitution of an Ala by Val enhances the conformational homogeneity (a study of these effects is currently ongoing).

cyclo(-D-Ala^1-Ala^2-MeAla^3-Ala^4-MeAla^5-) (11): This compound is obtained by formal N-methylation of **5** at Ala^3. Surprisingly, this small change induces the peptide bonds between Ala^2-Ala^3 and Ala^4-Ala^5 to adopt a *cis*- conformation (Figure 3.21). This avoids steric interaction of all the methyl groups from Ala^2 to Ala^5. ROE violations are observed only for Ala^{5}H$^\alpha$-D-Ala^{1}H^N and Ala^{5}H$^\beta$-D-Ala^{1}H^N but the rest of the ROEs are in total agreement to the MD calculations. To explain these ROE violations, we assume again that the Ala^5-D-Ala^1 peptide bond is flipping and directs D-Ala^{1}N^H above and below the plane.

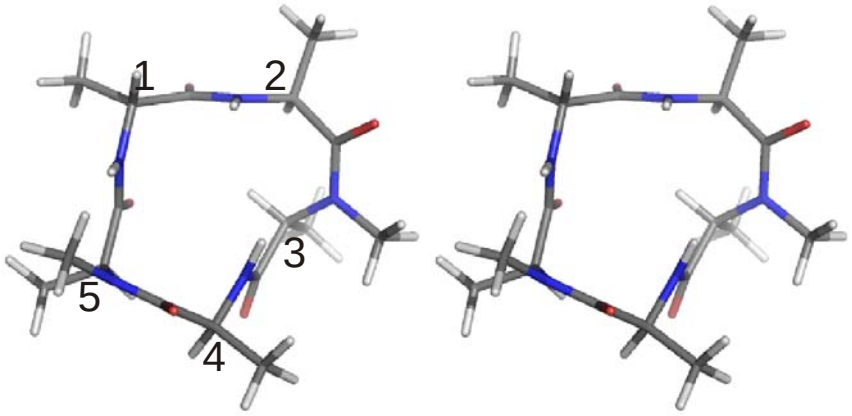

Figure 3.21. *Stereo picture of **11**.*

cyclo(-D-Ala^1-Ala^2-MeAla^3-MeAla^4-MeAla^5-) (16): The compound is obtained by additional N-methylation of **11** at Ala^3-Ala^4 peptide bond. Thus the compound has similar structural elements as **11** except the obvious rotation of the Ala^3-Ala^4 peptide bond by about 150° due to the N-methylation of the peptide bond (Figure 3.22). The peptide shows some violations in the ROEs, which again indicates some flexibility of the peptide bonds. There is a typical ROE between D-Ala^{1}H^N-Ala^{3}H$^\alpha$ which is violated by 0.25 Å; however, the other ROEs of D-Ala^{1}H^N are not violated. This suggests another orientation of the Ala^5-D-Ala^1 peptide bond than present in the average structure, where D-Ala^{1}H^N is close to Ala^{3}H$^\alpha$, formed by an anticlockwise rotation of the Ala^5-D-Ala^1 peptide bond. The Ala^{2}H^N also shows the following ROE violations Ala^{2}H^N–Ala^{4}NMe, Ala2H^N–Ala^{2}H$^\beta$, and Ala^{2}H^N–Ala^{3}H$^\alpha$. The first and the third violations restrict the Ala^{2}H^N to orient in a fashion so that it points towards Ala^{3}H$^\alpha$/Ala^{4}NMe and the second violation restricts the Ala^{2}H^N to a close proximity to Ala^{2}H$^\beta$; thus, these two sets of violations in the peptide points towards the flipping of Ala^5-D-Ala^1 and D-Ala^1-Ala^2 peptide bond. From the average structure one might conclude the presence of a γ turn about D-Ala^1; however, the temperature gradient values do not suggest that the Ala^{2}H^N is solvent shielded.

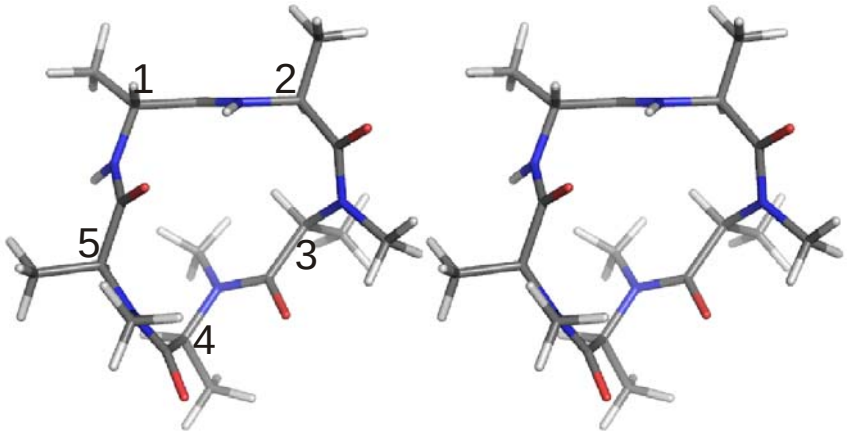

Figure 3.22. *Stereo picture of* ***16****.*

cyclo(-D-Ala^1-MeAla^2-Ala^3-MeAla^4-MeAla^5-) (21): Starting from **7**, **21** is formally N-methylated at Ala^5. It is evident from Figure 3.20 that N-methylation of Ala^5 is sterically forbidden. In fact, whereas the whole conformation between Ala^5-Ala^2 is retained in **7** and **21** (Figure 3.23), there is a change in the *cis*/*trans*- arrangement of the peptide bond (*cis*-peptide bond in **7** is between Ala^3-Ala^4, but in **21** between Ala^4-Ala^5) in addition to the backbone conformation in the region Ala^3-Ala^5. The spatial orientation of Ala^{4}NMe is defined by exactly the same ROEs as in **16**. The compound shows a major violation of 0.34 Å of the ROE between Ala^{2}H$^\alpha$ and Ala^{3}H^N. Additionally the Ala^{3}H^N shows a temperature gradient value of -2.00 ppb/K, suggesting it is solvent shielded. These data are consistent with rapid flipping of the Ala^3-Ala^2 peptide bond. The experimental D-Ala^1 ^3J(H^N,H$^\alpha$) coupling constant of 5.8 Hz is inconsistent with the average structure where the dihedral angle between D-Ala^{1}H$^\alpha$ and D-Ala^{1}H^N is -4.28°. This observation is also consistent with the observed minor violations of the ROEs between D-Ala^{1}H$^\alpha$-D-Ala^{1}H^N, D-Ala^{1}H^N-D-Ala^{1}H$^\beta$ and D-Ala^{1}H^N-Ala^{5}H$^\alpha$. These violations suggest an orientation wherein the Ala^5-D-Ala^1 peptide bond is rotated clockwise satisfying the observed ROE violations. However, as this is a sterically demanding situation, the structure relaxes energetically during the free MD run, resulting in the violation of the coupling constants and ROE.

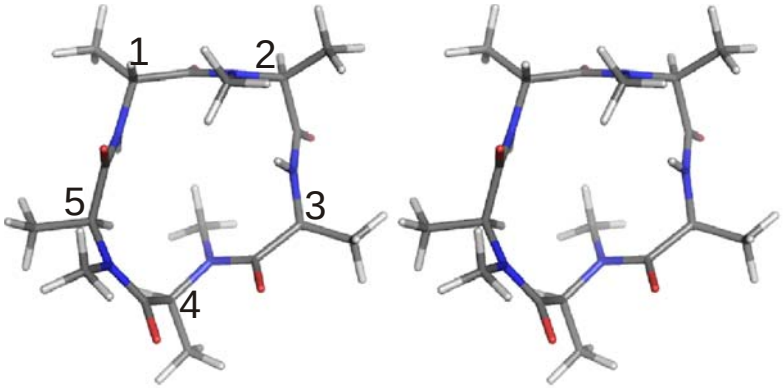

Figure 3.23. *Stereo picture of* ***21****.*

cyclo(-D-MeAla^1-MeAla^2-MeAla^3-Ala4-Ala^5-) (22): The compound can be obtained by further N-methylation of Ala^5-D-Ala^1 peptide bond of **6**. The compound as one expects from **6**, shows a *cis*-peptide bond about Ala^2-Ala^3 residue whereas all other peptide bonds are in the *trans*- configuration (Figure 3.24). The spatial orientation of D-Ala^{1}NMe is determined by the ROEs Ala^{5}H$^\alpha$-D-Ala^{1}NMe and Ala^{5}H^N-D-Ala^{1}NMe. The deep burying of the Ala^{3}H$^\beta$ is determined by the ROE Ala^{2}H$^\alpha$-Ala^{3}H$^\beta$ interaction. There are no major violations of the ROEs in the calculated structure except the intra-residual ROE between Ala^{5}H^N-Ala^{5}H$^\alpha$ suggesting dynamics of the Ala^4-Ala^5 peptide bond. The compound has similar structural elements as **6** and the N-methyl groups are spatially oriented in a fashion to have minimum possible steric clash with the N-methyl and β-protons. The low temperature coefficient value of -1.49 ppb/K for Ala^{5}HN indicates it is solvent shielded. However, the absence of the ROE between Ala^{5}H^N-Ala^{4}H^N and the absence of any violations, unlike the parent cyclo(-aA$_4$-), defines the orientation of the Ala^4-Ala^5 peptide bond and suggests the presence of a closed γ turn about Ala^4.

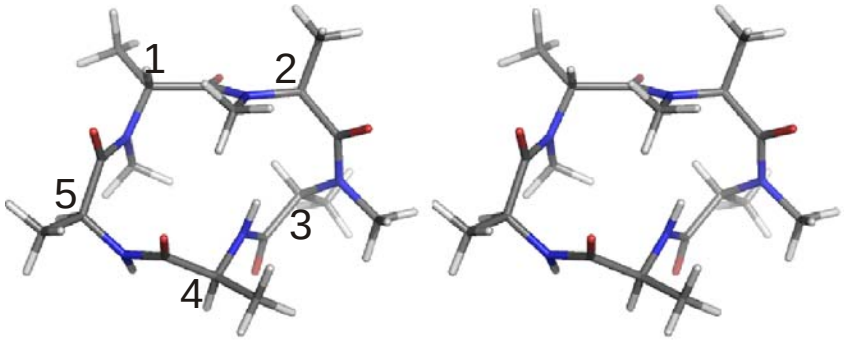

Figure 3.24. *Stereo picture of **22**.*

Table 3.4. Φ and Ψ values of conformationally in-homogeneous peptides.

#	Ala^1		Ala^2		Ala^3		Ala^4		Ala^5	
	Φ	**Ψ**	**Φ**	**Ψ**	**Φ**	**Ψ**	**Φ**	**Ψ**	**Φ**	**Ψ**
2	118	-81	-94	-61	-87	-66	-100	-67	-114	82
5	129	-94	-94	-64	-100	-61	-112	101	66	75
6	128	-87	-131	74	-110	11	-99	100	56	56
7	117	-90	-101	-89	-126	83	-128	-166	57	64
11	-55	-71	-138	79	-128	43	-138	72	-94	-23
16	86	-95	-134	84	-122	149	53	61	-112	151
21	116	-94	-80	-48	-129	80	58	74	-116	142
22	121	-84	-135	80	-109	48	-138	86	54	63

3.8 Conformational classes

With the detailed conformational characterization of the 15 out of the 30 N-methylated cyclic alanine pentapeptides, all of which prefer one conformation over 80%, can be analyzed into different classes. As a first approach, the peptides can be grouped into five different classes (Figure 3.25) based on the number and position of the *cis*-peptide bonds. It should also

be noted that in these conformationally homogeneous templates, we observe conformational dynamics (i.e., a rotation about Φ and Ψ) about peptide bonds, which are fast on the NMR shift time scale. Those processes are often found in peptides and are detected by non-agreement of observed and calculated distances in distinct areas.

In class I, there are six compounds possessing all-*trans*-peptide bonds. In class II, there are two compounds which have a *cis*-peptide bond between Ala^2-Ala^3, while class III contains three compounds with a single *cis*-peptide bond between Ala^4-Ala^5. Class IV has three compounds with two *cis*-peptide bonds (between Ala^2-Ala^3 and Ala^4-Ala^5), and finally class V has one compound, with a single *cis*-peptide bond between Ala^3-Ala^4. Thus combining all the possibilities of the occurrence of the *cis*-peptide bond, one can ascertain that the region between Ala^5 to Ala^3 is highly conserved, as under no circumstance there is the occurrence of a *cis*-peptide bond about Ala^5-D-Ala^1 and D-Ala^1-Ala^2. The region between Ala^2 to Ala^5 on the other hand is variable, where N-methylation of the peptide bond leads to the formation of one, two, or no *cis*-peptide bond varying with the pattern of N-methylation.

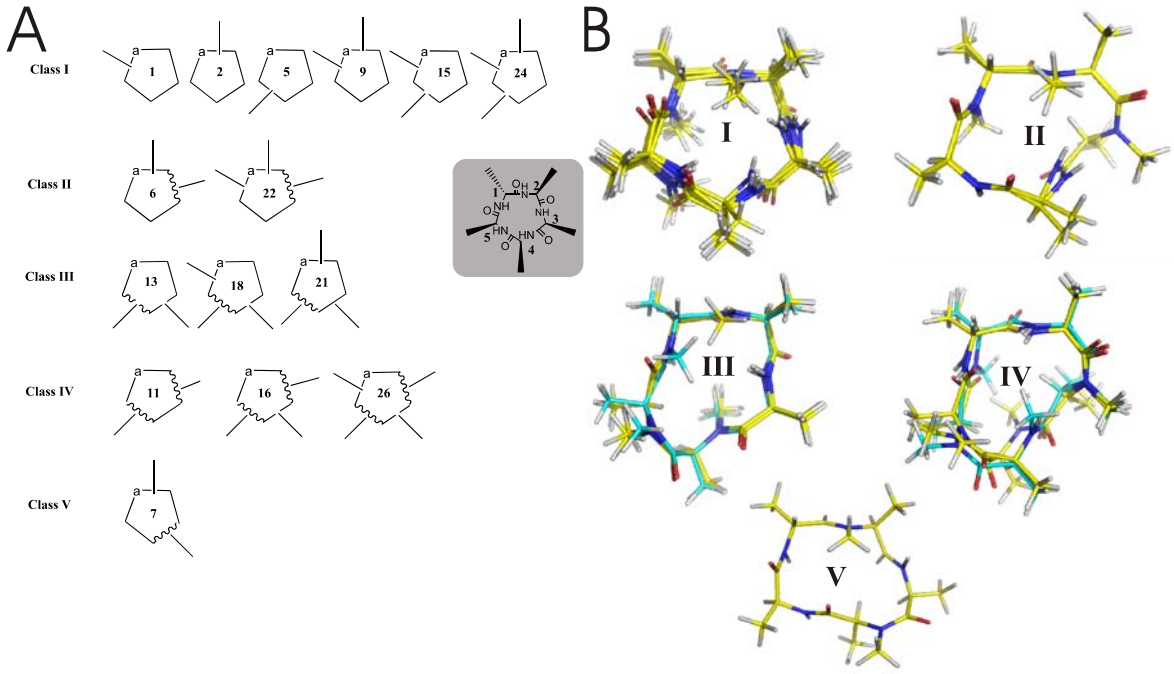

Figure 3.25. *A) Different classes of N-methylated cyclo(-D-Ala-Ala$_4$-); wavy lines: cis-peptide bond; a: D-Ala. B) Superimposed backbone conformation of the members in each class.* ***18*** *and* ***26*** *are in cyan highlighting differences in N-methyl orientation.*

In class II and IV, the compounds have a common N-methylated Ala^2-Ala^3 peptide bond leading to the formation of a *cis*-peptide bond in this position, owing to the strong steric interaction with the adjacent β-methyl groups. There is only one compound **7**, which has an N-methylated Ala^3-Ala^4 peptide bond in the *cis*- conformation. All other peptides, that is, **13**, **16**, **18**, **21**, and **26**, which have the Ala^3-Ala^4 N-methylated peptide bond, exhibit a *trans*-conformation. To understand this behavior we begin with **4**, wherein only Ala^4 is N-

methylated. Here we observe 50:50 abundance of two conformers (Figure 3.9) of this Ala^3-Ala^4 peptide bond in the *cis*- and *trans*- orientation (Figure 3.26). N-Methylation only at Ala^2 shifts the equilibrium to a strong *cis*- preference as in **7**, whereas N-methylation at any other sites shifts it to *trans*-.

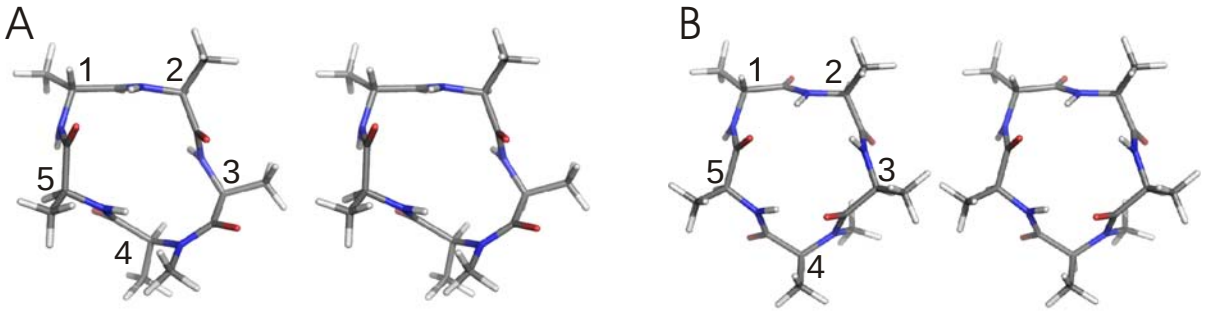

Figure 3.26. *Stereopictures of conformation of cyclo(-D-Ala^1-Ala^2-Ala^3-MeAla^4-Ala^5-) (**4**) A) cis- conformer, and B) trans- conformer.*

In class III, the three compounds possessing a *cis*-peptide bond at Ala^4-Ala^5 also have the adjacent *trans*- Ala^3-Ala^4 peptide bond N-methylated. It seems that only the N-methylation at the Ala^4-Ala^5 is not sufficient to introduce a *cis*-peptide bond at this position until the previous Ala^3-Ala^4 peptide bond is N-methylated (e.g., the mono-methylated compound, **5**, exhibits one abundant *trans*- conformer) and all the three compounds, **13**, **18**, and **21** have a common N-methylated Ala^3-Ala^4 peptide bond. However, similar to the previous case there is an exception to this pattern: compound **11**, where the Ala^4-Ala^5 peptide bond is *cis*-, despite the absence of the N-methylated Ala^3-Ala^4 peptide bond. An explanation to this observation can be extracted after taking all the six compounds into account which have N-methylated Ala^4-Ala^5 peptide bond. Here one observes that the single N-methylation of Ala^4-Ala^5 peptide bond or in conjunction with N-methylated Ala^5-D-Ala^1 and/or D-Ala^1-Ala^2 does not force Ala^4-Ala^5 into the *cis*- conformation. Instead when in conjunction with N-methylated Ala^2-Ala^3 and Ala^3-Ala^4 peptide bond, the Ala^4-Ala^5 peptide bond eventually orients in a *cis*-conformation. Thus, either N-methylation of Ala^2-Ala^3, Ala^3-Ala^4 or both is crucial to direct the N-methylated Ala^4-Ala^5 peptide bond into *cis*- conformation.

In class IV, all of the three compounds, **11**, **16** and **26**, have two *cis*-peptide bonds in equivalent positions; all three compounds are identical except for the orientation of the Ala^5-D-Ala^1 and Ala^3-Ala^4 peptide bonds, which exhibit *trans*-peptide bonds. The plane of the Ala^5-D-Ala^1 peptide bond in **11** has rotated by about 170° and in **26** by about 30° in comparison to **16**. Considering the Ala^3-Ala^4 peptide bond, the preferred orientation of the non N-methylated peptide bond is observed in **11**, however, the N-methylation of the Ala^3-Ala^4 peptide bond results in a different conformation of the peptide bond plane twisted by about 110° in **16**, as otherwise it would encounter strong steric clash with Ala^{3}NMe and

Ala^{4}H$^\beta$. This orientation is, however, violated in **26** as the N-methylation of Ala^5-D-Ala^1 peptide bond leads to a strong D-Ala^{1}NMe-Ala^{4}NMe steric clash and this eventually reorients the Ala^{4}NMe forcing the Ala^4-Ala^5 *cis*-peptide bond out providing a room for its spatial orientation. Thus in this series of N-methylated cyclic pentaalanine peptides, there is a systematic pattern in the orientation of peptide bond conformation and subsequently the side chain orientation based upon the site of N-methylation.

3.9 Systematic modulation of conformation by N-methylation

A clear picture of the conformational change by successive N-methylation can be obtained by classifying these peptides by virtue of their sites of N-methylation (Figure 3.27). Starting from compound **2**, N-methylation on either side (referring to the N-methylated site) results in **6** and **9**; in **9** the D-Ala^1 N-methylation is tolerated, as the D-Ala^{1}NH in **2** points down allowing the insertion of an N-methyl group without much deviation from backbone of **2**.

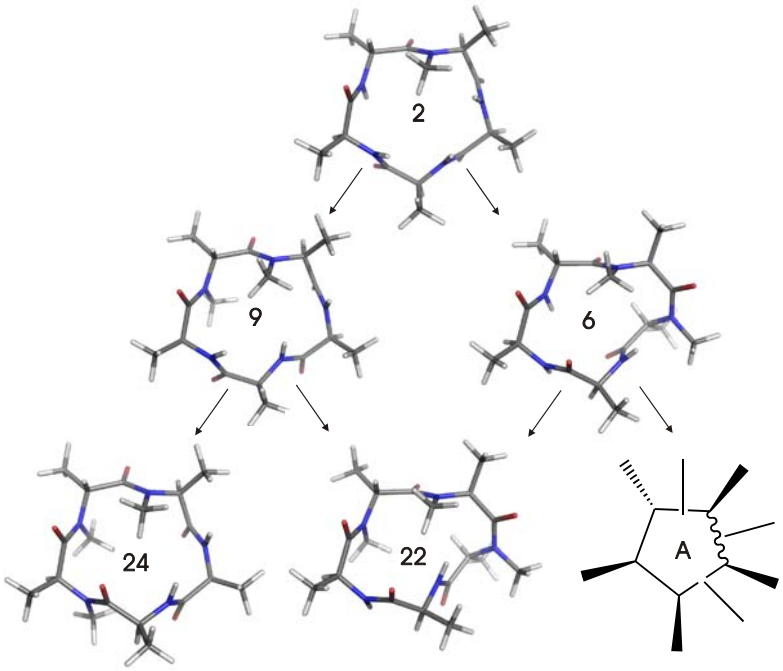

Figure 3.27. *Schematic diagram representing the correlation between the N-methylated cyclic peptides obtained by systematic shift and increasing the number of N-methylation of cyclo(-D-Ala^1-MeAla^2-Ala^3-Ala^4-Ala^5-). "A" shows two different conformation at the NMR spectrum having an abundance of (65:35), therefore the conformational details of this peptide omitted.*

In **6**, Ala^3 N-methylation leads to strong clash between two N-methyl groups eventually leading to Ala^2-Ala^3 *cis*-peptide bond. Extending the N-methylation of **6** and **9**, three peptides are obtained of which one is conformationally in-homogeneous. In **24**, Ala^5 N-methylation leads to the flip of Ala^4-Ala^5 peptide bond preferring a *trans*- conformation. In **22**, the backbone conformation is not much deviated from that of **6**, as D-Ala^1 N-methylation in **6** is

sterically allowed. N-Methylation on either side of **5** results in **15** and **13**. As shown in **24** (Figure 3.28), N-methylation of D-Ala[1] and Ala[5] is tolerated in **15** without enforcing a *cis*-peptide bond conformation.

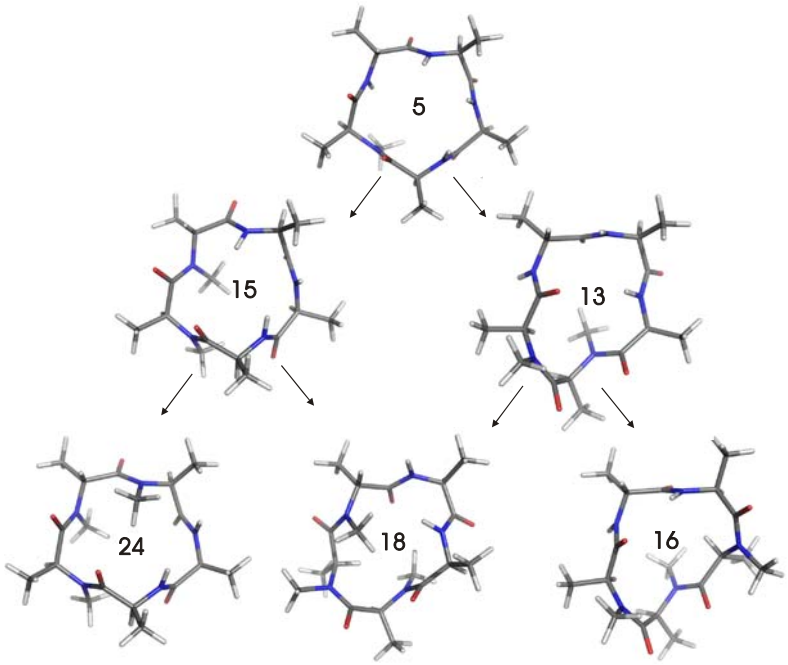

Figure 3.28. *Schematic diagram representing the correlation between the N-methylated cyclic peptides obtained by systematic shift and increasing the number of N-methyl group of the parent peptide* **5***, cyclo(-D-Ala[1]-Ala[2]-Ala[3]-Ala[4]-MeAla[5]-).*

N-Methylation of Ala[4] in **5** would have a strong clash with Ala[3] and Ala[4] methyl group, resulting in the 180° flip of Ala[3]-Ala[4] peptide bond (data not presented), which eventually forces the Ala[4]-Ala[5] peptide bond into *cis*- conformation. Further N-methylation of **13** and **15** leads to **16**, **18** and **24**; in **16**, Ala[3] N-methylation introduces *cis*-peptide bond as in **6** and in **18** D-Ala[1] N-methylation retains the backbone conformation as **13** with a minor change in the Ala[5]-D-Ala[1] peptide bond plane. Similarly, extending N-methylation on either side of **1** (Figure 3.29) results in **9** and **15**. Further N-methylation results in **18**, **22** and **24** which are discussed above. Ala[3] N-methylation of **18** leads to **26**, introducing an Ala[2]-Ala[3] *cis*-peptide resulting in a similar backbone conformation as **16**, however, the flip of the Ala[3]-Ala[4] peptide bond is noticeable which results from the steric clash of D-Ala[1] N-methyl which always points down the plane. Thus, based on the conformations of all the 15 peptides with a preferred conformation, we can summarize the results which are depicted in Table 3.5.

Table 3.5. *The figure depicts the cyclo(-aA$_4$-) with various pattern of N-methylation and the numbers refer to the corresponding peptide bond which is N-methylated.*

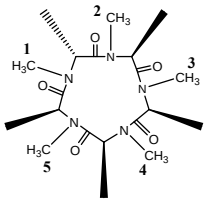

Peptide bond	Conformation
1	always trans-
2	always trans-
3	always cis-
4	always trans except **7** (cis)
5	trans- preferred but cis- when 3 and/or 4 N-methylated

Finally based on these results, we can predict the preferred orientation of the N-methylated peptide bonds in Figure 3.30. N-Methylation at D-Ala^1 and Ala^2 results only in subtle changes in the Φ and Ψ but N-methylation at Ala^4 and Ala^5 results in -180° flip of the respective peptide bond plane in comparison to the parent peptide bond, on the other hand, N-methylation only at Ala^3 results in a *cis*-peptide bond.

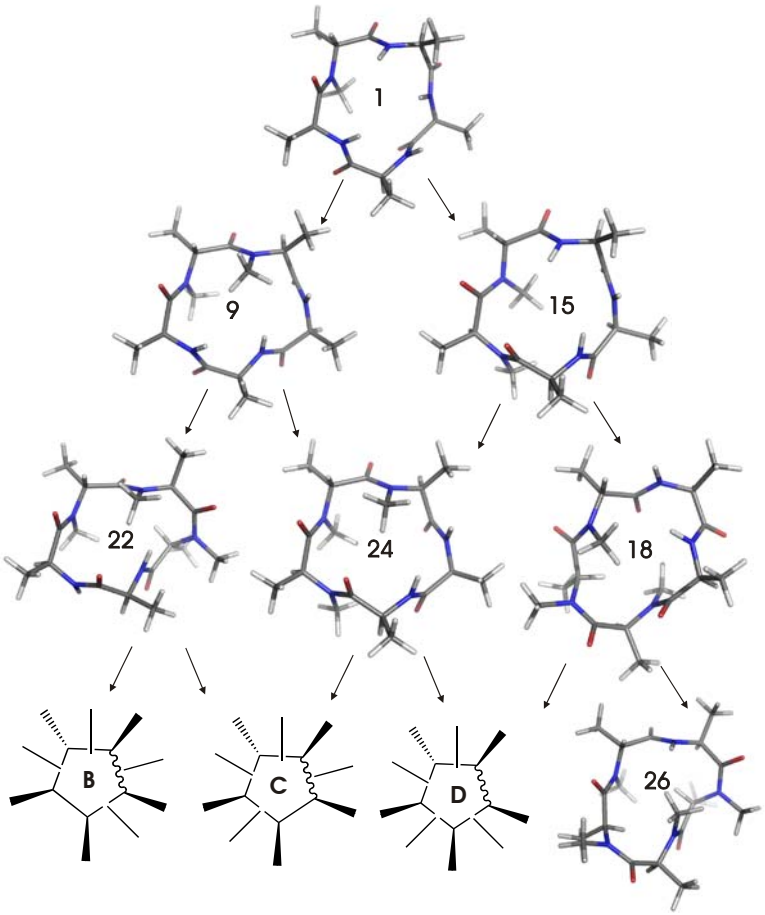

Figure 3.29. *Schematic diagram representing the correlation between the N-methylated cyclic peptides obtained by extending the pattern and number of N-methylation of* ***1****, cyclo(-D-MeAla^1-Ala^2-Ala^3-Ala^4-Ala^5-). Owing to conformational in-homogeneity, the conformations of* ***B****,* ***C*** *and* ***D*** *are omitted.*

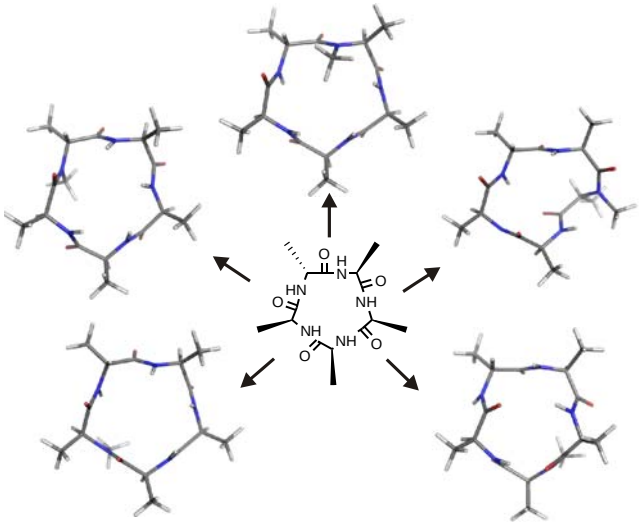

Figure 3.30. *The preferred orientation of the mono N-methylated peptide bonds. (It should be kept in mind that under sterically demanding conditions, the plane of the peptide bonds Ala*^{3}*-Ala*^{4} *and Ala*^{4}*-Ala*^{5} *can rotate).*

A similar N-methyl scan performed on cyclic hexapeptide: cyclo(-D-Ala-Ala$_5$-) in search of conformationally homogeneous templates and to investigate the effect of N-methylation on intestinal membrane permeability, revealed that N-methylation of the D-alanine results in conformational homogeneity and has been recently confirmed by McAlpine et al. in designing N-methylated cyclo-peptidic scaffolds against colon cancer.[104] Thus, the turn inducing property of N-methylated-D-alanine or probably any N-methylated-D-amino acid (except glycine) is equal or may be stronger than that of D-proline. This eventually opens a new dimension for the design of β-hairpin conformations[105] in cyclic protein epitope mimetics by using NMeD-Ala-L-Ala or NMeD-Ala-L-Pro or even NMeD-Xaa-L-Pro, NMeD-Xaa-L-MeXaa and NMeD-Xaa-L-Xaa as templates to induce a βII' turn instead of the conventionally used D-Pro-L-Pro (Figure 3.31), allowing use of wide range of functionalities by incorporating all the possible amino acids at the turn inducing region.

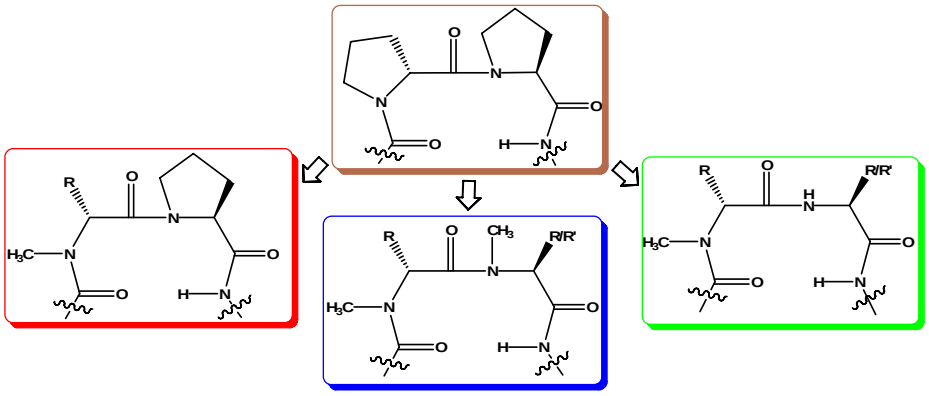

Figure 3.31. *Conventional β–hairpin turn inducer: D-Pro-L-Pro, which could be replaced by NMeD-Xaa-L-Pro, NMeD-Xaa-L-MeXaa, and NMeD-Xaa-L-Xaa. R and R' represents any amino acid side allowing the introduction of diverse functionalities.*

4. Oral bioavaiability of Peptides

4.1 Points to keep in mind

Drug design is an exciting and challenging issue in medicinal chemistry. The vision of a marketable drug from a lead structure is full of hurdles. To set standards for a rational and responsible approach to new molecules, the ADMET parameters were defined. ADME stands for **a**bsorption, **d**istribution, **m**etabolism, **e**xcretion, and **t**oxicology. These parameters are used as a rule of thumb for the screening of promising leads in pharmaceuticals. There are several factors that influence the oral bioavailability of a drug, however, the major factors that influence bioavailability was put forth by Lipinski et al.[17,106] They screened several thousand drugs from *Pfizer's* database and concluded the following five properties, commonly known as '*Pfizer's rule of five*'; which govern the drug likeliness nature of a molecule.

- molecular weight < 500 g/mol
- $4 \leq \log P \leq 5$
- $\sum$ hydrogen bond acceptors (N, O) < 10
- $\sum$ hydrogen bond donors (NH, OH) < 5
- one of the rules may be violated

However, one should bear in mind that these parameters are prerequisites but not indispensable for continuing drug research. One well known molecule violating these rules is the marketed immunosuppressive drug *Cyclosporin*.[24]

This rule of five was questioned by Veber et al. couple of years later and they put forth the importance of the rigidity and the surface area of the molecule, surpassing the importance of molecular weight.[18] They added that the number of rotatable bonds must be less than 10 and the polar surface area must not exceed 140$Å^2$.

4.2 Peptide drugs

Recent dramatic advances in recombinant DNA technology and modern synthetic methodologies, allow the production of vast quantities of various peptides possessing a diverse array of pharmacological effects. However, the clinical development of these peptide drugs has been restricted due to very poor absorption across cell membranes and rapid degradation leading to oral bioavailabilities typically less than 1-2% and short *in vivo* half-lives.[13,107,108] The successful design of such molecules as orally available drugs will be a major challenge confronting pharmaceutical scientists in the future. The rational drug design strategy involving the transformation of a peptide into a peptidomimetic[12,109] has led to the discovery of many therapeutically useful drugs, e.g. HIV protease inhibitors,[110,111] renin inhibitors,[112] and glycoprotein IIb/IIIa antagonists.[113] This strategy often involves the

replacement of a metabolically labile peptide bond with a peptide bond isostere, e.g. hydroxyethylamine,[110] hydroxyethylene,[114] dihydroxyethylene,[115] aminimide,[116] or pyrrolinone.[117] However, an effective 'minimalist' approach to accomplish this objective involves N-methylation of a metabolically labile peptide bond.[32,118] N-methylation strategy helps in stabilizing peptides to protease metabolism[119] and enhances their membrane permeation.[120,121] Thus, we were interested in the testing this hypothesis of improvement of pharmacokinetic properties of biologically active peptides by multiple N-methylation.

4.3 Barriers limiting peptide bioavailability

4.3.1 Biological barrier

Intestinal lumen

Physiologically, the gastrointestinal tract is designed to break down dietary proteins into subunits that are sufficiently small (e.g. di/tripeptides, amino acids) to be absorbed across the intestinal mucosa. Digestive processes for proteins and peptides are catalyzed by a variety of enzymes that are specialized in the hydrolysis of peptide bonds. Due to the wide substrate specificity of these proteases and peptidases, it is not surprising that the metabolic activity in the intestinal lumen is a major barrier limiting the absorption of peptide-based drugs. When peptides reach the duodenum, their degradation can be mediated by pancreatic proteases. The relative importance of this luminal hydrolysis in the overall degradation process is dependent on the size and amino acid composition of the peptide.[122] However, even when luminal peptide degradation occurs, as observed for simple glycine-containing di and tripeptides, it constitutes at best 20% of the total degradation in a given intestinal segment. This implies that significant degradation of the peptide requires at least contact with the brush-border membrane and/or uptake into the intestinal mucosal cells.

Intestinal mucosal cells

A typical biological barrier like the intestinal mucosa consists of both physical and biochemical components. The physical component of the barrier arises from both the tight intracellular junctions and the lipid characteristics of the cell membrane, whereas the biochemical component of the barrier arises from the proteins (e.g. enzymes, transporters) in the cell membrane. The ability of a peptide-based drug candidate to permeate this barrier may be limited by the physical and/or the biochemical component.

4.3.2 Physical barrier

The organization and architecture of the intestinal mucosa restrict peptides and proteins to either the paracellular or the transcellular route (Figure 4.1). The paracellular pathway is an aqueous, extracellular route across the epithelia. Translocation through the paracellular pathway is passive and the flux of the molecule is driven by electrochemical potential gradients originating from differences in concentration, electrical potential and hydrostatic pressure between the two sides of the epithelium.[123] The main barrier to the paracellular diffusion of molecules across the intestinal epithelium is the region of the tight junction or zonula occludens.[124] The structural features of these tight junctions and how they influence peptide transport across the intestinal epithelium are discussed in Section 4.4.

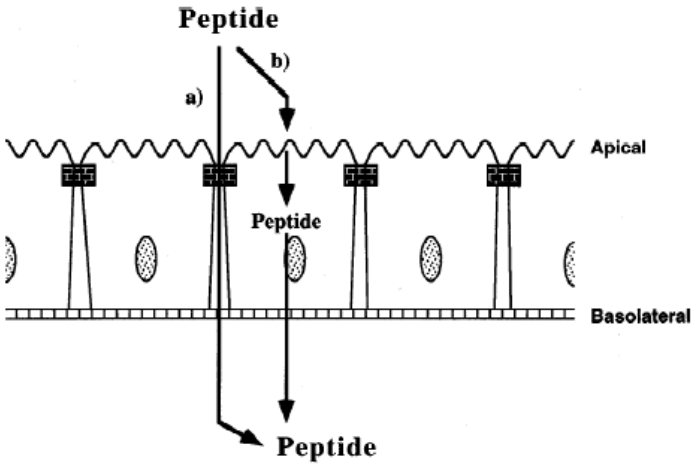

Figure 4.1. *The physical barrier properties of the intestinal mucosa limits peptide flux to (a) paracellular and (b) transcellular pathways.*[125]

The transcellular pathway involves movement of the solute across the apical cell membrane, through the cytoplasm of the cell and across the basolateral membrane by passive diffusion, or by a carrier- or vesicle-mediated process (Figure 4.2). In general, with peptides, transcellular flux by passive diffusion is minimal.[126] In addition, carrier-mediated processes (e.g. using di- or tripeptide transporters) for the transport of peptides and peptidomimetics are fairly substrate-specific and do not contribute significantly to the transport of non-substrates, although exceptions have been found (e.g. cephalosporins).[14]

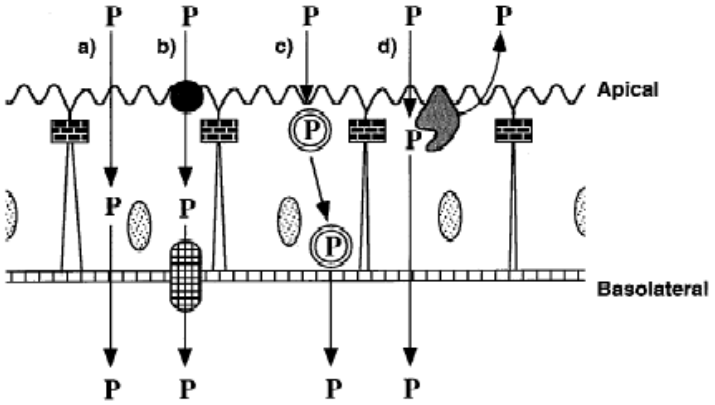

Figure 4.2. *Transcellular pathways for intestinal absorption of peptides: (a) passive, (b) carrier-mediated, and (c) vesicular. Transcellular transport can be reduced by (d) apically polarized efflux systems. P = peptide.*[125]

Cellular internalization of polypeptides by endocytosis is another important biological process whereby peptides that are too large to be absorbed by the di- and tripeptide transport systems may be taken up into intestinal mucosal cells. Fluid-phase endocytosis (pinocytosis) does not require any interaction between the polypeptide and the apical membrane. In contrast, receptor-mediated or absorptive endocytosis involves the binding of peptides and proteins to the plasma membrane before being incorporated into endocytic vesicles. Finally, some polypeptides can be carried in endosomes directly to the basolateral side (i.e., bypassing the lysosomes), where they are released into the extracellular space. This process is known as transcytosis. Although there is some evidence that mucosal peptide/protein uptake is mediated by endocytic processes, in most instances, this does not lead to transcytosis.[127] Although the cell layer contributes predominantly to the physical barrier of the intestinal mucosa, additional factors may hinder the passage of peptides and proteins. For example, like most epithelial surfaces, the intestinal mucosa is coated with a layer of mucus that serves as a lubricant and protective barrier. Mucus, in reality, is a constantly changing mix of many secretions, including exfoliated epithelial cells.[128] The main determinants of the physical and functional properties of mucus secretions are high molecular weight glycoproteins, termed mucins. Much research has been done in an attempt to understand the regulatory mechanisms of mucin secretion and its role in the modulation of tissue function. However, the role of the mucus layer as a physical barrier in the absorption of peptides from the gastrointestinal tract has not been well established.

4.3.3 Biochemical barrier

As mentioned above in Section 4.3.1, enzymes released from the pancreas into the intestinal lumen may play a role in the metabolism of peptides. However, the evidence strongly

suggests that significant degradation of peptides requires at least contact with the brush-border membrane and/or uptake into the intestinal mucosal cells. In general, it appears that brush-border peptidases are active mainly against tri-, tetra- and higher peptides, up to ten amino acid residues, while intracellular peptidases are active predominantly against dipeptides.[129] Today, a variety of intestinal peptidases are characterized and listed under the formal enzyme classification (EC) system, based on their site of action in a susceptible substrate.[130,131] Peptidases that are capable of cleaving the internal peptide bonds of a substrate are designated as endopeptidases (e.g. serine proteinases, metalloproteinases). For large peptides or those with blocked ends (e.g. acetylated N-terminus, amidated C-terminus), endopeptidases are required to initiate hydrolysis. The remaining peptidases are classified as exopeptidases (e.g. aminopeptidases, carboxypeptidases), which remove one or more residues from the termini of the peptide.

The regional distribution of intestinal peptidases, including their activities, has been studied recently. In rat and rabbit intestine, the activity of the brush-border exopeptidases, aminopeptidase P (EC3.4.11.9) and aminopeptidase W (EC 3.4.11.16), increases distally and reaches its highest level in the ileum.[132] The lowest activities, however, were measured at the ileo–caecal junction. Similar results were found in rabbits as well as in humans for aminopeptidase N (EC 3.4.11.2) and dipeptidyl peptidase IV (EC 3.4.14.5).[133,134] However, in recent years, it has been realized that the barrier function of the intestinal mucosa could not be adequately described by a combination of the metabolic and physical barriers alone.

In cancer cells, it has long been recognized that polarized efflux systems are present that pose a major barrier to the absorption of a wide variety of chemotherapeutic agents. Although these efflux systems are most commonly observed in tumor cells, they are also known to be present in normal intestinal cells.[135] These efflux systems are related to P-glycoprotein, the principal component of multidrug resistance in a variety of cell types. P-glycoprotein is a 170–180 kDa membrane glycoprotein that acts as an ATP-dependent efflux pump, thereby reducing the intracellular accumulation or the transcellular flux of a wide variety of drugs, including peptides (e.g. gramicidin D, valinomycin).[136] The polarized expression of these efflux systems suggests that their physiological role is to restrict the transcellular flux of some molecules (Figure 4.2). Thus, in the gastrointestinal epithelium, they serve as a major barrier by limiting the absorption of drugs, including peptides and peptidomimetics.[137]

4.4 Enhancement of passive diffusion across the intestinal mucosa

The organization and architecture of the intestinal mucosa, allow peptides to traverse the cell barrier via the paracellular and/or transcellular route (Figure 4.1). Permeation of peptides via

the paracellular pathway is primarily driven by passive diffusion. Translocation through the cells (i.e., transcellular pathway) involves either passive or active transport processes and can be restricted by polarized efflux systems (Figure 4.2).

4.4.1 Paracellular pathway

The paracellular pathway has gained interest for the delivery of peptides because of the perception that it is deficient in proteolytic activity.[138] Several peptide drugs, such as octreotide,[139] potent analogs of vasopressin (e.g. 1-deamino-8-D-arginine vasopressin (DDAVP),[140] and thyrotropin releasing hormone (TRH)[141] are assumed to permeate the intestinal mucosa predominantly via this route. In general, it is accepted that size, charge and the hydrophilicity of peptides are the crucial molecular characteristics for paracellular absorption. Since the paracellular pathway is an aqueous extracellular route across the epithelium, sufficient *hydrophilicity* is the most important prerequisite for a peptide to traverse the cell barrier via this pathway. The more *lipophilic* a peptide is, the more likely it is that it will interact with the cell membrane which, in fact, is the first step for the transcellular pathway. Transport of solutes via the paracellular route is primarily controlled by the region of the tightjunction or zonula occludens.[142] Adson et al. showed that the flux of a series of zwitterionic, metabolically stable peptides, D-Phe–Gly, D-Phe–D-Phe–Gly and D-Phe–D-Phe–D-Phe–Gly, decreased with increasing molecular radius.[143] Similar results were observed in a study performed in the laboratory of Borchardt et al., where they compared the permeation of metabolically stabilized neutral, positively and negatively charged amino acids, tripeptides and hexapeptides across Caco-2 cell monolayers, an *in vitro* model of the intestinal mucosa.[144] Apparent permeability coefficients, calculated for the hydrophilic, charged model peptides, increased on average by a factor of two when the molecular size was reduced from a hexapeptide to a tripeptide and finally to an amino acid, respectively. These findings underline the molecular sieving properties of the intestinal mucosa due to the presence of tight intercellular junctions. Although the degree of permeability at the tight junctions varies significantly within different epithelia, tight junctions are reported to be impermeable to molecules with radii larger than 11–15 Å.[145] These numbers truly represent the maximum hydrodynamic radius of a spherical rigid molecule, which is small enough to diffuse into the intercellular space. However, for peptide drugs possessing a high degree of conformational flexibility, it might be possible that even larger molecules can permeate the tight junctions. Recently, it was demonstrated by Borchardt et al. that the permeation characteristics of two model peptides (Ac–Tyr–Pro–X–Asp–Ile–NH ; X= Gly, Ile) across Caco-2 cell monolayers were not significantly different, although the Gly-containing pentapeptide exhibited a higher

degree of β turn structure than the Ile-containing analog.[125] In the literature, cyclic peptides (e.g. Cyclosporine[146] and a cyclic analog of Somatostatin[147]) have been reported to be highly permeable across the cellular barrier. However, it is unclear whether these favorable permeation characteristics are due to a reduction in their molecular size, resulting in enhanced paracellular flux, or a change in other physicochemical properties (e.g. lipophilicity), which would facilitate transport via a different route (e.g. transcellular pathway). Since linear peptides are in a dynamic equilibrium between open and folded structures, it was of interest to investigate the effect of restricted conformational flexibility of peptides on their transport properties. Borchardt et al. prepared cyclic analogs of linear hexapeptides (H–Trp–Ala–Gly–Gly–X–Ala–OH; X= Asp, Asn, Lys) by covalently linking the N-terminus to the C-terminus.[148] Transport experiments using the Caco-2 cell culture model revealed that the cyclic model hexapeptides were two–three times more capable of permeating the cell monolayer than were the linear analogs. Characterization of the molecular sizes performed by NMR spectroscopy and high-resolution size-exclusion chromatography did not show dramatic differences between the linear and cyclic peptides. However, cyclization seemed to increase the lipophilicity of the peptides, which was in accord with the formation of distinct intramolecular hydrogen bonds, as observed by NMR spectroscopy. These results suggest that enhanced permeation characteristics of the cyclic peptides may be due to a shift in the transport pathway that is related to the increased lipophilicity upon cyclization.

Experimental support for this hypothesis of a pathway shift was obtained from transport studies performed in the presence of 0.1 mM palmitoyl-DL-carnitine (PC). PC is a known tight junction modulator that can be used to increase the average pore radius at the junctional complex without completely destroying the physical barrier properties of the cell monolayer.[125] The flux of the linear Asp and Asn containing hexapeptides increased by approximately 90-fold, whereas the increase for the cyclic analogs was only ~25-fold. This implies that a significant fraction of the cyclic peptides may cross the cell monolayer via the transcellular pathway, which, per se, should not be sensitive to perturbation at the tight junctions. Using a quantitative biophysical model, the cyclic Asp and Asn containing hexapeptides were calculated to permeate the Caco-2 cell monolayers by at least 25% via the transcellular route. The linear analogs, in contrast, were found to traverse this biological membrane exclusively via the paracellular pathway.[144]

Proteins within the junctional complexes consist of polar amino acids with ionizable side chains. As a consequence, the junctional space exhibits an electrostatic field with a negative net charge that may affect the paracellular flux of molecules due to charge–charge interactions.[149a] Rubas et al.[149b] investigated the transport properties of cyclic RGD peptide

analogs, potent platelet aggregation inhibitors based on the Arg–Gly–Asp motif, with various net charges ranging from -3 to +1 using the Caco-2 cell culture model. Their conclusion was that peptides with net charges of -1 and -2 are able to permeate the intestinal mucosa most efficiently.[125] In contrast, a study from Borchardt et al. where they determined the transport properties of neutral, positively and negatively charged capped amino acids, tripeptides and hexapeptides,[144] suggests a favorable effect of a positive net charge for the trans mucosal transport of small peptides (≤ tripeptides). With increasing molecular size, however, the size sieving by the pores appeared to become more dominant. At the level of the hexapeptides, the charge selectivity of the cell monolayer (i.e., positive > negative) was almost negligible.

4.4.2 Transcellular pathway

Transcellular permeation requires a distinct interaction of the solute with the cell membrane. Chemically, the cell membrane represents a very complex environment, consisting of a lipid bilayer matrix with a variety of integral and peripheral proteins.[150] The proteins contribute to the structural integrity of the cell as well as its transport and metabolic capabilities. In contrast, the nature of the lipids influences the fluidity of the cell membrane, and anchors the protein structure to the core of the membrane via specific protein–lipid interactions.

To permeate the intestinal mucosa via the transcellular pathway, the ability of the molecule to partition into the cell membrane is of critical importance.[120] Therefore, most of the studies performed to date have focused on the individual contributions of physicochemical properties, including size and lipophilicity (hydrophobicity and hydrogen bonding potential), on the transcellular permeation of peptides. However, the controlling features for this route are still not well understood.

Traditionally, lipophilicity has been viewed as the most important molecular characteristic in determining passive diffusion through biological membranes, mainly because a membrane is simplistically considered a ‘‘lipophilic’’ barrier. Nevertheless, early *in vivo* data suggested that intestinal absorption may decline when lipophilicity becomes too high.[151] These results imply an ‘‘optimal’’ rather than a high lipophilicity for improved transmucosal permeation of a molecule. Since the energy necessary for a solute to enter from the aqueous phase to the membrane phase (i.e., desolvation energy) is the most significant factor for the membrane transport, the lipophilicity is usually described by parameters reflecting the relative affinity of the solute for an aqueous phase and a water-immiscible phase. It has been demonstrated for a variety of small organic based molecules that the octanol/water partition coefficient ($P_{o/w}$) is a good predictor of their permeation properties across a biological membrane.[152] However, for

peptide-based drugs, an increase in lipophilicity as expressed by a greater log$P_{o/w}$ value was not always correlated with enhanced transport properties across the intestinal mucosa.

In a systematic study, Conradi et al. have investigated the effect of lipophilicity on the transport of a series of metabolically stable oligomers of D-Phe and Gly using Caco-2 cell monolayers.[120,121] It was demonstrated that lipid solubility, as expressed by log $P_{o/w}$, did not correlate with their membrane permeation characteristics. A better predictor for the peptide permeation was the hydrogen bonding potential, which was experimentally assessed by the difference in partition coefficient determined in the octanol/water and the isooctane/water systems. The same conclusion was drawn when the transport of these model peptides was studied in an in situ perfused rat ileum model.[153] These results imply that the hydrogen bonding potential may represent a valuable parameter for characterizing the lipophilicity of peptides with respect to their membrane permeation via the transcellular pathway. This has been recently proven by Lokey et al., where they show the importance of hydrogen bonding potential by employing cyclic peptide diastereomers (Figure 4.3), which were highly permeable (comparable to Cyclosporin A).[154]

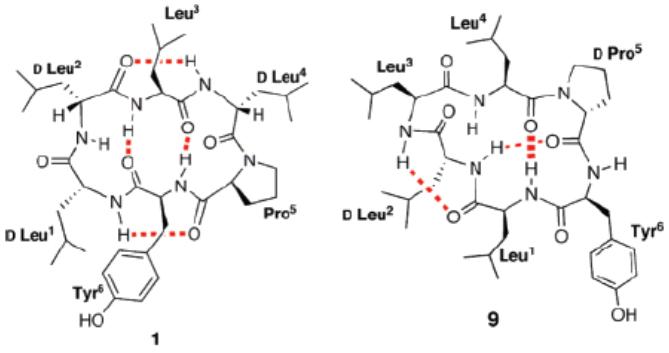

Figure 4.3. *Schematic diagrams of two cyclic peptides which were found to be high (left) and low (right) permeable through PAMPA (parallel artificial membrane permeability assay, which is a phospholipid impregnated membrane, the results of which correlate well with the passive diffusion across living cells). The red lines represent the hydrogen bonds observed.*[154]

For proteins, a reduction in hydrogen bonding potential has been shown to result from conformational changes that can lead to formation of intra-molecular hydrogen bonds. As a consequence, the free energy of transfer for an amide bond decreased from 25.9 kJ/mol, when solvated, to 2.3 kJ/mol, if it is involved in an intra-molecular hydrogen bond.[155] The mechanism of reducing hydrogen bonding potential due to conformational promotion of intra-molecular hydrogen bonding is not restricted only to proteins. Delta sleep-inducing peptide (DSIP) shows the unusual ability of passively diffusing across the blood–brain barrier both *in vivo*[156] and *in vitro*.[157] The solution structure of this peptide was shown to contain several intra-molecular hydrogen bonds, resulting in an overall amphiphilic structure that may account for its unexpectedly high permeation characteristics.[158]

With these examples, where the solution conformation of a molecule can ‘‘mask’’ polar groups and, therefore, improve its membrane permeation properties, it is appropriate to mention the idea of membrane-induced conformational changes that can favor a transient, more permeable structure of a molecule. Experimental lipophilicity determinations, combined with molecular dynamics simulations, revealed that molecules such as morphine glucuronides and cyclosporin A exhibit different conformations with significant differences in lipophilicity when going from a polar to an apolar environment.[159,160] This would support an earlier hypothesis that the membrane interface might act as a catalyst to promote conformational structures that might not necessarily be observed in aqueous solutions.[161]

4.5 Improving oral bioavailability of peptides by multiple N-methylation

Several strategies have been used in order to reduce the enzymatic cleavage and uptake into the systemic blood circulation of peptides, including prodrug approaches,[162] peptidomimetics and structural modifications such as covalent attachment of PEG,[163] lipidation,[164] and chemical modifications e.g. cyclization,[9] D-amino acid substitution and N-methylation.[45] Cyclic peptides show improved chemical stability and thereby display longer biological half-life compared to their linear counterparts.[37] Yet, additional modifications are required to generate peptides with enhanced enzymatic stability and improved oral bioavailability. One of the techniques suggested to improve the enzymatic stability of peptides is N-methylation.[119,165]

Inspired by the bioavailability of the highly N-methylated transplantation drug cyclosporin A (oral bioavailability 28±18%),[166] which violates all Lipinski’s rules,[106] we considered that multiple N-methylation together with cyclization might help to overcome the above mentioned bioavailability drawbacks of peptides, providing we retain the biological activity and receptor selectivity simultaneously.

To test our hypothesis, we considered the multiple N-methylation of the well known Somatostatin analogue Veber-Hirschmann cyclic hexapeptide cyclo(-PFwKTF-) developed at Merck Inc. in the late 70’s.[167]

4.5.1 Somatostatin

Somatostatin is one of the oldest peptides in neurobiology. It was discovered in 1972 as a part of the releasing hormones family for its property to inhibit the secretion of growth hormone from pituitary cell monolyers *in vitro*.[168] It was isolated from ovine hypothalamus and was shown to be a cyclic tetradecapeptide. Later it was found that the native somatostatin occurs in two biologically active forms, somatostatin-14 and a 28-residue peptide

somatostatin-28 (Figure 4.4). Both are derived from the same polypeptide precursor prosomatostatin.[169]

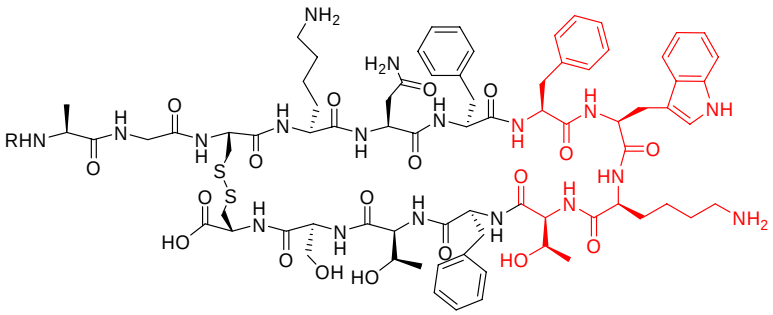

1. (SRIF-14) R = H
2. (SRIF-28) R = H-Ser-Ala-Asn-Ser-Asn-Pro-Ala-Met-Ala-Pro-Arg-Glu-Arg-Lys-

Figure 4.4. *Structures of the natural somatostatin peptide agonists SRIF-14 and SRIF-28. The pharmacophore is highlighted. SRIF, somatotropin-release inhibiting factor.*

SRIF's (somatotropin-release inhibiting factor) induces its biological effects, all inhibitory in nature, by binding to the G-protein-coupled receptors (GPCRs) on target cells, and function as neuromodulators and neurotransmitters, as well as potent inhibitors of various secretory process and cell proliferation.[170]

SRIFs have a broad inhibitory effect on both endocrine secretions – for example, of growth hormone, insulin, glucagon, gastrin, cholecystokinin, vasoactive intestinal peptide (VIP), and secretin – and exocrine secretion – for example, of gastric acid, intestinal fluid, and pancreatic enzymes.[171]

Because of its wide range of physiological functions, somatostatin play an important role in the treatment of numerous human diseases, including: diabetes type I and II; hypersecretory tumors, such as growth hormone-secreting pituitary adenomas, gastrinomas, insulinomas, glucagonomas, and vipomas; and gastrointestinal disorders, including bleeding gastric ulcers, pancreatitis, complications due to pancreatic surgery and pancreatic fistulae.[172,173] However, the clinical use of somatostatin has been hampered because of some disadvantages of the native hormone, such as its very short half-life in the circulation (<3 min) and its lack of selectivity. Therefore, there is an utmost need for the development of stable compounds with SRIF-like properties to show an improved clinical profile.[171]

4.5.1.1 Somatostatin receptor subtypes

Five different somatostatin receptors, referred to as sst1-5 have been cloned and characterized.[174] The receptor sequences ranges from 356 (sst2) to 418 (sst3) amino acids in length (Figure 4.5). There is a significant sequence similarity between SRIF receptor subtypes (39-57%) and a high similarity when compared across species (81-98% for mouse, human,

and rat homologues). The different properties and pharmacological behaviors of sst1-5 are summarized in Table 4.1.

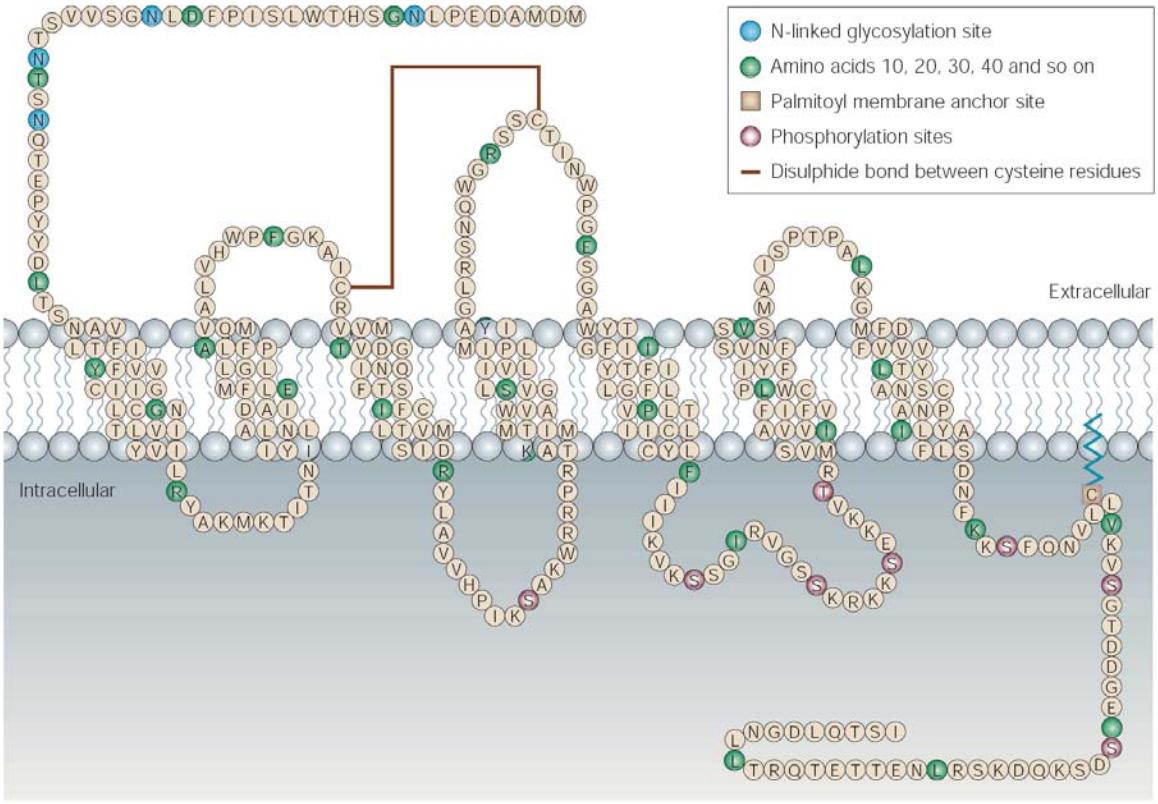

Figure 4.5. *Structure of receptors exemplified by subtype sst_{2A} receptor. Sites for potential N-linked glycosylation (blue) and phosphorylation (pink) are indicated. A predicted disulfide bond and the location of a potential palmitoyl anchor site are shown as well. Sst, somatostatin receptor.* Copyright © 2003.

SRIF receptors have seven α-helical transmembrane domains and are coupled to guanine-nucleotide-binding proteins.[175] In humans, sst1-5 are encoded by five non-allelic genes on chromosomes 14, 77, 22, 20, and 16 respectively. On the basis of structural, phylogenetic, and pharmacological features, SRIF receptors can be subdivided into two main classes: $SRIF_1$, which comprises sst2, sst3, and sst5; and $SRIF_2$, which includes sst1 and sst4 (Figure 4.6).

Table 4.1. *SRIF properties and signaling.* Copyright © 2003.

Criteria	Receptor subtype				
	sst_1	sst_2	sst_3	sst_4	sst_5
Signalling					
G-protein coupling	Yes	Yes	Yes	Yes	Yes
Adenylyl cyclase activity	↓	↓	↓	↓	↓
Phosphotyrosine phosphatase activity	↑	↑	↑	↑↓	↑
MAP kinase activity	↑	↑↓	↑↓	↑	↓
K^+ channels (GIRK)		↑	↑	↑	↑
Ca^{2+} channels	↓	↓			
Na^+/H^+ exchanger	↓		↓	↓	
AMPA/kainate glutamate channels	↑	↓			
Phospholipase C/IP_3 activity	↑	↑	↑	↑	↑↓
Phospholipase A_2 activity				↑	
Secretion					
Growth hormone	↓	↓		↓	↓
Insulin		↓			↓
Glucagon		↓			
Adrenocorticotropin		↓			↓
Ghrelin		↓			
Interferon-γ		↓			
IgM		↑			
Amylase					↓
Gastric acid		↓			
Cell growth and death					
Proliferation	↓	↑↓	↓	↑↓	↓
Apoptosis		↑	↑		
Properties of human SRIF receptors					
Gene	*SSTR1*	*SSTR2*	*SSTR3*	*SSTR4*	*SSTR5*
Chromosome	14q13	17q24	22q13.1	20p11.2	16p13.3
Number of amino acids	391	369/356	418	388	364
Swiss Prot ID	P30872	P30874-1/ P30874-2	P32745	P31391	P35346
Molecular weight (kDa)	42.7	41.3	45.9	41.9	39.2
Transcript size (kb)	4.3	1.1	1.1	1.2	1.1
Glycosylation sites	3	4	2	1	3
Reference sequence	NM_001049	NM_001050	NM_001051	NM_001052	NM_001053
Expression					
Tissue distribution (sst_{1-4} are rather ubiquitous)	Brain, pituitary, pancreas, stomach, liver, kidneys	Brain, pituitary, pancreas, lymphocytes, VSMC, stomach, kidneys	Brain, pituitary, pancreas, T cells, stomach	Brain, pancreas, stomach, lungs, placenta	Lymphoid cells, pituitary, pancreas, stomach

MAP, mitogen-activated protein; SRIF, somatotropin-release inhibiting factors; *SSTR*, somatostatin receptor gene; VSMC, vascular

All five SRIF receptor subtypes bind to their natural ligand SRIF-14 and SRIF-28 with nanomolar affinity. However, there is a selective binding profile for short synthetic SRIF analogs. The pharmacological characterization of SRIF receptor subtypes has been accelerated by the recent availability of a growing number of receptor-selective agonists and antagonists. However, their clinical utility is mainly limited by inadequate pharmacokinetic properties.

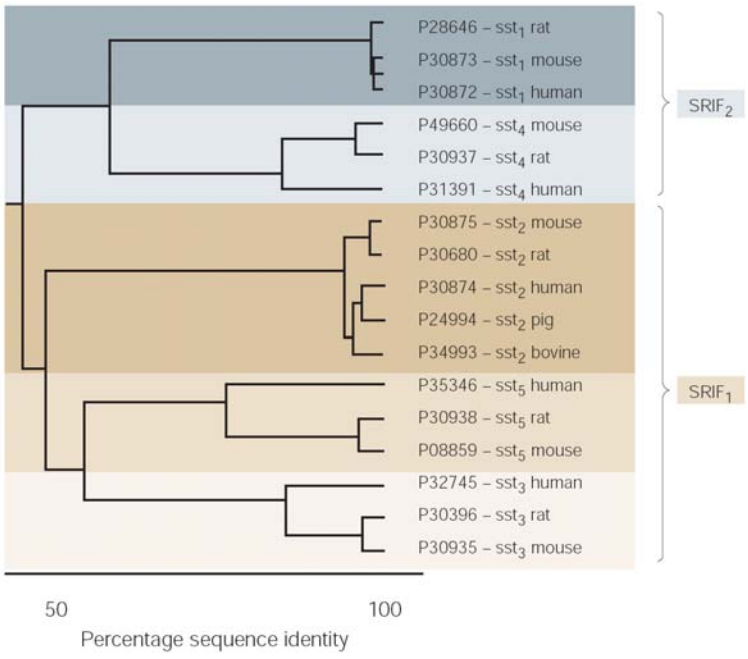

Figure 4.6. *Sequence homology between the respective receptor subtypes $SRIF_1$ (sst2,3,5) and $SRIF_2$ (sst1,4). SwissProt accession numbers are shown as well. $SRIF_2$ receptors fail to bind octreotide, whereas $SRIF_1$ receptors exhibit medium to high affinity for this ligand.*[176] Copyright © 2003.

4.5.1.2 Signal transduction

Signalling through SRIF receptors is a complex process involving the binding of somatostatins (SRIFs) to various SRIF receptor subtypes. Binding of these ligands to SRIF receptors induces G-protein activation and signaling through various pathways. As a consequence, the activities of several key enzymes, including adenylate cyclase, phosphotyrosine phosphatases (PTPases), and mitogen-activated protein kinase (MAPK) are modulated along with changes in the intracellular levels of calcium and potassium ions.

SRIF receptor stimulation is coupled to the respective intracellular signaling pathways through activation of specific G-proteins, including pertussis-toxin-sensitive $G_{\alpha i}$ and $G_{\alpha o}$, as well as pertussis-toxin-insensitive $G_{\alpha q}$, $G_{\alpha 14}$, and $G_{\alpha 16}$ proteins.[177] The interaction of certain G-proteins and SRIF receptor subtypes depends on factors such as their tissue-specific expression; for example, $G_{\alpha o}$ is found in neuronal cells, but is absent in B lymphocytes, whereas both cell types express sst2 receptor subtype (Figure 4.7).[177]

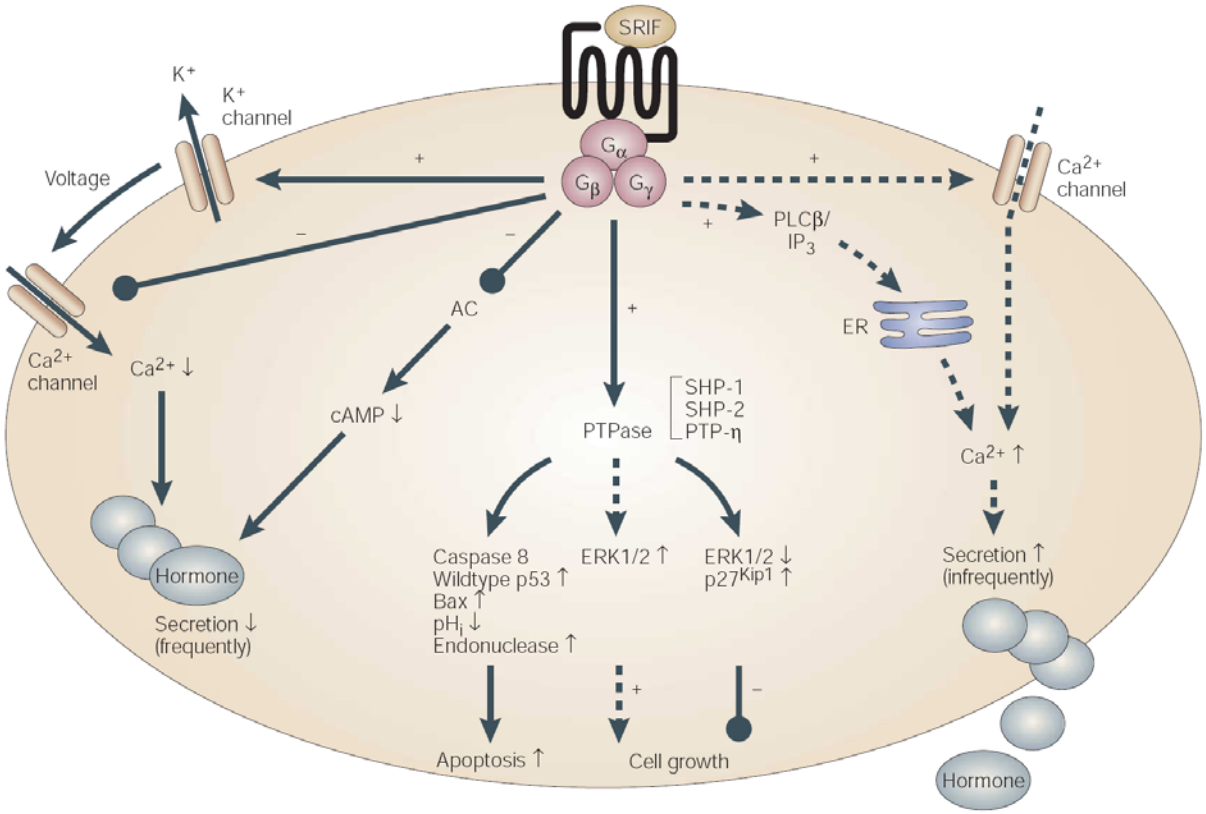

Figure 4.7. *SRIF-receptor-mediated modulation of signaling cascades leading to changes in hormone secretion, apoptosis and cell growth. In most cells, SRIF inhibits hormone as well as other secretions. Increased secretion is observed, for example in B-cells. SRIF plays a role in the control of cell growth and apoptosis. In a G-protein-dependant manner, PTPases, such as SHP-1, are activated, leading to dephosphorylation of signal-transducing proteins. SRIF-induced inhibition of ERK1/2 blocks degradation of the cyclin-dependant kinase inhibitor* $p27^{kip1}$*, leading to growth arrest. In rare cases, SRIF can stimulate proliferation. AC, adenylyl cyclase; ER, endoplasmic reticulum; ERK, extracellular signal-regulated kinase;* G_a*,* G_b*,* G_g*, G-protein subunit; PLC, phospholipase C;* IP_3*, inositol triphosphate; pHi, intracellular pH; PTPase, phosphotyrosine phosphatase.* Copyright © 2003.

All known human SRIF receptors can inhibit adenylate cyclase and hence decrease cyclic AMP levels.[178] This pertussis-toxin-sensitive action affects various downstream elements, in particular protein kinase A. The latter, in turn, acts as an activator of a cAMP-response-element-binding protein.

In most cells, Ca^{2+} signaling is downregulated by SRIF receptor activation owing to the inhibition of calcium channels and intracellular Ca^{2+} release or the activation of K^+ channels, which results in membrane hyperpolarization.[175] Accordingly, all human SRIF receptor-subtypes can be coupled to various phospholipase C (PLC) isoforms.[179] In certain systems, however, SRIF receptor activation increases the enzymatic activity of PLC_{b2} and PLC_{b3}, for example, and hence the intracellular levels of inositol triphosphate (IP_3) and Ca^{2+}.[180]

4.5.1.3 Somatostatin analogs

Biologically active SRIF analogs can be grouped into two classes: SRIF peptide agonists and antagonists. The availability of cloned SRIF receptor subtypes has enabled the detailed characterization of the binding properties of SRIF and SRIF analogs. To overcome the therapeutic limitation of SRIF-14 – namely its very short plasma half-life of <3 min – two strategies were undertaken. The first strategy focused on short-chain, metabolically stable analogs, typically showing selectivity for one (or a minority of) sst receptors, and the second strategy was based on larger SRIF analogs that bind to the majority of sst receptors, but which require metabolic stabilization through subsequent chemical modifications involving the incorporation of D-amino acids or N-methylated amino acids.

The initial work on the development of somatostatin analogs was carried out by the Salk group[181] they synthesized series of several somatostatin related peptides involving:

- shortening of the peptide from N- and C- terminus
- systematic deletion of residues
- replacement of single residues by alanine
- replacement of each residue by its D-counterpart
- replacement of each residue by different amino acids
- deletion and/or modification of multiple residues.

From these studies, it was revealed that replacing Trp^8 with D-Trp^8 the potency of SRIF increased by 6-8 times. Based on these results it was also suggested that 6-11 amino acid region is important in retaining the activity of the analog.

These results prompted Veber et al. to synthesize a series of reduced size somatostatin analogs, the most interesting of which was the highly active cyclic hexapeptidic analog: cyclo(-PFwKTF-) named L-363,301 (Figure 4.8).[167]

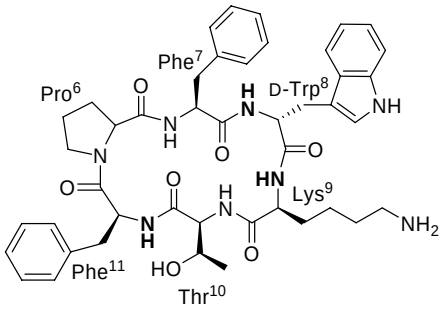

Figure 4.8. *L-363,301: Veber-Hirschmann peptide. The numbering in the sequence refers to the position of the residue in the native somatostatin. The amides showed in bold are the potential sites of N-methylation, which gave rise to bioactive analogs.*

The sequence consists of the amino acids from the native hormone, position 7-11, with L-Trp replaced by the D-isomer. A proline residue at position 6 was utilized to form the cyclic

hexapeptide derivative through an amide linkage. The molecule had higher activity than native somatostatin in inhibiting the release of GH, insulin, and glucagon.[182]

Further modification of L-363,301 resulted in the synthesis of MK-678 (Figure 4.9) also called seglitide:[183] which showed at least 10 fold greater potency than the parent compound in all biological tests and 50-100 times the potency of SRIF for the inhibition of insulin, glucagon, and GH release. It shows high affinity in binding to sst2 receptor and reduced affinity towards sst3 and sst5.

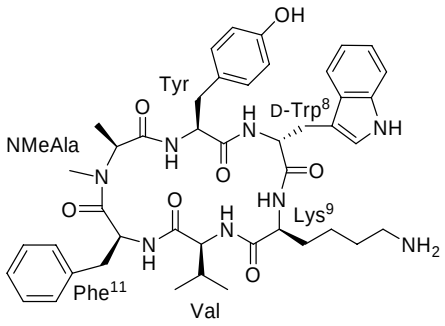

Figure 4.9. *MK-678: Seglitide. Note the NMeAla in place of the proline in Veber-Hirschmann peptide, which induces a cis-peptide bond formation.*

Bauer et al.[184] chose as a conformationally adequate surrogate for somatostatin sequence, the cyclic hexapeptide described first by Vale et al. cyclo(-Cys-Phe-D-Trp-Lys-Thr-Cys-), which, however, showed only 1/1000 of the activity of SRIF in pituitary cell culture *in vitro*. They proceeded to prepare close analogs of this hexapeptide in search of peptides that would selectively inhibit the secretion of GH and to be more stable than somatostatin by incorporating additional residues at both ends of the molecule. One of the amino acid residues of SRIF thought to be important is Phe^6, which in the cyclohexapeptide described by Vale et al. was replaced by Cys. Thus, D-Phe was added to the N-terminal of the hexapeptide, and eventually proved to be advantageous for the activity of the resulting peptide. The aromatic side chain of this additional amino acid can occupy at least some of the conformational space available to Phe^6 in somatostatin and being an unnatural amino acid also protects the disulfide bridge against enzymatic attack. Addition of the enzymatically stable amino alcohol, threoninol (Thr-ol), to the cycloheptapeptide C-terminal further increased the activity (Figure 4.10).

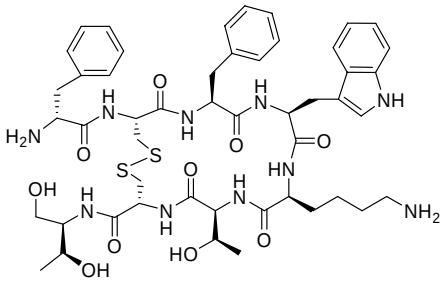

Figure 4.10. *SMS 201-995: Octreotide (Sandostatin).*

The resulting octapeptide SMS 201-995 or octreotide was characterized by greater potency than the native somatostatin, longer duration of action, and the half-life of octreotide is ~ 117 min, greater metabolic stability, and higher selectivity in GH inhibition compared with insulin and glucagon. Octreotide which is 70 times more potent in inhibiting GH *in vivo* than SRIF and 3 times more potent *in vitro* is protected against enzymatic degradation by the D-Phe residue at the N-terminus and by the amino alcohol at the C-terminus. It exhibits high affinity binding to sst2, along with intermediate binding to sst3 and sst5. SMS 201-995 was introduced into clinical practice in 1987 for the treatment of hormone-secreting pituitary adenomas and gastroenteropancreatic tumors.[185]

Recently, Bruns et al. reported the development of another cyclohexapeptide analog SOM230 (Figure 4.11), which exhibits for the first time, that near-universal, high affinity binding to sst1, sst2, sst3, and sst5.[186] This analog is based on the cyclohexapeptide template; however, it incorporates novel functionalized side-chains, such as tyrosylbenzyl, to mimic two essential Phe residues, and hydroxyproline with a basic extension to mimic Lys^4 of SRIF-14. SOM230 is a highly potent inhibitor of the growth hormone /IGF-1 axis in rats, dogs, and monkeys, as well as in healthy human subjects and acromegalic patients.[187]

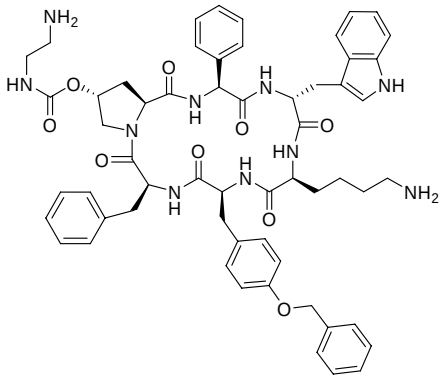

Figure 4.11. *SMS230. Potent high affinity binder to sst1, sst2, sst3, and sst5.*

Another promising approach towards the development of metabolically stable somatostatin analogs are the β-peptides (Figure 4.12). These analogs are intermediates to peptides and non-peptides due to their reduced number of peptide bonds. However, the potency of β-peptides so far has not surpassed 83 nM for sst4.[188]

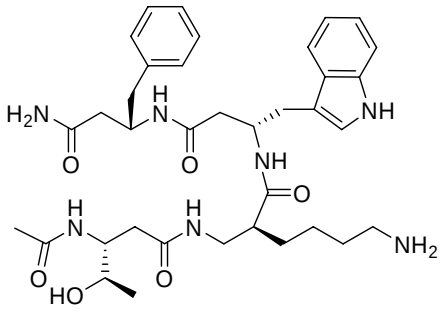

Figure 4.12. *β-peptidic analog of somatostatin showing affinity towards sst4.*

4.5.1.4 Multiply N-methylated Somatostatin analogs

In spite of a plethora of agonists available, none of them are orally available. Thus, we planned an multiple N-methyl scan of Veber-Hirschmann cyclic hexapeptide cyclo(-PFwKTF-). Although mono N-methylation has been employed by several other groups to modulate the activity and selectivity profile of somatostatin, multiple N-methylation has never been employed, probably owing to the difficulty in the synthesis of N-methylated amino acids of various functionalities, and their subsequent difficult coupling.[35,189]

4.5.1.5 Synthesis of multiply N-methylated library

Each peptide in the N-methyl scan library (Table 4.2) was synthesized by standard Fmoc strategy on TCP (Tritylchloride polystyrene) resin. N-Methylamino acids were before hand prepared in solution and then used on solid-phase. N-Methylated L-phenylalanine was obtained by using the procedure described by Freidinger et al.[49] However, to obtain N-methylated lysine(Boc), tryptophane(Boc) and threonine(t-Bu), we employed the approach of Fukuyama et *al.*,[54] where the amine of the amino acid methyl ester was protected by *o*-nitrobenzenesulfonyl group (*o*-NBS) followed by alkylation or Mitsunobu reaction on the activated nitrogen with the final deprotection of the *o*-NBS group.[57] The *o*-NBS group was introduced by treatment of the corresponding methyl ester with *o*-nitrobenzenesulfonylchloride in presence of triethylamine in dry methylene chloride.[190] The N-methylation was achieved by the treatment of the *o*-NBS protected amino acid with less expensive strong, hindered, non-ionic base DBU (1,8-diazabicyclo[5,4,0]undec-7-ene) and dimethylsulfate in DMF at 0°C for 15 min. giving quantitative yield. N^{α}-Protected-N^{α}-methylamino acids were coupled to the resin-bound amine free peptides by using HOBt/TBTU and DIPEA for one hour and couplings to N-methylated amino acids were achieved using HOAt/HATU and DIPEA for two hours in NMP (*N*-methyl-2-pyrollidone).[191] However, the coupling of threonine to the NMe-Phe was difficult and needed longer period (>4 hours), which is probably owing to the turn structure adopted by the peptide on the resin,

which prevented the exposure of the N-methylated amino group to undergo the coupling. Finally, the *o*-NBS group was removed with mercaptoethanol and DBU in DMF in 10 minutes (2 x 5 min).[191] During peptide synthesis, every step was monitored by reversed phase analytical HPLC and ESI-MS spectrometry for incomplete coupling and racemization.

Table 4.2. *HPLC and MS profile of all the synthesized N-methylated analogs of Veber-Hirschmann peptide. The binding affinities of the eight significant binders are elaborated. The one letter amino acid codes in gray are N-methylated. The pKd values are given towards hsst2 and hsst5 receptors expressed in CCL-39 cells and measured by radioligand binding assays with [125I]LTT-SRIF28 as radioligand.*[192]

Sequence						MW	HPLC	MS	pIC50	hSSt-2		hSST-5	
c(wKTFPF)							10-100%			pKd	Kd (nm)	pKd	Kd (nm)
w	K	T	F	P	F	806.4	16.2	807.4	<9	8.01	9.77	7.82	15.14
w	K	T	F	P	F	820.4	16.4	821.5	<8				
w	K	T	F	P	F	820.4	16.4	821.5	<9	7.82	15.14	8.03	9.33
w	K	T	F	P	F	820.4	16.3	821.4					
w	K	T	F	P	F	820.4	16.7	821.4	>9	8.6	2.51	8.19	6.46
w	K	T	F	P	F	820.4	17.0	821.5	<9	7.61	24.55	7.87	13.5
w	K	T	F	P	F	834.4	17.3	835.5	<7				
w	K	T	F	P	F	834.4	17.3	835.5	<8				
w	K	T	F	P	F	834.4	18.5	835.5	<8				
w	K	T	F	P	F	834.4	16.9	835.4	<8				
w	K	T	F	P	F	834.4	15.1	835.5	<7				
w	K	T	F	P	F	834.4	17.4	835.5	<9	7.96	10.96	7.39	40.74
w	K	T	F	P	F	834.4	17.4	835.5	<8	7.16	69.18	7.47	33.88
w	K	T	F	P	F	834.4	16.1	835.4	<7				
w	K	T	F	P	F	834.4	17.3	835.4	<7				
w	K	T	F	P	F	834.4	17.7	835.4	<9	7.6	25.12	7.19	64.56
w	K	T	F	P	F	848.5	16.6	849.4	<7				
w	K	T	F	P	F	848.5	18.9	849.5	<8				
w	K	T	F	P	F	848.5	18.1	849.4	<7				
w	K	T	F	P	F	848.5	17.7	849.5	<7				
w	K	T	F	P	F	848.5	17.3	849.5	<7				
w	K	T	F	P	F	848.5	17.3	849.5	<8				
w	K	T	F	P	F	848.5	16.3	849.5	<7				
w	K	T	F	P	F	848.5	16.8	849.5	<7				
w	K	T	F	P	F	848.5	18.3	849.5	<8	7.21	61.66	7.22	60.25
w	K	T	F	P	F	848.5	18.1	849.4	<7				
w	K	T	F	P	F	862.5	16.2	863.5	<7				
w	K	T	F	P	F	862.5	17.2	863.4	<7				
w	K	T	F	P	F	862.5	17.4	863.5	<7				
w	K	T	F	P	F	862.5	17.6	863.4	<7				
w	K	T	F	P	F	862.5	17.9	863.5	<7				
w	K	T	F	P	F	-	-	-					

The linear precursors were cleaved off the resin by treatment with a solution of CH_2Cl_2/AcOH/TFE (6:3:1) thrice for 1 hour followed by solvent evaporation, co-evaporation with toluene and lyophilization to remove traces of acetic acid. The cyclization was performed under high dilution condition (5mM) in DMF for 48 hours, using the solid base method with $NaHCO_3$ and DPPA.[193] After cyclization, monitored by ESI-MS spectrometry, the peptides were precipitated in brine and centrifuged, and washed two to three times in water to remove the cyclizing agents completely. The cyclized peptides were finally purified by RP-HPLC and lyophilized to obtain the hydrophobic protected peptides. The *t*-Bu and the Boc protecting group were finally cleaved by 1:1 (TFA:DCM) and the hydrophilic peptides precipitated over ether yielding >98% pure peptides.

Although the synthesis of linear peptides was straightforward, cyclization proved to be a crucial step. The site of cyclization was crucial in determining the final yield of the peptides. As the conformation of the stem peptide cyclo(-PFwKTF-) is known to have a βII' turn about D-Trp[8] and Lys[9] and a βVI turn about Phe[11] and Pro[6],[194] Lys[9] was chosen as the C-terminal amino acid to load the TCP resin in case of all the peptides, where Thr[10] was non N-methylated. On the other hand, when Pro[6] and Phe[7] were taken as C- and N- terminal respectively, the peptide completely failed to cyclize in spite of very high yield of the linear peptide compared to the previous case (Figure 4.13). Thus, terminals for efficient peptide cyclizations should be chosen in a way which results in the closure of a turn; preferably a βII turn, due to the strong propensity of the linear peptide to form a turn. Thus, during cyclization, though the linear peptide exhibits a dynamic nature in solution, a turn structure will always be preferred bringing the N-terminal and C-terminal ends in vicinity to enhance cyclization. It is also worth mentioning that during the scaling up the synthesis of analog **S8**, the cyclization with HATU/HOBt and collidine gave excellent results.[195]

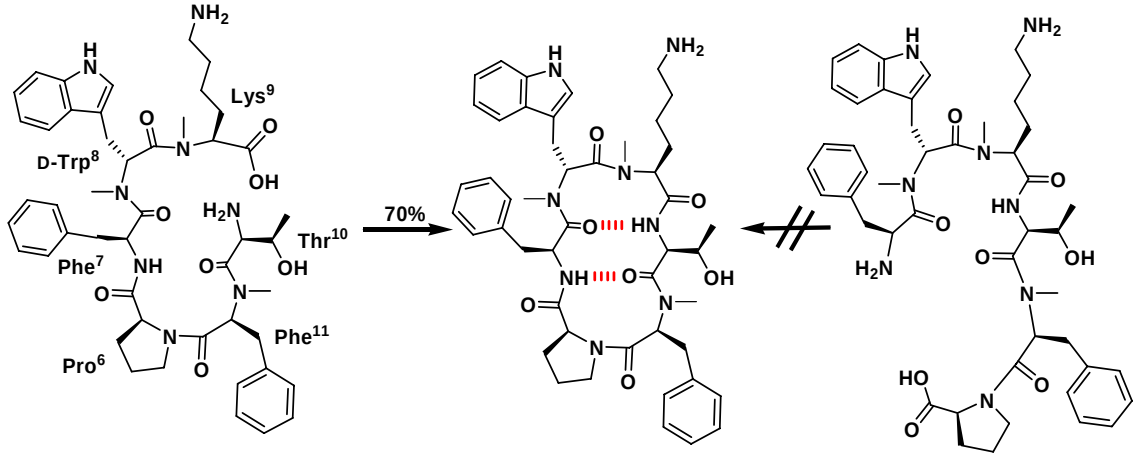

Figure 4.13. *Choice of preferred cyclization site in a linear peptide -PFMewMeKTMeF- (red lines: hydrogen bonds). The cyclization yield is given.*

4.5.1.6 Binding affinity and *in vivo* tests

In vitro screening of the N-methylated cyclic hexapeptide library by binding to all the human SRIF receptor subtypes (hsst1-5), resulted in only 7 analogs showing affinity in the nanomolar range towards receptor subtypes hsst2 and hsst5 (Table 4.2). All these 7 analogs were selective towards sst2 and sst5, like the parent peptide (Table 4.3); no other receptor subtype selectivity was obtained. These seven analogs had N-methylation at D-Trp^{8}, Lys^{9}, and Phe^{11} or a combination of these three. N-methylation at any other site resulted in the loss of binding affinity. It is interesting to note that the amide protons of these residues are not involved in any hydrogen bonding which stabilizes the bioactive form of the peptide. Thus, N-methylation of these residues does not cause any drastic change in the orientation of the side chains resulting in the loss of the binding affinity. These resulting 7 analogs were administered into rats to check their uptake into blood and interestingly, only **S1** and **S8** (given 10 mg/Kg p.o.) showed significant uptake into the blood stream with a plasma concentration of 242 ng/mL after 30 min and 151 ng/mL after 1 h of **S8**, compared to 158 ng/mL and 38 ng/mL at the same time points for the parent peptide **S1** (Table 4.3). Thus, we decided to characterize the detailed pharmacology including the mode of transport of **S1** and **S8**.

Table 4.3. *The pKd values and plasma concentration of the N-methylated bioactive peptides* ***S1-S8***.

Peptide	N-methylated amino acid	hsst 2 (pK_d)	hsst 5 (pK_d)	Time (hr) 0.5	1.0	3.0
Octreotide	None	9.18	7.71	-	-	-
S1	None	8.01	7.82	158	38	0
S2	Lys^{9}	8.60	8.19	38	9	0
S3	Phe^{11}	7.93	8.28	0	0	0
S4	D-Trp^{8}	7.61	7.87	0	0	0
S5	Lys^{9}, Phe^{11}	7.96	7.39	10	0	0
S6	D-Trp^{8}, Lys^{9}	7.60	7.19	28	0	0
S7	D-Trp^{8}, Phe^{11}	7.16	7.47	13	0	0
S8	D-Trp^{8}, Lys^{9}, Phe^{11}	7.21	7.22	242	151	0

4.5.1.7 Pharmacokinetics of the peptide sub-library

Enzymatic stability of the peptides

The stability of the peptide sub-library was evaluated in rat serum. No significant degradation was observed for any of the peptides up to 7 h incubation (Fig. 4.14).

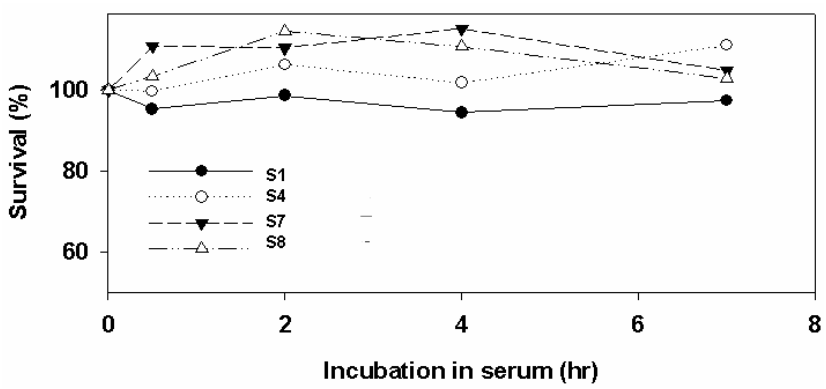

Figure 4.14. *Stability of peptides* ***S1****,* ***S4****,* ***S7,*** *and* ***S8*** *in rat serum. The tested molecules were mixed with fresh rat serum and incubated in 37°C for 7hrs, n=3.*

In addition to serum stability, analogs **S1** and **S8** were evaluated for their stability in the GI tract using enzymes isolated from the brush border (Brush Border Membrane Vesicles, BBMVs). These enzymes include a variety of peptidases which participate in the digestive function of peptides and proteins in the gut wall[196] thus can serve as an *in vitro* tool to evaluate peptide stability in the GI tract. As can be seen in Figure 4.15, the non-methylated stem peptide, analog **S1,** was degraded following exposure to intestinal enzymes. After 30 and 90 minutes incubation, 15% and 25%, respectively of the peptide was degraded. Comparably, analog **S8** was found to be completely stable to enzymatic degradation, under the assay conditions. Its concentration remained constant and similar to zero time concentration, up to 90 minutes.

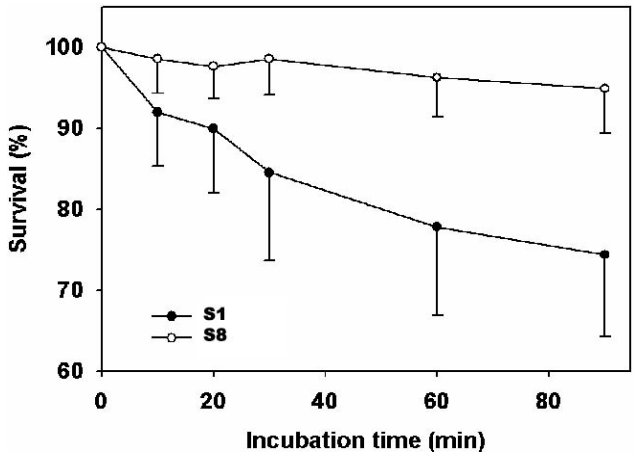

Figure 4.15. *Stability of* ***S1*** *and* ***S8*** *in brush border membrane vesicles (BBMVs). The tested molecules were mixed with BBMVs and incubated in 37 °C for 90 minutes, n=4. Data are expressed as the mean±SEM (standard error of the mean value). Statistical analysis gave a "student's t test" value of p<0.05.*

Intestinal permeability

The peptides were evaluated for their intestinal permeability using the Caco-2 *in vitro* model and compared to mannitol, a marker for paracellular permeability. The calculated

permeability coefficients (P apparent, P_{app}) of the tested compounds are depicted in Figure 4.16. The permeability of analogs **S1**-**S4** and **S6**-**S7** was lower than 1×10^{6} cm/sec.

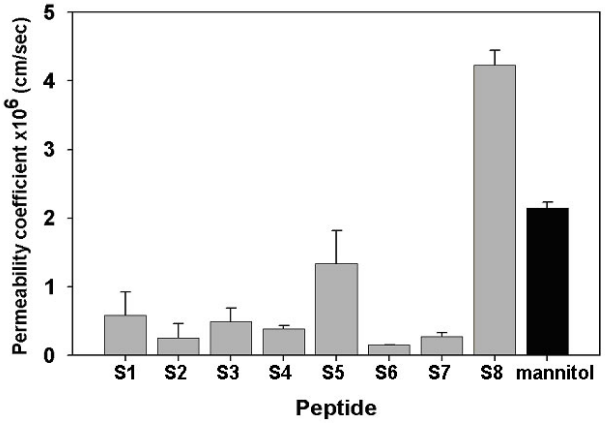

Figure 4.16. *Permeability coefficient (P apparent, Papp) of the 8 analogs compared to mannitol, a paracellular marker. Caco-2 monolayers were incubated with the tested molecules at 37°C, added to the apical side and further detected by HPLC-MS at the basolateral side (A to B) for 150 minutes.*

Analog **S5** was found to be relatively more permeable (1.8×10^{6}cm/sec), interestingly analog **S8** was found to have the highest P_{app} value (4×10^{6} cm/sec). The P_{app} of the analogs was found at the same order of magnitude as mannitol. In order to evaluate the involvement of active transport mechanism in the permeability process, analog **S8** was evaluated for its permeability from apical to basolateral (A to B) compared to basolateral to apical (B to A) (Figure 4.17). The permeability rate was found to be identical for both sides suggesting that no active transport is involved in the permeability of analog **S8**.

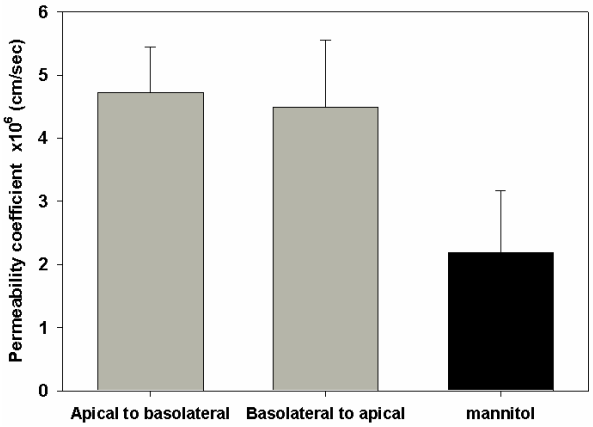

Figure 4.17. *Permeability of **S8** from A to B compared to B to A., n≥3 ± SEM.*

A novel colorimetric assay[197] was used to assess whether the peptides tend to interact with a bilayer liposome as a model of the cell membrane. When comparing a set of analogs with an identical number of N-methyl groups (Figure 4.18), there were two analogs (**S6** and **S7**) with enhanced interaction with the liposome (>85%) while analog **S5** interacted poorly with the vesicle membrane (<20%).

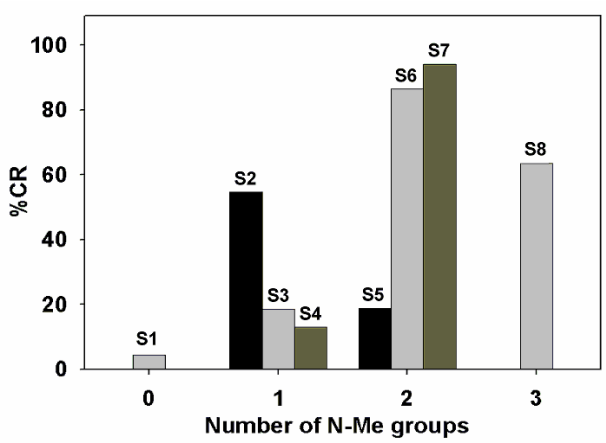

Figure 4.18. *The effect of N-methyl position on interaction with the liposomal model of the cell membrane (%CR). Analogs with identical number of N-Me groups (mono-methyl-peptides **S2-S4**, di-methyls-peptides **S5-S7**) were screened together with **S1** and **S8** for interaction with the bilayer liposomal model.*

Analog **S1** showed negligible interaction with the membrane, indicating that it is unable to penetrate through the model bilayer, while **S8** showed a significant interaction with the membrane. These results suggest that, although the increase in lipophilic nature of the analogs by additional N-methyl groups, as would be found by clogP values, results in an increased interaction with the membrane, there is no linear correlation between subsequent addition of N-methyl groups and enhanced interaction with the membrane (indicated by a significant color reaction). In other words, the data show the importance of the N-methyl position as different degrees of interaction derived from peptides having the same number of N-Me groups at different positions.

Oral bioavailability

The pharmacokinetic parameters of analogs **S1** and **S8** are significantly different including a five fold difference in the elimination half-life (15.5±2 and 74±6min, respectively) and a ten-fold difference in the volume of distribution at steady state (Vss, 0.3±0.1 and 3.7±1.3 L/kg, respectively). Additional distinctive characteristics were revealed following per oral (p.o.) administration. Following administration of **S1** and **S8** by oral gavage, at a dose which is one magnitude of order higher that the intravenous (i.v.) dose (i.e., 10 vs. 1 mg/kg, respectively), peptide **S1** could be detected only in one rat (out of 4); therefore a pharmacokinetic profile following oral administration could not be depicted. On the other hand, using the same dose for analog **S8** provided a full pharmacokinetic profile of concentration vs. time in blood (Figure 4.19). The calculated absolute oral bioavailability of analog **S8** was 9.9%.

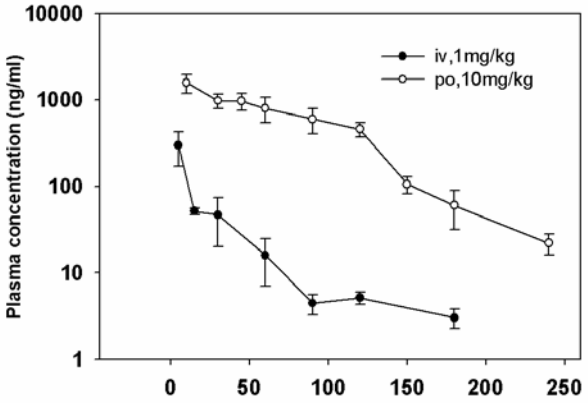

Figure 4.19. *Plasma concentration-time profiles (Mean ± SEM) following oral (○) and intravenous (●) administration of peptide* ***S8****, n≥4.*

The impact of N-methylation was evaluated in two different biological media, blood and intestinal wall (BBMV's) that contain different types of peptide degrading enzymes, and are very relevant in dictating the pharmacokinetic fate of the bioactive peptide in the body. As can be seen in Figure 4.14, the peptides were found to be stable in rat serum. This result was expected, in view of the fact that all the peptides in the sub-library are cyclic and the limited diversity of enzymes in plasma.[198,199] On the other hand, comparing the two extreme case of no N-Me vs. tri- N-Me peptides (i.e., peptides **S1** and **S8**) in purified brush border enzymes (Figure 4.15) revealed the significant contribution of multiple N-methylation to the enzymatic stability of peptide **S8**. This finding may explain the high stability of the drug cyclosporine A, in human serum[200] as indicated by its relatively long biological half life, 6.2 hours (in man).[201] Cyclosporine A, similarly to **S8,** is cyclic, multiply N-methylated, and also exhibits metabolic stability against the harsh peptidase activity in the intestinal wall. This stability against peptidases degradation is most probably attributed to the synergistic impact of cyclization together with multiple N-methylation. An additional factor that limits the oral bioavailability of peptides is their low permeation through the intestinal wall. In the case where there is no active transport involved in the peptide absorption, they may penetrate across the enterocytes via passive diffusion mechanisms, either through the membrane (transcellular) or between the enterocytes (i.e., the paracellular pathway). While hydrophilic molecules tend to pass via the paracellular route in order to be absorbed across the intestinal wall, lipophilic compounds can permeate transcellularly. This route provides extensive flux, in comparison to the paracellular route mainly due to the significantly larger surface area.[202] It was suggested that by increasing the lipophilicity of peptides, the permeability could be improved due to transcellular absorption.[203] A potential approach to achieve increased lipophilicity is by multiple N-methylation. Thus, this structural modification could provide a possible shift from paracellular towards transcellular absorption mechanism. According to our findings in the

Caco-2 permeability model, all the tested peptides, except for peptide **S8** were found to have Papp values which are lower or comparable than the Papp of mannitol, a marker for paracellular transport. Nevertheless, the permeability coefficient of analog **S8** was significantly higher (68% increase) than the non N-methylated analog **S1**, suggesting that multiple N-methylation improved the intestinal permeability, even in the aqueous media of the pores in the tight-junction that are available for paracellular transport. The possibility of increased permeation due to active transport mechanism of **S8** was ruled out by the finding that there was no observed difference in the permeation rate of the peptide when measured from apical to basolateral side and vice versa (Figure 4.17).

In order to eliminate the possibility of model-dependent results, additional *in vitro* methods including MDCK cells[204] and side by side diffusion chamber[205] were used to verify the transport characteristics of **S8**. The permeability coefficient found in these models was in the range of paracellular transport (data not shown). Analogs **S1** and **S8** were evaluated for their oral bioavailability *in vivo* following i.v. and p.o. administration to rats (Figure 4.19). While the *Veber-Hirschmann* peptide was not orally available, the absolute oral bioavailability of the N-methylated peptide **S8** was about 10% of the administered dose. In addition, changes were also found in additional pharmacokinetic parameters. The enhanced volume of distribution of **S8** compared to **S1** (3.7 and 0.3 L/kg, respectively) suggests that while the distribution of **S1** is limited to the blood and the interstitial fluid, **S8** can interact with biological membranes. A difference was also found in the plasma half-life of **S1** and **S8** which may have resulted from reduction of proteolytic digestion or enhanced hepatic and/or renal clearance. The transcellular transport includes an interaction of the molecule with the hydrophobic membrane followed by crossing the membranes (i.e., the apical and basolateral membranes) in order to reach the circulation. Indeed, an increase in the interaction of the N-methylated peptides with a model of the cell membrane was observed for the N-methylated peptides (Figure 4.18). Yet, this liposomal model is limited to evaluate the interaction with the membrane, which is a mandatory but not exclusive condition to cross the membrane. The enhanced interaction of **S8**, observed in the membrane vesicle liposome model may clarify the discrepancy between the *in vitro* permeability models which show limited absorption and the enhanced volume of distribution, compared to **S1**. The fact that peptides with identical numbers of N-methyl groups hold different degree of interaction with the liposomal membrane model suggest that there are additional factors, including conformation, that affect the interaction.

4.5.1.8 Conformational changes resulting from N-methylation

Due to the binding affinity of the seven compounds, the solution structure of the active analogs with different sites of N-methylation was determined by using NMR, distance geometry calculation, and molecular dynamics simulation. The inter and intra proton distances were calculated from ROESY spectrum measured with a mixing time of 150 ms. The isolated spin pair approximation was used, setting the Phe^2/Phe^6 β protons to a distance of 1.78 Å. Restraints were obtained by adding and subtracting 10% to the calculated experimental distances, accounting for errors from the two spin approximation and cross peak integration. Metric matrix DG calculations were carried as described earlier. About 65-70 structures were calculated for each peptide of which >95% had a conserved backbone along with slight deviations in the spatial orientation of side chains of Phe^2, D-Trp^3, Thr^5 and Phe^6. However, in some peptides there was considerable flexibility in the orientation of lysine side chain. As the structures obtained from distance geometry are based on only molecular connectivity, they were further subjected to refinement by molecular dynamics. The MD simulation was done by the program DISCOVER using CVFF force field, wherein the molecule was placed in a cubic box of length 45 Å and soaked with DMSO. The restrained simulation was carried out for 150 ps. And then the average structure resulted from the restrained simulation was further subjected to free dynamics for a further 150 ps.

The almost complete chemical shift assignment of each peptide was achieved barring some overlapped aromatic protons. The chemical shift of the peptide shows nice correlation, suggesting the alikeness of the chemical environment and subsequently the conformation of the peptides. In the *Veber-Hirschmann* peptide, the upper half i.e. Phe^7-Thr^{10} is involved in a βII' turn with the D-Trp^8 at *i*+1 position of the turn, which is stabilized by the hydrogen bonding between Phe^7CO and $Thr^{10}H^N$.[194] The lower half of the peptide adopts a βVI turn, with a *cis*-peptide bond between Phe^{11}-Pro^6, which is stabilized by again a hydrogen bond between $Thr^{10}CO$ and Phe^7H^N. There has been a lot of discussion regarding the bioactive conformation of the peptide, where it was suggested by Goodman et al. that the peptide exhibits a 'folded' conformation, where there is a kink in the backbone at Phe^7 and Thr^{10}, which results in a bend in the backbone conformation.[206] This 'folded' conformation is stabilized by the two additional hydrogen bonds between Pro^6CO-D-Trp^8H^N and Lys^9CO-$Phe^{11}H^N$, forming two closed γ turns (Figure 4.20). In addition to the kinked backbone, close proximity of the indole ring of tryptophane and aliphatic side chain of lysine is necessary for the significant binding. However, Veber et al. suggested that the flat conformation of the peptide with the absence of the two γ turns is the bioactive conformation and they discarded

the possibility of the 'folded' structure as the solution structure or the bioactive conformation.[207]

The conformations of the analogs are explained sequentially beginning with **S4** (as usually the starting point is the D-residue).

cyclo(-D-MeTrp-Lys-Thr-Phe-Pro-Phe-) (S4). This peptide is N-methylated at the D-Trp and shows comparatively lower binding constant than the parent peptide. The ROESY spectrum along with the characteristic ROEs listed in the experimental section shows cross-peaks between $TrpH^{\delta1}$-$TrpH^{\alpha}$, $TrpH^{\delta1}$-$Lys^{H\gamma}$, which in a way fixes the orientation of the indole ring of tryptophane with respect to the peptide backbone and lysine side chain. The spatial orientation of lysine side chain is confirmed by the intra-residual ROE between $LysH^{N}$-$LysH^{\gamma}$, $LysH^{N}$-$LysH^{\beta}$, $LysH^{\alpha}$-$LysH^{\gamma}$, $LysH^{\gamma}$-$LysH^{Z}$ and by inter residual ROE between $LysH^{\beta}$-$ThrH^{N}$. It is to be noted that the chemical shift of the lysine γ protons are reported to be shifted up-field due to the anisotropic shielding provided by the indole ring of the tryptophane owing to the close proximity, where the lysine γ protons are facing the indole ring (Figure 4.20).[194] However, in this peptide there is no abnormal up-field shift of the γ protons which suggests that orientation of lysine side chain is slightly different than in the parent in spite of its close proximity to indole ring (Figure 4.21). The low temperature gradient value of $ThrH^{N}$ suggests its solvent shielded nature and the short distance of 2.6 Å between $ThrH^{N}$-$ThrH^{\alpha}$ and 2.9 Å between $ThrH^{N}$-$LysH^{\alpha}$ suggests the anticlockwise rotation of the plane of Lys-Thr peptide bond in the parent peptide, placing the $ThrH^{N}$ in between $LysH^{\alpha}$ and $ThrH^{\alpha}$. On the other hand, the ROE's $LysH^{N}$-$ThrH^{N}$ and $LysH^{B}$-$ThrH^{N}$ corresponding to 2.4 Å and 3.2 Å respectively, suggests the orientation of the peptide bond plane similar as in the parent peptide. However, the average structure arising from the MD simulation represents a violation of ROE's $ThrH^{N}$-$LysH^{\alpha}$ and $ThrH^{N}$-$ThrH^{\alpha}$ by 0.4 Å and 0.33 Å respectively which eventually suggests the absence of a standard βII' turn and a dynamics of the peptide bond giving rise to an open and closed γ turn about lysine simultaneously.

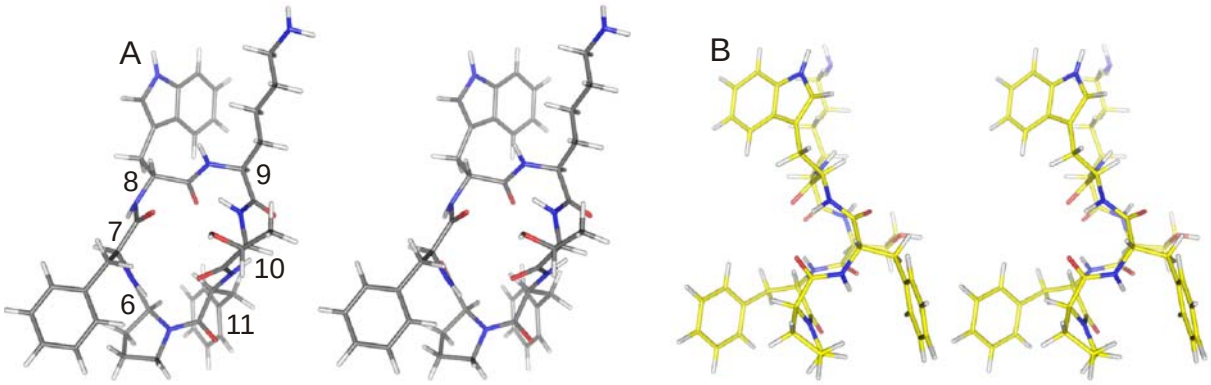

Figure 4.20. *Stereoview of the solution conformation of Veber-Hirschmann peptide* ***S1*** *A) Front view with the βII' and the βVI turn. B) Side view, note the fold in the backbone, resulting in the formation of two stabilizing γ turns between* $Pro^{6}CO$-D-$Trp^{8}H^{N}$ *and* $Lys^{9}CO$-$Phe^{11}H^{N}$.

This absence of βII' turn is actually owing to the N-methylation of tryptophane, as the N-methylated peptide bond twists anticlockwise with respect to the peptide bond in the parent accommodating the bulky N-methyl group, which otherwise experiences a strong steric clash with the α-methylene group of D-Trp and Phe^{7}. Concentrating on the other half of the peptide, the *cis*- peptide bond between Pro-Phe is conserved throughout the simulation forming a βVI turn which is confirmed by the low temperature gradient value of $Phe^{7}H^{N}$. The flexibility of the βVI turn is restricted by the ROE's between $Phe^{6}H^{N}$-$ProH^{\alpha}$, $Phe^{6}H^{N}$-$Phe^{11}H^{\alpha}$ and $Phe^{11}H^{N}$-$Phe^{11}H^{\alpha}$ corresponding to distances of 3.1 Å, 2.7 Å and 2.6Å respectively. The spatial orientation of the phenyl ring of Phe^{11} is dictated by the ROE's between $Phe^{11}H^{\delta}$-$ProH^{\alpha}$ and $Phe^{11}H^{\delta}$-$Phe^{11}H^{\alpha}$ corresponding to distances of 3.0 Å and 2.8 Å respectively exhibiting a *trans* rotamer of Phe^{11} side chain. The flexibility of Phe^{6} is also restricted and its spatial orientation directed by the presence of three characteristic ROE's between $Phe^{6}H^{\delta 2}$-$ProH^{\beta 1}$, $Phe^{6}H^{\delta 2}$-$ProH^{\gamma 1}$ and $Phe^{6}H^{\delta 1}$-D-$TrpH^{\alpha}$ corresponding to distances of 2.5 Å, 3.3 Å and 3.3 Å respectively. The threonine side chains' spatial orientation directed by the ROE's between $ThrH^{\beta}$-$Phe^{11}H^{N}$ and $ThrH^{\gamma}$-$Phe^{11}H^{N}$ corresponding to 2.2 Å and 3.5 Å respectively. The structure obtained by the MD calculation (Figure 4.21) shows the backbone of the peptide is partially bent, about the threonine residue. This kink about the threonine arouses the possibility of the existence of a γ turn about threonine stabilizing the 'partially-folded' structure, however, there is no kink observed about Phe^{6} owing to the N-methylation of the D-Trp residue, which would face a steric clash with ProCO in the 'folded' structure. The conformation of the peptide corroborates the biological activity, showing a moderate decrease in the binding affinity owing to the partial loss in the bioactive conformation i.e. 'folded' conformation by N-methylation.

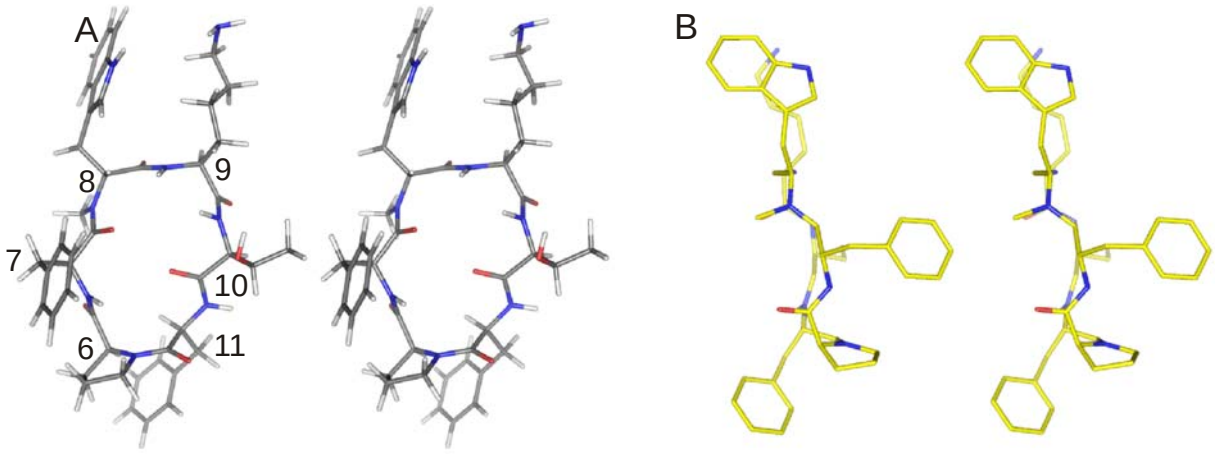

***Figure 4.21**. A) Stereopicture of **S4**, resulting from the energy minimization of the average structure obtained by 150 ps restrained MD simulation. B) Stereopicture of the side view of the backbone, the CO, NH and NMe group of the residues involved in bending of the peptide are shown. The peptide reveals a strong tendency to undergo a kink about Thr^{10}.*

cyclo(-D-Trp-MeLys-Thr-Phe-Pro-Phe-) (S2). The biological activity of this peptide is higher than that of the parent peptide as reported earlier by Merck Inc. and is also proven by our biological testing. A total of 58 relevant ROE's constrain the structure to a fixed conformation (Figure 4.22). The side chains of tryptophane and lysine are constrained in the three dimensional space by the characteristic ROE's between D-$TrpH^{D1}$-D-$TrpH^{\alpha}$, D-$TrpH^{D1}$-$MeLysH^{NMe}$, $MeLysH^{NMe}$-$MeLysH^{\beta}$, $MeLysH^{NMe}$-$MeLysH^{\gamma}$. Along with these, the γ protons of lysine are extremely upfield shifted at 0.54 and 0.74 ppm, suggesting the strong shielding provided by the indole ring of tryptophane, owing to their close proximity. Considering the existence of a βII' turn, the orientation of threonine NH with respect to $MeLysH^{\alpha}$ and $ThrH^{\alpha}$ ($ThrH^{N}$-$ThrH^{\alpha}$ and $ThrH^{N}$-$MeLysH^{\alpha}$ both are 2.6 Å) and the absence of any ROE between $MeLysH^{NMe}$-$ThrH^{\alpha}$ suggests the absence of a standard βII' turn. Thus like **S4**, the MeLys-Thr peptide bond is displaying a dynamics, which results in the violation of 0.35 and 0.38 Å in the two above mentioned ROE's, this disruption in the βII' turn is the resultant of the N-methylation of lysine, which forces the $Phe^{7}CO$ and $ThrH^{N}$ part to accommodate the bulky methyl group nullifying any chances of hydrogen bonding between them. This is clearly denoted by the deviation in the dihedrals about the D-Trp(*i*+1) and MeLys(*i*+2), where the Φ of D-Trp is 91˚ and Ψ of MeLys is -40˚ compared to the standard of 60˚ and 0˚ in a standard βII' turn, while Ψ of D-Trp(*i*+1) is -116˚ and Φ of MeLys(*i*+2) is -87˚ which deviate less from the standard of -120˚ and -80˚ respectively. The other half of the peptide has a conformation which is very similar to **S4** with a βVI turn (RMSD of the backbone superimposed **S4** and **S2** is 0.56), except the orientation of the phenyl ring of Phe^{7} which is owing to the twist in the structure about Phe^{7}. This clean twist in the structure is similar to the parent compound and revealing the tendency to form a γ turn about Phe^{7}. On the other side of the peptide, this kink

is not prominent which is probably owing to the dynamic nature of Lys-Thr peptide bond. The average structure represents the side chains of both Phe^{7} and Thr^{10} are axial with their close proximity which is a feature of the 'folded' conformation.

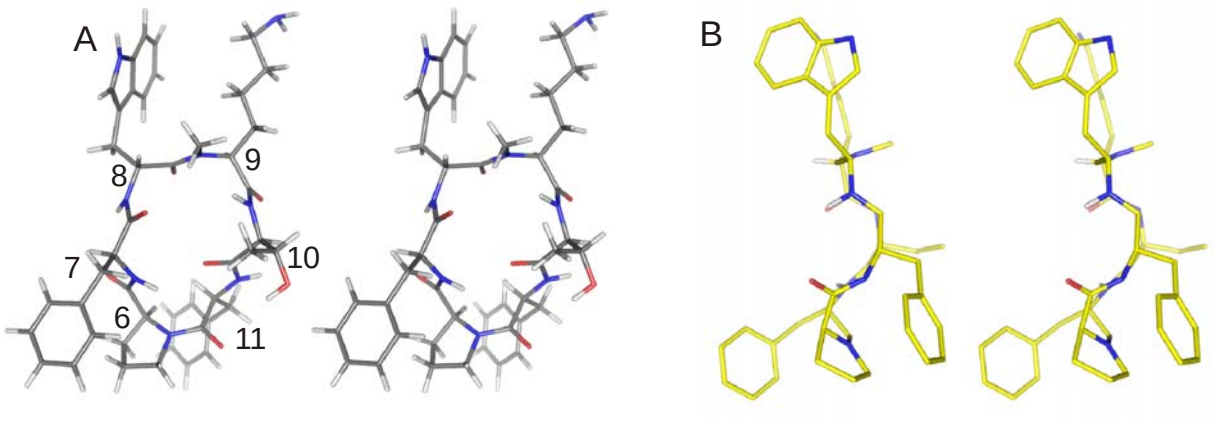

Figure 4.22. *A) Stereopicture of* ***S2****(energy minimized average structure of 150 ps restrained MD). B) Stereopicture of the side view of the backbone, the CO, NH and NMe group of the residues involved in bending of the peptide are shown. Note the kink about Phe^{7}, forming the γ turn, which in case of Thr^{10} is not so prominent owing to flexibility of peptide bond.*

cyclo(-D-Trp-Lys-Thr-MePhe-Pro-Phe-) (S3). This peptide N-methylated at Phe^{11} shows the biological activity slightly lower than the parent compound in binding to hsst 2 and binds best in the series to hsst 5. The absence of any N-methylation in the residues Trp to Thr, the ROE's ThrH^{N}-LysH^{N}, ThrH^{N}-TrpH$^{\alpha}$ corresponding to 2.4 Å and 3.5 Å respectively and the low temperature gradient of +0.2 ppb of ThrH^{N}, suggests the possibility of a standard βII' turn with D-Trp as (*i*+1) residue. The side chain of tryptophane and lysine are restrained by the characteristic pattern of ROE's between TrpH^{D1}-TrpH$^{\alpha}$, TrpH^{D1}-LysH^{N}, LysH^{N}-LysH$^{\gamma}$, LysH$^{\alpha}$-LysH$^{\gamma}$, LysH$^{\beta}$-ThrH^{N}. The orientation of the lysine side chain is similar to that in **S2**, as in this case also there is no up-field shift of the lysine γ protons due to anisotropic effect of the indole ring where the LysH$^{\gamma 1}$ is equidistant to LysH$^{\alpha}$ and LysH^{N}. The dihedral angles of the βII' turn is similar to a standard turn. The other half of the peptide adopts a βVI turn owing to the *cis*-peptide bond between Phe^{11}-Pro^{6} inspite of the N-methylation of Phe^{11}. The N-methylation leads to the increase in the steric bulk about H^{N}-N-C$^{\alpha}$-C$^{\beta}$ dihedral and eventually forces out the side chain of Phe^{11} to relieve the strain. The orientation of the phenyl ring of Phe^{11} in this peptide is similar to that in **S2** and **S3** but is drawn comparatively closer to the pyrrolidine ring of proline due to N-methylation, which is evident of the slight upfield shift of H$^{\beta 2}$(0.80 ppm). This peptide is kinked about Phe^{6} but on the other side about threonine, though the structure exhibits the tendency to adopt a γ turn, the stabilizing hydrogen bonding is blocked by the N-methyl group.

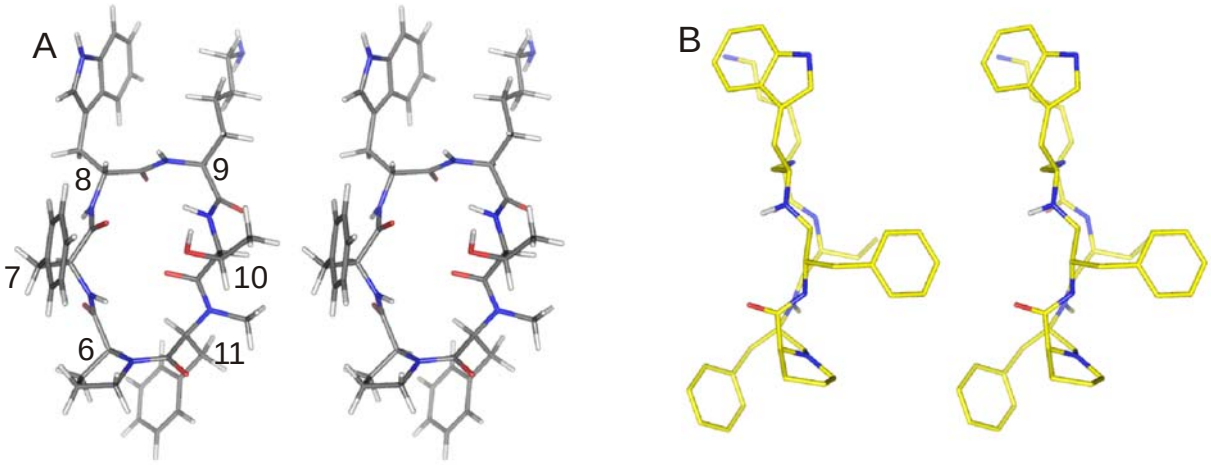

Figure 4.23. *A) Stereopicture of* ***3****(energy minimized average structure of 150 ps restrained MD). B) Stereopicture of the side view of the backbone, the CO, NH and NMe group of the residues involved in bending of the peptide are shown. The kink about Phe*^{7} *is stabilized by the γ turn, which in case of Thr*^{10} *is blocked by N-methylation.*

cyclo(-D-MeTrp-MeLys-Thr-MePhe-Pro-Phe-) (S8). Conformational analysis of compound **S8** showed that N-methylation at the selected positions (D-Trp^{8}, Lys^{9} and Phe^{11}) introduces distinct changes in the structure of the molecule; however, the orientations of the side chains are similar to the parent compound **S1** (Figure 4.24). Differences occur in the backbone over the residues MeLys^{9}-MePhe^{11} caused by the N-methylation of the lysine residue. The N-methyl group accommodates itself between the tryptophan and lysine in a way to avoid strong steric clash, and this eventually forces Thr^{10}H^{N} and Phe^{7}CO to move farther apart nullifying any chances of hydrogen bonding. However, the temperature gradient value of 0.43 ppb/K (shift to low field on warming) for Thr^{10}H^{N} suggests it is solvent shielded or hydrogen bonded. The MD structure exhibits an involvement of Thr^{10}H^{N} in a hydrogen bonding with Trp^{8}CO forming a γ turn. This is confirmed by a strong ROE between MeLys^{9}H$^{\alpha}$ and Thr^{10}H^{N} corresponding to a distance of 2.4 Å, and thus proves the absence of a βII' turn. Concentrating on the other half of the peptide, with the *cis*-proline peptide bond and the available Phe^{7}H^{N}, there is an indication of a βVI turn (Phe^{7}H^{N} shows a temperature gradient of 0 p.p.b/K, which could be accounted for its hydrogen bonded and hence solvent shielded nature in the hydrophobic environment). Thus, eventually as a result of the N-methylation at Trp^{8} and Phe^{11}, which does not take part in hydrogen bonding with Pro^{6}CO and Lys^{9}CO, respectively forming two closed γ turns, the peptide no more exhibits the 'folded' conformation.

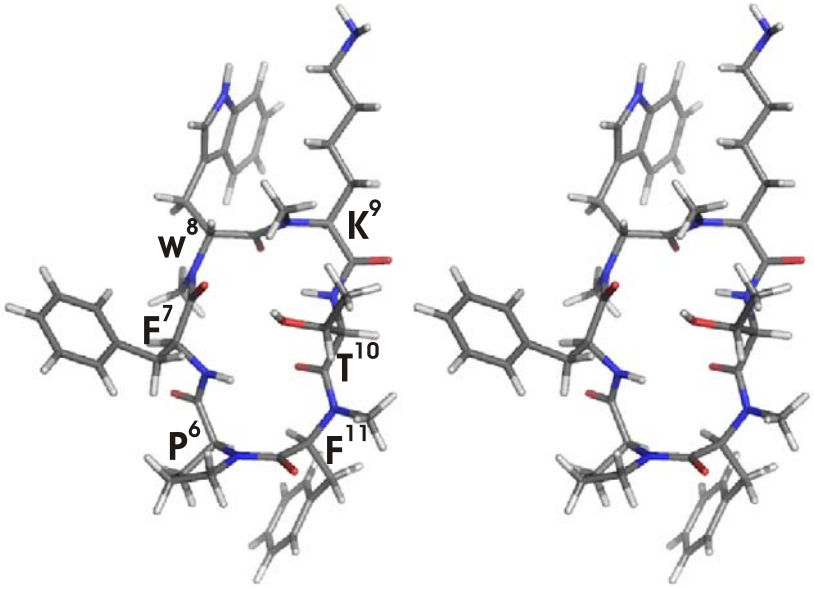

Figure 4.24. *Stereopicture of* ***S8*** *(energy minimized average structure of 150 ps restrained MD). The kink about Phe*[7] *and Thr*[10] *is completely lost presenting the peptide in a flat conformation.*

It is worth mentioning that, in order to determine the importance of the Phe[11] for bioactivity, we have synthesized the epimeric analog of **S8**, cyclo(-PFMewMeKTMef-) in which the MePhe[11] is substituted by the enantiomeric D-MePhe[11]. In contrast to **S8** this peptide exhibits a *trans*-peptide bond revealing a βII turn instead of a βVI turn about Phe[11] and Pro[6], resulting in the loss of deep burying of the phenyl ring and subsequent loss in the activity. The membrane permeability of this peptide was also compared with that of peptide **S8**, showing a dramatic loss in the paracellular permeability. From this we conclude that Phe[11] and its surrounding are important not only in maintaining the activity of the peptide but also in maintaining the permeability profile of a peptide.

In summary, we have characterized the effect of multiple N-methylation on the intestinal permeability and enzymatic stability of somatostatin analogs. Improving these parameters is a key factor in enhancing the oral bioavailability of peptides. The finding that multiple N-methylation of peptide improved oral bioavailability without modifying its biological activity and selectivity, as demonstrated in this work, can be a step towards the development of peptide based therapeutics. Thus, multiple N-methylation could be a simplistic way to achieve oral bioavailability of peptidic drugs.

5. N-Methylated cyclic hexapeptide GPIIb-IIIa ligands

5.1 Integrins

Integrins comprise a large family of cell surface receptors that are found in many animal species, ranging from sponges to mammals. This family of cell surface proteins mediates cell adhesion. Adhesion is of fundamental importance to a cell; it provides anchorage, cues for migration, and signal for growth and differentiation. There are two principal types of cell adhesion: cell-extracellular matrix adhesion and cell-cell adhesion. Integrins appear to be the primary mediators of cell-extracellular matrix adhesion, and they also serve as one of the many families of molecules active in cell-cell adhesion.[208,209]

Most integrins recognize several extracellular matrix (ECM) proteins. Conversely, individual matrix proteins, such as fibronectin, laminins, collagens, and vitronectin, bind to several integrins.[208] Integrins can signal through the cell membrane in either direction. The extracellular binding activity of integrins is regulated from the inside of the cell (inside-out signaling), while the binding of of the ECM elicits signals that are transmitted into the cell (out-inside signaling).[210]

Aside from their biological importance to fundamental cellular processes, the medical importance of the integrins has been rapidly being realized as well; integrins have been found to play a role in platelet aggregation, immune functions, tissue repair, and tumor invasion, and some diseases are already known to be caused by mutations in integrin genes. Moreover, knowledge of the target amino acid sequence for many integrins, the Arg-Gly-Asp (RGD) sequence,[211] can be exploited to design compounds controlling cell adhesion for therapeutic purposes.

5.2 Integrin families

Integrins are a family of glycoproteins consisting of two subunits, α and β. Each α and β subunit is a type I membrane glycoprotein which consists of a large extracellular domain (~1000 and ~750 residues), a transmembrane helix and a short cytoplasmic tail (~20 and ~50 residues, except β4). Until now, 18 α and eight β subunits are known in mammals to associate non-covalently forming 24 integrin heterodimers.[212] Half of the integrin a subunits contain an additional ~180 amino acid von-Willebrand factor A-type domain (often named αA or αI domain) in their extracellular domain. These αA-containing integrins recognize glutamate-based instead of aspartate-based sequence motifs in their ligands, but show similar basic features concerning bidirectional activation and signaling than the αA-lacking integrins.

Each of the 24 integrins appears to have a specific, nonredundant function. This can be concluded both from their ligand specificities and from phenotypes of knockout mice. The phenotypes range from a complete block in preimplantation development (β1), through major developmental defects (e.g. α4, α5, αv), to perinatal lethality (e.g. α6, αv, β4) and specific defects in leukocyte function (e.g. β7), inflammation (β6), hemostasis (e.g. αIIb, β3), bone remodeling (β3) and angiogenesis (α1, β3).[208] The largest number of integrins are members of the β1 integrin subfamily that are also known as the very late antigen (VLA) integrins. The best studied integrins among this family are the leukocyte integrin α4β1 (VLA-4) and the α5β1 receptor. α4β1 is a potential target for therapeutics in chronic inflammatory disease, whereas, α5β1 is involved in the angiogenesis process. β2-integrins, or leukocyte cell adhesion molecules (Leu-CAM), consist of four subtypes and have a major role concerning the immune system.[213] The most important β3-integrins are the platelet receptor αIIbβ3, which is responsible in hemostasis, and the vitronectin receptor αvβ3, which function in angiogenesis.[214]

5.3 Integrin structure

A major advance in our understanding of integrin function and ligand binding was provided by the X-ray crystal structures of the extracellular domain of αvβ3 in its unliganded state[215] and in complex with the cyclopeptide cyclo(-RGDfNMeV-) "Cilengitide"[216] developed in our group.[38] The integrin heterodimer has a jellyfish-like appearance with a globular "head" (*N*-terminal) from which two nearly parallel "tails" emerge (Figure 5.1). The integrin head has dimensions of ~90 Å x 60 Å x 45 Å which consists of a seven-bladed-β-propeller (438 residues) from αv and a so-called βA domain (243 residues) arising from an immunoglobulin (Ig)-like "hybrid" domain (133 residues) in β3. The αv tail is built up by three β-sandwich domains: the Ig-like "tight" domain and two "calf" domains. The β-tail is formed of six domains: an amino-terminal PSI-domain (plexins, semaphorins, integrins),[217] four epidermal growth factor (EGF) domains and a β-tail domain (βTD). Each integrin tail provides a thin cylinder of ~160 Å in length, when fully extended. In the crystal structure the head is folded back to the integrin tails, forming a V-shaped structure with a knee between the tight and the calf1-domain in the αv subunit, respectively between the EGF2-and EGF3-domain in β3. However, the relevance of these different conformations for the integrin activation is part of the actual discussion.[218]

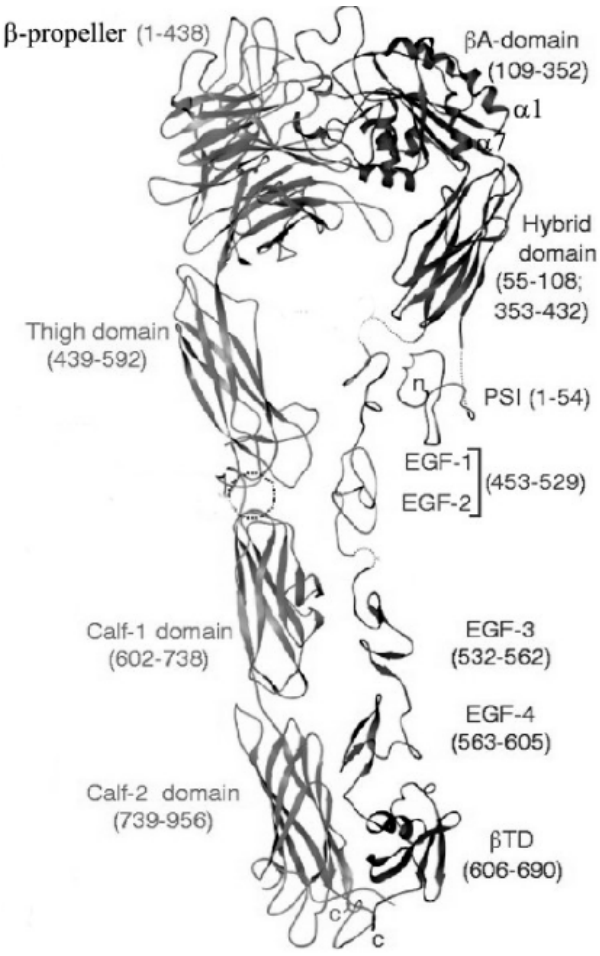

Figure 5.1. *Model of the straightened extracellular segment of αvβ3.*[215]

5.4 GPIIb-IIIa or αIIbβ3 integrin

αIIbβ3 is one of the best characterized integrins, studied not only for its importance in thrombosis but also as a prototypical integrin.[219] αIIbβ3 is by far the most abundant integrin on the platelet surface (40,000-80,000 copies) and is also present in internal pools.[220] The αIIb subunit undergoes posttranslational proteolytic cleavage, producing a 105-kDa extracellular fragment and a 23-kDa fragment containing the single transmembrane span and a 26-residue cytoplasmic domain.[219] The two chains are linked by a single disulfide bond. In contrast, β3 consists of a single polypeptide chain, including a single transmembrane span and a 45-residue cytoplasmic domain.

Platelet rich clot formation is important in many vasooclusive disorders such as unstable angina, acute myocardial infarction, reocclusion after percutaneous interventions, and stroke.[221] Platelet activation is produced by a wide variety of stimuli, but the final common event leading to platelet rich thrombus formation is the binding of the activated platelet integrin GPIIb-IIIa to the soluble plasma adhesive proteins fibrinogen (Fg) and von Willebrand factor (vWf).[222,223] Fibrinogen and von Willebrand factor are multivalent and

participate in the aggregation of platelets to form thrombi at the site of atherosclerotic plaque rupture. If GPIIb-IIIa is blocked from binding to adhesive proteins, then it should prevent formation and/or propagation of a platelet thrombus, no matter what the physiological stimuli was that initiated GPIIb-IIIa activation. Thus, compounds that compete with fibrinogen in binding to the activated GPIIb-IIIa in the final step of blood clot formation, can act as potent antithrombotic agents.[39]

5.5 GPIIb-IIIa antagonists

The use of intravenous GPIIb-IIIa inhibitors (eptifibatide, tirofiban, abciximab) in preventing vessel closure after percutaneous coronary angioplasty (PTCA) is now well established,[224] and GPIIb-IIIa receptor antagonists are considered to be the most potent antiplatelet drugs available to the clinician. So far, there is no orally available integrin antagonist in use; however, there are some compounds for αvβ3 reported by the Merck group which are orally available, but not yet as drugs on the market.[225] The antithrombotic activity of many molecules that inhibit the αIIbβ3-fibrinogen interaction has been assessed *in vitro* and *in vivo*. Most of these compounds fall into four categories: RGD-based peptides (small linear and cyclic peptides containing the RGD sequence or its equivalent),[37,39] snake venom peptides,[226] monoclonal antibodies raised against GPIIb-IIIa,[227] and non-peptide fibrinogen receptor antagonists that mimic the RGD tripeptide sequence.[228]

More than a decade ago, our group actively involved in the search of GPIIb-IIIa antagonists, synthesized a cyclic hexapeptide cyclo(-$G^1R^2G^3D^4f^5L^6$-) which was found to 2-4 fold more inhibitory than the linear -GRGDs- peptide in solid phase assays and showed similar inhibition as the fibrinogen ligand.[229] We chose this cyclic peptide as our lead structure to modify its oral bioavailability by multiple N-methylation.

5.6 The approach

Again in this work we envisioned a ‘Design Approach’ instead of the commonly used ‘Library Approach’. For this purpose, the prerequisite is the knowledge of the bioactive conformation of the stem peptide (lead structure). The chosen cyclic hexapeptide cyclo(-$G^1R^2G^3D^4f^5L^6$-) has a possibility to yield 63 different N-methylated analogs (Figure 5.2). However, we synthesized a small library of 7 derivatives in which only the externally oriented (solvent exposed) amide protons were N-methylated. This should lead us to structures in which the overall conformation is only slightly modified; retaining at least some activity but in addition may positively influence permeability when orally administered.

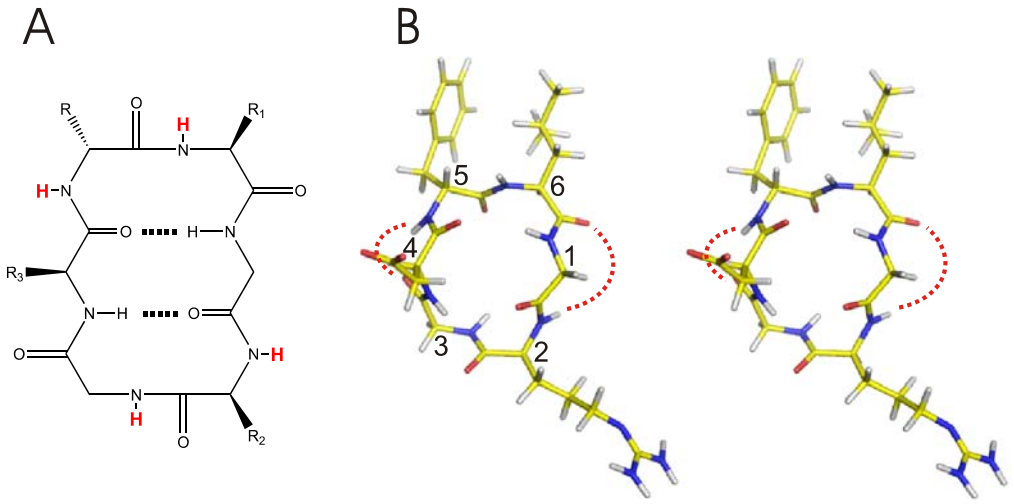

Figure 5.2. *A) Lead structure (**R1**) with two β turns and the solvent exposed amide protons (in red). B) Stereoview of cyclo(-GRGDfL-)(**R1**). Note the stabilizing γ turns about aspartic acid[4] and glycine[1] presenting the peptide in a 'folded conformation'.*

The cyclic peptides merely act as a scaffold to hold the side chains in proper spatial orientation. Detailed study of the impact of N-methylation on cyclic pentapeptides[92,93] and hexapeptides (unpublished results) suggested us that N-methylation of the externally oriented solvent-exposed amide protons may not drastically change the backbone peptide conformation (e.g. *trans*/*cis*-peptide bond inter-conversion); however, it helps in rigidifying the backbone conformation by i) restricting the peptide bond flip (180° rotation of the peptide bond about the adjacent C^{α}'s)[97] due to steric hindrance of the N-methyl group and ii) rules out the possibility of conformational equilibrium between interchangeable turn structures e.g. βII' to γ and vice versa.[9] The reason of choosing the cyclic hexapeptide rather than pentapeptide is the 'rigidity', as cyclic hexapeptides unlike cyclic pentapeptides usually exhibit a conformation with two internally oriented peptide bridges (often two β turns). Cyclic hexapeptide correspond to cyclohexanes (see discussion in Heller et al.)[98] and prefer to adopt a chair-like conformation.[68]

The cyclic peptide cyclo(-$G^1R^2G^3D^4f^5L^6$-) (**R1**), which was reported by Pfaff et al.[229] to be selective towards αIIbβ3 compared to αvβ3, reveals a βII' turn about D-Phe-Leu and a βII turn about Arg-Gly[230] which is the recognition motif; with two internal hydrogen bonds between Asp^4CO--HNGly^1 and Gly^1CO--HNAsp^4. This stem peptide cyclo(-GRGDfL-) has some flexibility (due to the two Gly residues) but allows to investigate the effect of N-methylation on the backbone to obtain highly active and selective αIIbβ3 integrin antagonist. We describe here a biased small library in which all externally oriented amide bonds except Gly^3, which is involved in the receptor binding[216] were N-methylated (Table 5.1).

Table 5.1. *The 7 N-methylated cyclic analogues with the stem peptide cyclo(-$G^1R^2G^3D^4f^5L^6$-) and their binding affinity (IC50 in nM) towards three different integrins. The N-methylated residues are highlighted in bold.*

No.	Analogue	$\alpha_5\beta_1$	$\alpha_v\beta_3$	$\alpha_{IIb}\beta_3$	$\alpha_v\beta_3/\alpha_{IIb}\beta_3$
R1	c(-GRGDfL-)	740	100	195	0.5
R2	c(-GRGDf**L**-)	3900	103	560	0.2
R3	c(-GRGDf**L**-)	4300	490	2000	0.2
R4	c(-G**R**GDfL-)	1200	770	12	64
R5	c(-GRGD**f**L-)	>20,000	1200	620	2
R6	c(-G**R**GDf**L**-)	~20,000	1300	15	86
R7	c(-G**R**GDf**L**-)	>20,000	2730	165	16
R8	c(-G**R**GD**f**L-)	>20,000	12,200	30	406

The linear peptides were obtained by standard solid phase technique with N-methylation either in solution[49] or on solid support[191] and finally the cyclization was carried out in solution using HATU/HOBt and Collidine.[231] It is worth noting that in spite of our previous report, we found no receptor selectivity for **R1**, and there is an inclination towards αvβ3 selectivity with N-methylated leucine (**R2**) or D-phenylalanine (**R3**). The different IC50 values and consequently different receptor selectivity can be explained by other experimental conditions used in this work compared to the work by Pfaff and colleagues.[229] The main difference is the composition of used integrins and thus the applied protein concentration which causes other IC50 values (details in experimental section).

Significant selectivity is first obtained in **R4** with N-methylated arginine residue, which corroborates with previous results.[33] Extending further the N-methylation of **R4** to leucine, there is almost no loss in the activity in **R6** but a further gain in selectivity. Exchanging the site of N-methylation from leucine to phenylalanine in **R7**, there is a sudden loss in the activity. However, interestingly the activity is gained back with an additional N-methylation of **R7** giving rise to **R8**, with a tremendous enhancement in the selectivity and still high activity for αIIbβ3. It is really surprising that a single N-methyl group when present at phenylalanine is responsible for the loss of activity in **R7** and gaining back the activity and enormous selectivity when present at leucine in **R8**.

These results prompted us to study the solution conformation of these analogues. It is well known that the selectivity between αvβ3 and αIIbβ3 can be achieved by fine tuning the distance between the carboxyl group of aspartic acid and the guanidine group of arginine in the ligands.[232] In our case, the selectivity first arises by N-methylation of the arginine residue (**R4**), which is primarily owing to the reduction in the flexibility about arginine[2] and glycine[3] (which resembles a βI' turn), presenting the peptidic backbone in an extended orientation. It is to be noted that the side chain of arginine is very flexible which could fit into αvβ3 and

αIIbβ3, thus the main selectivity is brought about by the rigidity in the scaffold by N-methylation.

In the stem peptide **R1** or when leucine (**R2**) and/or phenylalanine (**R3**) are N-methylated, there is considerable flexibility in the βII turn resulting in unspecific binding. In all the peptides lacking the N-methylated arginine residue, the NMR and the MD show the possibility of forming a γ turn about the glycine in position 3, which ultimately brings the side chains of the aspartic acid and arginine close to each other, resulting in a comparatively better fit into the αvβ3 binding pocket. In addition to the γ turn, we observe a 'kink' in the backbone conformations of **R1** and **R2**, giving rise to a 'folded' structure,[206] resulting in two further γ turns about Asp and Gly[1] (Figure 5.2).

This kinked conformation is probably favored for αvβ3 as both, **R1** and **R2**; bind better to αvβ3 than to αIIbβ3. This kink is lost by N-methylation of D-Phe and/or Arg which blocks the γ turns and presents the peptide in a flattened conformation. In case of **R8**, there is no indication of any γ turn about Gly[3] and the peptide is in a flat conformation (Figure 5.3), which eventually results in holding the aspartic acid and arginine side chains apart, fitting well into the αIIbβ3 pocket.

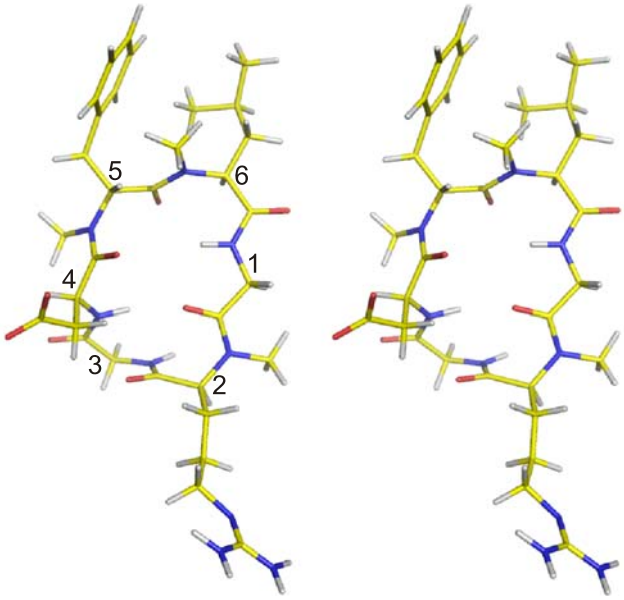

Figure 5.3. *Stereoview of cyclo(-G**R**GD**fL**-)(**R8**). The stabilizing γ turns about aspartic acid[4] and glycine[1] are absent resulting in a flat structure. Note the βI' turn about arginine[2] and glycine[3].*

The conformation of peptide **R8** is very similar to **R4**; the only difference is the slight clockwise rotation of the phenyl ring and anticlockwise rotation of the isopropyl group of the leucine side chain (as suggested by the ROE's). In addition, we observe a close resemblance to βI' turn about Arg and Gly[3] in **R8** owing to the reduced flexibility in this region (due to the NMe-D-Phe) and thus, there is no indication of the formation of γ turn about Gly[3], whereas,

the βI' turn in **R4** is flexible and there is a close resemblance to a γ turn about Gly^3 (Figure 5.4). This is probably one of the reasons for low binding of **R8** to αvβ3 in contrast to **R4**.

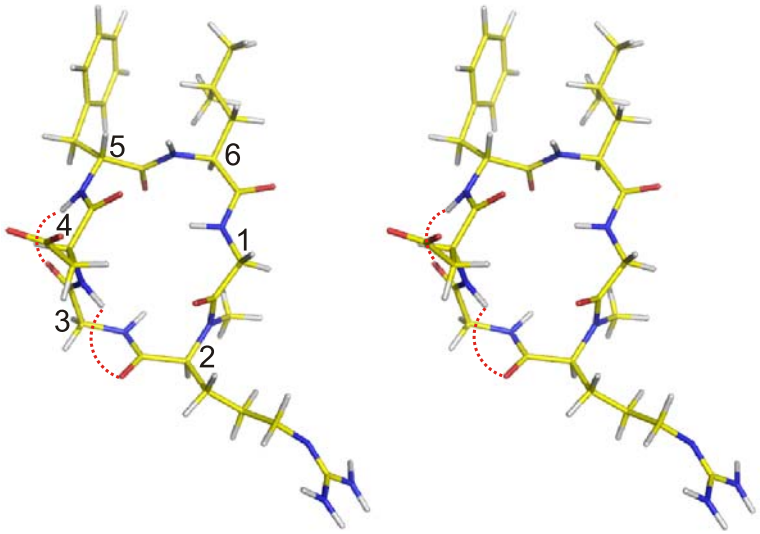

Figure 5.4. *Stereopicture of cyclo(-G**R**GDfL-)(**R4**). About Gly^3, the molecule has a tendency to adopt a γ turn (shown by curved line), forming a hydrogen bond between AspNH and Arg CO. Also interesting to note is the kink in the peptide backbone about Asp. This kink is stabilized by formation of a closed γ turn involving the PheNH and Gly^3CO.*

To have an insight into the binding modes of **R4** and **R8** into αIIbβ3, docking studies were performed using the software Autodock.[233]

In both peptides, the carboxylate group of Asp was found to coordinate the metal ion at the MIDAS region, whereas the Arg side chain extended into the deep β-propeller pocket forming hydrogen-bond to the αIIb-Asp 224 carboxylate group. The main difference between **R4** and **R8** binding modes comes from the upper part of peptides in the region from D-Phe^5-Leu^6 (Figure 2 and 3). Due to multiple N-methylation introduced in **R8**, and especially due to the N-methylation of D-Phe residue; **R8** when compared to **R4**, seems to lower its π-π interaction with β3-Tyr122 (shown by yellow arrow in Figure 5.5) and do not properly orient the Leu carbonyl group to hydrogen-bond with R214 side chain (shown by white arrow in Figure 5.5).

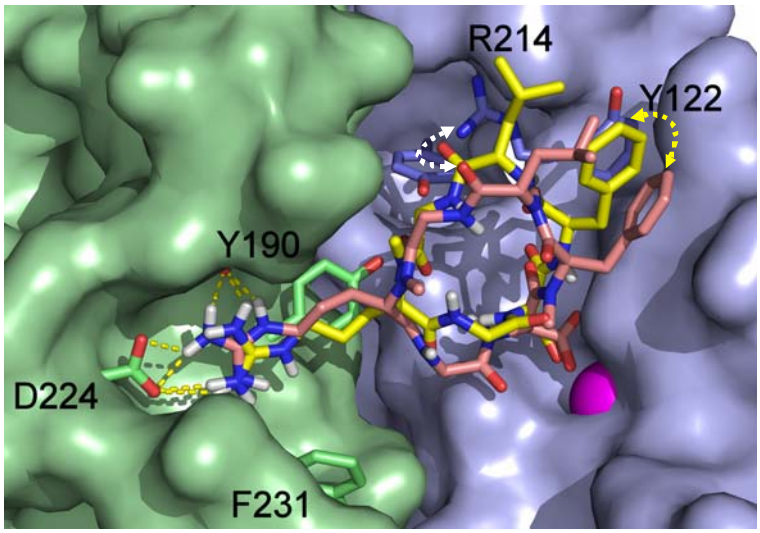

Figure 5.5. *Docked* ***R4****(yellow) and* ***R8****(pink) in the αIIbβ3 integrin. The αIIb subunit of the receptor is represented by green surface, while β3 subunit by violet surface. In both subunits, important side chains are highlighted as sticks. The metal ion in the MIDAS region is represented as magenta sphere. The loss in π–π interaction of D-Phe residue of* ***R8*** *with Tyr122 is shown by the yellow arrow and the improper orientation of Leu CO of* ***R8*** *to form hydrogen bond with Arg214 side chain is shown by white arrow.*

N-methylation was suggested also to affect permeability characteristics of peptides. [121] Therefore, the permeability of the library was assessed by Caco-2 model.[234] All the analogues had lower permeability (P_{app} between 3.0E-08 cm/sec and 1.5E-07cm/sec) compared to mannitol (9.0E-07 cm/sec) as standard.

Since N-methylation affects the hydrophobicity of the molecules, we examined whether N-methylation could improve the permeation of the compounds through biological membranes via the transcellular pathway. For that we used the PAMPA,[235] which is a non-cell based *in vitro* assay system that evaluates passive transcellular permeation. To our surprise, none of the analogues penetrated across the lipid artificial membrane, suggesting that these peptides have poor intestinal permeability which is limited exclusively to the paracellular pathway (via tight junctions) and N-methylation did not change or improve the transport in this series.

In conclusion, we demonstrate that a systematic multiple N-methylation by knowing the bioactive conformation of the stem peptide, can be employed for enhancing receptor selectivity and activity of a moderately active ligand, although in this case we failed to improve the bioavailability of the analogues. Using this conformational design approach, one can minimize the size of the library considerably. In this case, the selectivity of the analogue arises predominantly due to the reduced flexibility of the peptide. Multiple N-methylation results also in a better understanding of the bioactive conformation. Thus, multiple N-methylation of peptides could be a straightforward and simplistic approach to obtain highly potent and selective ligands.

6. Summary

The scope of this work was to investigate the N-methylation of peptides, especially cyclic peptides in context to improving their synthesis, investigating conformational impact and pharmacokinetic properties.

In this thesis an optimized, simplified procedure for N-methylation of peptides on solid support is reported which to our knowledge is the most inexpensive, least time consuming procedure and is applicable to every amino acid with diverse side chain functionalities till date. The efficient Mitsunobu alkylation conditions were employed for the key step of N-methylation, avoiding any side chain alkylations specifically in the case of cysteine and histidine, which are infamous to undergo side chain alkylations.

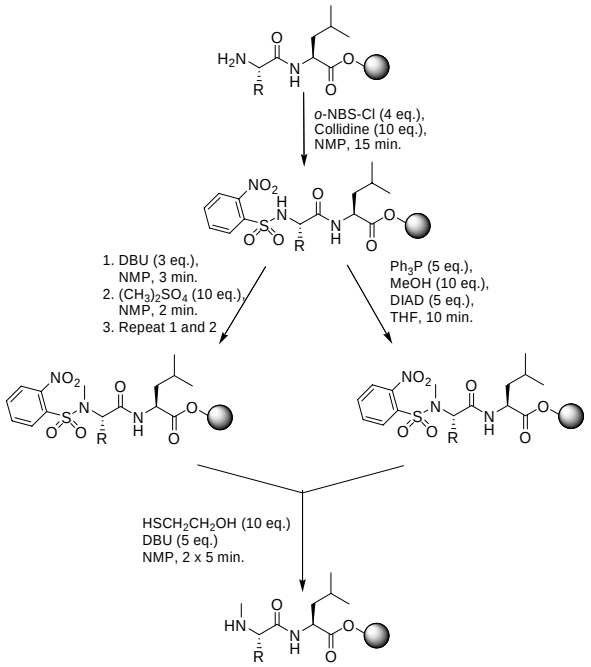

Figure 6.1. *Schematic representation of the optimized N-methylation procedure on solid phase.*

The successful development of the N-methylation on solid phase, equipped us to produce multiply N-methylated libraries of cyclic peptides in a reasonable period. Therefore, we approached towards a complete N-methyl scan of cyclo(-D-Ala-Ala_4-) to investigate in detail, the conformational impact of N-methylation on the cyclic peptide backbone.

The conformational study of the conformationally preferred N-methylated analogs (analogs with show an abundance of >80% at the NMR time scale) revealed the existence of 5 different template structures shown below.

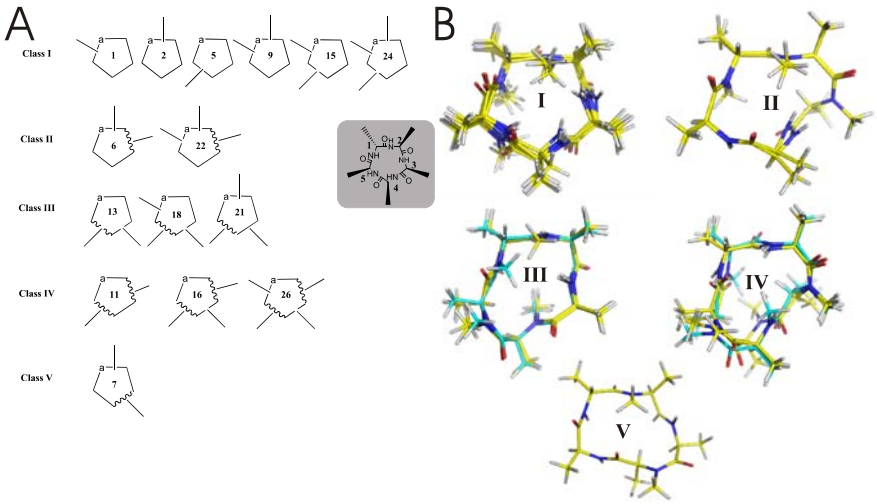

Figure 6.2. *A) Different classes of N-methylated cyclo(-D-Ala-Ala$_4$-); wavy lines: cis-peptide bond; a: D-Ala. B) Superimposed backbone conformation of the members in each class.* ***18*** *and* ***26*** *are in cyan highlighting differences in N-methyl orientation.*

These template structures can now be employed for 'spatial screening' to screen bioactive compounds by grafting the required functionalities in the desired spatial orientation.

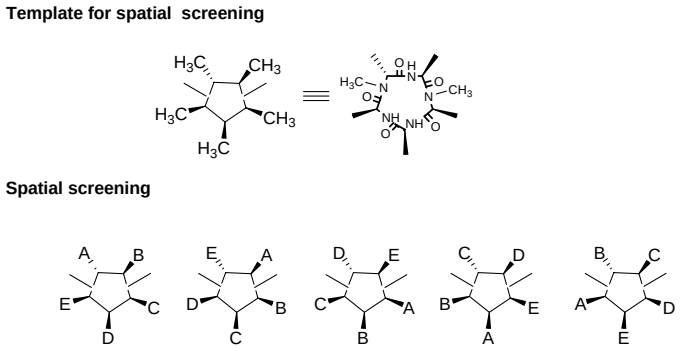

Figure 6.3. *A peptide with pharmacophoric groups A, B, C, D, and E can be screened for the spatial orientation in the bioactive conformation, by synthesis of the five position shifted cyclic isomers.*

A multiple N-methyl scan of a highly active somatostatin cyclic hexapeptidic analog: cyclo(-PFwKTF-) discovered by Merck Inc. in order to improve its oral bioavailability is reported. This multiple N-methyl scan yielded out of 31 only 7 high affinity N-methylated analog binding to somatostatin receptor subtypes 2 and 5. The detailed pharmacokinetic experiments revealed that out of these 7 only one analog was orally available (oral bioavailability of 10%). This analog had not only high paracellular permeability through the intestinal membrane, but also was notably stable against the brush border enzymes in the intestine, making the analog orally bioavailable. Hence, we arrived at the conclusion that multiple N-methylation of cyclic peptides can improve their pharmacokinetic properties making them orally available.

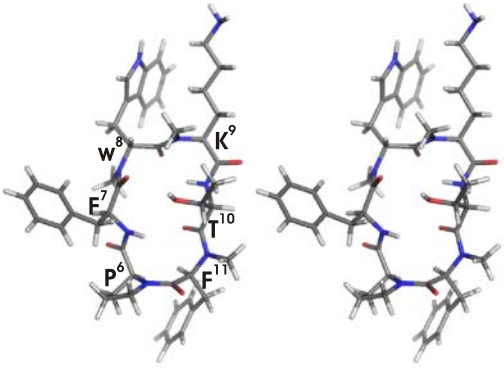

Figure 6.4. *Stereopicture of the orally bioavailable tri-N-methylated somatostatin analog.*

Finally, we turned our attention towards generalizing the method by applying the technique of multiple N-methylation on another cyclic peptide. This time however, we envisioned a 'designed approach' instead of the previously employed library approach. In this approach, the externally amide bonds were systematically N-methylated leaving out the internally oriented-hydrogen bonded amide bonds.

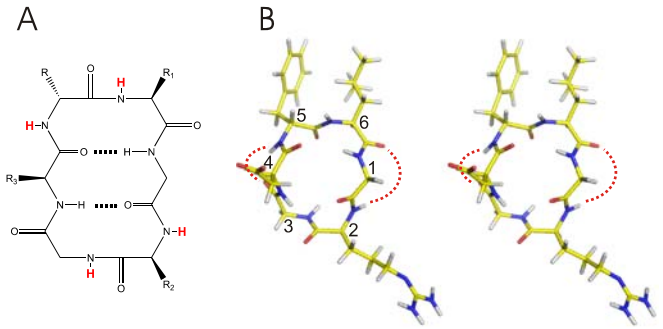

Figure 6.5. *A) Lead structure chosen for the N-methylation by 'Designed approach' with two β turns and the solvent exposed amide protons (in red). B) Stereoview of cyclo(-GRGDfL-).*

For this purpose, we chose the cyclic RGD peptide: cyclo(-GRGDfL-) synthesized in our lab more than a decade ago for the inhibition of blood clot acting as an antagonist of αIIbβ3 integrin. The synthesized N-methylated analogs showed very interesting activity profile. We found out that the selectivity of this ligand varies with the site of N-methylation. It was found out that the most N-methylated compound, cyclo(-GMeRGDMefMeL-) is highly selective towards the αIIbβ3 integrin compared to αvβ3 and α5β1 integrins. However, unfortunately we could not observe any transport of these peptides across the Caco-2 monolayer.

Thus, this thesis reports investigation of the versatile properties of N-methylation induced on the peptide backbone. However, although multiple N-methylation can not be a general approach to obtain oral bioavailability, but we encourage to employ this technique as it is highly dependant on the sequence of the amino acids in the cyclic peptide and can yield promising pharmacokinetic and bioactive profile.

7. Experimental Section:

7.1 General

Tritylchloride polystyrol (TCP) resin (0.94 mmol/g) was purchased from PepChem (Tübingen Germany). Coupling reagents and amino acid derivatives were purchased from Merck Biosciences (Läufelfingen, Switzerland), Perseptive Biosystems GmbH (Hamburg, Germany) and Neosystem (Strasbourg, France). All other reagents and solvents were purchased from Merck (Darmstadt, Germany), Aldrich (Steinheim, Germany) and Fluka (Neu-Ulm, Germany) and were used as received. Standard syringe techniques were applied for transferring dry solvents. Reactions on solid support were performed in filter columns (2 mL) from Abimed. RP-HPLC analyses were conducted on Amersham Pharmacia Biotech instruments using Omnicrom YMC columns (analytical: 2 mm × 250 mm, 5 μm C18, 1 mL/min) with different 30 min linear gradients from water (0.1% TFA) and CH3CN (0.1% TFA) and detection at 220 nm. Mass spectra (ESI) were performed on a LCQ Finnigan instrument.

Loading of TCP-resin

Peptide synthesis was carried out using TCP-resin (1 mmol/g) following standard Fmoc-strategy [44]. Fmoc-Leu-OH (1.2 eq.) was attached to the TCP resin with DIEA (2.5 eq.) in anhydrous DCM (2 mL) at room temperature for 1.5 h. After filtration the remaining trityl chloride groups were capped by a solution of DCM, MeOH, DIEA (17:2:1; v:v:v) for 15 min. The resin was filtered and washed thoroughly with DCM (2x), DMF (3x) and MeOH (5x). The loading capacity was determined by weight after drying the resin under vacuum and ranged from 0.75-0.8 mmol/g.

Fmoc Deprotection

The resin-bound Fmoc peptide was treated with 20% piperidine in NMP (v/v) for 15 minutes and a second time for 10 minutes. The resin was washed with NMP (5x).

N-Methylation by Freidinger's method

Fmoc-Xaa-OH (20 mmol) was suspended in 400 mL of toluene, and paraformaldehyde (4 g) and p-toluenesulfonic acid (200 mg) were added. The mixture was refluxed for 30 min with azeotropic water removal. The solution was cooled, washed with 1N $NaHCO_3$ (3 x 75 mL), dried over $MgSO_4$, and concentrated under reduced pressure. The oxazolidinone was dissolved in CH_2Cl_2 (60 mL), and trifluoroacetic acid (60 mL) and triethylsilane (9.5 mL, 60 mmol) were added. The solution was stirred at room temperature for 24 h followed by concentration *in vacuo* to oil. The oil was dissolved in diethyl ether and reconcentrated 3 times. The oil was dissolved in a minimum of diethyl ether and precipitated by adding hexane.

TBTU/HOBt Coupling

A solution of Fmoc-Xaa-OH (3 eq.), TBTU (3 eq.), HOBt (3 eq.), DIEA (6 eq.) in NMP was added to the resin-bound free amine peptide and shaken for 30 min at room temperature. The coupling was repeated another time and the resin was washed with NMP (5x).

HATU/HOAt Coupling

A solution of Fmoc-Ala-OH (3 eq.) or Fmoc-MeAla-OH, HATU (3 eq.), HOAt (3 eq.), DIEA (6 eq.) in NMP was added to the resin-bound N^{α}-methylamine free peptides and shaken for 3 hours at room temperature and then washed with NMP (5x). The peptides were cleaved from resin by treatment of a small amount of resin with 20% HFIP in DCM (v:v) for 10 min and analysed by RP-HPLC (ACN 30-100%) and ESI-MS.

Cleavage from resin and cyclization

The resin bound pentapeptide was cleaved off with a mild treatment of acetic acid/2,2,2-trifluoroethane (TFE) mixture in dichloromethane (DCM) (3:1:6), which was repeated 3 times with an hour each.

DPPA mediated cyclization:

The head-to-tail cyclization was performed with diphenylphosphorylacid azide (DPPA) (3 eq), applying the solid base method using $NaHCO_3$ (5 eq) in *N, N*-dimethylformamide (DMF) at a concentration of 0.1mM. After the completion of cyclization, which was monitored by ESI mass spectroscopy, DMF was evaporated and redissolved in minimum amount of dry acetonitrile, which precipitated the cyclization reagents and left the crude product dissolved in acetonitrile. The pure compound was obtained by reversed phase high-performane liquid chromatography (RP-HPLC) purification.

HATU/HOBt mediated cyclization:

The cyclization was also performed with HATU/HOBt and Collidine as a base under high dilution conditions. To a vigorously stirred solution of the linear peptide in DMF was added drop wise, a solution of HATU (1.5eq.), HOBt (1.5 eq.) and Collidine (1.5 eq.) in DMF, making a final concentration of 5mM of the linear peptide. The solution was stirred overnight and then the DMF was evaporated to dryness. To the crude product was added a saturated solution of $NaHCO_3$ and extracted with EtOAc thrice. The organic layer was washed with brine and dried with Na_2SO_4. The EtOAc is evaporated finally to obtain the crude product free of cyclization reagents.

7.2 Synthesis of N-methylated peptides:

_o_-NBS Protection

A solution of *o*-NBS-Cl (4 eq.) and collidine (10eq.) in NMP was added to the resin-bound free amine peptide **1a-k** and shaken for 15 min at room temperature. The resin was washed with NMP (5x). *o*-NBS-peptides **2a-k** were cleaved from resin by treatment of a small amount of resin with 20% HFIP in DCM (v:v) for 10 min and analysed by RP-HPLC (ACN 10-100%) and ESI-MS.

N-Methylation with DBU

A solution of DBU (3 eq.) in NMP was added to the resin-bound *o*-NBS-protected peptides **2a-k** and shaken for 3 min. A solution of dimethylsulfate (10 eq.) in NMP was then added to the reaction mixture and shaken for 2 min. The resin was filtered off, washed one time with NMP and the N-methylation procedure repeated one more time. The resin was washed with NMP (5x). N^{α}-Methyl-N^{α}-*o*-NBS-peptides **3a-k** were cleaved from resin by treatment of a small amount of resin with 20% HFIP in DCM (v:v) for 10 min and analysed by RP-HPLC (ACN 10-100%) and ESI-MS.

N-Methylation under Mitsunobu Conditions

A solution of triphenylphosphine (5 eq.) and MeOH (10 eq.) in dry THF was added to the resin-bound *o*-NBS-protected peptides **2a-k** and shaken 1 min. A solution of DIAD (5eq.) in dry THF was then added portionwise to the reaction mixture and shaken for 10 min at room temperature. The resin was filtered off, and washed with NMP (5x). N^{α}-Methyl-N^{α}-*o*-NBS-peptides **3a-k** were cleaved from resin by treatment of a small amount of resin with 20% HFIP in DCM (v:v) for 10 min and analysed by RP-HPLC (ACN 10-100%) and ESI-MS.

_o_-NBS Deprotection

For *o*-NBS deprotection, the resin-bound N^{α}-methyl-N^{α}-*o*-NBS-peptides **3a-k** was treated with a solution of mercaptoethanol (10 eq.) and DBU (5 eq.) in NMP for 5 minutes. The deprotection procedure was repeated one more time and the resin was washed with NMP (5x).

7.3 Synthesis of N-methylated cyclic pentaalanine peptides:

Combinatorial approach

The Library of compounds were obtained as shown in the Schemes 7.1-7.4, where a small 'a' stands for D-Ala and 'A' for L-Ala The underlined a or A indicates N-methylation. After each coupling the resin was divided into two halves, one for the coupling with non-methylated and the other for the coupling with methylated alanine. An unexpected reaction always occurred at the second coupling, when a N-methylated amino acid was tried to couple to a resin linked dipeptide, having the sequence Ala^{2}-D/L(Me)Ala^{1}, it always failed to couple and also resulted

in the loss of the peptide from the resin. Thus those compounds shown to fail in Scheme 7.2 and Scheme 7.3, which have similar sequence, were obtained by altering the sequence as given in Scheme 7.4.

Scheme 7.1. *Schematic approach showing the synthesis of the library of cyclic peptides starting with L-Alanine loaded to the resin, here none of the compound is having a major conformer having >98% conformational homogeneity.*

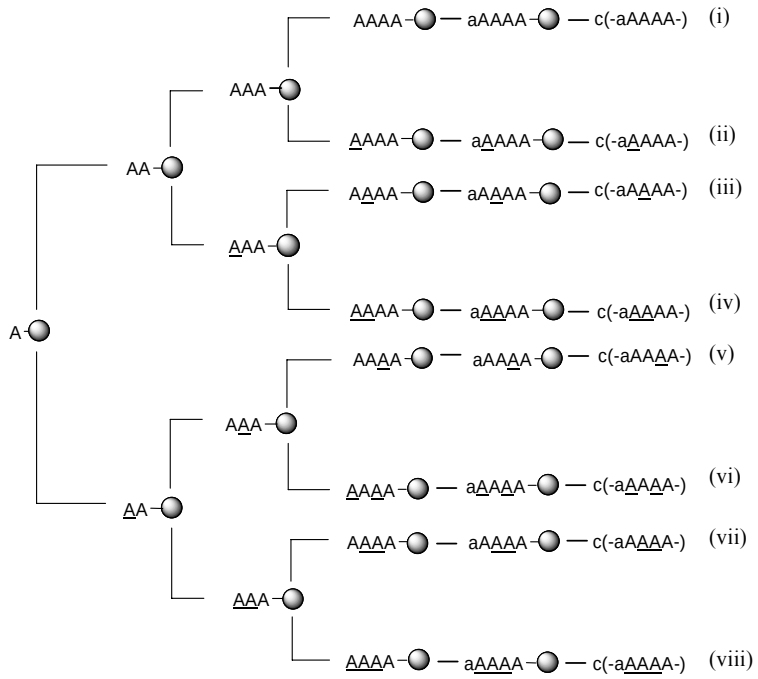

Scheme 7.2. *Schematic approach showing the synthesis of the library of cyclic peptides starting with (Me)L-Alanine loaded to the resin, the one shown in bold (**7**) is conformationally homogeneous. The compounds marked **a** and **b** were not obtained by this scheme.*

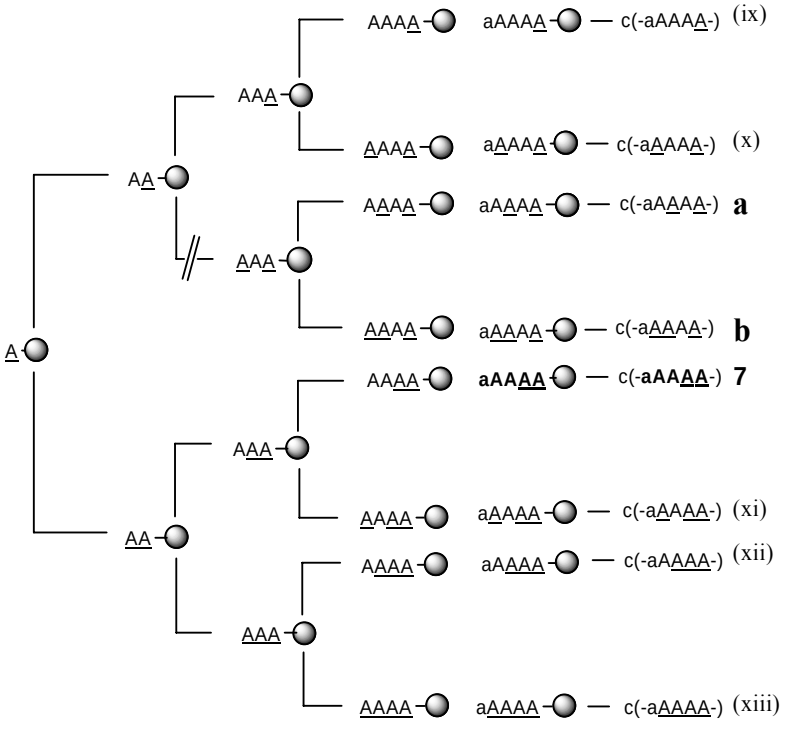

Scheme 7.3. *Schematic approach showing the synthesis of the library of cyclic peptides starting with (Me)D-Alanine loaded to the resin. The compounds shown in bold (denoted in arabic numerical) have either a single conformer or >98% of a major conformer. The compounds denoted with letters (* ***c****,* ***d****,* ***e*** *and* ***f****) were not obtained via this scheme.*

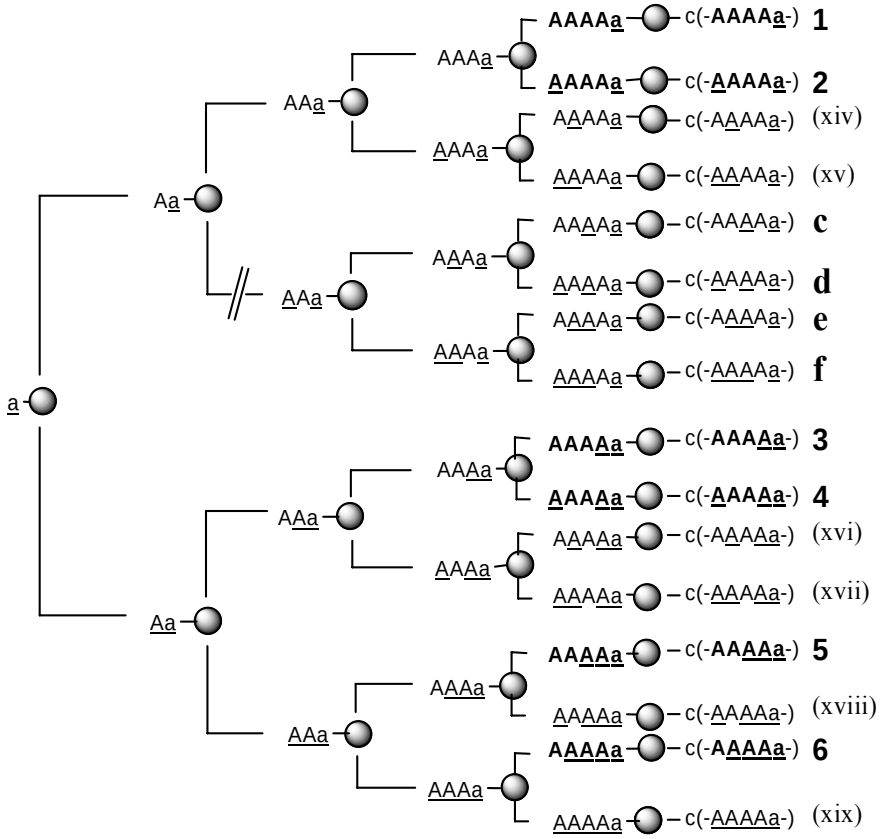

Scheme 7.4. *Schematic diagram showing the synthesis of the compounds which were obtained by altering the sequence.*

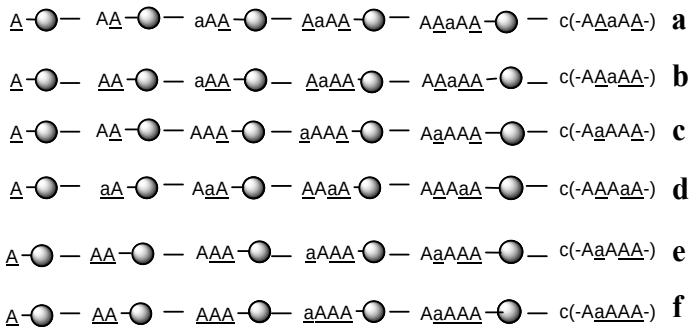

Table 7.1. *HPLC retention time, ESI-MS and yield of all cyclic peptides.*

Compound	t_R (min)[1]	$(M+H)^+$	Yield[2]
1	7.95	370.2	34%
2	10.2	384.2	28%
3	10.4	384.3	25%
4	13.9	398.3	26%
5	14.3	398.2	23%
6	16.6	412.2	12%
7	10.3	384.3	27%
(i)	7.28	356.2	66%
(ii)	8.1	370.2	32%
(iii)	8.2	370.2	34%
(iv)	9.9	384.2	28%
(v)	8.3	370.2	34%
(vi)	10.3	384.2	27%
(vii)	10.1	384.2	27%
(viii)	14.1	398.2	28%
(ix)	8.5	370.2	32%
(x)	10.7	384.2	22%
a	10.4	384.2	24%
b	14.2	398.2	25%
(xi)	14.5	398.2	19%
(xii)	14.1	398.2	20%
(xiii)	16.8	412.2	14%
(xiv)	10.3	384.2	16%
(xv)	13.9	398.2	24%
c	10.4	384.2	27%
d	14.2	398.2	21%
e	13.8	398.2	19%
f	16.6	412.2	12%
(xvi)	14.0	398.2	13%
(xvii)	16.8	412.2	11%
(xviii)	16.7	412.2	12%
(xix)	-	-	-

1. 10-50% ACN in 30 min.
2. Calculated after HPLC purification, relative to the amount of amino acid first coupled to the resin.

Chemical shifts and ROE violation list:

Conformationally homogeneous peptides:

cyclo(-D-MeAla^1-Ala^2-Ala^3-Ala^4-Ala^5)

Table 7.2. *^{1}H shifts of the respective protons.*

	H^β	H^α	H^N	N^{CH_3}
1.D-Ala	1.08(d, 7.0 Hz)	5.02(m)		2.51(s)
2.L-Ala	1.13(d, 6.7 Hz)	4.57(m)	7.89(d, 8.2 Hz)	
3.L-Ala	1.30(d, 7.5 Hz)	4.06(m)	7.82(d, 6.8 Hz)	
4.L-Ala	1.27(d, 7.2 Hz)	4.01(m)	8.07(d, 8.2 Hz)	
5.L-Ala	1.22(d, 7.0 Hz)	4.30(m)	7.35(d, 8.9 Hz)	

Table 7.3. *Distance restraints and their violations during the 150 ps rMD simulation. The calculated distances are obtained by $<r^{-3}>$ averaging.*

Atom 1	Atom 2	Low.	Upp.	Calc.	Viol.
1:D-ALA^1:CB	1:D-ALA^1:HA	2	2.44	2.11	0
1:D-ALA^1:CN	1:D-ALA^1:HA	2.82	3.45	3.5	0.05
1:D-ALA^1:CN	1:ALA^5:HN	2.76	3.38	3.5	0.11
1:D-ALA^1:CN	1:ALA^5:HA	1.9	2.32	2.63	0.31
1:D-ALA^1:CN	1:ALA^3:HN	3.56	4.35	4.35	0
1:D-ALA^1:CN	1:ALA^2:HN	3.07	3.75	3.6	0
1:ALA^5:CB	1:ALA^5:HA	1.97	2.41	2.15	0
1:ALA^5:CB	1:ALA^5:HN	2.72	3.33	3.18	0
1:ALA^5:HN	1:ALA^5:HA	2.36	2.88	2.95	0.06
1:ALA^5:HN	1:ALA^4:HA	2.7	3.3	3.49	0.19
1:ALA^5:HN	1:ALA^2:HN	2.99	3.65	3.42	0
1:ALA^4:CB	1:ALA^5:HN	2.77	3.39	3.13	0
1:ALA^4:HN	1:ALA^4:HA	2.08	2.55	2.97	0.41
1:ALA^4:HN	1:ALA^3:HA	3.06	3.74	3.48	0
1:ALA^4:HN	1:ALA^3:HN	1.61	1.97	2.26	0.28
1:ALA^3:CB	1:ALA^4:HN	2.07	2.53	2.85	0.31
1:ALA^3:CB	1:ALA^3:HN	3.3	4.03	3.04	-0.26
1:ALA^3:HN	1:ALA^3:HA	2.25	2.75	3.04	0.29
1:ALA^3:HN	1:ALA^3:HA	2.3	2.81	3.04	0.23
1:ALA^3:HN	1:ALA^2:HN	2.34	2.86	2.56	0
1:ALA^2:CB	1:ALA^3:HN	1.82	2.22	2.71	0.48
1:ALA^2:CB	1:ALA^2:HA	2	2.44	2.15	0
1:ALA^2:CB	1:ALA^2:HN	2.47	3.02	2.67	0
1:ALA^2:HN	1:D-ALA^1:HA	1.99	2.44	2.42	0
1:ALA^2:HN	1:ALA^2:HA	2.56	3.12	3.05	0

cyclo(-D-MeAla^1-MeAla^2-Ala^3-Ala^4-Ala^5)

Table 7.4. *^{1}H shifts of the respective protons.*

	H^β	H^α	H^N	N^{CH_3}
1.D-Ala	1.11(d, 6.0 Hz)	5.19(m)		2.49(s)
2.L-Ala	1.20(d, 6.7 Hz)	3.89(m)		3.09(s)
3.L-Ala	1.13(d, 6.1 Hz)	4.63(m)	7.37(d, 7.5 Hz)	
4.L-Ala	1.32(d, 7.5 Hz)	3.84(m)	7.93(d, 6.5 Hz)	
5.L-Ala	1.29(d, 7.1 Hz)	4.4(m)	6.88(d, 9.5 Hz)	

Table 7.5. *Distance restraints and their violations during the 150 ps rMD simulation. The calculated distances are obtained by $<r^{-3}>$ averaging.*

Atom 1	Atom 2	Low.	Upp.	Calc.	Viol.
1:ALA^5:CB	1:ALA^5:HA	1.95	2.39	2.13	0
1:ALA^5:CN	1:ALA^5:HA	1.72	2.1	2.48	0.38
1:ALA^5:CN	1:ALA^3:HA	3.28	4.01	4.57	0.55
1:ALA^5:CN	1:ALA^4:HA	1.8	2.2	2.42	0.22
1:ALA^5:CN	1:ALA^4:HN	3.33	4.07	4.29	0.21
1:D-ALA^1:HA	1:ALA^2:HN	2.22	2.72	2.48	0
1:D-ALA^1:CB	1:D-ALA^1:HA	1.97	2.41	2.14	0
1:D-ALA^1:CB	1:ALA^2:HN	3.17	3.88	3.93	0.05
1:D-ALA^1:CN	1:ALA^5:HA	1.91	2.34	2.78	0.43
1:D-ALA^1:CN	1:D-ALA^1:HA	2.68	3.27	3.45	0.17
1:D-ALA^1:CN	1:ALA^2:HN	2.41	2.95	3.02	0.06
1:ALA^2:HA	1:ALA^2:HN	2.61	3.19	3.07	0
1:ALA^2:HA	1:ALA^3:HN	2.66	3.25	3.46	0.21
1:ALA^2:CB	1:ALA^2:HA	1.93	2.36	2.12	0
1:ALA^2:CB	1:ALA^2:HN	2.46	3.01	2.87	0
1:ALA^2:CB	1:ALA^3:HN	1.98	2.42	2.55	0.12
1:ALA^2:HN	1:ALA^3:HN	3.19	3.9	3.09	-0.12
1:ALA^2:HN	1:ALA^4:HN	2.64	3.23	3.24	0
1:ALA^3:HA	1:ALA^3:HN	2.49	3.04	3.08	0.04
1:ALA^3:HA	1:ALA^4:HN	3.03	3.7	3.25	0
1:ALA^3:CB	1:ALA^3:HA	1.92	3.35	2.19	0
1:ALA^3:CB	1:ALA^4:HN	2.47	3.02	3.52	0.49
1:ALA^3:HN	1:ALA^4:HN	2.18	2.67	2.26	0
1:ALA^4:HA	1:ALA^4:HN	2.49	3.04	3.01	0
1:ALA^4:CB	1:ALA^4:HA	1.97	2.41	2.15	0
1:ALA^4:CB	1:ALA^4:HN	2.54	3.11	2.98	0

cyclo(-D-MeAla^1-Ala^2-Ala^3-Ala^4-MeAla^5)

Table 7.6. *^{1}H shifts of the respective protons.*

	H^{β}	H^{α}	H^{N}	N^{CH_3}
1.D-Ala	1.16(d, 7.0 Hz)	5.25(m)		2.72(s)
2.L-Ala	1.19(d, 7.0 Hz)	4.47(m)	8.04(d, 8.4 Hz)	
3.L-Ala	1.27(d)	4.05(m)	7.64(d, 7.5 Hz)	
4.L-Ala	1.33(d, 7.0 Hz)	4.10(m)	7.15(d, 7.6 Hz)	
5.L-Ala	1.27(d)	5.04(m)		2.9(s)

Table 7.7. *Distance restraints and their violations during the 150 ps rMD simulation. The calculated distances are obtained by $<r^{-3}>$ averaging.*

Atom 1	Atom 2	Low.	Upp.	Calc.	Viol.
1:D-ALA^1:CB	1:D-ALA^1:HA	1.97	2.41	2.12	0
1:D-ALA^1:CN	1:ALA^5:HA	1.89	2.31	2.6	0.29
1:D-ALA^1:CN	1:ALA^5:HN	2.68	3.27	3.46	0.18
1:ALA^5:HA	1:ALA^5:HN	2.3	2.81	2.9	0.09
1:ALA^5:CB	1:ALA^5:HA	1.97	2.41	2.15	0
1:ALA^5:CB	1:ALA^5:HN	2.68	3.27	3.23	0
1:ALA^4:HA	1:ALA^5:HN	2.35	2.88	3.32	0.43
1:ALA^4:HA	1:ALA^4:HN	2.3	2.81	3.01	0.2
1:ALA^4:CB	1:ALA^4:HA	1.97	2.41	2.13	0
1:ALA^4:HN	1:ALA^5:HN	2.38	2.9	2.43	0
1:ALA^4:HN	1:ALA^3:HN	2.7	3.3	2.73	0
1:ALA^3:CB	1:ALA^4:HN	2.2	2.69	2.86	0.16
1:ALA^3:CB	1:ALA^3:HA	1.97	2.41	2.14	0
1:ALA^3:CB	1:ALA^3:HN	2.49	3.04	2.72	0
1:ALA^3:HN	1:ALA^3:HA	2.4	2.94	3.03	0.08
1:ALA^3:HN	1:ALA^2:HA	2.49	3.04	3.42	0.38
1:ALA^2:CB	1:ALA^2:HA	1.98	2.42	2.08	0
1:ALA^2:CN	1:D-ALA^1:HA	1.81	2.21	2.6	0.38
1:ALA^2:CN	1:ALA^4:HN	2.94	3.6	3.83	0.21
1:ALA^2:CN	1:ALA^3:HN	2.38	2.9	2.66	0

cyclo(-D-MeAla[1]-MeAla[2]-Ala[3]-Ala[4]-MeAla[5])

Table 7.8. *^1H shifts of the respective protons.*

	H^{β}	H^{α}	H^{N}	N^{CH_3}
1.D-Ala	1,01(d, 6.5 Hz)	5,31(m)		2,45(s)
2.L-Ala	1,22(d, 6.7 Hz)	3,82(m)		3,10(s)
3.L-Ala	1,12(d, 6.9 Hz)	4,64(m)	7,07(d, 7.7 Hz)	
4.L-Ala	1,35(d, 7.4 Hz)	3,77(m)	7,76(d, 7.6 Hz)	
5.L-Ala	1,25(d, 7.6 Hz)	5,12(m)		2,87(s)

Table 7.9. *Distance restraints and their violations during the 150 ps rMD simulation. The calculated distances are obtained by $<r^{-3}>$ averaging.*

Atom 1	Atom 2	Low.	Upp.	Calc.	Viol.
1:D-ALA[1]:CB	1:D-ALA[1]:HA	1.98	2.42	2.11	0
1:D-ALA[1]:CN	1:D-ALA[1]:HA	2.91	3.55	3.5	0
1:D-ALA[1]:CN	1:ALA[5]:HA	1.99	2.43	2.63	0.19
1:ALA[5]:CB	1:ALA[5]:HA	1.97	2.41	2.09	0
1:ALA[5]:CN	1:ALA[5]:HA	2.01	2.45	2.56	0.1
1:ALA[5]:CN	1:ALA[4]:HA	1.85	2.26	2.53	0.27
1:ALA[4]:HA	1:ALA[4]:HN	2.59	3.17	3.06	0
1:ALA[4]:CB	1:ALA[4]:HA	2	2.44	2.13	0
1:ALA[4]:CB	1:ALA[4]:HN	2.55	3.12	2.89	0
1:ALA[4]:HN	1:ALA[3]:HN	2.52	3.08	2.61	0
1:ALA[3]:HA	1:ALA[3]:HN	2.34	2.86	3.02	0.15
1:ALA[3]:CB	1:ALA[4]:HN	2.61	3.19	3.18	0
1:ALA[3]:CB	1:ALA[3]:HA	1.99	2.43	2.13	0
1:ALA[3]:CB	1:ALA[3]:HN	2.49	3.04	2.69	0
1:ALA[2]:HA	1:ALA[3]:HN	2.4	2.93	3.39	0.46
1:ALA[2]:CB	1:ALA[3]:HN	2.38	2.9	2.62	0
1:ALA[2]:CB	1:ALA[2]:HA	1.99	2.43	2.08	0
1:ALA[2]:CN	1:D-ALA[1]:HA	1.78	2.17	2.57	0.39
1:ALA[2]:CN	1:ALA[4]:HN	2.44	2.99	3.14	0.14
1:ALA[2]:CN	1:ALA[3]:HN	2.52	3.08	2.99	0

cyclo(-D-MeAla[1]-Ala[2]-Ala[3]-MeAla[4]-MeAla[5])

Table 7.10. *^1H shifts of the respective protons.*

	H^{β}	H^{α}	H^{N}	N^{CH_3}
1.D-Ala	1.25(d, 7.0 Hz)	4,63(m)		3,10(s)
2.L-Ala	1,23(d, 7.5 Hz)	3,95(m)	8,73(d, 6.8 Hz)	
3.L-Ala	0,98(d, 6.4 Hz)	4,25(m)	6,86(d, 7.4 Hz)	
4.L-Ala	1,12(d, 6.4 Hz)	4,23(m)		2,79(s)
5.L-Ala	1,34(d, 7.0 Hz)	4,85(m)		2,68(s)

Table 7.11. *Distance restraints and their violations during the 150 ps rMD simulation.*

Atom 1	Atom 2	Low.	Upp.	Calc.	Viol.
1:D-ALA[1]:HA	1:ALA[3]:HN	2.86	3.49	3.61	0.11
1:D-ALA[1]:HA	1:ALA[2]:HN	1.85	2.26	2.1	0
1:D-ALA[1]:CB	1:D-ALA[1]:HA	1.91	2.33	2.07	0
1:D-ALA[1]:CN	1:D-ALA[1]:HA	2.52	3.08	2.59	0
1:D-ALA[1]:CN	1:ALA[5]:HA	1.79	2.18	2.86	0.67
1:ALA[5]:HA	1:ALA[4]:HA	1.54	1.88	2.23	0.34
1:ALA5:CB	1:ALA5:HA	1.97	2.41	2.15	0
1:ALA5:CN	1:ALA5:HA	2.71	3.32	3.43	0.11
1:ALA4:CB	1:ALA4:HA	1.88	2.3	2.1	0
1:ALA4:CN	1:ALA5:HA	2.21	2.71	2.7	0
1:ALA4:CN	1:ALA4:HA	1.65	2.02	2.47	0.44
1:ALA4:CN	1:ALA3:HN	2.49	3.04	3.48	0.43
1:ALA3:HA	1:ALA3:HN	2.34	2.86	3.02	0.16
1:ALA3:CB	1:ALA3:HA	1.9	2.32	2.13	0
1:ALA3:CB	1:ALA3:HN	2.43	2.97	3.01	0.03
1:ALA3:HN	1:ALA2:HN	2.16	2.64	2.51	0
1:ALA2:HA	1:ALA3:HN	2.91	3.55	3.39	0
1:ALA2:HA	1:ALA2:HN	2.46	3	3.01	0.01
1:ALA2:CB	1:ALA3:HN	2.53	3.1	3.39	0.28
1:ALA2:CB	1:ALA2:HA	1.88	2.29	2.15	0
1:ALA2:CB	1:ALA2:HN	2.45	3	2.57	0

cyclo(-D-MeAla[1]-Ala[2]-MeAla[3]-MeAla[4]-MeAla[5])

Table 7.12. *^1H shifts of the respective protons.*

	H^{β}	H^{α}	H^{N}	N^{CH_3}
1.D-Ala	1.16(d, 6.9 Hz)	5,07(m)		2,88(s)
2.L-Ala	1,11(d, 6.6 Hz)	4,74(m)	8,82(d, 9.7 Hz)	
3.L-Ala	1,26(d, 6.8 Hz)	4,39(m)		2,64(s)
4.L-Ala	1,08(d, 6.4 Hz)	4,77(m)		2,71(s)
5.L-Ala	1,36(d, 7.0 Hz)	4,49(m)		2,90(s)

Table 7.13. *Distance restraints and their violations during the 150 ps rMD simulation.*

Atom 1	Atom 2	Low.	Upp.	Calc.	Viol.
1:D-ALA[1]:HA	1:ALA[2]:HN	1.96	2.39	2.25	0
1:D-ALA[1]:CB	1:D-ALA[1]:HA	2.02	2.46	2.12	0
1:ALA[5]:CB	1:ALA[5]:HA	1.97	2.41	2.12	0
1:D-ALA[1]:CN	1:D-ALA[1]:HA	2.81	3.44	3.49	0.05
1:D-ALA[1]:CN	1:ALA[5]:HA	1.84	2.25	2.57	0.32
1:D-ALA[1]:CN	1:ALA[3]:HA	2.36	2.89	3.02	0.12
1:ALA[4]:CN	1:ALA[5]:HA	2.3	2.81	3.17	0.35
1:ALA[4]:CN	1:ALA[4]:HA	2.41	2.94	3.4	0.46
1:ALA[4]:CN	1:ALA[3]:HA	1.98	2.42	2.78	0.36
1:ALA[4]:CN	1:ALA[2]:HN	2.5	3.06	3.11	0.04
1:ALA[4]:HA	1:ALA[5]:HA	2.66	3.26	2.43	-0.23
1:ALA[3]:HA	1:ALA[2]:HA	1.69	2.07	2.34	0.26
1:ALA[3]:CB	1:ALA[3]:HA	1.96	2.4	2.12	0
1:ALA[3]:CB	1:ALA[2]:HA	2.19	2.68	2.86	0.18
1:ALA[3]:CN	1:ALA[3]:HA	2.63	3.21	3.44	0.23
1:ALA[2]:HA	1:ALA[2]:HN	2.57	3.14	3	0
1:ALA[2]:CB	1:ALA[2]:HA	1.72	2.1	2.14	0.04
1:ALA[2]:CB	1:ALA[2]:HN	2.55	3.12	3.1	0
1:ALA[2]:HN	1:ALA[3]:HA	2.56	3.12	2.93	0

cyclo(-D-Ala[1]-Ala[2]-Ala[3]-MeAla[4]-MeAla[5])

Table 7.14. *^1H shifts of the respective protons.*

	H^{β}	H^{α}	H^{N}	N^{CH_3}
1.D-Ala	1.23(d, 6.9 Hz)	4,16(m)	8,25(d, 6.2 Hz)	
2.L-Ala	1,24(d, 7.4 Hz)	3,93(m)	8,88(d, 6.6 Hz)	
3.L-Ala	0,98(d, 6.3 Hz)	4,29(m)	7,31(d, 7.7 Hz)	
4.L-Ala	1,14(d, 6.3 Hz)	3,97(m)		2,78(s)
5.L-Ala	1,47(d, 6.9 Hz)	4,12(m)		2,54(s)

Table 7.15. *Distance restraints and their violations during the 150 ps rMD simulation.*

Atom 1	Atom 2	Low.	Upp.	Calc.	Viol.
1:D-ALA[1]:CB	1:D-ALA[1]:HA	1.96	2.4	2.13	0
1:D-ALA[1]:CB	1:D-ALA[1]:HN	2.22	2.71	2.62	0
1:ALA[5]:HA	1:D-ALA[1]:HN	2.12	2.59	2.41	0
1:ALA[5]:CB	1:D-ALA[1]:HN	2.08	2.54	2.72	0.17
1:ALA[5]:CB	1:ALA[5]:HA	1.97	2.41	2.12	0
1:ALA[5]:CN	1:ALA[5]:CB	2	2.45	3	0.5
1:ALA[4]:HA	1:ALA[5]:HA	1.65	2.02	2.09	0.06
1:ALA[4]:CB	1:ALA[4]:HA	1.93	2.36	2.06	0
1:ALA[4]:CN	1:ALA[5]:HA	1.99	2.44	2.77	0.32
1:ALA[4]:CN	1:ALA[4]:HA	1.92	2.35	2.53	0.18
1:ALA[4]:CN	1:ALA[4]:CB	2.32	2.83	3.38	0.54
1:ALA[4]:CN	1:ALA[3]:HA	1.83	2.24	2.63	0.39
1:ALA[4]:CN	1:ALA[3]:HN	2.45	3	3.32	0.31
1:ALA[3]:CB	1:ALA3:HA	1.94	2.37	2.16	0
1:ALA[3]:HN	1:ALA[3]:HA	2.37	2.9	2.86	0
1:ALA[3]:HN	1:ALA[3]:CB	2.54	3.11	3.24	0.12
1:ALA[2]:HA	1:ALA[2]:HN	2.61	3.19	2.99	0
1:ALA[2]:CB	1:ALA[2]:HA	1.94	2.38	2.14	0
1:ALA[2]:CB	1:ALA[2]:HN	2.25	2.75	2.59	0
1:ALA[2]:HN	1:D-ALA[1]:HA	1.86	2.28	2.18	0
1:ALA[2]:HN	1:ALA[3]:HN	2.27	2.78	2.72	0

Cyclic peptides with preferred conformation:

cyclo(-D-Ala^1-MeAla^2-Ala^3-Ala^4-Ala^5-)

Table 7.16. *^{1}H shifts of the respective protons.*

	H^{β}	H^{α}	H^{N}	N^{CH_3}
1.D-Ala	1.18(d, 7.0 Hz)	4.61(m)	8.59(d, 6.2 Hz)	
2.L-Ala	1.25(d, 7.3 Hz)	4.95(m)		2.97(s)
3.L-Ala	1.37(d, 6.7 Hz)	4.16(m)	7.21(d, 7.2 Hz)	
4.L-Ala	1.28(d, 7.0 Hz)	4.00(m)	7.94(d, 6.8 Hz)	
5.L-Ala	1.19(d, 7.0 Hz)	4.29(m)	7.56(d, 8.4 Hz)	

Table 7.17. *Distance restraints and their violations during the 150 ps rMD simulation of **2**. The calculated distances are obtained by $<r^{-3}>$ averaging. (N:XX = residue number:atom)*

Atom 1	Atom 2	Low.	Upp.	Calc.	Viol.
1:D-ALA^1:HA	1:D-ALA^1:HN	2.59	3.16	2.89	0
1:D-ALA^1:HA	1:ALA^5:HN	2.27	2.8	2.23	-0.03
1:D-ALA^1:CB	1:D-ALA^1:HA	1.97	2.4	2.17	0
1:D-ALA^1:CB	1:D-ALA^1:HN	2.5	3.03	3.09	0.06
1:D-ALA^1:HN	1:ALA^2:HA	2.36	2.89	2.27	-0.08
1:D-ALA^1:HN	1:ALA^5:HN	2.51	3.05	3.14	0.09
1:ALA^2:CB	1:ALA^2:HA	1.97	2.4	2.07	0
1:ALA^2:NMe	1:D-ALA^1:HN	2.7	3.31	2.87	0
1:ALA^2:NMe	1:ALA^2:HA	2.04	2.47	2.54	0.07
1:ALA^2:NMe	1:ALA^3:HA	2.09	2.58	2.68	0.1
1:ALA^2:NMe	1:ALA^3:HN	3.54	4.32	3.68	0
1:ALA^3:HA	1:ALA^3:HN	2.52	3.08	3.03	0
1:ALA^3:CB	1:ALA^3:HA	2	2.45	2.14	0
1:ALA^3:CB	1:ALA^3:HN	2.56	3.14	3.05	0
1:ALA^3:HN	1:ALA^3:HN	2.25	2.75	2.66	0
1:ALA^4:HA	1:ALA^3:HN	2.84	3.48	3.56	0.08
1:ALA^4:HA	1:ALA^4:HN	2.47	3.02	3.01	0
1:ALA^4:CB	1:ALA^3:HN	2.65	3.24	3.08	0
1:ALA^4:CB	1:ALA^4:HA	1.97	2.4	2.13	0
1:ALA^4:CB	1:ALA^4:HN	2.65	3.24	2.67	0
1:ALA^4:HN	1:ALA^5:HA	2.51	3.06	3.41	0.05
1:ALA^4:HN	1:ALA^5:HN	2.73	3.34	2.72	0
1:ALA^5:HA	1:ALA^5:HN	2.5	3.06	3	0
1:ALA^5:CB	1:ALA^4:HN	2.01	2.44	2.52	0.09
1:ALA^5:CB	1:ALA^5:HA	1.99	2.43	2.14	0
1:ALA^5:CB	1:ALA^5:HN	2.47	3.02	3.07	0.05

cyclo(-D-Ala^1-Ala^2-Ala^3-Ala^4-MeAla^5-)

Table 7.18. *^{1}H shifts of the respective protons.*

	H^{β}	H^{α}	H^{N}	N^{CH_3}
1.D-Ala	1.19(d, 7.3 Hz)	4.38(m)	7.85(d, 8.4 Hz)	
2.L-Ala	1.28(d, 7.1 Hz)	4.26(m)	7.29(d, 8.2 Hz)	
3.L-Ala	1.32(d, 7.6 Hz)	4.02(m)	8.14(d, 7.6 Hz)	
4.L-Ala	1.13(d, 6.2 Hz)	4.55(m)	7.57(d, 7.0 Hz)	
5.L-Ala	1.22(d, 6.8 Hz)	3.63(m)		3.1(s)

Table 7.19. *Distance restraints and their violations during the 150 ps rMD simulation.*

Atom 1	Atom 2	Low.	Upp.	Calc.	Viol.
1:D-ALA^1:HA	1:D-ALA^1:HN	2.59	3.16	2.89	0
1:D-ALA^1:HA	1:ALA^2:HN	2.27	2.8	2.22	-0.03
1:D-ALA^1:CB	1:D-ALA^1:HA	1.97	2.4	2.17	0
1:D-ALA^1:CB	1:D-ALA^1:HN	2.5	3.03	3.09	0.06
1:D-ALA^1:HN	1:ALA^5:HA	2.36	2.89	2.26	-0.08
1:D-ALA^1:HN	1:ALA^2:HN	2.51	3.05	3.12	0.09
1:ALA^2:HA	1:ALA^2:HN	2.5	3.06	3	0
1:ALA^2:CB	1:ALA^3:HN	2.01	2.44	2.52	0.09
1:ALA^2:CB	1:ALA^2:HA	1.99	2.43	2.14	0
1:ALA^2:CB	1:ALA^2:HN	2.47	3.02	3.06	0.05
1:ALA^3:HA	1:ALA^4:HN	2.84	3.48	3.55	0.08
1:ALA^3:HA	1:ALA^3:HN	2.47	3.02	3.01	0
1:ALA^3:CB	1:ALA^4:HN	2.65	3.24	3.06	0
1:ALA^3:CB	1:ALA^3:HA	1.97	2.4	2.13	0
1:ALA^3:CB	1:ALA^3:HN	2.65	3.24	2.66	0
1:ALA^3:HN	1:ALA^2:HA	2.51	3.06	3.41	0.05
1:ALA^3:HN	1:ALA^2:HN	2.73	3.34	2.7	0
1:ALA^4:HA	1:ALA^4:HN	2.52	3.08	3.03	0
1:ALA^4:CB	1:ALA^4:HA	2	2.45	2.14	0
1:ALA^4:CB	1:ALA^4:HN	2.56	3.14	3.05	0
1:ALA^4:HN	1:ALA^3:HN	2.25	2.75	2.64	0
1:ALA^5:CB	1:ALA^5:HA	1.97	2.4	2.07	0
1:ALA^5:NMe	1:D-ALA^1:HN	2.7	3.31	2.85	0
1:ALA^5:NMe	1:ALA^5:HA	2.04	2.47	2.54	0.07
1:ALA^5:NMe	1:ALA^4:HA	2.09	2.58	2.67	0.1
1:ALA^5:NMe	1:ALA^4:HN	3.54	4.32	3.67	0

cyclo(-D-Ala^1-MeAla^2-MeAla^3-Ala^4-Ala^5-)

Table 7.20. *^{1}H shifts of the respective protons.*

	H^{β}	H^{α}	H^{N}	N^{CH_3}
1.D-Ala	1.09(d, 6.7 Hz)	4.67(m)	7.50(d, 9.0 Hz)	
2.L-Ala	1.11(d, 6.7 Hz)	5.38(m)		2.77(s)
3.L-Ala	1.31(d, 6.2 Hz)	4.50(m)		2.69(s)
4.L-Ala	1.20(d, 6.4 Hz)	4.27(m)	7.16(d, 8.1 Hz)	
5.L-Ala	1.21(d, 6.5 Hz)	3.95(m)	8.18(d, 7.7 Hz)	

Table 7.21. *Distance restraints and their violations during the 150 ps rMD simulation.*

Atom 1	Atom 2	Low.	Upp.	Calc.	Viol.
1:D-ALA^1:HA	1:D-ALA^1:HN	2.3	2.79	2.9	0.11
1:D-ALA^1:CB	1:D-ALA^1:HA	1.98	2.42	2.14	0
1:D-ALA^1:CB	1:D-ALA^1:HN	2.64	3.22	3.06	0
1:D-ALA^1:HN	1:ALA^5:HA	2.24	2.74	2.35	0
1:D-ALA^1:HN	1:ALA^5:HN	2.46	3.01	2.54	0
1:D-ALA^1:HN	1:ALA^3:HA	3.08	3.77	3.43	0
1:ALA^2:CB	1:ALA^2:HA	2.02	2.47	2.12	0
1:ALA^2:NMe	1:D-ALA^1:HA	2.02	2.47	2.59	0.12
1:ALA^2:NMe	1:D-ALA^1:HN	2.93	3.59	3.71	0.12
1:ALA^2:NMe	1:ALA^5:HN	3.55	4.34	4.47	0.13
1:ALA^2:NMe	1:ALA^4:HN	2.75	3.36	2.98	0
1:ALA^2:NMe	1:ALA^2:HA	3.05	3.73	3.46	0
1:ALA^3:HA	1:ALA^4:HN	2.55	3.11	2.65	0
1:ALA^3:HA	1:ALA^2:HA	1.66	2.04	2.16	0.12
1:ALA^3:CB	1:ALA^4:HN	3.08	3.77	3.84	0.07
1:ALA^3:CB	1:ALA^3:HA	2.08	2.54	2.1	0
1:ALA^3:CB	1:ALA^2:HA	2.73	3.34	3.3	0
1:ALA^3:NMe	1:ALA^4:HN	2.34	2.86	2.93	0.07
1:ALA^3:NMe	1:ALA^3:HA	3.1	3.79	3.51	0
1:ALA^4:HA	1:ALA^4:HN	2.43	2.97	3.07	0.1
1:ALA^4:CB	1:ALA^4:HA	1.82	2.23	2.13	0
1:ALA^4:CB	1:ALA^4:HN	2.61	3.19	2.79	0
1:ALA^5:HA	1:ALA^5:HN	2.18	2.66	2.35	0
1:ALA^5:CB	1:ALA^5:HA	1.97	2.4	2.09	0
1:ALA^5:CB	1:ALA^5:HN	2.44	2.98	3.37	0.39
1:ALA^5:HN	1:ALA^4:HA	2.15	2.63	2.44	0
1:ALA^5:HN	1:ALA^4:HN	2.39	2.92	3.22	0.3

cyclo(-D-Ala[1]-MeAla[2]-Ala[3]-MeAla[4]-Ala[5]-)

Table 7.22. *^{1}H shifts of the respective protons.*

	H^{β}	H^{α}	H^{N}	N^{CH_3}
1.D-Ala	1.26(-)	4.80(m)	8.12(d, 9.0 Hz)	
2.L-Ala	1.26(-)	4.93(m)		2.49(s)
3.L-Ala	1.11(d, 5.6 Hz)	4.67(m)	8.56(d, 8.3 Hz)	
4.L-Ala	1.27(-)	4.22(m)		2.53(s)
5.L-Ala	1.07(d, 6.2 Hz)	4.30(m)	8.04(d, 8.4 Hz)	

Table 7.23. *Distance restraints and their violations during the 150 ps rMD simulation.*

Atom 1	Atom 2	Low.	Upp.	Calc.	Viol.
1:D-ALA[1]:HA	1:D-ALA[1]:HN	2.43	2.98	3.05	0.07
1:D-ALA[1]:CB	1:D-ALA[1]:HA	1.87	2.28	2.11	0
1:D-ALA[1]:CB	1:D-ALA[1]:HN	2.52	3.08	2.75	0
1:D-ALA[1]:HN	1:ALA[5]:HA	2.13	2.6	2.2	0
1:ALA[2]:CB	1:ALA[2]:HA	1.87	2.32	2.07	0
1:ALA[2]:NMe	1:D-ALA[1]:HA	2.72	3.35	2.68	-0.03
1:ALA[2]:NMe	1:ALA[3]:HN	2.48	3.03	2.53	0
1:ALA[2]:NMe	1:ALA[2]:HA	2.92	3.57	3.47	0
1:ALA[3]:HA	1:ALA[3]:HN	2.57	3.14	2.97	0
1:ALA[3]:CB	1:ALA[3]:HA	1.97	2.4	2.14	0
1:ALA[3]:CB	1:ALA[3]:HN	2.73	3.33	3.19	0
1:ALA[3]:HN	1:ALA[2]:HA	2.55	3.12	3.46	0.04
1:ALA[4]:HA	1:ALA[3]:HA	1.82	2.23	2.15	0
1:ALA[4]:HA	1:ALA[3]:HN	2.71	3.32	2.99	0
1:ALA[4]:CB	1:ALA[3]:HA	2.35	2.88	2.83	0.04
1:ALA[4]:NMe	1:ALA[5]:HN	2.47	3.01	3.2	0.2
1:ALA[4]:NMe	1:ALA[4]:HA	2.94	3.59	3.47	0
1:ALA[5]:HA	1:ALA[5]:HN	2.35	2.88	2.87	0
1:ALA[5]:CB	1:ALA[5]:HA	1.97	2.4	2.15	0
1:ALA[5]:CB	1:ALA[5]:HN	2.66	3.25	3.08	0
1:ALA[5]:HN	1:ALA[4]:HA	2.14	2.61	2.41	0
1:ALA[5]:HN	1:ALA[3]:HN	2.35	2.88	3.06	0.19
1:ALA[2]:NMe	1:ALA[2]:HA	2.92	3.57	3.47	0

cyclo(-D-Ala[1]-Ala[2]-MeAla[3]-MeAla[4]-Ala[5]-)

Table 7.24. *^{1}H shifts of the respective protons.*

	H^{β}	H^{α}	H^{N}	N^{CH_3}
1.D-Ala	1.23(d, 6.5 Hz)	4.03(m)	8.52(d, 6.8 Hz)	
2.L-Ala	1.15(d, 6.5 Hz)	4.78(m)	7.58(d, 8.5 Hz)	
3.L-Ala	1.10(d, 7.0 Hz)	5.27(m)		2.74(s)
4.L-Ala	1.22(d, 6.2 Hz)	5.00(m)		2.73(s)
5.L-Ala	1.20(d, 6.7 Hz)	4.12(m)	8.20(d, 9.5 Hz)	

Table 7.25. *Distance restraints and their violations during the 150 ps rMD simulation.*

Atom 1	Atom 2	Low.	Upp.	Calc.	Viol.
1:D-ALA[1]:HA	1:D-ALA[1]:HN	2.59	3.09	2.289	-0.29
1:D-ALA[1]:HA	1:ALA[2]:HN	2.64	3.27	2.617	0
1:D-ALA[1]:CB	1:D-ALA[1]:HA	2.12	2.59	2.107	-0.01
1:D-ALA[1]:CB	1:D-ALA[1]:HN	2.47	3.02	3.072	0.05
1:D-ALA[1]:CB	1:ALA[2]:HN	3.16	3.84	3.951	0.01
1:D-ALA[1]:HN	1:ALA[5]::HA	1.99	2.44	2.768	0.33
1:D-ALA[1]:HN	1:ALA[2]:HN	2.81	3.44	2.982	0
1:ALA[2]:HA	1:ALA[2]:HN	2.73	3.34	3.005	0
1:ALA[2]:CB	1:ALA[2]:HA	1.97	2.4	2.157	0
1:ALA[2]:CB	1:ALA[2]:HN	2.63	3.21	2.918	0
1:ALA[3]:CB	1:ALA[3]:HA	2.03	2.51	2.099	0
1:ALA[3]:NME	1:ALA[2]:HA	2.15	2.58	2.614	0.04
1:ALA[4]:CB	1:ALA[4]:HA	2.05	2.57	2.098	0
1:ALA[4]:NMe	1:ALA[4]:HA	3.13	3.83	3.288	0
1:ALA[4]:NMe	1:ALA[3]:HA	2.09	2.55	3.057	0.51
1:ALA[5]:HA	1:ALA[5]:HN	2.77	3.39	3.062	0
1:ALA[5]:CB	1:ALA[5]:HA	1.97	2.4	2.149	0
1:ALA[5]:CB	1:ALA[5]::HN	2.25	2.75	2.79	0.04
1:ALA[5]:HN	1:ALA[4]:HA	2.31	2.82	2.881	0.1

cyclo(-D-Ala[1]-Ala[2]-MeAla[3]-Ala[4]-MeAla[5]-)

Table 7.26. *^1H shifts of the respective protons.*

	H^{β}	H^{α}	H^{N}	N^{CH_3}
1.D-Ala	1.16(-)	4.15(m)	7.97(d, 8.1 Hz)	
2.L-Ala	1.15(-)	4.40(m)	8.08(d, 7.5 Hz)	
3.L-Ala	1.22(d, 7.0 Hz)	4.31(m)		2.51(s)
4.L-Ala	1.13(-)	4.65(m)	8.18(d, 8.0 Hz)	
5.L-Ala	1.34(d, 6.8 Hz)	4.05(m)		2.90(s)

Table 7.27. *Distance restraints and their violations during the 150 ps rMD simulation.*

Atom 1	Atom 2	Low.	Upp.	Calc.	Viol.
1:D-ALA[1]:HA	1:D-ALA[1]:HN	1.87	2.28	2.38	0
1:D-ALA[1]:HA	1:ALA[2]:HN	2.11	2.58	2.33	0
1:D-ALA[1]:CB	1:D-ALA[1]:HA	1.94	2.37	2.1	0
1:D-ALA[1]:CB	1:D-ALA[1]:HN	2.59	3.15	3.17	0.04
1:D-ALA[1]:HN	1:ALA[5]:HA	2.12	2.59	3.07	0.5
1:ALA[2]:HA	1:ALA[2]:HN	1.75	3.14	2.87	0
1:ALA[2]:CB	1:ALA[2]:HA	1.85	2.27	2.16	0
1:ALA[2]:CB	1:ALA[2]:HN	2.5	3.05	3.22	0.07
1:ALA[3]:HA	1:ALA[2]:HA	1.83	2.24	2.24	0.01
1:ALA[3]:HA	1:ALA[2]:HN	2.1	2.53	2.55	0.04
1:ALA[3]:CB	1:ALA[3]:HA	1.95	2.38	2.11	0
1:ALA[3]:NMe	1:ALA[4]:HN	2.37	2.9	3.05	0.06
1:ALA[4]:HA	1:ALA[4]:HN	2.49	3.04	3.04	0.01
1:ALA[4]:CB	1:ALA[4]:HA	1.92	2.32	2.13	0
1:ALA[4]:CB	1:ALA[4]:HN	2.47	3.02	2.99	0
1:ALA[4]:HN	1:ALA[3]:HA	2.4	2.93	2.47	0
1:ALA[5]:HA	1:ALA[4]:HA	1.61	1.96	2.11	0.05
1:ALA[5]:HA	1:ALA[4]:HN	2.65	3.24	3.31	0.08
1:ALA[5]:CB	1:D-ALA[1]:HN	2.56	3.12	3.45	0.34
1:ALA[5]:CB	1:ALA[5]:HA	1.97	2.4	2.1	0
1:ALA[5]:NMe	1:D-ALA[1]:HN	2.52	3.08	2.5	0

cyclo(-D-Ala[1]-Ala[2]-MeAla[3]-MeAla[4]-MeAla[5]-)

Table 7.28. *^1H shifts of the respective protons.*

	H^{β}	H^{α}	H^{N}	N^{CH_3}
1.D-Ala	1.14(d, 7.5 Hz)	4.37(m)	8.25(d, 8.7 Hz)	
2.L-Ala	1.10(d, 6.4 Hz)	4.76(m)	8.70(d, 9.8 Hz)	
3.L-Ala	1.26(d, 7.0 Hz)	4.45(m)		2.68(s)
4.L-Ala	1.08(d, 6.7 Hz)	4.24(m)		2.80(s)
5.L-Ala	1.37(d, 7.2 Hz)	3.95(m)		2.84(s)

Table 7.29. *Distance restraints and their violations during the 150 ps rMD simulation.*

Atom 1	Atom 2	Low.	Upp.	Calc.	Viol.
1:D-ALA[1]:HA	1:D-ALA[1]:HN	2.7	3.3	3.06	0
1:D-ALA[1]:HA	1:ALA[2]:HN	1.98	2.42	2.54	0.03
1:D-ALA[1]:CB	1:D-ALA[1]:HA	1.98	2.42	2.13	0
1:D-ALA[1]:CB	1:D-ALA[1]:HN	2.42	2.96	2.68	0
1:D-ALA[1]:HN	1:ALA[5]:HA	2.1	2.57	2.14	0
1:D-ALA[1]:HN	1:ALA[3]:HA	2.94	3.59	3.83	0.25
1:ALA[2]:HA	1:ALA[2]:HN	2.74	3.35	2.7	-0.03
1:ALA[2]:CB	1:ALA[2]:HA	1.96	2.39	2.16	0
1:ALA[2]:CB	1:ALA[2]:HN	2.53	3.09	3.36	0.23
1:ALA[2]:HN	1:ALA[3]:HA	1.47	1.79	2.13	0.31
1:ALA[3]:HA	1:ALA[2]:HA	1.69	2.06	2.18	0.04
1:ALA[3]:CB	1:ALA[3]:HA	2.04	2.5	2.13	0
1:ALA[3]:CB	1:ALA[2]:HA	2.17	2.65	2.88	0.06
1:ALA[3]:NMe	1:ALA[3]:HA	3.19	3.9	3.48	0
1:ALA[4]:NMe	1:D-ALA[1]:HN	2.82	3.45	3.06	0
1:ALA[4]:NMe	1:ALA[5]:HA	2.29	2.8	2.77	0
1:ALA[4]:NMe	1:ALA[3]:HA	1.97	2.41	2.54	0.09
1:ALA[4]:NMe	1:ALA[2]:HN	2.85	3.48	3.86	0.29
1:ALA[5]:HA	1:ALA[4]:HA	2.28	2.79	2.15	0
1:ALA[5]:CB	1:D-ALA[1]:HN	2.48	3.03	3.13	0.01
1:ALA[5]:CB	1:ALA[5]:HA	1.97	2.4	2.07	0

cyclo(-D-Ala[1]-MeAla[2]-Ala[3]-MeAla[4]-MeAla[5]-)

Table 7.30. *^{1}H shifts of the respective protons.*

	H^{β}	H^{α}	H^{N}	N^{CH_3}
1.D-Ala	1.27(d, 6.5 Hz)	4.67(m)	8.42(d, 5.8 Hz)	
2.L-Ala	1.34(d, 7.2 Hz)	4.78(m)		3.09(s)
3.L-Ala	1.00(d, 6.5 Hz)	4.32(m)	7.04(d, 7.4 Hz)	
4.L-Ala	1.15(d, 6.5 Hz)	3.96(m)		2.74(s)
5.L-Ala	1.49(d, 7.2 Hz)	4.10(m)		2.51(s)

Table 7.31. *Distance restraints and their violations during the 150 ps rMD simulation.*

Atom 1	Atom 2	Low.	Upp.	Calc.	Viol.
1:D-ALA[1]:HA	1:D-ALA[1]:HN	2.32	2.84	3.06	0.23
1:D-ALA[1]:CB	1:D-ALA[1]:HA	1.79	2.18	2.11	0
1:D-ALA[1]:CB	1:D-ALA[1]:HN	2.13	2.6	2.73	0.14
1:D-ALA[1]:HN	1:ALA[5]:HA	2.26	2.77	2.16	-0.08
1:ALA[2]:CB	1:ALA[2]:HA	1.79	2.19	2.07	0
1:ALA[2]:NMe	1:D-ALA[1]:HA	2.33	2.71	2.64	0
1:ALA[2]:NMe	1:ALA[3]:HN	2.26	2.74	2.73	0.05
1:ALA[3]:HA	1:ALA[3]:HN	2.52	3.05	3.05	0.01
1:ALA[3]:CB	1:ALA[3]:HA	1.86	2.28	2.12	0
1:ALA[3]:CB	1:ALA[3]:HN	2.28	2.81	2.87	0.09
1:ALA[3]:HN	1:ALA[2]:HA	2.67	3.21	3.55	0.34
1:ALA[4]:CB	1:ALA[4]:HA	1.82	2.23	2.07	0
1:ALA[4]:NMe	1:ALA[5]:HA	2.46	2.97	2.92	0
1:ALA[4]:NMe	1:ALA[4]:HA	2.12	2.5	2.57	0.08
1:ALA[4]:NMe	1:ALA[3]:HA	2.32	2.71	2.69	0
1:ALA[4]:NMe	1:ALA[3]:HN	3.31	4	4	0.09
1:ALA[4]:NMe	1:ALA[2]:HA	4.31	5.27	5.17	0
1:ALA[5]:HA	1:ALA[4]:HA	1.67	2.02	2.1	0.09
1:ALA[5]:CB	1:D-ALA[1]:HN	2.57	3.09	3.17	0.11
1:ALA[5]:CB	1:ALA[5]:HA	1.97	2.4	2.09	0

cyclo(-D-MeAla[1]-MeAla[2]-MeAla[3]-Ala4-Ala[5]-)

Table 7.32. *^{1}H shifts of the respective protons.*

	H^{β}	H^{α}	H^{N}	N^{CH_3}
1.D-Ala	1.10(-)	5.42(m)		2.42(s)
2.L-Ala	1.10(-)	5.26(m)		2.76(s)
3.L-Ala	1.32(d, 6.7 Hz)	4.07(m)		2.69(s)
4.L-Ala	1.27(d, 7.3 Hz)	4.39(m)	7.49(d, 9.2 Hz)	
5.L-Ala	1.15(d, 6.8 Hz)	4.43(m)	7.74(d, 9.3 Hz)	

Table 7.33. *Distance restraints and their violations during the 150 ps rMD simulation.*

Atom 1	Atom 2	Low.	Upp.	Calc.	Viol.
1:D-ALA[1]:CB	1:D-ALA[1]:HA	2.01	2.45	2.11	0
1:D-ALA[1]:NMe	1:ALA[5]:HA	2.05	2.52	2.52	0
1:D-ALA[1]:NMe	1:ALA[5]:HN	2.54	3.06	3.15	0.02
1:ALA[2]:CB	1:ALA[2]:HA	1.75	2.14	2.13	0
1:ALA[2]:NMe	1:D-ALA[1]:HA	2.09	2.48	2.59	0.11
1:ALA[2]:NMe	1:ALA[5]:HN	2.6	3.17	3.16	0
1:ALA[2]:NMe	1:ALA[4]:HN	2.38	2.91	3.21	0.11
1:ALA[3]:HA	1:ALA[4]:HN	2.43	2.97	2.84	0
1:ALA[3]:HA	1:ALA[2]:HA	1.73	2.07	2.11	0.04
1:ALA[3]:CB	1:ALA[3]:HA	2.01	2.46	2.08	0
1:ALA[3]:CB	1:ALA[2]:HA	2.36	2.89	3.12	0.13
1:ALA[3]:NMe	1:ALA[4]:HN	2.12	2.59	2.8	0.12
1:ALA[4]:HA	1:ALA[4]:HN	2.4	2.91	2.92	0.02
1:ALA[4]:CB	1:ALA[5]:HN	2.6	3.18	3.15	0
1:ALA[4]:CB	1:ALA[4]:HA	1.97	2.4	2.11	0
1:ALA[4]:CB	1:ALA[4]:HN	2.49	3.05	2.57	0
1:ALA[5]:HA	1:ALA[5]:HN	1.82	2.23	2.69	0.26
1:ALA[5]:CB	1:ALA[5]:HA	1.97	2.4	2.17	0
1:ALA[5]:CB	1:ALA[5]:HN	2.71	3.32	3.26	0

7.4 Synthesis of N-methylated Somatostatin analogs:

Synthesis of all the analogs was done on solid support on the TCP resin. To obtain successful cyclization of the linear peptides, lysine (except the analogs where threonine was N-methylated) was chosen as the C-terminal to be coupled to the resin. All the cyclizations were done in solution with the HATU/HOBt method and final work up of the dry crude product with $NaHCO_3$. The product was then purified by RP-HPLC.

The deprotection of the protecting groups: Boc and *t*-Bu in the prurified product was done in a 50% solution of dry DCM and TFA for 1 h. The solution was then evaporated and ether was added to precipitate the polar deprotected peptide.

cyclo(-wKTFPF-): MW- 806.4, R_t- 16.2, MS- 807.4, yield- 45%
cyclo(-wKTFPMeF-): MW- 820.4, R_t- 16.4, MS- 821.5, yield- 32%
cyclo(-wKTMeFPF-): MW- 820.4, R_t- 16.4, MS- 821.5, yield- 27%
cyclo(-wKMeTFPF-): MW- 820.4, R_t- 16.3, MS- 821.4, yield- 19%
cyclo(-wMeKTFPF-): MW- 820.4, R_t - 16.7, MS- 821.4, yield- 24%
cyclo(-MewKTFPF-): MW- 820.4, R_t - 17.0, MS- 821.5, yield- 28%
cyclo(-wKTMeFPMeF-): MW- 834.4, R_t - 17.3, MS- 835.5, yield- 18%
cyclo(-wKMeTFPMeF-): MW- 834.4, R_t - 17.3, MS- 835.5, yield- 12%
cyclo(-wMeKTFPMeF-): MW- 834.4, R_t- 18.5, MS- 835.5, yield- 14%
cyclo(-MewKTFPMeF-): MW- 834.4, R_t- 16.9, MS- 835.5, yield- 13%
cyclo(-wKMeTMeFPF-): MW- 834.4, R_t- 15.1, MS- 835.5, yield- 12%
cyclo(-wMeKTMeFPF-): MW- 834.4, R_t- 17.4, MS- 835.5, yield- 18%
cyclo(-MewKTMeFPF-): MW- 834.4, R_t- 17.4, MS- 835.5, yield- 15%
cyclo(-wMeKMeTFPF-): MW- 834.4, R_t- 16.1, MS- 835.5, yield- 16%
cyclo(-MewKMeTFPF-): MW- 834.4, R_t- 17.3, MS- 835.5, yield- 11%
cyclo(-MewMeKTFPF-): MW- 834.4, R_t- 17.7, MS- 835.5, yield- 15%
cyclo(-wKMeTMeFPMeF-): MW- 848.5, R_t- 16.6, MS- 849.4, yield- 8%
cyclo(-wMeKTMeFPMeF-): MW- 848.5, R_t- 18.9, MS- 849.4, yield- 6%
cyclo(-MewKTMeFPMeF-): MW- 848.5, R_t- 18.1, MS- 849.4, yield- 7%
cyclo(-wMeKMeTFPMeF-): MW- 848.5, R_t- 17.7, MS- 849.4, yield- 6%
cyclo(-MewKMeTFPMeF-): MW- 848.5, R_t- 17.3, MS- 849.4, yield- 8%
cyclo(-MewMeKTFPMeF-): MW- 848.5, R_t- 17.3, MS- 849.4, yield- 7%
cyclo(-wMeKMeTMeFPF-): MW- 848.5, R_t- 16.3, MS- 849.4, yield- 5%
cyclo(-MewKMeTMeFPF-): MW- 848.5, R_t- 16.8, MS- 849.4, yield- 5%
cyclo(-MewMeKTMeFPF-): MW- 848.5, R_t- 18.3, MS- 849.4, yield- 8%

cyclo(-MewMeKMeTFPF-): MW- 848.5, R_t - 18.1, MS- 849.4, yield- 4%
cyclo(-wMeKMeTMeFPMeF-): MW- 862.5, R_t- 16.2, MS- 863.5, yield- 2%
cyclo(-MewKMeTMeFPMeF-): MW- 862.5, R_t- 17.2, MS- 863.4, yield- 3%
cyclo(-MewMeKTMeFPMeF-): MW- 862.5, R_t- 17.4, MS- 863.5, yield- 1%
cyclo(-MewMeKMeTFPMeF-): MW- 862.5, R_t- 17.6, MS- 863.4, yield- 2%
cyclo(-MewMeKMeTMeFPF-): MW- 862.5, R_t- 17.9, MS- 863.5, yield- 1%

Somatostatin receptor activation: The affinity of every N-Methylated analog for five different human somatostatin receptors (hsst1-5, expressed in CCL-39 cells) was measured by using radioligand binding assays. Competition experiments for the specific binding of [125I]LTT-SRIF28 to these receptors were carried out and the affinities are reported as pKD values.
In vitro permeability study: Growth and maintenance of cells: Caco-2 cells were obtained from ATCC and then grown in 75 cm2 flasks with approximately 0.5·106 cells/flask at 37oC in 5% CO2 atmosphere and at relative humidity of 95%. The culture growth medium consisted of Dulbecco's Modified Eagle Medium (DMEM) supplemented with 10% heat-inactivated fetal bovine serum (FBS), 1% nonessential amino acids (NEAA), and 2mM L-glutamine. The medium was replaced twice weekly.
Preparation of cells for transport studies: For the transport studies, cells in a passage range of 52-60, were seeded at density of 25·105 cells/cm2 on untreated culture inserts of polycarbonate membrane with 0.4 μM pores and surface area of 1.1 cm2. The culture inserts containing Caco-2 monolayer were placed in 24 transwells plates 12mm, CostarTM. The culture medium was changed every other day. Transport studies were performed 21-23 days after seeding, when the cells were fully differentiated and the TEER values were stable (300-500 Ω·cm2).
Experiment protocol: Transport study (apical to basolateral ,A to B) was initiated by medium removal from both sides of the monolayer and replacement with apical buffer (600 μl) and basolateral buffer (1500μL), both warmed to 37oC. The cells were incubated for 30 minute period at 37oC with shaking (100 cycles/min). After incubation period the buffers were removed and replaced with 1500 μL basolateral buffer at the basolateral side. Test solutions were warmed previously to 37oC and added (600 μL) to the apical side of the monolayer. 50 μL samples were taken from the apical side immediately at the beginning of the experiment, resulting in 550 μL apical volume during the experiment. For the period of the experiment the cells were kept at 37oC with shaking. At predicted times (30, 60, 90, 120 and 150), the 200 μL samples were taken from the basolateral side and replaced with the same volume of flesh basolateral buffer to maintain a constant volume.

Interaction with the liposome bilayer

Vesicle preparation: All lipid constituents were dissolved in chloroform/ethanol (1:1, v/v) and dried *in vacuo* to a constant weight. All lipids were suspended in deionized water, followed by probe sonication on a Misonix Incorporated sonicator (Farmingdale, NY, USA), applying an output power of ~100 W. Vesicles containing lipid components and PDA were sonicated at 70°C for 3-4 min. The vesicle suspensions were then cooled to room temperature, incubated overnight at 4°C, and polymerized by irradiation at 254 nm for 20-30 s, resulting in solutions with an intense blue color. Vesicle suspensions were allowed to anneal for 30 min and centrifuged for 15 min at 6000 g to remove titanium particles.

UV-Vis measurements: Peptides at a concentration of 30 μM were added to 60 μL of polydiacetylene (PDA) containing vesicle solutions consisting of ~0.2 M phospholipids in 25 mM Tris-base (pH 8.0). Following addition of the peptides, the solutions were diluted to 1 ml and spectra were acquired at 28°C, between 400 nm and 700 nm, on a Jasco V-550 spectrophotometer (Jasco Corp., Tokyo, Japan), using a 1-cm optical path cell. To quantify the extent of blue-to-red color transitions within the vesicle solutions, the percentage colorimetric response (% CR) was defined and calculated as follows:

$$\% \text{ CR} = (PB0 - PBI / PB0) \times 100$$

Where PB = Ablue/(Ablue + Ared), and A is the absorbance at 640 nm (the 'blue' component), or 500 nm (the 'red' component). The colors 'blue' and 'red' refer to the visual appearance of the material, not the actual absorbance. $PB0$ is the blue/red absorption ratio of the control sample before the induction of a color change, and PBI is the value obtained for the vesicle solution after the colorimetric transition occurred.

Fluorescence quenching measurements: NBD-PE was added to lipids from a 1 mM chloroform stock solution, yielding a final concentration of 4 μM, and then dried together by vacuum sonication (see Vesicle preparation above). Samples were prepared by adding peptides, at a bound concentration of 30 μM, to 60 μL of vesicle solutions at ~0.2 mM total lipid concentration in 25 nm Tris-base (pH 8.0). The quenching reaction was initiated by adding sodium dithionite from a 0.6 M solution, prepared in 50 mM Tris base (pH 11.0) buffer, to a final concentration of 0.6 mM. The decrease in fluorescence was recorded for 210 s at 28°C using 468 nm excitation and 538 nm emissions on an Edinburgh FL920 spectrofluorimeter. The fluorescence decay was calculated as a percentage of initial fluorescence measured before the addition of sodium dithionite.

Preparing brush border membrane vesicles (BBMVs)

BBMVs were prepared from combined duodenum, jejunum and upper ileum of rats by a Ca2+ precipitation method. The intestines of five rats, 200-250 g, were rinsed with ice cold

0.9% NaCl and freed of mucous; the mucosa was scraped off the luminal surface with glass slides and put immediately into buffer containing 50 nM KCl and 10 mM Tris-HCl (pH 7.5, 4°C) and the mixture homogenized by Polytron (Polytron PT 1200, Kinematica AG, Switzerland). CaCl2 was added to a final concentration of 10 mM. The homogenate was left shaking for 30 min at 4°C and subsequently centrifuged at 10,000 g for 10 min. The supernatant was then centrifuged at 400,000 g for 30 min and additional two purification steps were performed by suspending the pellet in 300 mM mannitol and 10 mM Hepes/Tris (pH 7.5) and centrifuged (400,000 g, 1 hr). Purification of brush border membranes was assayed using the brush border membrane enzyme markers GGT, LAP and alkaline phosphatase. During the course of these studies, enrichment in brush border membrane enzymes varied between 13- and 18-fold.

The enzymatic reaction was performed as follows: 2 μM stock solutions of the peptides were diluted with purified BBMV's solution to a final 0.5 μM. The solution was incubated at 37°C and sampled at time 0, 10, 20, 30, 60 and 90 min. The enzymatic reaction was stopped by adding 1:1 v/v of ice-cold acetonitrile and centrifuged (4,000 g, 10 min) before analysis.

Animals

All surgical and experimental procedures were reviewed and approved by the Animal Experimentation Ethics Committee of The Hebrew University Hadassah Medical School, Jerusalem. Adult male Wistar rats (Harlan, Israel) weighting 310-330 g were kept under a 12h light/dark cycle with free access to water and food (standard rat chow) prior to investigation. The rats underwent cannulation of right jugular vein one day prior to the drug administration. The rats were anesthetized with ketamine and xylazine solution (9:1 IP, 0.1 ml /100g body weight). A polyethylene cannula (PE-50, Becton Dickinson, MD) was inserted into the right jugular vein and was further used for IV drug administration and blood sampling. After implantation, the cannula was flushed with a normal saline solution containing heparin (100 units). Rats were then placed in individual metabolic cages and allowed to recover overnight. The animals were euthanized by overexposure to CO2 after the last sample collection.

Experimental procedure: Stock solutions of the peptides were freshly prepared immediately prior to administration. The final dose for IV and PO administration were 1 mg/kg and 10mg/kg body weight respectively. After dosing, the animals were housed in metabolic cages. Rats were fasted during the experiment. Drinking water was available *ad libitum*. Blood samples of 350μl were obtained at 0,5,15,30,60,90,120,180,240,480 min and 7 hr post infusion.

Heparinized saline (450 μL) was administered after each sampling. Blood was collected into heparinized tubes, immediately centrifuged at 4,000 rpm 6oC for 7 min and stored at -20oC pending analysis.

The plasma samples were diluted 1:3 in acetonitrile, centrifuged (4,000g, 10min), the supernatant was evaporated re-suspended in water and analyzed for peptide content.

Data analysis: The pharmacokinetic parameters of the drugs were determined from the experimental plasma concentration-time data by non-compartmental methods. PK analysis was performed with a WinNonlinTM 4.0.1 computer program (Pharsight Company; Mount View, CA). All data is presented as mean ± SEM, if not stated otherwise.

HPLC-MS analysis: Instrument: HPLC-MS Waters Millenium equipped with Micromass ZQ detector, Waters 600 Controller gradient pump and Waters 717 auto sampler. Nitrogen flow: 500L/Hr; Source temperature: 400oC; Cone Voltage 30V. Column: Atlantis MS C18 2.1x150mm (Waters). Mobile phase: 0.3ml/minute; 35% Acetonitrile, 0.1%formic acid, 0.05%Trifluoroacetic acid.

Table 7.34. *Chemical shift assignment of the active analogs (**S2-S8**) (**S1** is reported earlier somewhere else). The similar chemical shifts and shifts of N-methyl residues are highlighted.*

Residue		S2	S3	S4	S5	S6	S7	S8
Pro[6]	Ha	3.74	3.87	3.69	3.85	3.81	3.82	3.88
	Hb	1.61	0.81	1.7	0.62	0.99	0.83	0.64
		1.04	1.73	1.06	1.57	1.7	1.72	1.65
	Hg	1.3	0.94	1.22	0.93	1.36	0.99	0.95
		1.46	1.4	1.5	1.33	1.5	1.41	1.35
	Hd	3.25	2.81	3.11	2.86	3.16	2.98	2.92
		3.11	3.25	3.22	3.29	3.28	3.26	3.28
Phe[7]	Ha	4.7	4.65	4.86	4.86	5.04	4.99	5.15
	Hb	2.87	2.73	2.68	2.88	2.86	2.74	2.79
		2.87	2.98	2.87	2.72	2.86	2.92	2.88
	Hd	6.78		6.71				
		6.78		6.71				
	HN	6.94	7.59	7.58	7.2	7.36	8.05	7.53
D-Trp[8]	Ha	4.94	4.48	5.21	4.85	5.59	4.96	5.33
	Hb	2.8	3.03	3.06	2.77	3.19	3.12	2.92
		3.09	2.79	2.96	3.08	2.87	3.02	3.2
	Hd	7.53		7.11				
	HN/NCH3	8.78	8.42	2.98	8.97	3.07	3.04	3.17
Lys[9]	Ha	4.8	3.83	3.87	4.77	4.79	3.89	4.81
	Hb	1.28	1.43	1.65	1.21	1.82	1.44	1.2
		1.8	1.69	1.48	1.75	1.31	1.69	1.79
	Hg	0.54	0.98	1.05	0.39	0.66	0.99	0.64
		0.74	0.98	1.05	0.64	0.85	0.99	0.79
	Hd	1.36	1.39	1.42	1.28	1.42	1.41	1.38
		1.36	1.39	1.42				
	He	2.64	2.63	2.65	2.57	2.68	2.64	2.67
		2.64	2.63	2.65				
	Hz	7.67	7.63	7.65	7.62	7.76	7.63	7.69
	HN	2.72	8.58	8.63	2.64	2.63	8.53	2.56
Thr[10]	Ha	4.1	4.81	4.14	4.77	4.07	4.79	4.76
	Hb	3.97	3.93	4.01	3.84	4.02	3.91	3.84
	Hg	0.92	1.07	1.02	0.99	0.95	1.04	1
	HN	6.69	7.19	6.96	6.67	6.69	7.08	6.83
Phe[11]	Ha	4.47	4.89	4.2	5.02	4.4	4.73	4.94
	Hb	2.8	3.12	2.9	3.05	2.89	3.15	3.05
		3.09	3.12	2.9			3.07	
	Hd	7.17	7.25	7.22				
		7.17	7.25	7.22				
	HN	8.18	3.17	8.35	3.16	8.23	3.15	3.17

ROE violation list of the calculated structures:

Table 7.35. *ROE list and violation of* ***S2****.*

Atom 1	Atom 2	Low.	Upp.	Calc.	Viol.
1:MELYS_9:HA	1:MELYS_9:HB2	2.01	2.45	2.43	0
1:MELYS_9:HA	1:THR_10:HN	2.33	2.84	2.983	0.134
1:MELYS_9:HB1	1:MELYS_9:HB2	1.6	1.95	1.744	0
1:MELYS_9:HB1	1:MELYS_9:CN	2	2.45	2.721	0.265
1:MELYS_9:HD1	1:MELYS_9:HA	2.18	2.67	2.585	0
1:MELYS_9:HD1	1:MELYS_9:HZ1	2.2	2.69	2.732	0.011
1:MELYS_9:HE1	1:MELYS_9:HZ1	1.9	2.32	2.439	0.108
1:MELYS_9:HG1	1:MELYS_9:HA	2.44	2.98	2.623	0
1:MELYS_9:HG1	1:MELYS_9:CN	2.46	3.01	3.201	0.173
1:MELYS_9:HG2	1:MELYS_9:HG1	1.7	2.08	1.695	-0.009
1:MELYS_9:HG2	1:MELYS_9:CN	2.9	3.55	3.848	0.278
1:MELYS_9:CN	1:MELYS_9:HA	2.44	2.99	3.429	0.438
1:MELYS_9:CN	1:TRP_8:HA	1.66	2.03	2.511	0.478
1:PRO_6:HA	1:PHE_7:HN	2.77	3.39	3.31	0
1:PRO_6:HB1	1:PRO_6:HA	2.39	2.92	2.767	0
1:PRO_6:HB1	1:PHE_7:HD2	2.75	3.36	3.418	0.037
1:PRO_6:HB2	1:PRO_6:HA	1.99	2.44	2.368	0
1:PRO_6:HB2	1:PRO_6:HB1	1.58	1.93	1.775	0
1:PRO_6:HD1	1:PRO_6:HD2	1.61	1.97	1.787	0
1:PRO_6:HD2	1:PHE_7:HN	2.48	3.04	2.984	0
1:PRO_6:HG1	1:PRO_6:HD2	2.26	2.76	2.375	0
1:PRO_6:HG1	1:PHE_7:HD2	2.53	3.09	3.118	0
1:PRO_6:HG1	1:PHE_7:HN	2.7	3.3	3.214	0
1:PRO_6:HG2	1:PRO_6:HD1	2.21	2.7	2.41	0
1:THR_10:CG2	1:MELYS_9:CN	2.43	2.96	3.282	0.315
1:THR_10:CG2	1:THR_10:HA	2.22	2.72	3.05	0.328
1:THR_10:CG2	1:THR_10:HB	1.98	2.42	2.14	0
1:THR_10:CG2	1:THR_10:HN	2.49	3.04	3.019	0
1:THR_10:CG2	1:PHE_11:HN	2.47	3.02	3.135	0.099
1:THR_10:HN	1:MELYS_9:CN	2.19	2.68	2.85	0.157
1:THR_10:HN	1:THR_10:HA	2.33	2.85	3.015	0.162
1:THR_10:HN	1:THR_10:HB	2.6	3.18	3.278	0.088
1:TRP_8:HA	1:TRP_8:HB2	2.39	2.92	2.452	0
1:TRP_8:HA	1:TRP_8:HN	2.52	3.08	2.938	0
1:TRP_8:HA	1:PHE_7:HD1	2.78	3.4	3.706	0.293
1:TRP_8:HB1	1:TRP_8:HB2	1.54	1.88	1.755	0
1:TRP_8:HB1	1:TRP_8:HN	2.06	2.51	2.514	0
1:TRP_8:HB2	1:TRP_8:HD1	2.44	2.98	3.009	0.016
1:TRP_8:HB2	1:TRP_8:HN	2.33	2.85	2.648	0
1:TRP_8:HD1	1:MELYS_9:CN	2.8	3.42	3.537	0.097
1:TRP_8:HD1	1:TRP_8:HA	2.23	2.73	2.55	0
1:PHE_7:HA	1:TRP_8:HN	1.86	2.28	2.225	0
1:PHE_7:HA	1:PHE_7:HD1	2.36	2.89	3.274	0.375
1:PHE_7:HA	1:PHE_7:HN	2.37	2.9	3.056	0.154
1:PHE_7:HB1	1:PHE_7:HN	2.5	3.05	2.637	0
1:PHE_7:HD2	1:PHE_7:HA	2.41	2.94	3.169	0.218
1:PHE_11:HA	1:PRO_6:HA	1.66	2.03	2.071	0.035
1:PHE_11:HA	1:PHE_7:HN	2.58	3.15	3.115	0
1:PHE_11:HA	1:PHE_11:HN	2.48	3.03	3.05	0.018
1:PHE_11:HB1	1:PRO_6:HA	2.56	3.12	3.4	0.274
1:PHE_11:HB1	1:PHE_11:HA	1.97	2.41	2.339	0
1:PHE_11:HB1	1:PHE_11:HN	2.01	2.45	2.657	0.195
1:PHE_11:HD1	1:PRO_6:HA	2.51	3.07	2.919	0
1:PHE_11:HD1	1:PHE_11:HA	2.36	2.89	2.837	0
1:PHE_11:HN	1:THR_10:HA	2.07	2.53	2.651	0.108
1:PHE_11:HN	1:THR_10:HB	2.34	2.87	3.098	0.223

Table 7.36. *ROE list and violation of* ***S3****.*

Atom 1	Atom 2	Low.	Upp.	Calc.	Viol.
1:LYS_9:HA	1:LYS_9:HN	2.47	3.02	3.018	0
1:LYS_9:HB1	1:LYS_9:HA	2.11	2.59	2.797	0.205
1:LYS_9:HB1	1:LYS_9:HN	2.15	2.62	2.539	0
1:LYS_9:HB1	1:THR_10:HN	3.03	3.7	2.911	-0.135
1:LYS_9:HB2	1:LYS_9:HB1	1.54	1.88	1.737	0
1:LYS_9:HD1	1:LYS_9:HZ1	2.17	2.66	2.802	0.109
1:LYS_9:HG1	1:LYS_9:HA	2.21	2.7	2.916	0.202
1:LYS_9:HG1	1:LYS_9:HE1	2.13	2.6	2.458	0
1:LYS_9:HG1	1:LYS_9:HN	2.31	2.82	2.832	0
1:LYS_9:HG1	1:LYS_9:HZ1	2.72	3.33	3.729	0.358
1:LYS_9:HG1	1:TRP_8:HD1	2.96	3.62	3.759	0.117
1:LYS_9:HN	1:TRP_8:HD1	3.03	3.7	2.992	-0.063
1:LYS_9:HZ1	1:LYS_9:HE1	2.17	2.66	2.522	0
1:PRO_6:HA	1:MEPHE_11:HD1	2.45	2.99	2.304	-0.157
1:PRO_6:HA	1:MEPHE_11:HE1	3.13	3.83	3.818	0
1:PRO_6:HB1	1:PRO_6:HA	2.39	2.92	2.707	0
1:PRO_6:HB1	1:PRO_6:HB2	1.6	1.95	1.764	0
1:PRO_6:HB2	1:PRO_6:HA	2.02	2.46	2.391	0
1:PRO_6:HB2	1:MEPHE_11:HD1	2.8	3.43	3.572	0.123
1:PRO_6:HB2	1:MEPHE_11:HE1	3.04	3.71	3.521	0
1:PRO_6:HD2	1:PRO_6:HD1	1.54	1.88	1.807	0
1:PRO_6:HG1	1:PRO_6:HD2	2.19	2.68	2.309	0
1:PRO_6:HG1	1:PHE_7:HD1	2.76	3.38	3.659	0.264
1:PRO_6:HG1	1:PHE_7:HN	2.81	3.43	3.624	0.183
1:PRO_6:HG2	1:PRO_6:HD1	2.13	2.61	2.391	0
1:THR_10:HB	1:THR_10:HA	1.79	2.19	2.417	0.221
1:THR_10:CG2	1:THR_10:HA	2.25	2.65	2.756	0.099
1:THR_10:CG2	1:THR_10:HB	1.91	2.34	2.13	0
1:THR_10:CG2	1:THR_10:HN	2.59	3.17	3.133	0
1:THR_10:HN	1:LYS_9:HN	2.2	2.69	2.473	0
1:THR_10:HN	1:THR_10:HA	2.34	2.86	2.949	0.086
1:TRP_8:HA	1:LYS_9:HN	1.81	2.21	2.161	0
1:TRP_8:HA	1:THR_10:HN	3.07	3.76	3.747	0
1:TRP_8:HA	1:TRP_8:HN	2.3	2.81	2.957	0.145
1:TRP_8:HB1	1:TRP_8:HA	2.14	2.61	2.821	0.208
1:TRP_8:HB1	1:TRP_8:HN	2.19	2.68	2.642	0
1:TRP_8:HB2	1:TRP_8:HA	2.28	2.79	2.484	0
1:TRP_8:HB2	1:TRP_8:HD1	2.59	3.17	2.964	0
1:TRP_8:HB2	1:TRP_8:HN	2.43	2.97	3.118	0.134
1:TRP_8:HD1	1:TRP_8:HA	2.52	3.08	2.736	0
1:PHE_7:HA	1:TRP_8:HN	1.93	2.35	2.172	0
1:PHE_7:HA	1:PHE_7:HN	2.39	2.92	2.993	0.07
1:PHE_7:HB1	1:PHE_7:HA	2.2	2.69	2.499	0
1:PHE_7:HB1	1:PHE_7:HD1	2.01	2.45	2.368	0
1:PHE_7:HB2	1:PHE_7:HA	2	2.45	2.809	0.356
1:PHE_7:HD2	1:PHE_7:HA	2.2	2.69	2.907	0.205
1:PHE_7:HN	1:PRO_6:HA	2.65	3.24	3.359	0.114
1:PHE_7:HN	1:PRO_6:HD2	1.64	2.01	2.325	0.301
1:PHE_7:HN	1:TRP_8:HN	2.73	3.34	3.548	0.198
1:MEPHE_11:HA	1:PRO_6:HA	1.69	2.06	2.081	0.014
1:MEPHE_11:HA	1:PHE_7:HN	2.36	2.89	3.254	0.353
1:MEPHE_11:HB1	1:PRO_6:HA	2.22	2.71	3.048	0.325
1:MEPHE_11:HD1	1:MEPHE_11:HA	2.1	2.57	2.922	0.339
1:MEPHE_11:CN	1:THR_10:HA	1.72	2.11	2.491	0.377

Table 7.37. *ROE list and violation of* ***S4****.*

Atom 1	Atom 2	Low.	Upp.	Calc.	Viol.
1:LYS_9:HA	1:LYS_9:HN	2.33	2.85	2.885	0.032
1:LYS_9:HA	1:THR_10:HN	2.55	3.12	3.512	0.389
1:LYS_9:HB2	1:THR_10:HN	2.74	3.35	2.953	0
1:LYS_9:HB1	1:LYS_9:HA	2.03	2.48	2.998	0.516
1:LYS_9:HB2	1:LYS_9:HB1	1.6	1.95	1.689	0
1:LYS_9:HB2	1:LYS_9:HN	2	2.45	2.65	0.25
1:LYS_9:HG1	1:LYS_9:HA	1.95	2.39	2.641	0.238
1:LYS_9:HG1	1:LYS_9:HN	2.13	2.6	2.766	0.149
1:LYS_9:HN	1:THR_10:HN	1.97	2.4	2.659	0.246
1:PRO_6:HB1	1:PHE_7:HD1	2.56	3.13	3.254	0.102
1:PRO_6:HB1	1:PRO_6:HA	2.2	2.69	2.795	0.101
1:PRO_6:HB2	1:PRO_6:HA	1.9	2.32	2.3	0
1:PRO_6:HB2	1:PRO_6:HB1	1.38	1.69	1.771	0.077
1:PRO_6:HD2	1:PHE_7:HN	2.37	2.9	2.936	0.007
1:PRO_6:HG1	1:PHE_7:HD1	2.55	3.12	2.414	-0.153
1:PRO_6:HG1	1:PRO_6:HB1	1.64	2.01	2.278	0.261
1:PRO_6:HG1	1:PRO_6:HD2	2.06	2.52	2.322	0
1:PRO_6:HG1	1:PRO_6:HG2	1.5	1.84	1.77	0
1:PRO_6:HG1	1:PHE_7:HN	2.53	3.09	3.237	0.125
1:PRO_6:HG2	1:PRO_6:HD1	2.05	2.5	2.371	0
1:THR_10:CG2	1:THR_10:HA	2.01	2.96	2.653	0
1:THR_10:CG2	1:THR_10:HB	1.78	2.98	2.127	0
1:THR_10:CG2	1:THR_10:HN	2.38	3.41	3.539	0.117
1:THR_10:CG2	1:PHE_11:HN	2.5	3.56	3.859	0.291
1:THR_10:HN	1:THR_10:HA	2.18	2.66	2.987	0.325
1:THR_10:HN	1:THR_10:HB	2.46	3	3.297	0.291
1:METRP_8:HA	1:LYS_9:HN	1.72	2.1	2.223	0.115
1:METRP_8:HD1	1:LYS_9:HG1	2.86	3.49	3.379	0
1:METRP_8:HD1	1:METRP_8:HA	2.29	2.8	2.575	0
1:LYS_9:HZ1	1:LYS_9:HD1	2.03	2.49	2.436	0
1:LYS_9:HZ1	1:LYS_9:HE1	1.92	2.35	2.69	0.319
1:LYS_9:HZ1	1:LYS_9:HG1	2.57	3.14	3.195	0.013
1:METRP_8:HA	1:PHE_7:HD2	2.77	3.39	3.604	0.201
1:METRP_8:CN	1:PHE_7:HA	1.43	2.25	2.583	0.328
1:PHE_7:HA	1:PHE_7:HN	2.24	2.73	2.977	0.244
1:PHE_7:HB1	1:PHE_7:HA	1.99	2.44	2.42	0
1:PHE_7:HB1	1:PHE_7:HN	2.48	3.03	3.344	0.309
1:PHE_7:HB2	1:PHE_7:HA	1.15	1.41	1.848	0.433
1:PHE_7:HB2	1:PHE_7:HN	2.72	3.33	3.386	0.044
1:PHE_7:HN	1:PHE_7:HD1	2.44	2.98	2.841	0
1:PHE_7:HN	1:PRO_6:HA	2.58	3.15	3.386	0.232
1:PHE_11:HA	1:PRO_6:HA	1.57	1.92	2.26	0.331
1:PHE_11:HA	1:PHE_7:HN	2.27	2.78	3.182	0.391
1:PHE_11:HB1	1:PHE_11:HN	1.84	2.25	2.363	0.101
1:PHE_11:HN	1:THR_10:HA	1.88	2.3	2.249	0
1:PHE_11:HN	1:THR_10:HB	2.13	2.6	2.553	0
1:PHE_11:HN	1:PHE_11:HA	2.18	2.66	2.941	0.277

Table 7.38. *ROE list and violation of* ***S8****.*

Atom 1	Atom 2	Low.	Upp.	Calc.	Viol.
1:PRO_6:HA	1:PHE_7:HN	2.54	3.1	3.21	0.11
1:PRO_6:HA	1:MePHE_11:HD1	2.38	2.9	2.42	0
1:PRO_6:HA	1:MePHE_11:HA	1.58	1.93	2	0.08
1:PRO_6:HG2	1:PRO_6:HD2	2.12	2.6	2.71	0.11
1:PRO_6:HB2	1:PRO_6:HA	2.28	2.78	2.3	0
1:PRO_6:HD1	1:MePHE_11:HD1	2.44	2.98	2.84	0
1:PRO_6:HB2	1:PRO_6:HA	1.96	2.4	2.56	0.16
1:PRO_6:HB2	1:MePHE_11:HD1	2.66	3.26	2.91	0
1:PRO_6:HB2	1:MePHE_11:HE1	2.78	3.4	2.87	0
1:PRO_6:HG2	1:PRO_6:HD1	2.11	2.57	2.39	0
1:PRO_6:HG1	1:PHE_7:HD1	2.63	3.21	3.36	0.15
1:PHE_7:HA	1:PHE_7:HD2	2.07	2.53	2.5	0
1:PHE_7:HA	1:PHE_7:HN	2.43	2.97	3.01	0.04
1:PHE_7:HB1	1:PHE_7:HD1	1.7	2.08	2.34	0.27
1:PHE_7:HB1	1:PHE_7:HN	1.81	2.21	2.28	0.07
1:PHE_7:HB1	1:PHE_7:HA	2.08	2.51	2.76	0.26
1:PHE_7:HB2	1:PHE_7:HD1	1.89	2.27	2.5	0.23
1:PHE_7:HB2	1:PHE_7:HN	1.91	2.33	2.44	0.12
1:PHE_7:HB2	1:PHE_7:HA	2.54	2.88	2.89	0.01
1:MeTRP_8:CN	1:PHE_7:HD2	3.13	3.89	3.93	0.05
1:MeTRP_8:CN	1:PHE_7:HA	2.47	2.85	2.76	0
1:MeTRP_8:HA	1:MeTRP_8:HD1	2.43	2.98	3.16	0.19
1:MeTRP_8:HB1	1:MeTRP_8:HE3	2.1	2.57	2.6	0.04
1:MeTRP_8:HB2	1:MeTRP_8:HA	2	2.45	2.33	0
1:MeTRP_8:HB2	1:MeTRP_8:HD1	2.12	2.59	2.77	0.19
1:MeLYS_9:CN	1:MeTRP_8:HD1	3.48	4.25	3.88	0
1:MeLYS_9:CN	1:MeTRP_8:HE3	3.69	4.55	4.79	0.24
1:MeLYS_9:CN	1:MeTRP_8:HA	1.85	2.25	2.45	0.2
1:MeLYS_9:CN	1:THR_10:HN	2.58	3.25	3.24	0
1:MeLYS_9:HA	1:THR_10:HN	2.04	2.49	2.56	0.08
1:MeLYS_9:CN	1:MeLYS_9:HA	3.23	3.94	3.47	0
1:MeLYS_9:HZ1	1:MeLYS_9:HE1	1.85	2.26	2.32	0.07
1:MeLYS_9:HE2	1:MeTRP_8:HD1	2.85	3.48	3.74	0.27
1:MeLYS_9:HG1	1:MeTRP_8:HD1	2.86	3.49	3.68	0.2
1:MeLYS_9:HG1	1:MeLYS_9:CN	2.55	3.12	3.37	0.26
1:MeLYS_9:HG1	1:MeLYS_9:HG2	1.58	1.93	1.71	0
1:MeLYS_9:HG2	1:MeTRP_8:HD1	2.97	3.64	3.57	0
1:MeLYS_9:HG2	1:MeLYS_9:CN	3.06	3.75	2.84	-0.22
1:THR_10:HB	1:THR_10:HN	2.61	3.19	3.51	0.33
1:THR_10:HB	1:THR_10:HA	1.85	2.26	2.51	0.25
1:THR_10:CG2	1:MeLYS_9:CN	2.5	3.05	3.35	0.3
1:THR_10:CG2	1:THR_10:HN	2.53	3.1	3.3	0.21
1:THR_10:CG2	1:THR_10:HG1	2.55	3.12	2.53	0
1:THR_10:CG2	1:THR_10:HA	2.16	2.64	2.65	0.02
1:THR_10:CG2	1:THR_10:HB	1.85	2.26	2.12	0
1:THR_10:CG2	1:MePHE_11:CN	3.72	4.58	4.92	0.38
1:MePHE_11:CN	1:THR_10:HG1	2.97	3.94	3.56	0
1:MePHE_11:CN	1:THR_10:HA	3.09	3.76	3.92	0.16
1:MePHE_11:CN	1:THR_10:HB	2.65	3.48	3.59	0.11
1:MePHE_11:CN	1:MePHE_11:HA	2.02	2.29	2.49	0.2
1:MePHE_11:HA	1:PHE_7:HN	2.59	3.14	3.4	0.27
1:MePHE_11:HA	1:MePHE_11:HD1	2.16	2.61	2.88	0.27
1:MePHE_11:HB1	1:MePHE_11:HD2	1.74	2.13	2.3	0.17
1:MePHE_11:HB1	1:MePHE_11:HA	1.8	2.2	2.47	0.27
1:MeLYS_9:HG1	1:MeLYS_9:HE1	2.32	2.83	2.72	0
1:MeLYS_9:HG2	1:MeLYS_9:HE2	2.28	2.79	2.38	0
1:PHE_7:HN	1:THR_10:HG1	2.49	3.04	2.74	0

7.5 Synthesis of N-methylated GPIIb-IIIa antagonists:

Synthesis of all the analogs was done on solid support on the TCP resin. To obtain high yields of the cyclic peptide and free of racemization, glycine was chosen as the C-terminal to be loaded to the TCP resin. The linear peptides were synthesized on solid support and cleaved from resin and cyclized in solution using the HATU/HOBt method. After the cyclization, the work up was done and to the vaccum dried crude cyclized peptide, a solution of TFA:TIPS:H_2O (95%:5%:5%) (minimal amount, just to dissolve the peptide) was added and

stirred for 1 hour (monitored by MS spectra) to remove the –Pbf and –Boc protection. The solution was finally evaporated to dryness, dissolved in ACN/H_2O and purified by RP-HPLC.

Table 7.39. *HPLC retention time, ESI-MS and yield of all analogues. The bold residues indicate the N-methylation.*

No.	Analogue	t_R (min)[1]	$(M+H)^+$	Purity[2]	Yield[3]
R1	c(-GRGDfL-)	12.85	646.3	>99%	72%
R2	c(-GRGDf**L**-)	13.87	660.3	>99%	60%
R3	c(-GRGD**f**L-)	13.51	660.3	>99%	55%
R4	c(-G**R**GDfL-)	13.25	660.3	>99%	63%
R5	c(-GRGD**f**L-)	14.19	674.3	>99%	58%
R6	c(-G**R**GDf**L**-)	14.07	674.3	>99%	59%
R7	c(-G**R**GD**f**L-)	13.76	674.3	>99%	57%
R8	c(-G**R**GD**f**L-)	14.71	688.3	>99%	54%

1. RP-HPLC in Pharmacia C18 column with a gradient of 10-100% (ACN:H2O)]+0.1%TFA
2. Calculated from ^{1}H NMR
3. The cyclization yields.

Solid phase binding assay:

Inhibiting activity and integrin selectivity of the integrin inhibitors were determined in a solid phase binding assay using soluble integrins and coated extracellular matrix protein. Binding of integrins was than detected by specific antibodies in an enzyme-linked immunosorbant assay. Fibronectin and vitronectin were purchased from Sigma (St Louis, MO) and fibrinogen from Calbiochem (EMD Biosciences, Darmstadt, Germany). The integrin $\alpha_5\beta_1$ extracellular domain Fc-fusion protein was a generous gift from M. Humphries (University of Manchester), $\alpha_V\beta_3$ was purchased from Chemicon (Chemicon Europe, Germany) and αIIbβ3 from Kordia (Kordia Life Science, Leiden, Netherlands). The integrin antibodies were purchased from Pharmingen, BD Bioscience Europe ($\alpha_V\beta_3$, and αIIbβ3) and Sigma (anti-human-Fc-HRP antibody conjugate and anti-mouse-HRP conjugate). The detection of HRP was performed using HRP substrate solution 3.3.5.5'-tetramethylethylenediamine (TMB, Seramun, Germany) and 1M H_2SO_4 for stopping the reaction. The developed color was measured at 450nm with SpectraMax Plus reader (Molecular Devices). The resulting inhibition curves were analyzed using SoftMaxPro 4.0 software, the turning point describes the IC50 value.

$\alpha_5\beta_1$:Nunc-Immuno maxisorp plates (Nalge Nunc Europe Ltd) were coated over night at 4°C with fibronectin (0.25 µg/ml) in 15 mM Na_2CO_3, 35 mM $NaHCO_3$, pH 9.6. All subsequent washing and binding were performed in 25 mM Tris, pH7.6, 150 mM NaCl, 1 mM $MnCl_2$, 1 mg/ml BSA. The plates were blocked with 3 % BSA in PBS 0.1% Tween20 for 1 hour at room temperature. Soluble integrin $\alpha_5\beta_1$ (0.5 µg/ml) and a serial dilution of integrin inhibitor were incubated in the coated wells for one hour at room temperature. The detection antibody (anti-human-Fc-HRP antibody conjugate) was then applied for 1 hour at room temperature

and the binding visualized as described above. For the $\alpha_V\beta_3$ assay, plates were coated with vitronectin (1 µg/ml) and blocked as described for $\alpha_5\beta_1$. Soluble $\alpha_V\beta_3$ (1 µg/ml) was incubated with a serial dilution of integrin inhibitor for one hour at room temperature. Primary (anti-$\alpha_V\beta_3$) and secondary antibody (anti-mouse-HRP conjugate) were applied for 1 hour at room temperature and the binding visualized as described above.

For the αIIbβ3 assay, plates were coated with fibrinogen (10 µg/ml) and blocked as described for α5β1. Soluble αIIbβ3 (5 µg/ml) was incubated with a serial dilution of integrin inhibitor (25 mM Tris, pH7,6, 150 mM NaCl, 1 mM $MnCl_2$, 1 mg/mL BSA 1 mM $MgCl_2$, 1 mM $CaCl_2$) for one hour at room temperature. Primary (anti-CD41b) and secondary antibody (anti-mouse-HRP conjugate) were applied for 1 hour at room temperature and the binding visualized as described above.

HRP – horse radish peroxidase

Molecular docking.

Molecular modelling calculations and graphics manipulations were performed on a Silicon Graphics Octane2 workstation equipped with two 2600 MHz R14000 processors using the SYBYL7.3 software package. Automated docking calculations were performed using version 3.0.5 of the AutoDock program.

Ligand setup: for peptides **R4** and **R8**, the conformations in solution as experimentally determined by NMR, distance geometry and subsequent molecular dynamics (restrained MD), were used as starting conformation. During the docking process the backbone conformation was held fix, while the side chain dihedral angles were free to rotate. Partial atomic charges were assigned by using the Gasteiger-Marsili formalism.

Protein setup: Crystal coordinates of the extracellular segment of the αIIbβ3-integrin in complex with Eptifibatide were taken from the Brookhaven Protein Databank (PDB entry code = 1TY6). For the purpose of ligand docking, the binding region between the so called propeller and the A domain on the integrin head was selected. The receptor was set up for docking as follows: polar hydrogens were added using the BIOPOLYMERS module of the SYBYL program, Kollman united-atom partial charges were assigned and all waters were removed. ADDSOL utility of the AutoDock program was used to add salvation parameters to the protein structures and the grid maps representing the proteins in the docking process were calculated using AutoGrid. The grids, one for each atom type in the ligand, plus one for electrostatic interactions, were chosen to be large enough to include the RGD binding site. For docking calculations, the dimensions of grids map was 60 x 60 x 60 Å̊ with a grid-point spacing of 0.375 Å̊ and the center of the grid was set to be coincident with the mass center of Eptifibatide in the crystal complex.

Docking simulation: Docking simulations of compounds **R4** and **R8** were carried out using the Lamarckian Genetic Algorithm and applying a protocol with an initial population of 50 randomly placed individuals, a maximum number of 1.0 x 10^6 energy evaluations, a mutation rate of 0.02, a crossover rate of 0.80, and an elitism value of 1. The pseudo-Solis and Wets algorithm with a maximum of 300 interactions was applied for the local search. 50 independent docking runs were carried out for each ligand, clustering together the resulting conformations which differ by less than 1.5 Å in positional root-mean-square deviation (RMSD). The result with the lowest free energy of binding was taken as the representative of each cluster.

Structure calculation:

Table 7.40. *Chemical shifts of the residues of analog* ***R4****.*

Residue	H^{α}	H^{β}	H^{γ}	H^{δ}	H^{ε}	H^{N}/H^{NMe}
Glycine[1]	3.97					7.34
Arginine[2]	3.95	1.95/1.76	1.45	3.09	7.47	3.02
Glycine[3]	3.37/3.85					8.28
Aspartic acid[4]	4.63	2.42/2.58				7.40
D-Phenylalanine[5]	4.49	2.78/2.99				8.55
Leucine[6]	3.97	1.38	1.04	0.57/0.70		8.27

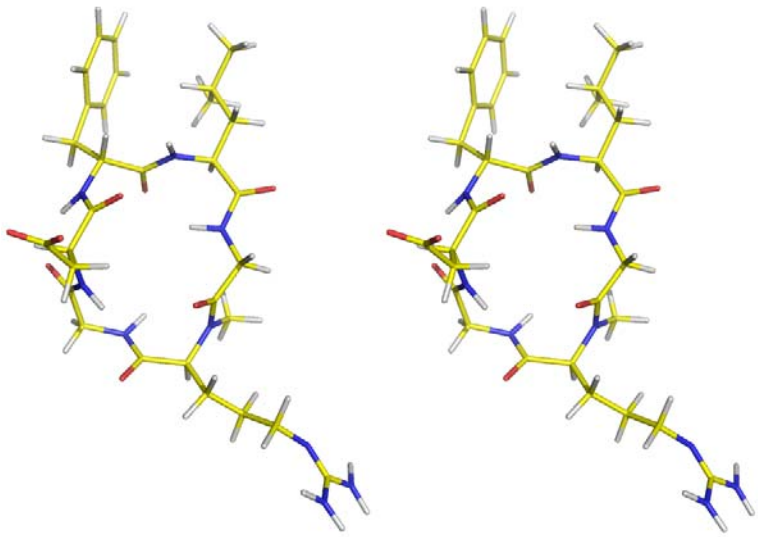

Figure 7.1. *Stereopicture of analog* ***R4****.*

Table 7.41. *Restraints and violations of the rMD simulation of analog* ***R4****.*

Atom 1	Atom 2	Low.	Upp.	Calc.	Viol.
1:NRG_2:HA	1:NRG_2:HB2	2.05	2.5	2.59	0.09
1:NRG_2:HA	1:NRG_2:HG1	1.81	2.21	2.287	0.077
1:NRG_2:HB1	1:NRG_2:HB2	1.58	1.93	1.743	0
1:NRG_2:CN	1:NRG_2:HA	1.9	2.32	2.431	0.111
1:NRG_2:CN	1:GLY_1:HA1	1.66	2.03	2.327	0.297
1:NRG_2:CN	1:GLY_3:HN	2.38	2.91	3.045	0.135
1:ASP-_4:HA	1:PHE_5:HN	1.82	2.23	2.341	0.111
1:ASP-_4:HB1	1:ASP-_4:HN	1.68	2.05	2.258	0.208
1:ASP-_4:HB2	1:ASP-_4:HN	2.35	2.87	2.702	0
1:ASP-_4:HN	1:ASP-_4:HA	2.2	2.7	2.858	0.158
1:LEU_6:HA	1:LEU_6:CD1	1.93	2.36	2.647	0.287
1:LEU_6:HA	1:LEU_6:HN	1.88	2.3	2.661	0.361
1:LEU_6:HA	1:GLY_1:HN	1.9	2.32	2.59	0.27
1:LEU_6:HB1	1:LEU_6:CD2	2.01	2.45	2.624	0.174
1:LEU_6:HB1	1:LEU_6:HN	2.02	2.47	2.518	0.048
1:LEU_6:CD1	1:LEU_6:HB1	2.16	2.64	2.992	0.352
1:LEU_6:HG	1:LEU_6:HN	2.15	2.62	2.764	0.144
1:PHE_5:HA	1:LEU_6:HN	1.71	2.09	2.188	0.098
1:PHE_5:HA	1:PHE_5:HD1	2.14	2.62	2.659	0.039
1:PHE_5:HA	1:PHE_5:HN	2.19	2.68	2.901	0.221
1:PHE_5:HB1	1:PHE_5:HN	2.12	2.59	2.56	0
1:PHE_5:HB2	1:PHE_5:HD1	2.1	2.57	2.607	0.037
1:PHE_5:HN	1:ASP-_4:HN	2.7	3.3	3.41	0.11
1:PHE_5:HN	1:PHE_5:HB2	2.13	2.61	2.709	0.099
1:GLY_1:HN	1:LEU_6:HN	2.08	2.55	2.761	0.311
1:GLY_1:HN	1:GLY_1:HA1	1.9	2.32	2.544	0.224
1:GLY_3:HA1	1:GLY_3:HN	1.85	2.26	2.447	0.187
1:GLY_3:HA2	1:ASP-_4:HN	2.43	2.97	2.863	0
1:GLY_3:HN	1:ASP-_4:HN	2.23	2.72	2.981	0.261
1:GLY_3:HN	1:GLY_3:HA1	1.88	2.3	2.547	0.247

Table 7.42. *Chemical shifts of the residues of analog* ***R8****.*

Residue	H^{α}	H^{β}	H^{γ}	H^{δ}	H^{ε}	H^{N}/H^{NMe}
Glycine[1]	3.94/3.94					6.67
Arginine[2]	3.87	2.02/1.78	1.52	3.12/3.08	7.44	3.07
Glycine[3]	3.49/3.73					8.29
Aspartic acid[4]	5.01	2.21/2.73				7.56
D-Phenylalanine[5]	5.74	2.87/3.22				3.03
Leucine[6]	4.94	1.54/1.35	0.41	0.67/0.63		2.83

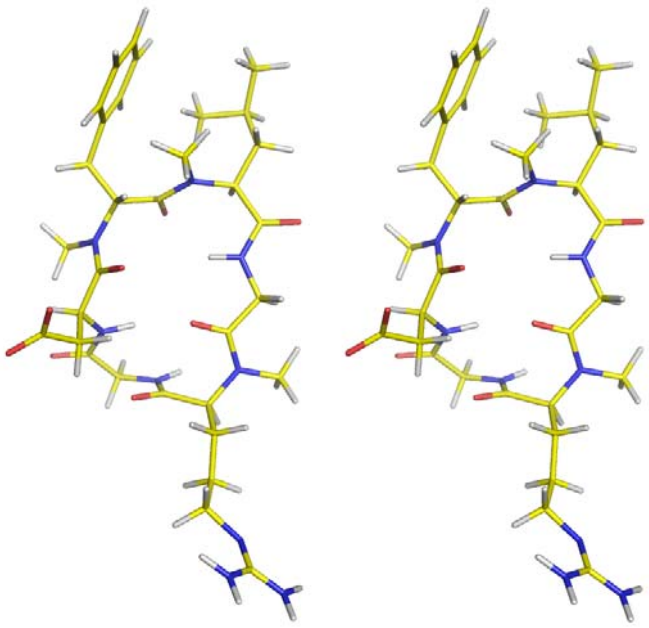

Figure 7.2. *Stereopicture of analog* ***R8****.*

Table 7.43. *Restraints and violations of the rMD simulation of analog* ***R8****.*

Atom 1	Atom 2	Low.	Upp.	Calc.	Viol.
1:NRG_2:HA	1:GLY_3:HN	2.36	2.88	2.41	0
1:NRG_2:HB1	1:NRG_2:HA	2.1	2.56	2.51	0
1:NRG_2:HB1	1:NRG_2:HB2	1.58	1.93	1.75	0
1:NRG_2:HG1	1:NRG_2:HA	2.15	2.63	2.47	0
1:NRG_2:CN	1:NRG_2:HA	1.75	2.13	2.29	0.16
1:NRG_2:CN	1:GLY_1:HA1	1.85	2.26	2.4	0.14
1:NRG_2:CN	1:GLY_3:HN	2.45	3	3.09	0.09
1:ASP-_4:HA	1:ASP-_4:HB1	2.09	2.56	2.59	0.03
1:ASP-_4:HA	1:ASP-_4:HN	2.38	2.91	2.97	0.06
1:ASP-_4:HB1	1:ASP-_4:HB2	1.58	1.93	1.74	0
1:ASP-_4:HB1	1:ASP-_4:HN	2.44	2.99	3.23	0.24
1:ASP-_4:HB2	1:ASP-_4:HB1	1.6	1.96	1.74	0
1:ASP-_4:HB2	1:ASP-_4:HN	2.4	2.93	3.03	0.10
1:NFE_5:HA	1:NFE_5:HD1	2.16	2.64	2.25	0
1:NFE_5:HB1	1:NFE_5:HB2	1.59	1.94	1.71	0
1:NFE_5:HB1	1:NFE_5:HD1	2.57	3.14	3.46	0.32
1:NFE_5:HD1	1:NFE_5:HB2	2.16	2.64	2.76	0.12
1:NFE_5:CN	1:ASP-_4:HA	1.68	2.05	2.35	0.30
1:NFE_5:CN	1:ASP-_4:HN	2.72	3.32	3.57	0.25
1:NFE_5:CN	1:NFE_5:HA	2.63	3.21	3.44	0.23
1:NFE_5:CN	1:NFE_5:HB2	2.11	2.57	2.84	0.273
1:NMLU_6:HA	1:GLY_1:HN	2.26	2.77	2.96	0.192
1:NMLU_6:HB1	1:NMLU_6:HB2	1.58	1.93	1.73	0
1:NMLU_6:HB2	1:NMLU_6:HA	2.1	2.57	2.85	0.288
1:NMLU_6:CD1	1:NMLU_6:HA	2.03	2.48	2.78	0.301
1:NMLU_6:HG	1:NMLU_6:HA	2.35	2.87	2.66	0
1:NMLU_6:CN	1:NFE_5:HA	1.68	2.06	2.26	0.20
1:NMLU_6:CN	1:NFE_5:HD1	2.65	3.24	3.48	0.24
1:NMLU_6:CN	1:NMLU_6:HA	2.58	3.16	3.44	0.28
1:NMLU_6:CN	1:NMLU_6:HB1	2.06	2.51	2.74	0.23
1:NMLU_6:CN	1:GLY_1:HN	2.21	2.71	2.97	0.26
1:GLY_1:HN	1:GLY_1:HA1	2.22	2.71	2.919	0.209
1:GLY_3:HN	1:ASP-_4:HN	2.41	2.95	3.122	0.172
1:GLY_3:HN	1:GLY_3:HA1	2.03	2.48	2.578	0.098

Bibliograhy

1. Marx, V. Watching peptide drugs grow up. *Chem. Eng. News* **83**, 17-24 (2005).
2. Banta, S., Megeed, Z., Casali, M., Rege, K. & Yarmush, M.L. Engineering protein and peptide building blocks for nanotechnology. *J. Nanosci. Nanotechnol.* **7**, 387-401 (2007).
3. Merrifield, B. Concept and early development of solid-phase peptide synthesis. *Methods Enzymol.* **289**, 3-13 (1997).
4. Fischer, E. & Fourneau, E. A derivative from glykocolls. *Ber. Dtsch. Chem. Ges.* **34**, 2868-2877 (1901).
5. Kochendoerfer, G.G., Chen, S.Y., Mao, F., Cressman, S., Traviglia, S., Shao, H.Y., Hunter, C.L., Low, D.W., Cagle, E.N., Carnevali, M., Gueriguian, V., Keogh, P.J., Porter, H., Stratton, S.M., Wiedeke, M.C., Wilken, J., Tang, J., Levy, J.J., Miranda, L.P., Crnogorac, M.M., Kalbag, S., Botti, P., Schindler-Horvat, J., Savatski, L., Adamson, J.W., Kung, A., Kent, S.B.H., Bradburne, J.A. Design and chemical synthesis of a homogeneous polymer-modified erythropoiesis protein. *Science* **299**, 884-887 (2003).
6. Bergmann, M. & Zervas, L. A general procedure of the peptide synthesis. *Ber. Dtsch. Chem. Ges.* **65**, 1192-1201 (1932).
7. Wieland, T. & Bernhard, H. Uber Peptid-Synthesen .3. Die Verwendung Von Anhydriden Aus N-Acylierten Aminosauren Und Derivaten Anorganischer Sauren. *Liebigs Ann. Chem.* **572**, 190-194 (1951).
8. Merrifield, R.B. Solid Phase Peptide Synthesis .1. Synthesis of a tetrapeptide. *J. Am. Chem. Soc.* **85**, 2149-2154 (1963).
9. Kessler, H. Peptide Conformations .19. Conformation and biological-activity of cyclic-peptides. *Angew. Chem.-Int. Ed.* **21**, 512-523 (1982).
10. Goodman, M. & Chorev, M. Concept of linear modified retro-peptide structures. *Accounts Chem. Res.* **12**, 1-7 (1979).
11. Simon, R.J. Kania, R. S., Zuckermann, R. N., Huebner, V. D., Jewell, D. A., Banville, S., Ng, S., Wang, L., Rosenberg, S., Marlowe, C. K., Spellmeyer, D. C., Tan, R. Y., Frankel, A. D., Santi, D. V., Cohen, F. E., Bartlett, P. A. Peptoids - A modular approach to drug discovery. *Proc. Natl. Acad. Sci. U. S. A.* **89**, 9367-9371 (1992).
12. Giannis, A. peptidomimetics for receptor ligands discovery, development, and medical perspectives. *Angew. Chem.-Int. Ed.* **32**, 1244-1267 (1993).
13. Amidon, G.L. & Lee, H.J. Absorption of peptide and peptidomimetic drugs. *Annual Review of Pharmacology and Toxicology* **34**, 321-341 (1994).

14. Pauletti, G.M., Gangwar, S., Knipp, G. T., Nerurkar, M. M., Okumu, F. W., Tamura, K., Siahaan, T. J., Borchardt, R. T. Structural requirements for intestinal absorption of peptide drugs. *J. Control. Release* **41**, 3-17 (1996).

15. Matthews, D.M., Gandy, R.H., Taylor, E. & Burston, D. Influx of 2 dipeptides, Glycylsarcosine and L-Glutamyl-L-Glutamic acid, into hamster jejunum in vitro. *Clinical Science and Molecular Medicine* **56**, 15-23 (1979).

16. Bundgaard, H. Prodrugs as a means to improve the delivery of peptide drugs .1. *Adv. Drug Deliv. Rev.* **8**, 1-38 (1992).

17. Lipinski, C.A., Lombardo, F., Dominy, B.W. & Feeney, P.J. Experimental and computational approaches to estimate solubility and permeability in drug discovery and development settings. *Adv. Drug Deliv. Rev.* **46**, 3-26 (2001).

18. Veber, D.F., Johnson, S. R., Cheng, H. Y., Smith, B. R., Ward, K. W., Kopple, K. D. Molecular properties that influence the oral bioavailability of drug candidates. *J. Med. Chem.* **45**, 2615-2623 (2002).

19. Borel, J.F., Feurer, C., Gubler, H.U. & Stahelin, H. Biological Effects of Cyclosporin-a - new antilymphocytic agent. *Agents and Actions* **6**, 468-475 (1976).

20. Fusetani, N. & Matsunaga, S. Bioactive sponge peptides. *Chem. Rev.***93**, 1793-1806 (1993).

21. Davidson, B.S. Ascidians - producers of amino-acid derived metabolites. *Chem. Rev.***93**, 1771-1791 (1993).

22. Wipf, P. Synthetic studies of biologically-active marine cyclopeptides. *Chem. Rev.***95**, 2115-2134 (1995).

23. Rüegger, A., Kuhn, M., Lichti, H., Loosli, H. R., Huguenin, R., Quiquerez, C., Wartburg, A. V. Cyclosporin-a, a peptide metabolite from Trichoderma polysporum (Link Ex Pers) Rifai, with a remarkable immunosuppressive activity. *Helv. Chim. Acta* **59**, 1075-1092 (1976).

24. Wenger, D.M. Total Syntheses of 'Cyclosporin A' and 'Cyclosporin H', Two fungal metabolites isolated from the species Tolypocladium Inflaturn1 GAMS. *Helv. Chim. Acta* **67**, 502-525 (1984).

25. Pettit, G.R., Kamano, Y., Herald, C. L., Fujii, Y., Kizu, H., Boyd, M. R., Boettner, F. E., Doubek, D. L., Schmidt, J. M., Chapuis, J. C., Michel, C. Isolation of Dolastatins 10-15 from the marine mollusk Dolabella-Auricularia. *Tetrahedron* **49**, 9151-9170 (1993).

26. Sterner, O., Etzel, W., Mayer, A. & Anke, H. Omphalotin, a new cyclic peptide with potent nematicidal activity from Omphalotus olearius .2. Isolation and structure determination. *Natural Product Letters* **10**, 33-38 (1997).

27. Thern, B., Rudolph, J. & Jung, G. Total synthesis of the nematicidal cyclododecapeptide omphalotin A by using racemization-free triphosgene-mediated couplings in the solid phase. *Angew. Chem.-Int. Ed.* **41**, 2307-2309 (2002).

28. Sewald, N. Efficient, racemization-free peptide coupling of N-alkyl amino acids by using amino acid chlorides generated in situ - Total syntheses of the cyclopeptides cyclosporin O and omphalotin A. *Angew. Chem.-Int. Ed.* **41**, 4661-4663 (2002).

29. Cruz, L.J., Insua, M. M., Baz, J. P., Trujillo, M., Rodriguez-Mias, R. A., Oliveira, E., Giralt, E., Albericio, F., Canedo, L. M. IB-01212, a new cytotoxic cyclodepsipeptide isolated from the marine fungus Clonostachys sp ESNA-A009. *J. Org. Chem.* **71**, 3335-3338 (2006).

30. Cruz, L.J., Cuevas, C., Canedo, L.M., Giralt, E. & Albericio, F. Total solid-phase synthesis of marine cyclodepsipeptide IB-01212. *J. Org. Chem.* **71**, 3339-3344 (2006).

31. Haviv, F., Fitzpatrick, T. D., Swenson, R. E., Nichols, C. J., Mort, N. A., Bush, E. N., Diaz, G., Bammert, G., Nguyen, A., Rhutasel, N. S., Nellans, H. N., Hoffman, D. J., Johnson, E. S., Greer, J. Effect of N-methyl substitution of the peptide-bonds in luteinizing hormone-releasing hormone agonists. *J. Med. Chem.* **36**, 363-369 (1993).

32. Cody, W.L., He, J. X., Reily, M. D., Haleen, S. J., Walker, D. M., Reyner, E. L., Stewart, B. H., Doherty, A. M. Design of a potent combined pseudopeptide endothelin-A/endothelin-B receptor antagonist, Ac-DBhg(16)-Leu-Asp-Ile-[NMe]Ile-Trp(21) (PD 156252): Examination of its pharmacokinetic and spectral properties. *J. Med. Chem.* **40**, 2228-2240 (1997).

33. Bach, A.C., Espina, J. R., Jackson, S. A., Stouten, P. F. W., Duke, J. L., Mousa, S. A., DeGrado, W. F. Type II' to type I beta-turn swap changes specificity for integrins. *J. Am. Chem. Soc.* **118**, 293-294 (1996).

34. Pierson, M.E., Comstock, J. M., Simmons, R. D., Kaiser, F., Julien, R., Zongrone, J., Rosamond, J. D. Synthesis and biological evaluation of potent, selective, hexapeptide CCK-A agonist anorectic agents. *J. Med. Chem.* **40**, 4302-4307 (1997).

35. Rajeswaran, W.G., Hocart, S.J., Murphy, W.A., Taylor, J.E. & Coy, D.H. Highly potent and subtype selective ligands derived by N-methyl scan of a somatostatin antagonist. *J. Med. Chem.* **44**, 1305-1311 (2001).

36. Laufer, R., Wormser, U., Friedman, Z. Y., Gilon, C., Chorev, M., Selinger, Z. Neurokinin-B is a preferred agonist for a neuronal substance-P receptor and its action is antagonized by enkephalin. *Proc. Natl. Acad. Sci. U. S. A.* **82**, 7444-7448 (1985).

37. Samanen, J., Ali, F., Romoff, T., Calvo, R., Sorenson, E., Vasko, J., Storer, B., Berry, D., Bennett, D., Strohsacker, M., Powers, D., Stadel, J., Nichols, A. Development of a small RGD peptide fibrinogen receptor antagonist with potent antiaggregatory activity in vitro. *J. Med. Chem.* **34**, 3114-3125 (1991).

38. Dechantsreiter, M.A., Planker, E., Mathä, B., Lohof, E., Hölzemann, G., Jonczyk, A., Goodman, S. L., Kessler, H. N-methylated cyclic RGD peptides as highly active and selective alpha(v)beta(3) integrin antagonists. *J. Med. Chem.* **42**, 3033-3040 (1999).

39. Barker, P.L., Bullens, S., Bunting, S., Burdick, D. J., Chan, K. S., Deisher, T., Eigenbrot, C., Gadek, T. R., Gantzos, R., Lipari, M. T., Muir, C. D., Napier, M. A., Pitti, R. M., Padua, A., Quan, C., Stanley, M., Struble, M., Tom, J. Y. K., Burnier, J. P. Cyclic RGD peptide analogs as antiplatelet antithrombotics. *J. Med. Chem.* **35**, 2040-2048 (1992).

40. Piriou, F., Lintner, K., Fermandjian, S., Fromageot, P., Khosla, M. C., Smeby, R. R., Bumpus, F. M. Amino-acid side-chain conformation in angiotensin-II and analogs - correlated results of circular-dichroism and H-1 nuclear magnetic-resonance. *Proc. Natl. Acad. Sci. U. S. A.-Biological Sciences* **77**, 82-86 (1980).

41. Kessler, H. Detection of intramolecular mobility by NMR spectroscopy .13. Detection of hindered rotation and inversion by NMR spectroscopy. *Angew. Chem.-Int. Ed.* **9**, 219-& (1970).

42. Gordon, D.J., Tappe, R. & Meredith, S.C. Design and characterization of a membrane permeable N-methyl amino acid-containing peptide that inhibits A beta(1-40) fibrillogenesis. *J. Pept. Res.* **60**, 37-55 (2002).

43. Hess, S., Ovadia, O., Shalev, D. E., Senderovich, H., Qadri, B., Yehezkel, T., Salitra, Y., Sheynis, T., Jelinek, R., Gilon, C., Hoffman, A. Effect of structural and conformation modifications, including backbone cyclization, of hydrophilic hexapeptides on their intestinal permeability and enzymatic stability. *J. Med. Chem.* **50**, 6201-6211 (2007).

44. Sugano, H., Higaki, K. & Miyoshi, M. Synthesis and biological-activity of peptides related to eledoisin .1. Hexapeptide amides containing alpha-hydroxy acids. *Bulletin of the Chemical Society of Japan* **46**, 226-230 (1973).

45. Gilon, C., Dechantsreiter, M.A., Burkhart, F., Friedler, A. & Kessler, H. Synthesis of peptides and peptidomimetics. in *Houben-Weyl Methods of Organic Chemistry.*, Vol.

E22c (eds. Goodman, M., Felix, A., Moroder, L. & Tonolio, C.) 215-291 (Georg Thieme Verlag, Stuttgart, Germany, 2002).

46. Cheung, S.T. & Benoiton, N.L. N-Methylamino acids in peptide-synthesis .5. Synthesis of N-tert-Butyloxycarbonyl, N-methylamino acids by N-methylation. *Can. J. Chem.* **55**, 906-910 (1977).
47. Di Gioia, M.L., Leggio, A., Le Pera, A., Liguori, A., Napoli, A., Siciliano, C., Sindona, G. "One-Pot" methylation of N-nosyl-alpha-amino acid methyl esters with diazomethane and their coupling to prepare N-methyl dipeptides. *J. Org. Chem.* **68**, 7416-7421 (2003).
48. Prashad, M., Har, D., Hu, B., Kim, H. Y., Repic, O., Blacklock, T. J. An efficient and practical N-methylation of amino acid derivatives. *Org. Lett.* **5**, 125-128 (2003).
49. Freidinger, R.M., Hinkle, J.S., Perlow, D.S. & Arison, B.H. Synthesis of 9-Fluorenylmethyloxycarbonyl-protected N-alkyl amino-acids by reduction of oxazolidinones. *J. Org. Chem.* **48**, 77-81 (1983).
50. Mcdermot.Jr & Benoiton, N.L. N-Methylamino acids in peptide synthesis .3. Racemization during deprotection by saponification and acidolysis. *Can. J. Chem.* **51**, 2555-2561 (1973).
51. Cheung, S.T. & Benoiton, N.L. N-Methylamino acids in peptide-synthesis .7. Studies on enantiomeric purity of N-methylamino acids prepared by various procedures. *Can. J. Chem.* **55**, 916-921 (1977).
52. Zhang, S., Govender, T., Norstrom, T. & Arvidsson, P.I. An improved synthesis of Fmoc-N-methyl-alpha-amino acids. *J. Org. Chem.* **70**, 6918-6920 (2005).
53. Govender, T. & Arvidsson, P.I. Facile synthesis of Fmoc-N-methylated alpha- and beta-amino acids. *Tetrahedron Lett.* **47**, 1691-1694 (2006).
54. Fukuyama, T., Jow, C.K. & Cheung, M. 2-Nitrobenzenesulfonamides and 4-Nitrobenzenesulfonamides - Exceptionally versatile means for preparation of secondary-amines and protection of amines. *Tetrahedron Lett.* **36**, 6373-6374 (1995).
55. Miller, S.C. & Scanlan, T.S. Site-selective N-methylation of peptides on solid support. *J. Am. Chem. Soc.* **119**, 2301-2302 (1997).
56. Reichwein, J.F. & Liskamp, R.M.J. Site-specific N-alkylation of peptides on the solid phase. *Tetrahedron Lett.* **39**, 1243-1246 (1998).
57. Biron, E. & Kessler, H. Convenient synthesis of N-methylamino acids compatible with Fmoc solid-phase peptide synthesis. *J. Org. Chem.* **70**, 5183-5189 (2005).

58. Ohfune, Y., Kurokawa, N., Higuchi, N., Saito, M., Hashimoto, M., Tanaka, T. An efficient one-step reductive N-monoalkylation of alpha-amino-Acids. *Chemistry Letters*, 441-444 (1984).

59. Müller, P. & Siegfried, B. SN2 reactions with carboxylic esters - Selective cleavage of methyl-esters. *Helv. Chim. Acta* **57**, 987-994 (1974).

60. Magnus, P. & Gallagher, T. Studies on the synthesis of the antitumour agent CC-1065 - Synthesis of the cyclopropapyrroloindole portion. *Chem. Commun.* 389-390 (1984).

61. Miller, S.C. & Scanlan, T.S. oNBS-SPPS: A nem method for solid-phase peptide synthesis. *J. Am. Chem. Soc.* **120**, 2690-2691 (1998).

62. Yang, L.H. & Chiu, K.L. Solid phase synthesis of Fmoc N-methyl amino acids: Application of the Fukuyama amine synthesis. *Tetrahedron Lett.* **38**, 7307-7310 (1997).

63. Teixido, M., Albericio, F. & Giralt, E. Solid-phase synthesis and characterization of N-methyl-rich peptides. *J. Pept. Res.* **65**, 153-166 (2005).

64. Falb, E., Yechezkel, T., Salitra, Y. & Gilon, C. In situ generation of Fmoc-amino acid chlorides using bis(trichloromethyl) carbonate and its utilization for difficult couplings in solid-phase peptide synthesis. *J. Pept. Res.* **53**, 507-517 (1999).

65. Thern, B., Rudolph, J. & Jung, G. Triphosgene as highly efficient reagent for the solid-phase coupling of N-alkylated amino acids - total synthesis of cyclosporin O. *Tetrahedron Lett.* **43**, 5013-5016 (2002).

66. Rose, G.D., Gierasch, L.M. & Smith, J.A. Turns in peptides and proteins. *Advances in Protein Chemistry* **37**, 1-109 (1985).

67. Weide, T., Modlinger, A. & Kessler, H. Spatial screening for the identification of the bioactive conformation of integrin ligands. *Bioactive Conformation I* **272**, 1-50 (2007).

68. Kessler, H., Gratias, R., Hessler, G., Gurrath, M. & Muller, G. Conformation of cyclic peptides. Principle concepts and the design of selectivity and superactivity in bioactive sequences by 'spatial screening'. *Pure Appl. Chem.* **68**, 1201-1205 (1996).

69. Haubner, R., Gratias, R., Diefenbach, B., Goodman, S. L., Jonczyk, A., Kessler, H. Structural and functional aspects of RGD-containing cyclic pentapeptides as highly potent and selective integrin alpha(v)beta(3) antagonists. *J. Am. Chem. Soc.* **118**, 7461-7472 (1996).

70. Tonelli, A.E. Effects of isolated N-methylated residues on conformational characteristics of polypeptides. *Biopolymers* **15**, 1615-1622 (1976).

71. Patel, D.J. & Tonelli, A.E. N-Methylleucine Gramicidin-S and (Di-N-Methylleucine) Gramicidin-S conformations with cis L-Orn-L-N-Meleu peptide-bonds. *Biopolymers* **15**, 1623-1635 (1976).

72. Barlos, K., Gatos, D., Kallitsis, J., Papaphotiu, G., Sotiriu, P., Yao, W. Q., Schafer, W. Synthesis of protected peptide-fragments using substituted triphenylmethyl resins. *Tetrahedron Lett.* **30**, 3943-3946 (1989).

73. Barlos, K., Chatzi, O., Gatos, D. & Stavropoulos, G. 2-Chlorotrityl chloride resin - studies on anchoring of Fmoc-amino acids and peptide cleavage. *Int. J. Pept. Protein Res.* **37**, 513-520 (1991).

74. Anteunis, M.J.O. & Vanderauwera, C. The remarkable sensitivity to acid-catalyzed peptolysis of peptide chains (Endopeptolysis) having a succession of 3 N-alkylated amino-acid residues. *Int. J. Pept. Protein Res.* **31**, 301-310 (1988).

75. Knorr, R., Trzeciak, A., Bannwarth, W. & Gillessen, D. New coupling reagents in peptide chemistry. *Tetrahedron Lett.* **30**, 1927-1930 (1989).

76. Carpino, L.A., Elfaham, A., Minor, C.A. & Albericio, F. Advantageous applications of azabenzotriazole (triazolopyridine)-aased coupling reagents to solid-phase peptide-synthesis. *Chem. Commun.* 201-203 (1994).

77. Albericio, F., Bofill, J.M., El-Faham, A. & Kates, S.A. Use of onium salt-based coupling reagents in peptide synthesis. *J. Org. Chem.* **63**, 9678-9683 (1998).

78. Carpino, L.A. 1-Hydroxy-7-Azabenzotriazole - an efficient peptide coupling additive. *J. Am. Chem. Soc.* **115**, 4397-4398 (1993).

79. Kaiser, E., Colescot.Rl, Bossinge.Cd & Cook, P.I. Color test for detection of free terminal amino groups in solid-phase synthesis of peptides. *Anal. Biochem.* **34**, 595-& (1970).

80. Shioiri, T., Yamada, S. & Ninomiya, K. Diphenylphosphoryl azide - New convenient reagent for a modified curtius reaction and for peptide synthesis. *J. Am. Chem. Soc.* **94**, 6203-& (1972).

81. Brady, S.F., Varga, S. L., Freidinger, R. M., Schwenk, D. A., Mendlowski, M., Holly, F. W., Veber, D. F. Practical Synthesis of cyclic-peptides, with an example of dependence of cyclization yield upon linear sequence. *J. Org. Chem.* **44**, 3101-3105 (1979).

82. Brady, S.F., W. J.; Arison, B. H.; Freidinger, R. M.; Nutt, R. F.; Veber, D. F. peptides'83: Structure and Function. in *8th Annual Peptide Symposium* (ed. Hruby, V.J., Rich, D. H.,) 127-130 (Pierce Chemical Co.:Rockford, IL. 1983, 1983).

83. Bax, A. & Summers, M. F. H-1 and C-13 assignments from sensitivity-enhanced detection of heteronuclear multiple-bond connectivity by 2d multiple quantum NMR. *J. Am. Chem. Soc.* **108**, 2093-2094 (1986).

84. Kessler, H., Gehrke, M. & Griesinger, C. Two-dimensional NMR-spectroscopy - background and overview of the experiments. *Angew. Chem.-Int. Ed.* **27**, 490-536 (1988).

85. Bothnerby, A.A., Stephens, R.L., Lee, J.M., Warren, C.D. & Jeanloz, R.W. Structure determination of a tetrasaccharide - transient nuclear overhauser effects in the rotating frame. *J. Am. Chem. Soc.* **106**, 811-813 (1984).

86. Jeener, J., Meier, B.H., Bachmann, P. & Ernst, R.R. Investigation of exchange processes by 2-dimensional NMR-spectroscopy. *J. Chem. Phys.* **71**, 4546-4553 (1979).

87. Griesinger, C. & Ernst, R.R. Frequency offset effects and their elimination in NMR rotating-frame cross-relaxation spectroscopy. *J. Magn. Reson.* **75**, 261-271 (1987).

88. Havel, T.F. An evaluation of computational strategies for use in the determination of protein-structure from distance constraints cbtained by nuclear-magnetic-resonance. *Prog. Biophys. Mol. Biol.* **56**, 43-78 (1991).

89. Mierke, D.F., Scheek, R.M. & Kessler, H. Coupling-constants as restraints in ensemble distance driven dynamics. *Biopolymers* **34**, 559-563 (1994).

90. Mierke, D.F., Geyer, A. & Kessler, H. Coupling-constants and hydrogen-bonds as experimental restraints in a distance geometry refinement protocol. *Int. J. Pept. Protein Res.* **44**, 325-331 (1994).

91. Lifson, S., Hagler, A.T. & Dauber, P. Consistent force-field studies of inter-molecular forces in hydrogen-bonded crystals .1. Carboxylic-acids, amides, and the C=O...H-hydrogen-bonds. *J. Am. Chem. Soc.* **101**, 5111-5121 (1979).

92. Chatterjee, J., Mierke, D. & Kessler, H. N-methylated cyclic pentaalanine peptides as template structures. *J. Am. Chem. Soc.* **128**, 15164-15172 (2006).

93. Chatterjee, J., Mierke, D.F. & Kessler, H. Conformational preference and potential templates of N-methylated cyclic pentaalanine peptides. *Chem.-Eur. J.* **14**, 1508-1517 (2008).

94. Snyder, J.P. Probable unimportance of intramolecular hydrogen-Bonds for determining the secondary structure of cyclic hexapeptides - roseotoxin-B. *J. Am. Chem. Soc.* **106**, 2393-2400 (1984).

95. Laufer, B., Chatterjee, J. & Kessler, H. Making double-minded pepticles strong-willed? The side chain impact on the backbone conformation of N-methylated cyclic pentapeptides. *Biopolymers* **88**, 585-585 (2007).

96. Kessler, H., Anders, U. & Schudok, M. An unexpected cis peptide-bond in the minor conformation of a cyclic hexapeptide containing only secondary amide bonds. *J. Am. Chem. Soc.* **112**, 5908-5916 (1990).

97. Mierke, D.F., Kurz, M. & Kessler, H. Peptide flexibility and calculations of an ensemble of molecules. *J. Am. Chem. Soc.* **116**, 1042-1049 (1994).

98. Heller, M., Sukopp, M., Tsomaia, N., John, M., Mierke, D. F., Reif, B., Kessler, H. The conformation of cyclo(-D-Pro-Ala(4)-) as a model for cyclic pentapeptides of the DL4 type. *J. Am. Chem. Soc.* **128**, 13806-13814 (2006).

99. Mierke, D.F. & Kessler, H. Molecular-dynamics with dimethyl-sulfoxide as a solvent - conformation of a cyclic hexapeptide. *J. Am. Chem. Soc.* **113**, 9466-9470 (1991).

100. Hutchinson, E.G. & Thornton, J.M. A revised set of potentials for beta-turn formation in proteins. *Protein Sci.* **3**, 2207-2216 (1994).

101. Nagarajaram, H.A. & Ramakrishnan, C. Stereochemical studies on cyclic peptides: Detailed energy minimization studies on hydrogen bonded all-trans cyclic pentapeptide backbones. *J. Biosci.* **20**, 591-611 (1995).

102. Bystrov, V. F., Ivanov, V. T., Portnova, S. L., Balashov, T. A., & Ovchinni,Y. A. Refinement of angular dependence of peptide vicinal NH-C Alpha H coupling-constant. *Tetrahedron* **29**, 873-877 (1973).

103. Keller, B., Christen, M., Oostenbrink, C. & van Gunsteren, W. F. On using oscillating time-dependent restraints in MD simulation. *J. Biomol. NMR* **37**, 1-14 (2007).

104. Otrubova, K., McGuire, K.L. & McAlpine, S.R. Scaffold targeting drug-resistant colon cancers. *J. Med. Chem.* **50**, 1999-2002 (2007).

105. Robinson, J.A. The design, synthesis and conformation of some new beta-hairpin mimetics: Novel reagents for drug and vaccine discovery. *Synlett*, 429-441 (2000).

106. Lipinski, C.A., Lombardo, F., Dominy, B.W. & Feeney, P.J. Experimental and computational approaches to estimate solubility and permeability in drug discovery and development settings. *Adv. Drug Deliv. Rev.* **23**, 3-25 (1997).

107. Modi, N.B. Pharmacokinetics and pharmacodynamics of recombinant proteins and peptides. *J. Control. Release* **29**, 269-281 (1994).

108. Zhou, X.H. Overcoming enzymatic and absorption barriers to non-parenterally administered protein and peptide drugs. *J. Control. Release* **29**, 239-252 (1994).

109. Gante, J. Peptidomimetics - Tailored enzyme-inhibitors. *Angew. Chem.-Int. Ed.* **33**, 1699-1720 (1994).

110. Roberts, N.A., Martin, J. A., Kinchington, D., Broadhurst, A. V., Craig, J. C., Duncan, I. B., Galpin, S. A., Handa, B. K., Kay, J., Krohn, A., Lambert, R. W., Merrett, J. H., Mills, J. S., Parkes, K. E. B., Redshaw, S., Ritchie, A. J., Taylor, D. L., Thomas, G. J., Machin, P. J. Rational design of peptide-based HIV proteinase-inhibitors. *Science* **248**, 358-361 (1990).

111. Rich, D.H., Prasad, J. V. N. V., Sun, C. Q., Green, J., Mueller, R., Houseman, K., Mackenzie, D., Malkovsky, M. New hydroxyethylamine HIV protease inhibitors that suppress viral replication. *J. Med. Chem.* **35**, 3803-3812 (1992).

112. Kempf, D. J., Delara, E., Stein, H. H., Cohen, J., Egan, D. A., Plattner, J. J. Renin inhibitors based on dipeptide analogs - Incorporation of the hydroxyethylene isostere at the P2/P3 sites. *J. Med. Chem.* **33**, 371-374 (1990).

113. Xue, C.B., Roderick, J., Jackson, S., Rafalski, M., Rockwell, A., Mousa, S., Olson, R. E., DeGrado, W. F. Design, synthesis, and in vitro activities of benzamide-core glycoprotein IIb/IIIa antagonists: 2,3-diaminopropionic acid derivatives as surrogates of aspartic acid. *Bioorg. Med. Chem.***5**, 693-705 (1997).

114. Sakurai, M., Higashida, S., Sugano, M., Handa, H., Komai, T., Yagi, R., Nishigaki, T., Yabe, Y. Studies of human-immunodeficiency-virus type-1 (HIV-1) protease inhibitors .3. Structure-activity relationship of HIV-1 protease inhibitors containing cyclohexylalanylalanine hydroxyethylene dipeptide isostere. *Chem. Pharm. Bull.* **42**, 534-540 (1994).

115. Thaisrivongs, S., Turner, S. R., Strohbach, J. W., Tenbrink, R. E., Tarpley, W. G., Mcquade, T. J., Heinrikson, R. L., Tomasselli, A. G., Hui, J. O., Howe, W. J. Inhibitors of the protease from human-immunodeficiency-virus - Synthesis, enzyme-inhibition, and antiviral activity of a series of compounds containing the dihydroxyethylene transition-state isostere. *J. Med. Chem.* **36**, 941-952 (1993).

116. Peisach, E., Casebier, D., Gallion, S. L., Furth, P., Petsko, G. A., Hogan, J. C., Ringe, D. Interaction of a peptidomimetic aminimide inhibitor with elastase. *Science* **269**, 66-69 (1995).

117. Smith, A.B., Hirschmann, R., Pasternak, A., Yao, W. Q., Sprengeler, P. A., Holloway, M. K., Kuo, L. C., Chen, Z. G., Darke, P. L., Schleif, W. A. An orally bioavailable pyrrolinone inhibitor of HIV-1 protease: Computational analysis and x-ray crystal structure of the enzyme complex. *J. Med. Chem.* **40**, 2440-2444 (1997).

118. Roemer, D., Buescher, H. H., Hill, R. C., Pless, J., Bauer, W., Cardinaux, F., Closse, A., Hauser, D., Huguenin, R. Synthetic enkephalin analog with prolonged parenteral and oral analgesic activity. *Nature* **268**, 547-549 (1977).

119. Yu, J., Butelman, E.R., Woods, J.H., Chait, B.T. & Kreek, M.J. Dynorphin A (1-8) analog, E-2078, is stable in human and rhesus monkey blood. *J. Pharmacol. Exp. Ther.* **280**, 1147-1151 (1997).

120. Conradi, R.A., Hilgers, A.R., Ho, N.F.H. & Burton, P.S. The influence of peptide structure on transport across caco-2 cells. *Pharm. Res.* **8**, 1453-1460 (1991).

121. Conradi, R.A., Hilgers, A.R., Ho, N.F.H. & Burton, P.S. The influence of peptide structure on transport across caco-2 cells .2. Peptide-bond modification which results in improved permeability. *Pharm. Res.* **9**, 435-439 (1992).

122. Adibi, S. Intestinal transport of dipeptides in man - Potentially important mechanism for amino acid absorption. *Gastroenterology* **60**, 637-& (1971).

123. Balda, M.S., Gonzalezmariscal, L., Matter, K., Cereijido, M. & Anderson, J.M. Assembly of the tight junction - the role of diacylglycerol. *J. Cell Biol.* **123**, 293-302 (1993).

124. Madara, J.L. & Dharmsathaphorn, K. Occluding junction structure-function relationships in a cultured epithelial monolayer. *J. Cell Biol.* **101**, 2124-2133 (1985).

125. Pauletti, G.M., Gangwar, S., Siahaan, T.J., Aube, J. & Borchardt, R.T. Improvement of oral peptide bioavailability: Peptidomimetics and prodrug strategies. *Adv. Drug Deliv. Rev.* **27**, 235-256 (1997).

126. Conradi, R.A., Burton, P.S. & Borchardt, R.T. Physico-chemical and biological factors that influence a drug's cellular permeability by passive diffusion. in *Lipophilicity in Drug Action and Toxicology* (ed. V. Pliska, B.T., H.Van de Waterbeemd) 233-250 (VCH, Weinheim, 1996).

127. Siminoski, K., Gonnella, P., Bernanke, J., Owen, L., Neutra, M., Murphy, R. A. Uptake and trans-epithelial transport of nerve growth-factor in suckling rat ileum. *J. Cell Biol.* **103**, 1979-1990 (1986).

128. Strous, G.J. & Dekker, J. Mucin-type glycoproteins. *Crit. Rev. Biochem. Mol. Biol.* **27**, 57-92 (1992).

129. Kim, Y.S., Kim, Y.W. & Birtwhis.W. Peptide hydrolases in brush border and soluble fractions of small intestinal-mucosa of rat and man. *J. Clin. Invest.* **51**, 1419-& (1972).

130. Barrett, A.J. & McDonald, J.K. *Mammalian proteases: a glossary and bibliography*, (Academic Press, New York, 1980).

131. McDonald, J.K. & Barrett, A.J. *Mammalian proteases: a glossary and bibliography*, (Academic Press, New York, 1980).

132. Bai, J.P.F. Comparison of distribution of brush-border exopeptidases and endopeptidases in rat and rabbit intestine. *J. Pharm. Pharmacol.* **46**, 928-930 (1994).

133. Leitch, G.J. Regional variations in composition of purified brush borders isolated from infant and adult rabbit small intestine. *Archives Internationales De Physiologie Et De Biochimie* **79**, 279-& (1971).

134. Lindberg, T. Intestinal dipeptidases - Dipeptidase activity in mucosa of gastrointestinal tract of adult human. *Acta Physiol. Scand.* **66**, 437-443 (1966).

135. Peters, W.H.M., Boon, C. E. W., Roelofs, H. M. J., Wobbes, T., Nagengast, F. M., Kremers, P. G. Expression of drug-metabolizing-enzymes and P-170-glycoprotein in colorectal-carcinoma and normal mucosa. *Gastroenterology* **103**, 448-455 (1992).

136. Gottesman, M.M. & Pastan, I. Biochemistry of multidrug-resistance mediated by the multidrug transporter. *Annu. Rev. Biochem.* **62**, 385-427 (1993).

137. Burton, P.S., Conradi, R.A., Hilgers, A.R. & Ho, N.F.H. Evidence for a polarized efflux system for peptides in the apical membrane of caco-2 cells. *Biochem. Biophys. Res. Commun.* **190**, 760-766 (1993).

138. Lee, V.H.L. Enzymatic barriers to peptide and protein-absorption. *Crit. Rev. Ther. Drug Carr. Syst.* **5**, 69-97 (1988).

139. Drewe, J., Fricker, G., Vonderscher, J. & Beglinger, C. Enteral absorption of octreotide - absorption enhancement by polyoxyethylene-24-cholesterol ether. *Brit. J. Pharmacol.***108**, 298-303 (1993).

140. Lundin, S. & Artursson, P. Absorption of a vasopressin analog, 1-Deamino-8-D-arginine-vasopressin (Ddavp), in a human intestinal epithelial-cell line, caco-2. *Int. J. Pharm.* **64**, 181-186 (1990).

141. Thwaites, D.T., Hirst, B.H. & Simmons, N.L. Passive transepithelial absorption of thyrotropin-releasing-hormone (Trh) via a paracellular route in cultured intestinal and renal epithelial-cell lines. *Pharm. Res.* **10**, 674-681 (1993).

142. Cereijido, M., Meza, I. & Martinezpalomo, A. Occluding junctions in cultured epithelial monolayers. *Am. J. Physiol.* **240**, C96-C102 (1981).

143. Adson, A. Raub, T. J., Burton, P. S., Barsuhn, C. L., Hilgers, A. R., Audus, K. L. Ho, N. F. H. Quantitative approaches to delineate paracellular diffusion in cultured epithelial-cell monolayers. *J. Pharm. Sci.* **83**, 1529-1536 (1994).

144. Pauletti, G.M., Okumu, F.W. & Borchardt, R.T. Effect of size and charge on the passive diffusion of peptides across caco-2 cell monolayers via the paracellular pathway. *Pharm. Res.* **14**, 164-168 (1997).

145. Ho, N.F.H., Day, J.S., Barsuhn, C.L., Burton, P.S. & Raub, T.J. Biophysical model approaches to mechanistic transepithelial studies of peptides. *J. Control. Release* **11**, 3-24 (1990).

146. Augustijns, P.F., Bradshaw, T.P., Gan, L.S.L., Hendren, R.W. & Thakker, D.R. Evidence for a polarized efflux system in caco-2 cells capable of modulating cyclosporine-a transport. *Biochem. Biophys. Res. Commun.* **197**, 360-365 (1993).

147. Mcmartin, C., Hutchinson, L.E.F., Hyde, R. & Peters, G.E. Analysis of structural requirements for the absorption of drugs and macromolecules from the nasal cavity. *J. Pharm. Sci.* **76**, 535-540 (1987).

148. Okumu, F.W., Pauletti, G.M., VanderVelde, D.G., Siahaan, T.J. & Borchardt, R.T. Effect of restricted conformational flexibility on the permeation of model hexapeptides across caco-2 cell monolayers. *Pharm. Res.* **14**, 169-175 (1997).

149. (a) Hochman, J. & Artursson, P. Mechanisms of absorption enhancement and tight junction regulation. *J. Control. Release* **29**, 253-267 (1994). (b) Lee, V.H.L., Dodda-Kashi, S., Grass, G.M. & Rubas, W. Oral route of peptide and protein delivery. in *Peptide and Protein Drug Delivery* (ed. Lee, V.H.L.) pp. 691-738 (Marcel Dekker, New York, 1991).

150. Singer, S.J. & Nicolson, G.L. Fluid mosaic model of structure of cell-membranes. *Science* **175**, 720-731 (1972).

151. Hansch, C. & Fujita, T. Rho-Sigma-Pi Analysis . Method for correlation of biological activity + chemical structure. *J. Am. Chem. Soc.* **86**, 1616-1626 (1964).

152. Smith, R.N., Hansch, C. & Ames, M.M. Selection of a reference partitioning system for drug design work. *J. Pharm. Sci.* **64**, 599-606 (1975).

153. Kim, D.C., Burton, P.S. & Borchardt, R.T. A correlation between the permeability characteristics of a series of peptides using an in-vitro cell-culture model (Caco-2) and those using an in-situ perfused rat ileum model of the intestinal-mucosa. *Pharm. Res.* **10**, 1710-1714 (1993).

154. Rezai, T., Yu, B., Millhauser, G.L., Jacobson, M.P. & Lokey, R.S. Testing the conformational hypothesis of passive membrane permeability using synthetic cyclic peptide diastereomers. *J. Am. Chem. Soc.* **128**, 2510-2511 (2006).

155. Roseman, M.A. Hydrophobicity of the Peptide C=O...H-N Hydrogen-bonded group. *J. Mol. Biol.***201**, 621-623 (1988).

156. Banks, W.A., Kastin, A.J., Coy, D.H. & Angulo, E. Entry of dsip peptides into dog csf - role of physicochemical and pharmacokinetic parameters. *Brain Res. Bull.* **17**, 155-158 (1986).

157. Raeissi, S. & Audus, K.L. In-vitro characterization of blood-brain-barrier permeability to delta sleep-inducing peptide. *J. Pharm. Pharmacol.* **41**, 848-852 (1989).

158. Gray, R.A., Vandervelde, D. G., Burke, C. J., Manning, M. C., Middaugh, C. R., Borchardt, R. T. Delta-sleep-inducing peptide - solution conformational studies of a membrane-permeable peptide. *Biochemistry* **33**, 1323-1331 (1994).

159. Carrupt, P.A., Testa, B., Bechalany, A., Eltayar, N., Descas, P., Perrissoud, D. morphine 6-glucuronide and morphine 3-glucuronide as molecular chameleons with unexpected lipophilicity. *J. Med. Chem.* **34**, 1272-1275 (1991).

160. Eltayar, N., Mark, A.E., Vallat, P., Brunne, R.M., Testa, B., van Gunsteren, W.F. Solvent-dependent conformation and hydrogen-bonding capacity of cyclosporine-a - evidence from partition-coefficients and molecular-dynamics simulations. *J. Med. Chem.* **36**, 3757-3764 (1993).

161. Kaiser, E.T. & Kezdy, F.J. Amphiphilic secondary structure - design of peptide-hormones. *Science* **223**, 249-255 (1984).

162. Rautio, J., Kumpulainen, H., Heimbach, T., Oliyai, R., Oh, D., Jarvinen, T., Savolainen, J. Prodrugs: design and clinical applications. *Nat. Rev. Drug Discov.* **7**, 255-270 (2008).

163. Roberts, M.J., Bentley, M.D. & Harris, J.M. Chemistry for peptide and protein PEGylation. *Adv. Drug Deliv. Rev.* **54**, 459-476 (2002).

164. Flinn, N., Hussain, I., Shaw, A., Artursson, P., Gibbons, W. A., Toth, I. Oral absorption studies of lipid-polylysine conjugates of thyrotropin releasing hormone (TRH) and luteinizing hormone releasing hormone (LHRH). *Int. J. Pharm.* **138**, 167-174 (1996).

165. Yu, J., Butelman, E.R., Woods, J.H., Chait, B.T. & Kreek, M.J. Dynorphin A (1-8) analog, E-2078, crosses the blood-brain barrier in rhesus monkeys. *J. Pharmacol. Exp. Ther.* **282**, 633-638 (1997).

166. Thummel, K.E. & Shen, D.D. Design and optimization of dosage regimens: pharmacokinetic data. in *The pharmacological Basis of Therapeutics* (eds. Hardman, J.G., Limbird, L.E. & Gilman, A.G.) (Mc.Graw-Hill, USA, 2001).

167. Veber, D.F., Freidinger, R. M., Perlow, D. S., Paleveda, W. J., Holly, F. W., Strachan, R. G., Nutt, R. F., Arison, B. H., Homnick, C., Randall, W. C., Glitzer, M. S.,

Saperstein, R., Hirschmann, R. A potent cyclic hexapeptide analog of somatostatin. *Nature* **292**, 55-58 (1981).

168. Brazeau, P., Vale, W., Burgus, R., Ling, N., Butcher, M., Rivier, J., Guillemi, R. Hypothalamic polypeptide that inhibits secretion of immunoreactive pituitary growth-hormone. *Science* **179**, 77-79 (1973).
169. Benoit, R. Esch, F., Bennett, H. P. J., Ling, N., Ravazzola, M., Orci, L., Mufson, E. J. Processing of prosomatostatin. *Metab.-Clin. Exp.* **39**, 22-25 (1990).
170. Gillies, G. Somatostatin: The neuroendocrine story. *Trends in Pharmacol. Sci.* **18**, 87-95 (1997).
171. Weckbecker, G., Lewis, I., Albert, R., Schmid, H. A., Hoyer, D., Bruns, C. Opportunities in somatostatin research: Biological, chemical and therapeutic aspects. *Nat. Rev. Drug Discov.* **2**, 999-1017 (2003).
172. Reichlin, S. Somatostatin .1. *New Engl. J. Med.* **309**, 1495-1501 (1983).
173. Reichlin, S. Somatostatin .2. *New Engl. J. Med.* **309**, 1556-1563 (1983).
174. Yamada, Y., Post, S. R., Wang, K., Tager, H. S., Bell, G. I., Seino, S. Cloning and functional-characterization of a family of human and mouse somatostatin receptors expressed in brain, Gastrointestinal-Tract, and Kidney. *Proc. Natl. Acad. Sci. U. S. A.* **89**, 251-255 (1992).
175. Patel, Y.C. Somatostatin and its receptor family. *Front. Neuroendocrinol.* **20**, 157-198 (1999).
176. Hannon, J.P., Nunn, C., Stolz, B., Bruns, C., Weckbecker, G., Lewis, I., Troxler, T., Hurth, K., Hoyer, D. Drug design at peptide receptors - Somatostatin receptor ligands. *J. Mol. Neurosci.* **18**, 15-27 (2002).
177. Rosskopf, D., Schurks, M., Manthey, I., Joisten, M., Busch, S., Siffert, W. Signal transduction of somatostatin in human B lymphoblasts. *Am. J. Physiol.-Cell Physiol.* **284**, C179-C190 (2003).
178. Bruns, C. Raulf, F., Hoyer, D., Schloos, J., Lubbert, H., Weckbecker, G. Binding properties of somatostatin receptor subtypes. *Metab.-Clin. Exp.* **45**, 17-20 (1996).
179. Akbar, M., Okajima, F., Tomura, H., Majid, M. A., Yamada, Y., Seino, S., Kondo, Y. Phospholipase-C Activation and Ca2+ Mobilization by cloned human somatostatin receptor subtypes-1-5, in transfected cos-7 cells. ***FEBS Lett.* 348**, 192-196 (1994).
180. Cheng, H., Yibchok-anun, S., Coy, D.H. & Hsu, W.H. SSTR2 mediates the somatostatin-induced increase in intracellular Ca2+ concentration and insulin secretion in the presence of arginine vasopressin in clonal beta-cell HIT-T15. *Life Sci.* **71**, 927-936 (2002).

181. Rivier, J., Brown, M. & Vale, W. D-Trp8-Somatostatin - Analog of somatostatin more potent than native molecule. *Biochem. Biophys. Res. Commun.* **65**, 746-751 (1975).

182. Nutt, R.F., Veber, D.F., Curley, P.E., Saperstein, R. & Hirschmann, R. Somatostatin analogs which define the role of the lysine-9 amino group. *Int. J. Pept. Protein Res.* **21**, 66-73 (1983).

183. Veber, D.F., Saperstein, R., Nutt, R.F., Freidinger, R.M., Brady, S.F., Curley, P., Perlow, D.S., Paleveda, W.J., Colton, C.D., Zacchei, A.G., Tocco, D.J., Hoff, D.R., Vandlen, R.L., Gerich, J.E., Hall, L., Mandarino, L., Cordes, E.H., Anderson, P.S., Hirschmann, R. A super active cyclic hexapeptide analog of somatostatin. *Life Sci.* **34**, 1371-1378 (1984).

184. Bauer, W., Briner, U., Doepfner, W., Haller, R., Huguenin, R., Marbach, P., Petcher, T.J., Pless, J. SMS 201-995 - a very potent and selective octapeptide analog of somatostatin with prolonged action. *Life Sci.* **31**, 1133-1140 (1982).

185. Lamberts, S.W.J., vanderLely, A.J., deHerder, W.W. & Hofland, L.J. Drug therapy - Octreotide. *New Engl. J. Med.* **334**, 246-254 (1996).

186. Bruns, C., Lewis, I., Briner, U., Meno-Tetang, G. & Weckbecker, G. SOM230: a novel somatostatin peptidomimetic with broad somatotropin release inhibiting factor (SRIF) receptor binding and a unique antisecretory profile. *Eur. J. Endocrinol.* **146**, 707-716 (2002).

187. Lamberts, S.W.J., van der Lely, A.J. & Hofland, L.J. New somatostatin analogs: will they fulfil old promises? *Eur. J. Endocrinol.* **146**, 701-705 (2002).

188. Gademann, K., Kimmerlin, T., Hoyer, D. & Seebach, D. Peptide folding induces high and selective affinity of a linear and small beta-peptide to the human somatostatin receptor 4. *J. Med. Chem.* **44**, 2460-2468 (2001).

189. Rajeswaran, W.G., Hocart, S.J., Murphy, W.A., Taylor, J.E. & Coy, D.H. N-methyl scan of somatostatin octapeptide agonists produces interesting effects on receptor subtype specificity. *J. Med. Chem.* **44**, 1416-1421 (2001).

190. Bowman, W.R. & Coghlan, D.R. A facile method for the N-alkylation of alpha-amino esters. *Tetrahedron* **53**, 15787-15798 (1997).

191. Biron, E., Chatterjee, J. & Kessler, H. Optimized selective N-methylation of peptides on solid support. *J. Pept. Sci.* **12**, 213-219 (2006).

192. Hannon, J.P., Pertucci, C., Fehlmann, D., Viollet, C., Epelbaum, J., Hoyer, D. Somatostatin sst(2) receptor knock-out mice: localisation of sst(1-5) receptor mRNA and binding in mouse brain by semi-quantitative RT-PCR, in situ hybridisation

histochemistry and receptor autoradiography. *Neuropharmacology* **42**, 396-413 (2002).

193. Brady, S.F., W. J.; Arison, B. H.; Freidinger, R. M.; Nutt, R. F.; Veber, D. F. An improved procedure for peptide cyclization. in *Peptides: Structure and Function. Proceedings of the 8th American Peptide Symposium;* (eds Hruby, V.J., Rich, D. & H.) 127-130 (Rockford, IL,, 1983).
194. Kessler, H., Bernd, M., Kogler, H., Zarbock, J., Sorensen, O. W., Bodenhausen, G., Ernst, R. R. Peptide conformations .28. Relayed heteronuclear correlation spectroscopy and conformational-analysis of cyclic hexapeptides containing the active sequence of somatostatin. *J. Am. Chem. Soc.* **105**, 6944-6952 (1983).
195. Carpino, L.A., Imazumi, H., El-Faham, A., Ferrer, F. J., Zhang, C. W., Lee, Y. S., Foxman, B. M., Henklein, P., Hanay, C., Mugge, C., Wenschuh, H., Klose, K., Beyermann, M., Bienert, M. The uronium/guanidinium peptide coupling reagents: Finally the true uronium salts. *Angew. Chem.-Int. Ed.* **41**, 442-445 (2002).
196. Holmes, R. & Lobley, R.W. Intestinal brush-border revisited. *Gut* **30**, 1667-1678 (1989).
197. Kolusheva, S., Boyer, L. & Jelinek, R. A colorimetric assay for rapid screening of antimicrobial peptides. *Nature Biotechnol.* **18**, 225-227 (2000).
198. Tugyi, R., Mezo, G., Fellinger, E., Andreu, D. & Hudecz, F. The effect of cyclization on the enzymatic degradation of herpes simplex virus glycoprotein D derived epitope peptide. *J. Pept. Sci.* **11**, 642-649 (2005).
199. Byk, G., Halle, D., Zeltser, I., Bitan, G., Selinger, Z., Gilon, C. Synthesis and biological activity of NK-1 selective, N-backbone cyclic analogs of the C-terminal hexapeptide of substance P. *J. Med. Chem.* **39**, 3174-3178 (1996).
200. Hows, J.M. & Smith, J.M. In-vitro stability of cyclosporin-A. *J. Clin. Pathol.* **36**, 720-721 (1983).
201. Sangalli, L., Bortolotti, A., Jiritano, L. & Bonati, M. Cyclosporine pharmacokinetics in rats and interspecies comparison in dogs, rabbits, rats, and humans. *Drug Metab. Dispos.* **16**, 749-753 (1988).
202. Fasano, A. Modulation of intestinal permeability: An innovative method of oral drug delivery for the treatment of inherited and acquired human diseases. *Mol. Genet. Metab.* **64**, 12-18 (1998).
203. Knipp, G.T., Velde, D.G.V., Siahaan, T.J. & Borchardt, R.T. The effect of beta-turn structure on the passive diffusion of peptides across Caco-2 cell monolayers. *Pharm. Res.* **14**, 1332-1340 (1997).

204. Irvine, J.D., Takahashi, L., Lockhart, K., Cheong, J., Tolan, J. W., Selick, H. E., Grove, J. R. MDCK (Madin-Darby canine kidney) cells: A tool for membrane permeability screening. *J. Pharm. Sci.* **88**, 28-33 (1999).

205. Lennernas, H. Human intestinal permeability. *J. Pharm. Sci.* **87**, 403-410 (1998).

206. He, Y.B., Huang, Z.W., Raynor, K., Reisine, T. & Goodman, M. Syntheses and conformations of somatostatin-related cyclic hexapeptides incorporating specific alpha-methylated and beta-methylated residues. *J. Am. Chem. Soc.* **115**, 8066-8072 (1993).

207. Veber, D.F. Design and discovery in the development of peptide analogs. in *Proc. Am. Pept. Symp., 12th* (eds Smith, J.A. & Rivier, J.E.) 3-14 (ESCOM, Leiden, Cambridge, MA, 1991).

208. Hynes, R.O. Integrins - a family of cell-surface receptors. *Cell* **48**, 549-554 (1987).

209. Humphries, J.D., Byron, A. & Humphries, M.J. Integrin ligands at a glance. *J. Cell Sci.* **119**, 3901-3903 (2006).

210. Schlaepfer, D.D. & Hunter, T. Integrin signalling and tyrosine phosphorylation: just the FAKs? *Trends Cell Biol.* **8**, 151-157 (1998).

211. Hemler, M.E. Vla proteins in the integrin family - Structures, functions, and their role on leukocytes. *Annu. Rev. Immunol.* **8**, 365-400 (1990).

212. Arnaout, M.A. Integrin structure: new twists and turns in dynamic cell adhesion. *Immunol. Rev.* **186**, 125-140 (2002).

213. Arnaout, M.A. Structure and function of the leukocyte adhesion molecules Cd11 Cd18. *Blood* **75**, 1037-1050 (1990).

214. Mousa, S.A. Anti-integrin as novel drug-discovery targets: potential therapeutic and diagnostic implications. *Curr. Opin. Chem. Biol.* **6**, 534-541 (2002).

215. Xiong, J.P., Stehle, T., Diefenbach, B., Zhang, R. G., Dunker, R., Scott, D. L., Joachimiak, A., Goodman, S. L., Arnaout, M. A. Crystal structure of the extracellular segment of integrin alpha V beta 3. *Science* **294**, 339-345 (2001).

216. Xiong, J.P., Stehle, T., Zhang, R. G., Joachimiak, A., Frech, M., Goodman, S. L., Aranout, M. A. Crystal structure of the extracellular segment of integrin alpha V beta 3 in complex with an Arg-Gly-Asp ligand. *Science* **296**, 151-155 (2002).

217. Bork, P., Doerks, T., Springer, T.A. & Snel, B. Domains in plexins: links to integrins and transcription factors. *Trends Biochem. Sci.* **24**, 261-263 (1999).

218. Takagi, J. & Springer, T.A. Integrin activation and structural rearrangement. *Immunol. Rev.* **186**, 141-163 (2002).

219. Du, X. & Ginsberg, M.H. Integrin alpha(IIb)beta(3) and platelet function. *Thromb. Haemostasis* **78**, 96-100 (1997).

220. Vorchheimer, D.A., Badimon, J.J. & Fuster, V. Platelet glycoprotein IIb/IIIa receptor antagonists in cardiovascular disease. *JAMA-J. Am. Med. Assoc.* **281**, 1407-1414 (1999).

221. Mehrotra, M. M., Heath, J. A., Smyth, M. S., Pandey, A., Rose, J. W., Seroogy, J. M., Volkots, D. L., Nannizzi-Alaimo, L., Park, G. L., Lambing, J. L., Hollenbach, S. J., Scarborough, R. M. Discovery of novel 2,8-diazaspiro[4.5]decanes as orally active glycoprotein IIb-IIIa antagonists. *J. Med. Chem.* **47**, 2037-2061 (2004).

222. Phillips, D.R., Charo, I.F., Parise, L.V. & Fitzgerald, L.A. The platelet membrane glycoprotein-IIb-IIIa complex. *Blood* **71**, 831-843 (1988).

223. Scarborough, R.M., Naughton, M. A., Teng, W., Rose, J. W., Phillips, D. R., Nannizzi, L., Arfsten, A., Campbell, A. M., Charo, I. F. Design of potent and specific integrin antagonists - peptide antagonists with high specificity for glycoprotein-IIb-IIIa. *J. Biol. Chem.* **268**, 1066-1073 (1993).

224. Lincoff, A.M., Califf, R.M. & Topol, E.J. Platelet glycoprotein IIb-IIIa receptor blockade in coronary artery disease. *J. Am. Coll. Cardiol.* **35**, 1103-1115 (2000).

225. Coleman, P.J., Brashear, K.M., Askew, B.C., Hutchinson, J.H., McVean, C.A., Duong, L.T., Feuston, B.P., Fernandez-Metzler, C., Gentile, M.A., Hartman, G.D., Kimmel, D.B., Leu, C.T., Lipfert, L., Merkle, K., Pennypacker, B., Prueksaritanont, T., Rodan, G.A., Wesolowski, G.A., Rodan, S.B., Duggan, M.E. Nonpeptide alpha(v)beta(3) antagonists. Part 11: Discovery and preclinical evaluation of potent alpha v beta(3) antagonists for the prevention and treatment of osteoporosis. *J. Med. Chem.* **47**, 4829-4837 (2004).

226. Dennis, M.S., Henzel, W.J., Pitti, R.M., Lipari, M.T., Napier, M.A., Deisher, T.A., Bunting, S., Lazarus, R.A. Platelet glycoprotein-IIb-IIIa protein antagonists from snake-venoms - evidence for a family of platelet-aggregation inhibitors. *Proc. Natl. Acad. Sci. U. S. A.* **87**, 2471-2475 (1990).

227. Yasuda, T., Gold, H.K., Fallon, J.T., Leinbach, R.C., Guerrero, J.L., Scudder, L.E., Kanke, M., Shealy, D., Ross, M.J., Collen, D., Coller, B.S. Monoclonal-antibody against the platelet glycoprotein (Gp) IIb-IIIa receptor prevents coronary-artery reocclusion after reperfusion with recombinant tissue-type plasminogen-activator in dogs. *J. Clin. Invest.* **81**, 1284-1291 (1988).

228. Zablocki, J.A., Miyano, M., Garland, R.B., Pireh, D., Schretzman, L., Rao, S.N., Lindmark, R.J., Panzerknodle, S.G., Nicholson, N.S., Taite, B.B., Salyers, A.K., King,

L.W., Campion, J.G., Feigen, L.P. Potent in-vitro and in-vivo inhibitors of platelet-aggregation based upon the Arg-Gly-Asp-Phe sequence of fibrinogen - a proposal on the nature of the binding interaction between the Arg-Guanidine of RGDX mimetics and the platelet GP IIb-IIIa receptor. *J. Med. Chem.* **36**, 1811-1819 (1993).

229. Pfaff, M., Tangemann, K., Müller, B., Gurrath, M., Müller, G., Kessler, H., Timpl, R., Engel, J. Selective recognition of cyclic RGD peptides of NMR defined conformation by Alpha-II-Beta-3, Alpha-V-Beta-3, and Alpha-5-Beta-1 integrins. *J. Biol. Chem.* **269**, 20233-20238 (1994).

230. Gurrath, M., Müller, G., Kessler, H., Aumailley, M. & Timpl, R. Conformation activity studies of rationally designed potent antiadhesive RGD peptides. *Eur. J. Biochem.* **210**, 911-921 (1992).

231. Enholm, E. & Bharadwaj, A. RGD mounted on an L-proline scaffold. *Bioorg. Med. Chem.Letters* **15**, 3470-3471 (2005).

232. Müller, G., Gurrath, M. & Kessler, H. Pharmacophore refinement of GpIIb-IIIa antagonists based on comparative-studies of antiadhesive cyclic and acyclic RGD peptides. *J. Comput. Aid. Mol. Des.* **8**, 709-730 (1994).

233. Morris, G.M., Goodsell, D.S., Halliday, R.S., Huey, R., Hart, W.E., Belew, R.K., Olson, A.J. Automated docking using a Lamarckian genetic algorithm and an empirical binding free energy function. *J. Comput. Chem.* **19**, 1639-1662 (1998).

234. Artursson, P. & Karlsson, J. Correlation between oral-drug absorption in humans and apparent drug permeability coefficients in human intestinal epithelial (caco-2) cells. *Biochem. Biophys. Res. Commun.* **175**, 880-885 (1991).

235. Kansy, M., Senner, F. & Gubernator, K. Physicochemical high throughput screening: Parallel artificial membrane permeation assay in the description of passive absorption processes. *J. Med. Chem.* **41**, 1007-1010 (1998).